

ENHANCED OIL RECOVERY BY CO₂ FOAM FLOODING

Final Report for the Period October 1, 1981—December 31, 1985

**By
John T. Patton**

September 1986

**New Mexico State University
Las Cruces, New Mexico**

MOOREHEAD ENERGY



**Bartlesville Project Office
U. S. DEPARTMENT OF ENERGY
Bartlesville, Oklahoma**

DISCLAIMER

This report was prepared as an account of work sponsored by an agency of the United States Government. Neither the United States Government nor any agency thereof, nor any of their employees, makes any warranty, express or implied, or assumes any legal liability or responsibility for the accuracy, completeness, or usefulness of any information, apparatus, product, or process disclosed, or represents that its use would not infringe privately owned rights. Reference herein to any specific commercial product, process, or service by trade name, trademark, manufacturer, or otherwise, does not necessarily constitute or imply its endorsement, recommendation, or favoring by the United States Government or any agency thereof. The views and opinions of authors expressed herein do not necessarily state or reflect those of the United States Government or any agency thereof.

Printed in the United States of America. Available from:
National Technical Information Service
U.S. Department of Commerce
5285 Port Royal Road
Springfield, VA 22161

NTIS price codes
Paper copy: **A10**
Microfiche copy: **A01**

ENHANCED OIL RECOVERY BY CO₂ FOAM FLOODING

**Final Report for the Period
October 1, 1981—December 31, 1985**

**By
John T. Patton**

Work Performed Under Contract No. AC21-81MC16551

**Prepared for
U.S. Department of Energy
Assistant Secretary for Fossil Energy**

**Royal Watts, Project Manager
Morgantown Energy Technology Center
P.O. Box 880
Morgantown, WV 26505**

**Prepared by
New Mexico State University
Engineering Research Center
Box 3449
Las Cruces, NM 88003**

Table of Contents

| <u>Title</u> | <u>Page</u> |
|---|-------------|
| SECTION ONE. | 1 |
| INTRODUCTION | 1 |
| 1.1 General. | 1 |
| 1.2 Background | 2 |
| 1.3 Project Summary 1979-1983. | 8 |
| SECTION TWO. | 13 |
| DYNAMIC SCREENING - THE MINI-FLOW TEST | 13 |
| 2.1 Introduction | 13 |
| 2.2 Dynamic Screening. | 13 |
| 2.3 Apparatus and Procedure | 14 |
| 2.3.1 Mathematical Analysis | 17 |
| 2.4 Results and Conclusions | 25 |
| SECTION THREE. | 39 |
| CO ₂ RELATIVE PERMEABILITIES IN THE PRESENCE OF RESIDUAL OIL | 39 |
| 3.1 Introduction | 39 |
| 3.1.1 Need for Present Study | 39 |
| 3.1.2 Experimental Approach | 40 |
| 3.2 Calculation of Relative Permeabilities | 42 |
| 3.2.1 Model Equations | 42 |
| 3.2.2 Limitations | 44 |
| 3.2.3 Methods to Scale Relative Permeability Curves | 46 |
| 3.3 Equation for Water Production Vs. CO ₂ Injection. | 48 |
| 3.3.1 Shape of Water Production Curve | 48 |
| 3.3.2 Curve Modeled After CO ₂ Breakthrough. | 51 |

Table of Contents (Cont'd)

| <u>Title</u> | <u>Page</u> |
|--|-------------|
| 3.3.3 Equation to Fit L_p Data | 51 |
| 3.3.4 Other Forms Considered | 51 |
| 3.4 Equation for Cumulative Volume of Injected CO_2 | 55 |
| 3.4.1 Four-Parameter Equation | 55 |
| 3.4.2 Need to Correct the Injected Gas Volumes | 55 |
| 3.4.3 Initial Attempts to Correct for or Avoid CO_2 Dis- solution Problem | 57 |
| 3.5 CO_2 Solubility Corrections | 57 |
| 3.5.1 Comparison Between Injected Gas and Produced Water. | 57 |
| 3.5.2 Further Corrections to G_i | 59 |
| 3.6 Apparatus | 59 |
| 3.6.1 Reservoir Condition Model | 59 |
| 3.6.2 Carbon Dioxide | 63 |
| 3.6.3 Effluent Collection | 63 |
| 3.6.4 Modification of Valves | 64 |
| 3.7 Procedure | 64 |
| 3.7.1 Preparation of Model | 64 |
| 3.7.2 Permeability to Brine | 65 |
| 3.7.3 Oil Saturation | 65 |
| 3.7.4 Start-up Procedure for CO_2 Injection | 66 |
| 3.7.5 Operation | 67 |
| 3.7.6 Data Collection | 67 |
| 3.8 Results | 68 |
| 3.8.1 Surfactants Selection | 68 |

Table of Contents (Cont'd)

| <u>Title</u> | <u>Page</u> |
|--|-------------|
| 3.8.2 Performance of Surfactants During Immiscible CO ₂ Floods | 68 |
| 3.8.3 Additional Favorable Performance Factors | 71 |
| 3.8.4 Interaction of Surfactants With Oil | 74 |
| 3.8.5 Relative Permeability Curves | 75 |
| SECTION FOUR | 85 |
| MISCIBLE DISPLACEMENT | 85 |
| 4.1 Apparatus | 85 |
| 4.1.1 Reservoir Condition Flow Model | 85 |
| 4.1.2 Injection Pump | 88 |
| 4.2 Materials | 90 |
| 4.3 Procedure | 90 |
| 4.3.1 Saturation of the Model | 90 |
| 4.3.2 Water and Surfactant Flood | 92 |
| 4.3.3 Carbon Dioxide Tertiary Flood | 92 |
| 4.3.4 Sample Analysis | 93 |
| 4.4 Results | 94 |
| 4.5 Conclusions | 103 |
| SECTION FIVE | 105 |
| IMMISCIBLE OIL DISPLACEMENT TESTS | 105 |
| 5.1 Introduction | 105 |
| 5.2 Equipment | 105 |
| 5.3 Analytical Procedure | 110 |
| 5.4 Experimental Procedure | 115 |
| 5.5 Results | 117 |

Table of Contents (Cont'd)

| <u>Title</u> | <u>Page</u> |
|--|-------------|
| SECTION SIX | 125 |
| RESERVOIR SIMULATION OF MOBILITY CONTROLLED CO ₂ FLOODS | 125 |
| 6.1 Introduction | 125 |
| 6.2 Immiscible Displacement | 126 |
| 6.3 Miscible Displacement | 137 |
| SELECTED BIBLIOGRAPHY | 141 |
| PATENTS & THESES | 148 |
| APPENDIX A | 149 |
| APPENDIX B | 159 |
| APPENDIX C | 177 |
| APPENDIX D | 189 |

List of Tables

| <u>Tables</u> | | <u>Page</u> |
|----------------|---|-------------|
| 2.1 | Terms Used in Equations. | 19 |
| 2.2 | Mobility Control Surfactants | 26 |
| 2.3 | A Comparison of Mobility Ratios at 77° and 170°F | 28 |
| 2.4 | Mobility Ratio After Breakthrough for Various Surfactants at 0.5% Concentration. | 33 |
| 3.1 | Parameters of Reservoir Model. | 62 |
| 3.2 | Gas Saturation at Breakthrough Increased by Surfactants . | 71 |
| 4.1 | Physical Properties of N-Octane. | 91 |
| 4.2 | Mobility Control Surfactants | 91 |
| 4.3 | Mobility Control Floods | 95 |
| 5.1 | Immiscible Displacement. | 118 |
| 5.2 | Immiscible CO ₂ Flood Results | 118 |
| 6.1 | Reservoir and Fluid Parameters - Immiscible CO ₂ Simulation | 130 |
| 6.2 | Comparison of 3-D Vs. 2-D Simulation of Immiscible CO ₂ Flooding | 132 |
| 6.3 | Reservoir and Fluid Parameters - Miscible CO ₂ Simulation . | 139 |
| APPENDIX A | | |
| A-1 | Relative Permeabilities to Gas and Water When No Surfactant is Present | 156 |
| A-2 | Relative Permeabilities to Gas and Water When Pluradyne SF-27 Present | 156 |
| A-3 | Relative Permeabilities to Gas and Water When Stepanflo- 50 Present | 157 |

List of Tables (continued)

| <u>Tables</u> | <u>Page</u> |
|---------------|--|
| APPENDIX D | |
| D-1 | Simulation Initialization Data 190 |
| D-2 | Saturation Functions - Relative Perms 191 |
| D-3 | Immiscible CO ₂ Flood - Mobility Ratio = 1.0 192 |
| D-4 | Immiscible CO ₂ Flood - Mobility Ratio = 1.5 193 |
| D-5 | Immiscible CO ₂ Flood - Mobility Ratio = 2.0 194 |
| D-6 | Immiscible CO ₂ Flood - Mobility Ratio = 10.0 195 |

List of Figures

| <u>Figure</u> | <u>Page</u> |
|---|-------------|
| 1.1 Carbon Dioxide Required to Produce Tertiary Oil | 3 |
| 2.1 Dynamic Flow Test Apparatus | 15 |
| 2.2 Dynamic Flow Test Column | 18 |
| 2.3 Mobility Ratio vs PV Injected for Pluradyne SF-27 in Brine | 30 |
| 2.4 Mobility Ratio vs Time for Exxon LD776-52 in Brine 77 DEG.F | 31 |
| 2.5 Mobility Ratio vs PV Inected for Exxon LD776-52 in R.0 Water | 32 |
| 2.6 Mobility Ratio vs Time - Exxon LD776-52 in Tap Water . . . | 34 |
| 2.7 Mobility Ratio vs Time for Pluronic F68, pH = 2.9 | 35 |
| 2.8 Mobility Ratio vs Time for Alipal CD-128, pH = 2.85 | 36 |
| 2.9 Mobility Ratio vs Time for Neodol 23-6.5, pH-2.9 | 37 |
| 3.1 Water Saturation and Permeability Drop Abruptly when CO ₂ Breaks Through the Sand Pack. | 47 |
| 3.2 Gas Permeability at End of Flood Permits Scaling of k _{rg} Curve | 49 |
| 3.3 Water Production Rate Decreases after CO ₂ Breaks Through the Sand Pack | 50 |
| 3.4 Eq. 3.3.1 Used to Smooth Water Production Data Following CO ₂ Breakthrough. | 52 |
| 3.5 Eq. 3.4.1 Used to Smooth Gas Injection Data | 56 |
| 3.6 Volume of CO ₂ Injected Exceeds Water Production Before Gas Breakthrough | 58 |

List of Figures

| <u>Figure</u> | | <u>Page</u> |
|---------------|--|-------------|
| 3.7 | Undissolved Fraction of Injected CO ₂ (dashed line) Provides Values for G _i to be Used in Eqs. 3.2.1-4 | 60 |
| 3.8 | Schematic Diagram of Apparatus Used for CO ₂ Mobility Study | 61 |
| 3.9 | Effect of Surfactants on Gas Permeability | 70 |
| 3.10 | Mobility Control with Stepanflo-50 Increases Displacement Efficiency | 72 |
| 3.11 | Breakthrough of CO ₂ Delayed by Pluradyne SF-27 | 73 |
| 3.12 | Performance of Pluradyne SF-27 Unchanged When Concentration Was Doubled | 76 |
| 3.13 | Permeability to Gas in the Absence of Surfactant | 77 |
| 3.14 | Permeability to Water in Absence of Surfactant | 78 |
| 3.15 | Permeability to Gas when Pluradyne SF-27 Present | 79 |
| 3.16 | Permeability to Water when Pluradyne SF-27 Present | 80 |
| 3.17 | Permeability to Gas when Stepanflo-50 Present | 81 |
| 3.18 | Permeability to Water when Stepanflo-50 Present | 82 |
| 4.1 | Miscible Displacement Apparatus | 86 |
| 4.2 | Model Entrance Construction | 87 |
| 4.3 | Injected Fluid Filter | 89 |
| 4.4 | Conventional CO ₂ Flood | 96 |
| 4.5 | Stepanflo-50 Mobility Controlled CO ₂ Flood | 98 |
| 4.6 | Pluradyne SF-27 Mobility Controlled CO ₂ Flood | 100 |
| 4.7 | Exxon LD776-52 Mobility Controlled CO ₂ Flood | 102 |
| 5.1 | Reservoir Condition Flow Apparatus | 106 |

List of Figures (Cont'd)

| <u>Figure</u> | | <u>Page</u> |
|---------------|--|-------------|
| 5.2 | Absorption Spectra for Crude Oil-Toluene Solutions | 113 |
| 5.3 | Calibration Curve for Spectra Photometric Analysis of Oil Concentration | 114 |
| 5.4 | Immiscible CO ₂ Displacement of Wilmington Tar Zone Crude Oil | 120 |
| 5.5 | Pluronic F68 Mobility Controlled Immiscible CO ₂ Displacement of Wilmington Tar Zone Crude Oil | 121 |
| 5.6 | Carbon Dioxide Displacement of Upper Terminal Zone Crude . | 123 |
| 6.1 | Enhanced Oil Production - Immiscible CO ₂ | 129 |
| 6.2 | Base Case - No Mobility Control CO ₂ Saturation Profile @0.24 P.V. Injected; 1/4 five spot pattern | 133 |
| 6.3 | MR = 1.5 - CO ₂ Saturation Profile @0.24 P.V. Injected; 1/4 five spot pattern | 134 |
| 6.4 | MR = 2.0 - CO ₂ Saturation Profile @0.24 P.V. Injected, 1/4 five spot pattern | 135 |
| 6.5 | MR = 10.0 - CO ₂ Saturation Profile @0.24 P.V. Injected; 1/4 five spot pattern | 136 |
| 6.6 | EOR - Miscible CO ₂ | 140 |

List of Figures (Cont'd)

| | |
|---|-----|
| APPENDIX B | 159 |
| B.1 Static Foam Test #1: Alipal CD-128. | 160 |
| B.2 Static Foam Test #'s 1 & 2: Alipal CD-128 w/10cc of Crude | 161 |
| B.3 Static Foam Test #4: Witcolate 1276. | 162 |
| B.4 Static Foam Test #'s 7 & 8: Witcolate 1276 w/10cc of Crude | 163 |
| B.5 Static Foam Test #2: Neodol 23-6.5 | 164 |
| B.6 Static Foam Test #'s 3 & 4: Neodol 23-6.5, w/10cc of Crude | 165 |
| B.7 Static Foam Test #3: Pluronic F-68 | 166 |
| B.8 Static Foam Test #'s 5 & 6: Pluronic F-68, w/10cc of Crude | 167 |
| B.9 Static Foam Test #5: Stepanflo #50. | 168 |
| B.10 Static Foam Test #'s 9 & 10: Stepanflo-50 w/10cc of Crude | 169 |
| B.11 Static Foam Test #6: Tetronic 1508 | 170 |
| B.12 Static Foam Test #'s 11 & 12: Tetronic 1508 w/10cc of Crude | 171 |
| B.13 Static Foam Test #7: Iconol | 172 |
| B.14 Static Foam Test #'s 13 & 14: Iconol w/10cc of Crude . . . | 173 |
| B.15 Static Foam Test #'s 15 & 16: Pluradyne OF-90 | 174 |
| B.16 Static Foam Test #'s 17 & 18: Pluradyne OF-90 w/10cc of Crude | 175 |
| APPENDIX C | 177 |
| C.1 Mobility Ratio vs Time for Brine pH = 2.8 | 178 |

List of Figures (Cont'd)

| <u>Figure</u> | | <u>Page</u> |
|---------------|---|-------------|
| C.2 | Mobility Ratio vs Time for Alipal CD-128, pH = 2.85, 20/11/82 | 179 |
| C.3 | Mobility Ratio vs Time for Witcolate 1276, pH = 2.5, 29/11/82 | 180 |
| C.4 | Mobility Ratio vs Time for Neodol 23-3 | 181 |
| C.5 | Mobility Ratio vs Time for Pluronic F68, pH = 2.9, 1/27/83 | 182 |
| C.6 | Mobility Ratio vs Time for Stepanflo 50, pH = 2.8 | 183 |
| C.7 | Mobility Ratio vs Time for Tetronic 1508, pH = 2.6, 11/26/83 | 184 |
| C.8 | Mobility Ratio vs Time for Iconol, pH = 2.5, 24/1/83 | 185 |
| C.9 | Mobility Ratio vs Time for Pluradyne OF-90, pH = 2.75, 22/1/83 | 186 |
| C.10 | Mobility Ratio vs Time for Sun Tech 4 | 187 |

Executive Summary

Objective: Identify commercially available additives which are effective in reducing the mobility of carbon dioxide, CO₂, thereby improving its efficiency in the recovery of tertiary oil, and which are low enough in cost to be economically attractive.

Summary: During the course of the project significant progress has been made in developing a commercial method of reducing the mobility of carbon dioxide in enhanced oil recovery processes. Interest in the industry is high and several major oil companies have agreed to underwrite a portion of funding necessary to continue the research over the next two years.

Experiments on gas mobility control, conducted in linear sand-pack models, show only a general correlation with the static foam test. The static test, which utilizes a blender to generate foam from an aqueous surfactant solution, is useful mainly for studying the effects of pH, temperature, salinity and crude oil on the relative foamability of any given surfactant. In general, surfactants that produce reasonable quantities of foam in the blender test also impart some degree of mobility control to gas during two-phase flow. The best mobility control additives however, are only modest foam volume producers. In addition, the best additives spontaneously produce a viscous foam under flow conditions and rates typical of petroleum reservoirs.

Three basic chemical structures listed below appear to show most promise for gas mobility control;

1. Ethoxylated adducts of $C_8 - C_{14}$ linear alcohols
2. Sulfate esters of ethoxylated $C_9 - C_{16}$ linear alcohols
3. Low molecular weight co-polymers of ethylene oxide and propylene oxide.

Each of the above types are compatible with normal oil field brines, unaffected by the presence of crude oil and stable under conditions common in a petroleum reservoir. Additive stability is of real concern. Limited experimentation suggests that only the sulfate esters might degrade at an unacceptable rate. This could limit their application to lower temperature reservoirs, below about 130°F. No degradation was noted for structures 1 and 3 in aging tests lasting two weeks at 125°F.

Computer simulation of mobility controlled CO_2 floods provided mixed results. For an immiscible CO_2 flood, reducing CO_2 mobility by a factor of 10 increased overall recovery by 20 percent. More importantly, incremental oil production was more than doubled during the early phase when only CO_2 was injected. The earlier oil kick resulting from mobility control could be more significant commercially than the final incremental improvement.

Attempts to simulate the mobility controlled miscible CO_2 process were not successful. Current simulation adequately predicted the base case flood without problems. However, it was not possible within the time frame of this project to model miscible CO_2 mobility lowering without generating spurious effects on the reservoir oil phase. More work is planned.

SECTION ONE

INTRODUCTION

1.1 General

For more than 30 years oil recovery experts have known that carbon dioxide possesses a unique ability to displace crude oil from reservoir rock. Although many gases have been tested for their crude-displacing efficacy, only carbon dioxide has the ability to reduce residual oil saturations to near zero and also to produce significant quantities of tertiary oil in models that have been previously waterflooded to the economic limit. Early studies have provided the fundamental understanding required to explain the high efficiency of carbon dioxide, and yet the depressed price of crude until 1973 made most, if not all, CO₂ field applications appear to be unprofitable.

Oil displacement by gas can occur under both miscible and immiscible conditions. CO₂ is unique in that it can effectively displace oil in both modes. The determining factor is the CO₂ pressure in the reservoir and depth controls the maximum pressure at which the flood can be conducted. All factors being equal, it is desirable to conduct the flood under pressure high enough to achieve miscible conditions if at all possible.

A common problem among gas-driven oil recovery processes is the severe gas channeling which occurs in the reservoir due to high gas mobility. Optimistic oil recoveries obtained in laboratory flow tests using small diameter linear models, have never been achieved in the field.

Both miscible and immiscible drive processes suffer because gas channeling causes most of the oil reservoir to be bypassed and the oil left behind.

Because of the high potential for miscible drives using enriched gas mixtures, considerable study was undertaken in the late 1950's on techniques to mitigate gas channeling. A few visionary investigators considered the use of foams as a possible solution to the problem. The earliest reported work was conducted by Bond and Holbrook whose 1958 patent describes the use of foams in gas-drive processes [106]. Because of the high cost of carbon dioxide relative to crude oil during this period, carbon dioxide processes were ignored. The use of foams in conjunction with carbon dioxide was not contemplated until much later when rising crude prices coupled with an increase in value of hydrocarbon gases revived interest in the carbon dioxide displacement technique.

1.2 Background

Before embarking on the experimental phase of this research project, an extensive literature review was undertaken to evaluate the current state-of-the-art and to identify techniques, both good and bad, that had been investigated in the past. The resulting bibliography is included in this report.

The majority of both field and laboratory results which appear in the literature have been summarized by Patton [56] and are presented in Figure 1.1. These data have been normalized to a constant CO₂ injection equal to 0.2 pore volumes. It is apparent that above an oil viscosity of 2 centipoises the experiments indicate an almost constant displacement efficiency for carbon dioxide processes.

The earliest work relative to the problem of lowering the mobility of carbon dioxide does not involve carbon dioxide at all. Carbon dioxide exists as a gas or super critical phase under most reservoir conditions; therefore, experiments on controlling gas mobility are usually applicable to carbon dioxide even though they may have been conducted with nitrogen, methane or even air. Concurrent with Bond and Holbrook's work, whose 1958 patent describes the use of foams, Fried, working at the Bureau of Mines Laboratory in San Francisco, demonstrated the potential of foam to lower the mobility of an injected gas phase [27].

Fried generated the foam in a cylinder by dispersing fine air bubbles beneath the surface of a surfactant solution. This foam was flowed but only with much difficulty through a highly permeable matrix. A high foam-viscosity was indicated, suggesting that, indeed, foam might be the answer to mobility control in gas drive processes. Oil displacement tests in an Aloxite core showed that foam could reduce the saturation of a 350 centipoise oil to half the value obtained by waterflooding. The reduction in oil saturation was purely a viscous flow effect as the waterflood contained the same surfactant concentration as the foam.

Fried conducted additional studies in a 30 cm long glass-bead pack, 0.78 cm diameter, that indicated foam might be too good as a mobility control agent. Although the permeability of the pack was about 12 darcys, the foam was too viscous to flow even at a pressure gradient of 15 psi/ft. Microscopic examination of the linear model indicated that the injected foam coalesced, and was regenerated as the gas and water moved through the tiny pores. The regenerated foam had smaller bubbles and had presumably, a much higher viscosity. After a substantial amount

of regenerated foam had been formed, the mobility was lowered to the point that steady-state flow could not be maintained. From these experiments Fried concluded that a highly stable foam would not be desirable in an oil recovery process.

Fried's work was followed by some excellent work by Bond, Bernard and Holm [5,7,10,38] whose experimental technique involved in-situ foam generation promoted by injecting alternate slugs of surfactant solution and gas. Especially pertinent is their patent related to the use of foam for mobility control in CO₂ processes [104].

Laboratory work was encouraging enough that Union Oil Company conducted a field test in the Siggins Field, Illinois [35]. Foam generation by alternate slug-injection as well as simultaneous gas-solution injection was tested. This test indicated that the foaming agent, a modified ammonium lauryl sulfate, at concentrations below 1%, did not produce an effective foam. Above 1%, reduced gas mobility was obtained; however, it required 0.06 PV of surfactant solution be injected to achieve lasting mobility control. Inasmuch as the tests were conducted sequentially with the higher concentrations injected last, it is possible that the required amount of surfactant may be understated. Possibly a 0.10 PV surfactant bank might be more realistic for lasting mobility control. The results also indicated that adsorption may reduce the effectiveness of a surfactant. Future tests might benefit by selection of agents which are less strongly adsorbed than lauryl sulfate.

Work from the mid-60's to the early 70's proceeded sporadically due to the low incentive provided by the depressed price of crude oil. Interest was maintained largely through the impressive attempt by Chevron to commercialize the CO₂ process at Sacroc. Although this proj-

ect suffered from the same gas channeling noted earlier, CO₂ was effective in displacing commercial quantities of oil. Sacroc is regarded as the pioneering success for CO₂ processes.

The recent publications are especially pertinent. The first by Kanda and Schechter [44], corroborated much of the earlier work by Union, Amoco and Professor Marsden at Stanford University. It served to highlight the mechanisms and pertinent variables related to foam mobility control. Specifically they concluded that:

1. Displacement efficiency of foams is inversely related to the surface tension between the gas and liquid constituents.
2. High surface-viscosities are beneficial to displacement efficiency.
3. Permeability reduction, interpreted as meaning mobility control, is achieved more by films forming across the pore openings than by the physical movement of foam past mineral surfaces in the pore matrix.
4. By far the most important variable is the ability of the surfactant solution to wet the mineral surfaces in the matrix.

This last item has not been widely recognized and bears additional discussion. Experiments were conducted in sand packs conditioned to provide varying degrees of water-wetness. When the matrix was oil wet, drastic reduction in displacement efficiency occurred. The mere presence of oil had little influence on mobility control; however, when the oil was initially allowed to contact the dry, sand surfaces, it reduced water-wetness and subsequent displacement efficiency. A similar result was obtained when the sand grain surfaces were treated with an oil-wetting silicone prior to being saturated with water.

Accurate interpretation of these results in terms of reservoir performance is difficult because of two factors. First, the displacement

tests were conducted in a sand pack having a permeability of 27 darcys and a porosity of 42%. The pore dimensions in these media are unrealistically high and may have caused anomalous experimental results. The second factor involves the very low concentration of surfactants employed. Kanda & Schechter believe surfactant concentrations above the critical micelle concentrations are of no advantage and, hence, used very dilute solutions, about 10^{-3} M [44]. Tests by Holm et al. [36], indicate that there is a concentration effect and that this variable should be investigated in the future.

A more recent theoretical study by Slattery [74] suggests that displacement efficiency is proportional to surface tension. It then follows that the optimum foaming agent is one which lowers surface tension only the minimum required for spontaneous foaming to occur in the reservoir. Slattery's predictions are supported in part by experimental observations reported by other authors [35,43,47]. It is possible that deviations from theory are the result of grossly different pore dimensions utilized by the different investigators. Slattery's work also supports the dominant effect wettability exerts on the control of CO₂ mobility by foam.

The recent work by Bernard, et al. [85] provides the most definitive experimental data supporting the use of surfactants to control the mobility of CO₂. This study included linear flow tests conducted in sandstone and carbonate cores both with and without oil present in the matrix. Tests were conducted using supercritical CO₂ at pressures ranging from 1000-3050 psig. Many surfactants were screened and one, Alipal CD-128 was judged superior for lowering the mobility of CO₂. Alipal CD-128 is an anionic surfactant synthesized by ethoxylating a linear alcohol and reacting the subsequent product with SO₃ to obtain

an anionic surfactant. Tests were made utilizing this surfactant at two concentrations, 0.1% wt and 1.0% wt. These concentrations are based on the commercially available form of the surfactant, which is listed as being only 58% active.

Although the mobility reduction was evident in both carbonate and sandstone cores the effect in the sandstone was more dramatic. CO₂ mobility was reduced 99% in sandstone as opposed to only 85% in the carbonate core. Similar tests were repeated in carbonate cores after an oil saturation had been established in the pore spaces. As was the case when no oil was present, mobility of CO₂ was reduced; however, this time it was in excess of 95% over a large number of individual experiments. The fact that mobility was reduced even more in the presence of oil strongly supports the feasibility of the concept.

With oil present, tests were run at two surfactant concentrations, 0.1% and 1.0%. In every case the more concentrated solution achieved much greater mobility lowering, 10 fold or more, than in the 0.1% experiments. This is somewhat surprising since the c.m.c. for Alipal CD-128 is thought to be well below 0.1%. In all of the experiments the lower concentration was tested first and the results may be reflecting the adsorption of the surfactant on the mineral surfaces and the residual oil droplets.

1.3 Project Summary 1979-1983

Static foam tests, performed on 113 commercial surfactant samples, have identified some optimum chemical structures for mobility control additives. A unique dynamic screening process involving a mini-flow test has been developed to quickly identify new more-promising additives. The

potential of additives, identified in these tests, have been confirmed in linear, two-phase flow tests in tight, unconsolidated sand packs.

Linear flow experiments on gas mobility control, conducted in the sand-pack models, show only a general correlation with the static foam test. The static test, which utilizes a blender to generate foam from an aqueous surfactant solution, is useful mainly for studying the effects of pH, temperature, salinity and crude oil on the relative foamability of any given surfactant. In general, all surfactants that produce reasonable quantities of foam in the blender test also impart some degree of mobility control to gas during two-phase flow. Some of the best mobility control additives however, are only modest foam volume producers. In addition, the best additives spontaneously produce a viscous foam under flow conditions present in a petroleum reservoir.

Results of the dynamic screening tests correlate very well with both the linear mobility as well as oil displacement experiments. There is considerable evidence that the four basic chemical structures listed below appear to show most promise for gas mobility control;

1. Ethoxylated adducts of $C_8 - C_{14}$ linear alcohols
2. Sulfate esters of ethoxylated $C_9 - C_{16}$ linear alcohols
3. Low molecular weight co-polymers of ethylene oxide and propylene oxide
4. Synthetic organic sulfonates.

The first three types are compatible with normal oil field brines, unaffected by the presence of crude oil and stable under conditions common in a petroleum reservoir. At least one sulfonate also meets the above criteria. Additive stability is of real concern. Limited experimentation suggests that only the sulfate esters might degrade at an unacceptable rate. This could limit their application to

lower temperature reservoirs. No degradation was noted for structures 1 and 3 in aging tests lasting 2 weeks at 125°F. Some synergism exists between additives. Amine oxides and amides improve foam stability for many anionic surfactants but at the expense of some mobility control.

Data collected at different shear rates show foam is mildly pseudoplastic in nature and several orders of magnitude more viscous, (i.e. 10-100 cp) than its gas or liquid fraction. Of a special significance is the fact that foam viscosity has been shown to be an inverse function of foam density over a wide range of compositions. This fact is very advantageous in oil displacement processes. In areas where gas fingering is pronounced, foam viscosity would be increased by the high gas saturation and, thereby, tend to mitigate further gas channeling.

This high viscosity exhibited by foam at the low shear rates characteristic of oil reservoirs suggests that the displacement of oil by foam, envisioned by early investigators, may not be the dominant mechanism enhancing oil recovery. Alternately, the spontaneous generation of a viscous foam phase may serve to artificially reduce the flowing-gas saturation and thus provide a dramatic lowering of gas mobility due largely to a relative permeability effect. This mechanism could be especially important in the WAG process utilizing carbon dioxide or enriched gas mixtures for the displacement of oil in both miscible and immiscible processes.

The efficacy of CO₂ mobility control in enhancing oil recovery was demonstrated experimentally. Flow tests were conducted with a viscous oil under immiscible displacement conditions. Mobility control increased recovery by 40% over a CO₂ enhanced waterflood and 93% over a conventional waterflood plus primary production. No adverse effects,

such as emulsion formation, due to mobility control additives were noted. Mass transfer of CO₂ from the foam to the oil did not appear to be impeded. In fact, the mobility control experiment was performed without the severe gas and liquid slugging which characterized conventional CO₂ laboratory floods.

Additional experiments involved the miscible displacement of oil by carbon dioxide. They corroborate the immiscible results and, thus, provide additional evidence to support the commercial feasibility of CO₂ mobility control. Equally significant is the fact that the improvement in miscible displacement efficiency correlates with the two-phase flow mobility control data obtained in the dynamic screening experiments.

Information on the various facets of the project have been the subject of five technical papers. Two papers were presented at the 1981 SPE/DOE Symposium held in Tulsa, Oklahoma, the third at the 182nd ACS National meeting held in New York City, August 1981, the fourth at the SPE Annual Fall meeting held in San Francisco, California, September 1983, and the fifth at the 187th ACS National meeting held in St. Louis, Missouri, April 1984. In addition, many informal discussions have been held with industry and government personnel who have visited the laboratory facilities in Las Cruces.

During the course of the project, 8 graduate and 43 undergraduate students have assisted in various phases of the research, 6 M.S. degrees in Chemical Engineering have been awarded and 14 of the undergraduates accepted positions in the oil industry following their graduation. The specialized training in EOR technology that the students receive is of significant value in addition to the project's technical progress and accomplishments.

SECTION TWO

DYNAMIC SCREENING - THE MINI-FLOW TEST

2.1 Introduction

New additives are screened by conducting two tests that provide a rapid initial evaluation of given additives potential for reducing the mobility of carbon dioxide in a reservoir environment. The initial test involves generation of foam under high shear and measuring the key parameters, quality of foam produced and the stability of this foam with respect to time. The procedure involved in these tests as well as the static screening results on 92 additives have been reported previously [88].

To provide a more critical evaluation of those additives showing a high potential in the static foam test, a mini-flow test involving the two-phase flow of air and brine was developed. The results obtained with the dynamic flow test program show that the instrument is useful for predicting the efficacy of various surfactants for lowering the mobility of gases commonly injected into oil reservoirs. It has been possible to determine with reasonable accuracy, which of the numerous surfactant structures are the most effective. Also the effect of salinity temperature and pressure drop on surfactant performance can be determined.

2.2 Dynamic Screening

The mini-flow test was developed to provide rapid evaluation of the effect of surfactant additives on gas-liquid flow in an oil reservoir. Analysis of the ability of various surfactants to lower the

mobility of gas flowing in a porous medium was accomplished by comparing its mobility to the mobility of water in the same porous media, i.e., mobility ratio of gas to liquid during sequential flow. Mobility was chosen as the basis for analysis to avoid any controversy that may exist concerning the mechanism of the flow of foam in porous media. Since mobility of any fluid is known to be proportional to the ratio $q/\Delta P$, mobility ratio is easily calculated by the following formula:

$$\frac{M_g}{M_l} = \frac{q_g \Delta P_l}{q_l \Delta P_g}$$

Mobility control is evidenced by a lowering of this mobility ratio.

It was found that the presence of a surfactant in the brine lowers the pressure required to initiate gas flow in the liquid filled porous medium. In addition, a permanent pressure increase or resistance to flow in the porous medium is consistently observed when a surfactant foaming agent is added to the aqueous phase. This confirms the hypothesis that the presence of a surfactant does lower the mobility of a flowing gas stream in a porous medium.

2.3 Apparatus and Procedure

The ratio of mobility for gas and brine, with and without surfactants, was evaluated by displacing these fluids through a porous medium at a constant flow rate and recording the pressure drop as a function of time. A schematic of the apparatus used to obtain experimental data is shown in Figure 2.1.

The dynamic flow test apparatus consists of a small packed bed through which surfactant solution can be passed followed by gas to produce in-situ foam. The pressure drop through the column is measured at constant volumetric flow rate. From the recorded data, relative

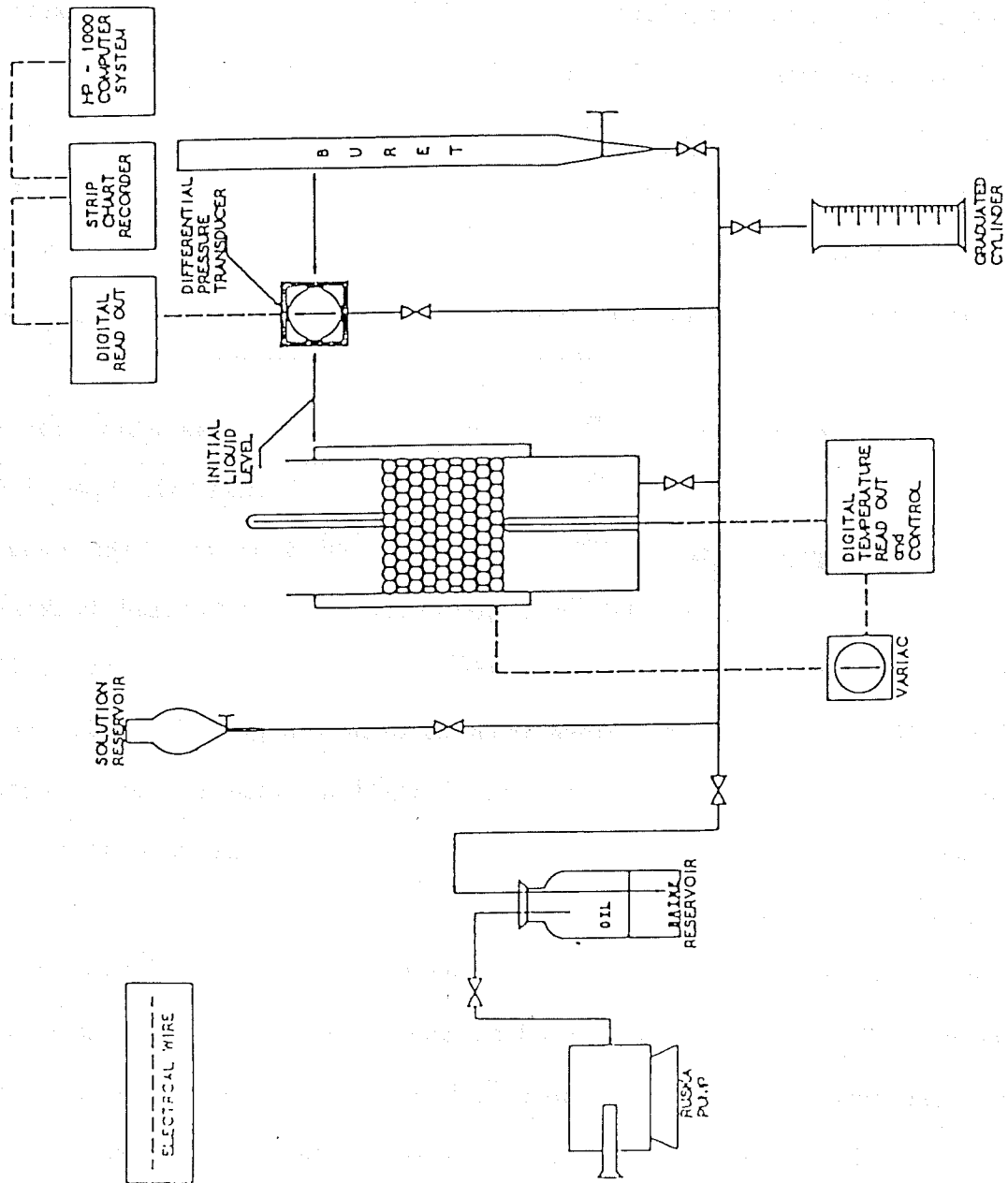


Figure 2.1 Dynamic Flow Test Apparatus

mobilities of the liquid and gas phases may be calculated. The change in gas mobility due to the presence of the surfactant is very closely related to the effectiveness of that surfactant for mobility control in oil core studies.

One flow column consists of a 1 1/4" (3.17 cm) inside diameter plexiglass tube which contains the porous bed. The porous bed used consists of -150+200 Tyler mesh glass beads (0.105 mm to 0.210 mm) supported by a 65-mesh screen. A bed approximately four inches in depth was used to test the surfactants and brine. A small layer of +65 mesh beads was used to prevent the smaller beads from going through the screen.

A second flow column for higher temperature tests was also fabricated. The tubing for the column is 1 1/2", schedule 40, type 316 stainless-steel pipe with an inside diameter of 4.01 cm. The upper section is 23 cm long and has a thermostatically controlled heating mantle to maintain the operating temperature. The lower section is 43 cm long. The two parts are joined with weld-on flanges (150 psi, type 316 ss). A 65-mesh copper screen is installed between the flanges to support the bed. The beads used for the bed are the same sizes as those used in the plastic column.

During operation the column is filled with the test solution from the buret. The glass beads are added and bead volume determined by liquid displaced. Solution is then withdrawn from the bottom of the flow column with a Ruska proportioning pump. The pump is capable of pumping or withdrawing fluid at a rate of 10 to 1200 cc/hr by the action of a 500 cc piston in a cylinder, powered by a 1/4 horsepower drive motor. Typically a rate of flow of 1 to 2 cc/min was used in the tests.

At the start of the runs a fast rate, 10-15 cc/min, was used briefly to establish, with more accuracy, the initial permeability of the bed.

Differential pressure across the bed was measured with a Validyne Model DP215 ± 15 psi differential pressure transducer connected to a Validyne Model CD223 dual channel digital readout. The transducer output is demodulated, amplified and filtered to produce an input proportional to CD output. For this work, a Cole-Parmer, model number 385, x-y strip chart recorder was connected to the digital readout to record the pressure differential profile as an experiment was being run.

During the flow tests, differential pressure, ΔP , vs. time data were automatically recorded into a computer (HP-1000). It was programmed to analyze the results and provide calculated relative mobilities as a function of the flow volumes, which were then plotted.

The ability of various surfactants to lower mobility of a gas flowing in a porous medium was evaluated by comparing the ratio of the gas mobility to that of the liquid during the course of the experiment.

Mobility was chosen as the basis for analysis as this avoids the necessity of defining the mechanism of flow control by foam in porous media. Mobility of a fluid is defined as the ratio of the permeability of the media with respect to that fluid divided by the fluid viscosity.

2.3.1 Mathematical Analysis

The calculations for mobilities from the experimental results require the separation of several different phenomena. Basically, the overall pressure drop must be analyzed with respect to hydrostatic effects, dynamic flow effects and capillary effects. Figure 2.2 and Table 2.1 show the notation used in the equations.

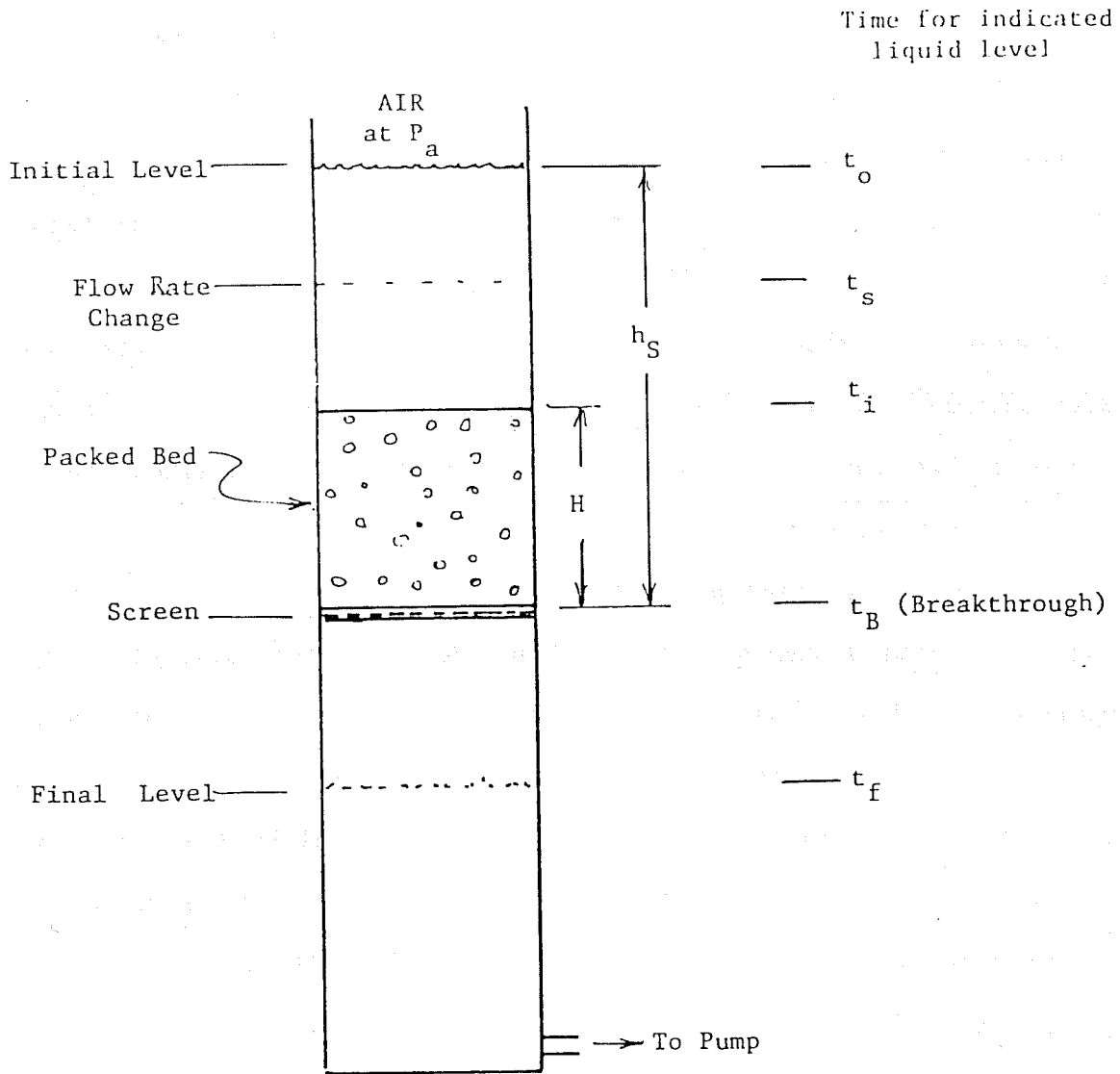


Figure 2.2 Dynamic Flow Test Column

Table 2.1. Terms Used in Equations

| | |
|--|---|
| μ = viscosity of fluid | ρ = fluid density |
| k = permeability of bed | Q = liquid flow rate used for most of the run |
| H = height of bed | Q' = fast rate at start of run |
| z = vertical height of interface | ϕ = porosity |
| P_H = pressure at bottom of bed | A = cross sectional area of tube |
| P_a = atmospheric pressure | M = mobility where $M = k/\mu$ |
| P_o = pressure at time = 0 (transducer) | Z = liquid height |
| P_t = pressure read by the transducer | W_B = weight of beads |
| P_c = pressure due to capillary effect | V = void volume in bed |
| S_{rL} = residual liquid saturation | V_G = volume of gas in the bed and is equal to liquid displaced |
| t = time | |
| P_f = pressure drop due to flow | |
| P_o' = pressure when interface enters the bed (transducer) | |
| P_h = pressure due to hydrostatic effects. | |

Period I, Before the Interface Enters the Bed

The hydrostatic effect on pressure is

$$\Delta P_h = \frac{\rho g z}{g_c} = P_h - P_o$$

Since $z = Q t/A$, P_h is a function of t ,

$$P_h = \frac{\rho g Q t}{g_c A} \quad \text{or} \quad \Delta P_h = \frac{\rho g Q t}{g_c A} - P_o$$

It is helpful to calculate the slope of this expression when P is plotted vs. t ,

$$\frac{dP}{dt} = \frac{\rho g Q}{g_c A}$$

The flow equation can be represented by Darcy's Law,

$$Q = \frac{k}{\mu} \frac{A \Delta P_f}{H} = M_L \frac{A \Delta P_f}{H}$$

or

$$M_L = \frac{QH}{A \Delta P_f}$$

Either flow rate Q or Q' may be used to calculate the mobility of the solution as long as the appropriate ΔP_f is used. It is preferable to use the faster rate Q' since $\Delta P'_f$ can be more accurately measured.

The transducer reads the total pressure which includes both the hydrostatic and the flow effects. The mobility calculation must include both terms as follows:

$$\Delta P'_f = (P_t - P_o) - \frac{\rho g Q' t}{A g_c} - P_o = P_t - \frac{\rho g Q' t}{g_c A}$$

$$M_L = \frac{Q'H}{A} \frac{1}{P_t - \rho g Q' t / A g_c}$$

The mobility during this part of the run is a constant since there is no composition change in the bed. Therefore $\Delta P'_f$ is also a constant. An accurate calculation of mobility must take into account the fluctuations in readings due to random error. The time readings are very

accurate and can be assumed to be free of error. The pressure readings are not error free. Therefore either mobility or pressure may be expressed as a function of time, and a least-square fit may be utilized to calculate an accurate value of mobility. In the first case, the fit should be made for the best line of zero slope through the data. In the second case, the slope of the pressure-time curve should be $P gQ'/g_c A$. The intercept of this line is the value of $\Delta P'_f$ from which the mobility can be readily calculated.

$$M_L \text{ (least sq. fit)} = \frac{Q'H}{A\Delta P'_f} \text{ (least sq.)}$$

In this study the second method was used. By similar calculations the ΔP_f for the lower flow rate can be calculated. The mobility should be the same at both flow rates so that the ΔP_f values should have the same ratio as the flow rates Q and Q' .

Period II, Interface Passing through the bed.

When the gas phase enters the bed, liquid is displaced. The permeability to the two phases changes in a non-steady state manner.

Although these changes can be handled rigorously it is not necessary for the purpose of this study to do so. The changes can be approximated from the variation in the liquid height in the bed.

During this period capillary forces must be taken into account. As the gas-liquid interface starts to enter the bed, sufficient pressure must be applied to initiate flow. This pressure is that needed to overcome the capillary pressure at the interface for the particular bed geometry. At this point a sharp rise in the pressure difference can be observed.

At gas breakthrough the capillary force is no longer opposing the flow, and a decrease in the pressure drop is apparent. When foam is

present, however, this effect may be so screened by the mobility control effects that it cannot be differentiated. The magnitude of this pressure recovery is a function of liquid composition, flow rate, liquid drainage time and wettability of the tube walls and support screen. It was found that a copper screen was superior to a stainless-steel one because the drainage was appreciably more consistent.

The calculations necessary for this period are the bed height, porosity, residual liquid saturation and breakthrough time. These values are needed for the calculations for the next period, i.e., after breakthrough.

The bed height may be readily calculated from the flow rates and the corresponding time intervals. The fast flow rate, Q' , begins at time zero and ends at t_s , the time when the flow rate is reduced to the slower rate, Q . With t_i being the time for entry of the interface into the bed, the cumulative volume of flow at this time is as follows:

$$\text{Vol.} = Q'(t_s - t_o) + Q(t_i - t_s)$$

The values of t_s and t_i are easily determined by the computer software because of the abrupt changes of slope of the pressure-time curve. The corresponding change of liquid height is

$$Z_i = \frac{Q'(t_s - t_o) + Q(t_i - t_s)}{A}$$

If h_s is the measured height of the liquid interface above the support screen, then the bed height, H , is equal $(h_s - Z_i)$. The porosity, ϕ , can now be calculated. The bed volume less the volume of beads gives the void volume, V_v , and the porosity is then

$$\phi = \frac{HA - W_B/2.473}{HA} = V_v/V$$

where 2.473 is the density of the beads and V is the bulk bed volume.

The residual liquid saturation is best determined by weighing the bed at the end of the run.

The time for gas breakthrough, t_B , can now be calculated as will be shown below. Alternately, but less desirably, it could be visually observed or else determined from the pressure trace in the same manner as were t_s and t_i . The difficulty is that the first is subject to human error and also would require a separate computer entry. Determining t_B from the change of slope of the pressure trace is an adequate method for some systems, but for some of the better mobility control agents the slope change is very gradual. Consequently, the breakthrough time would be difficult to determine with sufficient accuracy.

With a known value of residual liquid saturation, S_{rL} , the gas volume or the volume of liquid displaced by the gas flowing through the bed, V_G , can be calculated

$$V_g = \phi V(1 - S_{rL})$$

The corresponding time is calculated as follows:

$$Q(t_B - t_i) = \phi V(1 - S_{rL})$$

$$t_B = \frac{\phi V}{Q} (1 - S_{rL}) + t_i$$

Period III, Gas flowing through the bed after breakthrough.

During this period, it is again necessary to separate the pressure difference into a hydrostatic component and a flow component. The hydrostatic component can be readily calculated from the system geometry and the breakthrough time. The hydrostatic head at the breakthrough point is that sustained by the column of liquid of a height equal to the height of the support screen. The pressure loss due to the change in head from the start of the run is as follows:

$$P_{h_B} = \frac{\rho g h_s}{g_c}$$

The hydrostatic pressure, P_h , for the latter part of the run is then

$$P_h = \frac{Q(t-t_B)}{A} \frac{\rho g}{g_c} + \frac{\rho g h_s}{g_c} - P_o \quad \text{or}$$

$$P_h = \frac{\rho g}{g_c} (h_s + Q(t - t_B)/A) - P_o$$

The pressure drop due to flow is due to the resistance encountered by the gas in flowing through the wetted bed. It is as follows:

$$\Delta P_f = \frac{Q_G H \mu}{k(1-S_{rL})A}$$

Note: the term for permeability is approximated by $k(1 - S_{rL})$ because part of the pore structure is blocked by liquid.

The pressure drop through the bed for this period is often sufficiently high that a correction is needed for the gas expansion. The actual flow rate of gas at the top of the column is less than the liquid flow rate (pump rate). Since the flow ΔP varies essentially linearly through the bed an average may be used, and the new effective flow rate for the gas is

$$Q_G = Q \frac{(P_a - \Delta P_f/2)}{P_a}$$

with this addition the following equation may be written:

$$\Delta P_f = \frac{Q H \mu}{k A P_a} \frac{(P_a - \Delta P_f/2)}{(1-S_{rL})}$$

or in terms of Mobility

$$M_G = k/\mu = \frac{QH}{A \Delta P_f} \frac{(P_a - \Delta P_f/2)}{(1-S_{rL})P_a}$$

Expressing ΔP_f in terms of the transducer pressure P_t yields, where

$$\Delta P_f + \Delta P_h = \Delta P_t :$$

$$\Delta P_f = (P_t - P_o) - \left[\frac{\rho g}{g_c} (h_s + Q(t-t_B)/A) - P_o \right]$$

$$\Delta P_f = P_t - \frac{\rho g}{g_c} (h_s + Q(t-t_B)/A)$$

The gas mobility is therefore:

$$M_G = \frac{QH}{A(1-S_{rL})P_a} \left[\frac{P_a - 1/2(P_t - \rho g (h_s + Q(t-t_B)/A)/g_c)}{P_t - \rho g (h_s + Q(t-t_B)/A)/g_c} \right]$$

The mobility ratio of gas to liquid is therefore:

$$R = \frac{M_G}{M_L}$$

where $M_L = \frac{Q'H}{A \Delta P'_f}$ from the least squares fit as previously mentioned.

The mobility ratio is then plotted as a function of pore volume displaced.

2.4 Results & Conclusions

The dynamic flow test results provided means for comparing surfactants for mobility control applications. It was possible to compare the performance of various surfactants one against another; but, in addition, the effect on surfactant performance with changes in reservoir temperature and brine concentration were also delineated.

The best surfactants for mobility control as screened by the dynamic flow test are given in Table 2.2.

There are two ethoxylated alcohols, Pluradyne SF-27 and Neodol 23-6.5, both of which are excellent, based on tests in a typical brine solution, 3% sodium chloride with 100 PPM calcium ion. Other surfactants chosen from this same structural group were tested, and it was found that the chain length and degree of ethoxylation were both important for optimum mobility control. This is also true for the ethoxylated alcohol sulfates. It was found that the optimum ethoxylated type surfactant is a mixture with an average alcohol chain length of about 13 carbon atoms. The degree of ethoxylation is also important. It was

Table 2.2. Mobility Control Surfactants

| <u>Surfactant</u> | <u>Company</u> | <u>Chemical Structure</u> |
|-------------------|----------------------|---|
| Pluronic F-68 | BASF Wyandotte Corp. | Ethylene oxide - Propylene oxide co-polymer |
| Alipal CD-128 | GAF Corp. | Sulfated Ethoxylated alcohol |
| Neodol 23-6.5 | Shell Chemical Co. | Ethoxylated alcohol |
| Witcolate 1276 | Witco Chemical | Alcohol ether sulfate |
| Pluradyne SF-27 | BASF Wyandotte Corp. | Ethoxylated alcohol |
| Stepanflo-50 | Stepan Chemical Co. | Sulfate ester of ethoxylated alcohol |
| Exxon LD 776-52 | Exxon Co. | Sulfonate |

NOTE: Surfactant names are registered trademarks

found that the six ethoxylate groups was about optimum. Formation of the sulfate ester tended to minimize the effect of chain length and reduce the degree of ethoxylation required to produce maximum activity.

Neodol 23-6.5 is synthesized from a blend of mostly of C₁₂ and C₁₃ linear alcohols with an average of 6.5 ethoxylate groups per molecule.

Pluradyne SF-27 is a blend of ethoxylated alcohols having chain lengths varying between C₁₁ and C₁₅. It is superior to all other ethoxylated alcohol additives tested. The mobility reduction, immediately after breakthrough, was about the same for both surfactants but the Pluradyne SF-27 was more persistent in maintaining the high degree of mobility lowering with continued gas flow.

The superior performance of surfactants consisting of blends of similar chain lengths as opposed to relatively pure compounds was found

to be a consistent effect. The question of separation of mixtures during flow in reservoirs should be considered. Fractionation of mixtures often occurs as a consequence of successive adsorption-desorption steps similar to that in chromatographic procedures. The compounds in such a mixture are very similar; and the effect, consequently, should be greatly minimized. Also, because of the structural similarity, the result of separation would have minor consequence in mobility control applications.

Ethoxylated alcohol sulfates are not as stable as some of the other good surfactants, but preliminary hydrolysis studies at reservoir conditions indicated that for lower temperature reservoirs they are sufficiently stable to be practical. Further, the hydrolysis product, ethoxylated alcohol, is also effective for mobility control.

The temperature effect on the degree of mobility control was investigated. The mobility is defined as the ratio of the permeability of the bed to a fluid divided by the viscosity of that fluid. The mobility ratio expressed in terms of these variables is as follows:

$$MR = \frac{M_g}{M_L} = \frac{k_g/\mu_g}{k_L/\mu_L}$$

The variable that will be most affected by temperature is the liquid viscosity, μ_L . The gas viscosity, μ_g , will also be affected but to much less extent. The gas permeability may change because of changes in residual water saturation, but this effect is not likely to be very large. The liquid permeability should be constant.

With negligible changes in k_g , the following equation may be used to predict the change in mobility ratio with temperature where the subscripts indicate different temperatures:

$$\frac{MR_1}{MR_2} = \frac{(\mu_L/\mu_g)_1}{(\mu_L/\mu_g)_2}$$

The Pluradyne SF-27 was tested at several different temperatures. The results are shown in Figure 2.3, where the mobility ratio (gas to liquid) is plotted as a function of the pore volumes of gas injected. The mobility ratio during the displacement at 170°F is significantly less after breakthrough than that performed at 77°F. The derived equation can be used to predict this difference.

A comparison of the values is shown in Table 2.

Table 2.3. A Comparison of Mobility Ratios at 77° and 170 °F

| Temperature, °F | Exp. Value | Viscosity Ratios |
|-----------------|------------|-------------------|
| 77 | 0.020 | 0.89/0.018 = 49.4 |
| 125 | 0.0101 | 0.53/0.019 = 27.9 |
| 170 | 0.0077 | 0.37/0.020 = 18.5 |
| Ratio 77-170 | 2.61 | 2.67 |
| Ratio 125-170 | 1.31 | 1.51 |

These results at 177 °F show excellent agreement between the measured and values predicted from viscosity ratios.

The MR ratio at 125 °F was 1.31 while that calculated from the viscosity ratios was 1.51. This is not quite as good agreement between predicted and measured ratios as the previous case. During this run the temperature control was slightly erratic. The small temperature deviations were not thought to be important but apparently did have some effect.

A similar comparison of the effect of temperature on the mobility after breakthrough was made for Exxon 776-52 at 72 °F and 170 °F. The measured ratio was 2.6 which is in close agreement with the 2.67 value calculated from the viscosities.

Exxon LD776-52 was included as the only sulfonate-type surfactant that had sufficient brine tolerance to perform well in the tests. The results are shown in Figure 2.3 for brine and Figure 2.4 for deionized water. The water runs were made at 77 °F and 170 °F.

Note in Figure 2.4 that the breakthrough point occurs earlier at the lower temperature. This effect can also be seen in the Pluradyne SF-27 data. This effect is due to the difference in residual water saturation in the two cases. With little or no mobility control, the residual water saturation is typically 0.40 to 0.60. With good mobility control, the value is typically between 0.15 and 0.25. The time for breakthrough is thus extended since more liquid is displaced from the column. In the case of the best mobility control agents residual liquid saturations of about 0.10 have been achieved.

The Exxon LD776-52 tests included a run with tap water of about 50 PPM calcium ion and negligible NaCl. The test was sensitive enough to differentiate between the deionized water runs and the tap water run. The plot is shown as Figure 2.5. A comparison with Figure 2.4 shows a value of mobility ratio after breakthrough of 0.0106 as compared with 0.0059 for the purified water run. A corresponding point for the brine run at the same temperature is about 0.036. These results clearly show the strong effect of the aqueous phase composition on the mobility control effectiveness for this surfactant.

MOBILITY RATIO VS PV. INJECTED FOR PLURADYNE SF-27 IN BRINE

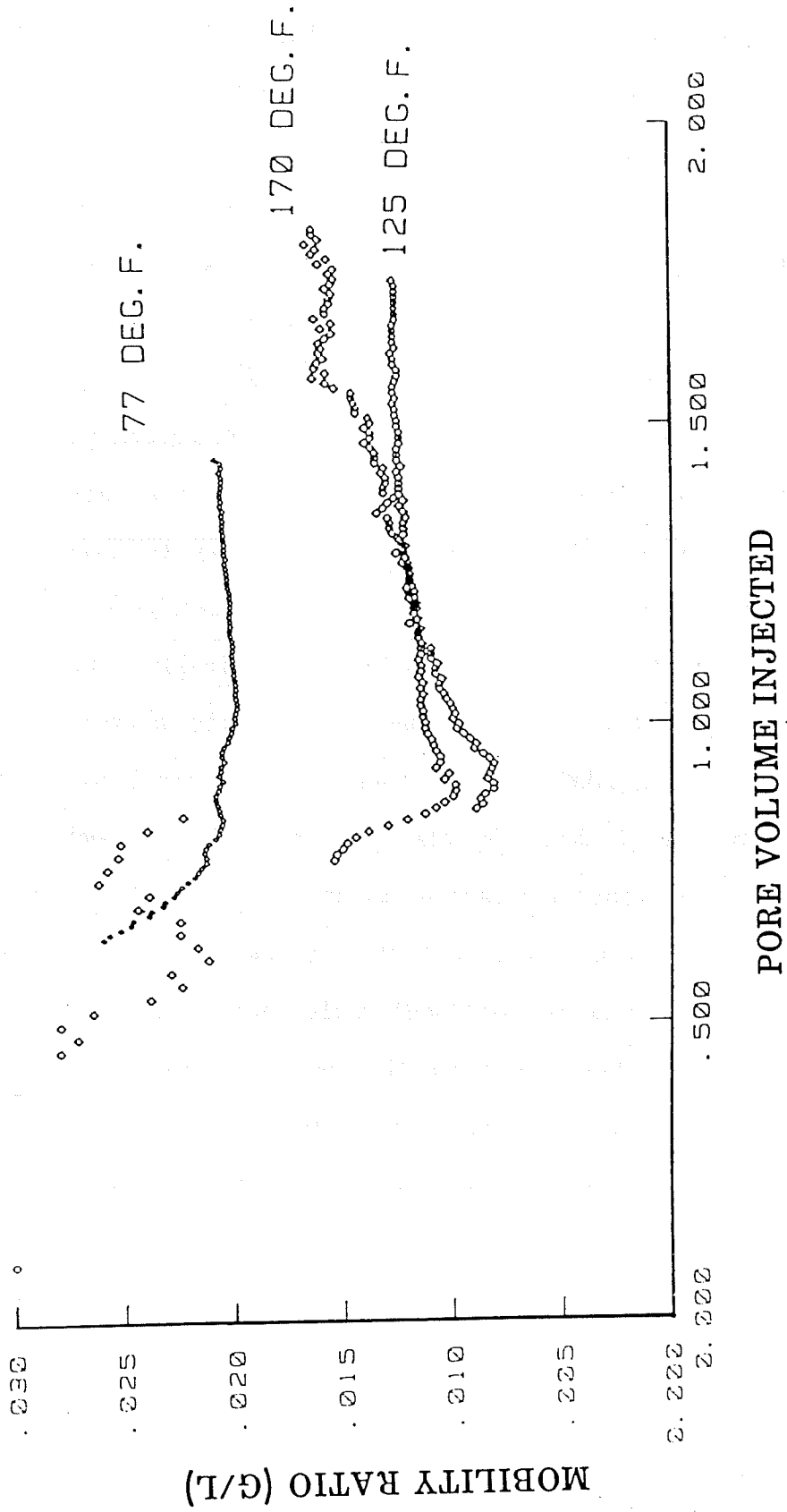


Figure 2.3

MOBILITY RATIO VS TIME FOR EXXON LD776-52 IN BRINE 77 DEG. F.

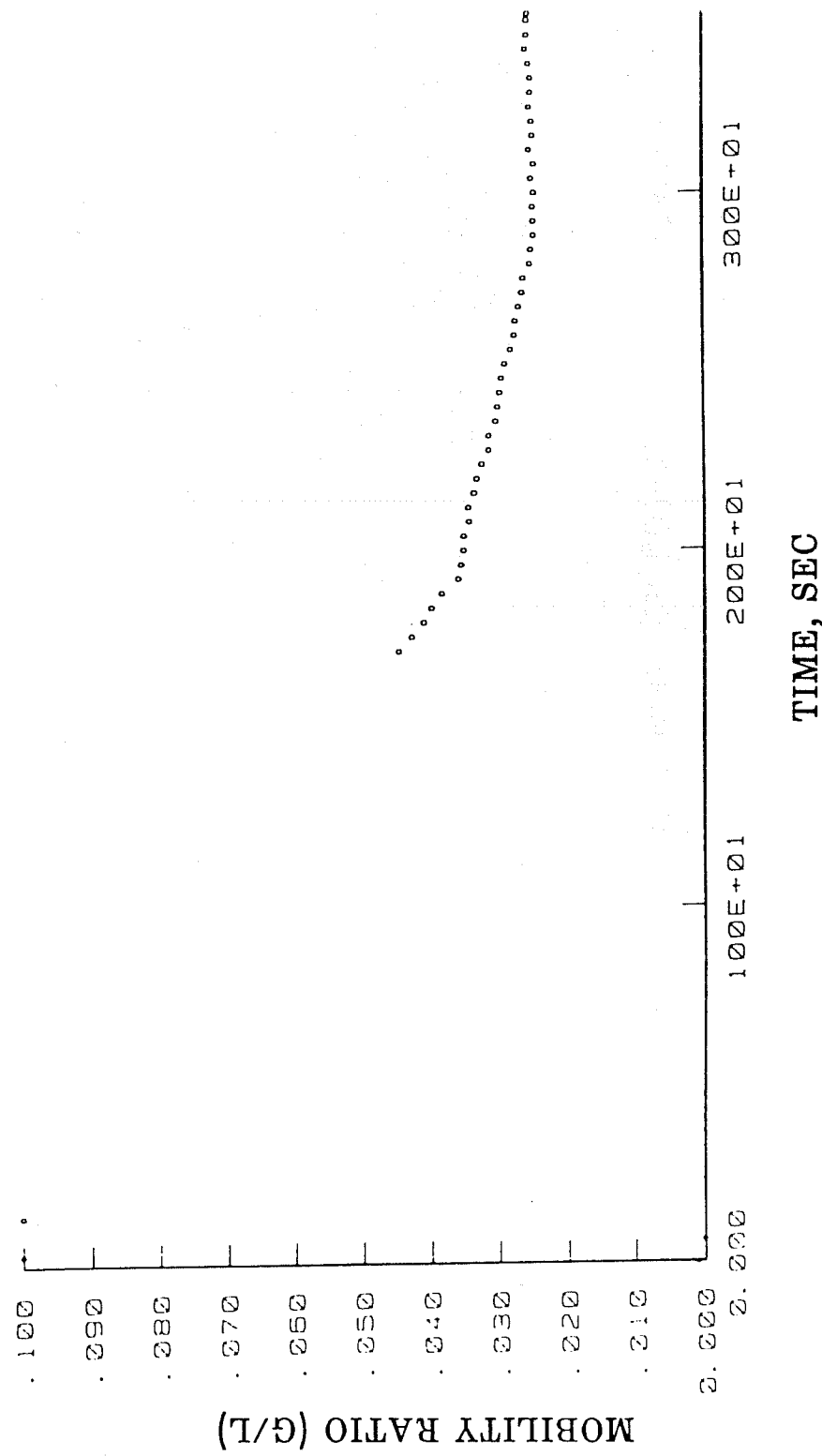


Figure 2.4

MOBILITY RATIO VS PV INJECTED FOR EXXON LD776-52 IN R.O. WATER

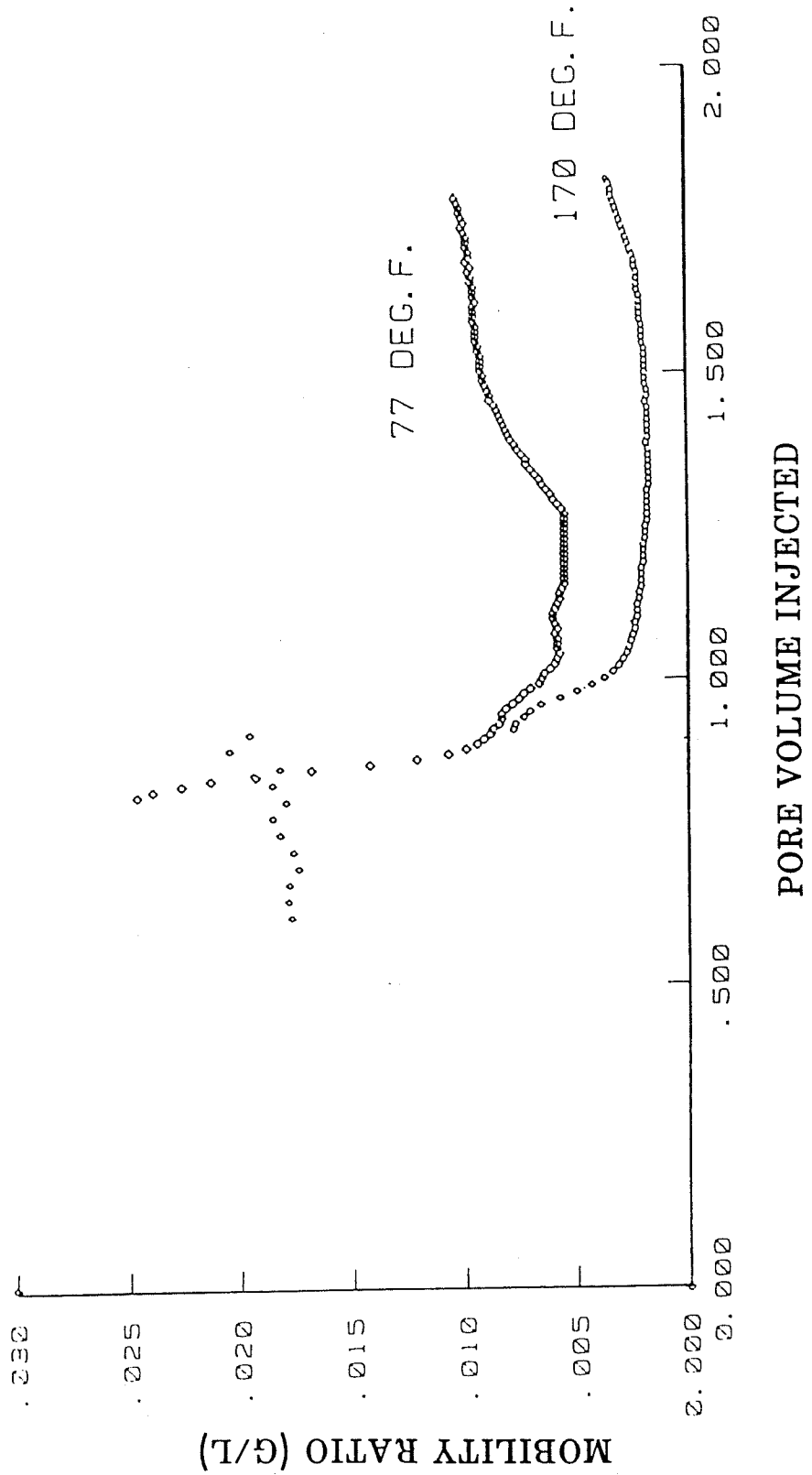


Figure 2.5

A table showing a comparison of these surfactants and the others which proved to be superior is shown in Table 2.4. A value of mobility ratio after breakthrough is used for the comparison. A more in depth comparison can be made by a comparison of the mobility ratio plots which are included. The ones not already referred to are shown as Figures 2.6 through 2.9.

The results of this study demonstrate the effectiveness of the dynamic flow test apparatus for the rapid evaluation of surfactant performance under various conditions. Its use should contribute significantly to the development of superior mobility control agents.

Table 2.4. Mobility Ratio After Breakthrough for Various Surfactants at 0.5% Concentration.

| Surfactant | Mobility Ratio | Temp. °F | Solution |
|-----------------|----------------|-------------|--------------|
| Pluronic F-68 | 0.056 | 77 | Brine |
| Alipal CD-128 | 0.024 | 77 | Brine |
| Neodol 23-6.5 | 0.018 | 77 | Brine |
| Witcolate 127.6 | 0.017 | 77 | Brine |
| Stepanflo-50 | 0.019 | 77 | Brine |
| Pluradyne SF-27 | 0.020 | 77 | Brine |
| Pluradyne SF-27 | 0.0101 | 125 | Brine |
| Pluradyne SF-27 | 0.0077 | 170 | Brine |
| Exxon LD776-52 | 0.036 | 77 | Brine |
| " | 0.0059 | 77 | Deion. Water |
| " | 0.0023 | 170 | Deion. Water |
| " | 0.0106 | 77 | Tap Water |

MOBILITY RATIO VS TIME-EXXON LD776-52 IN TAP WATER

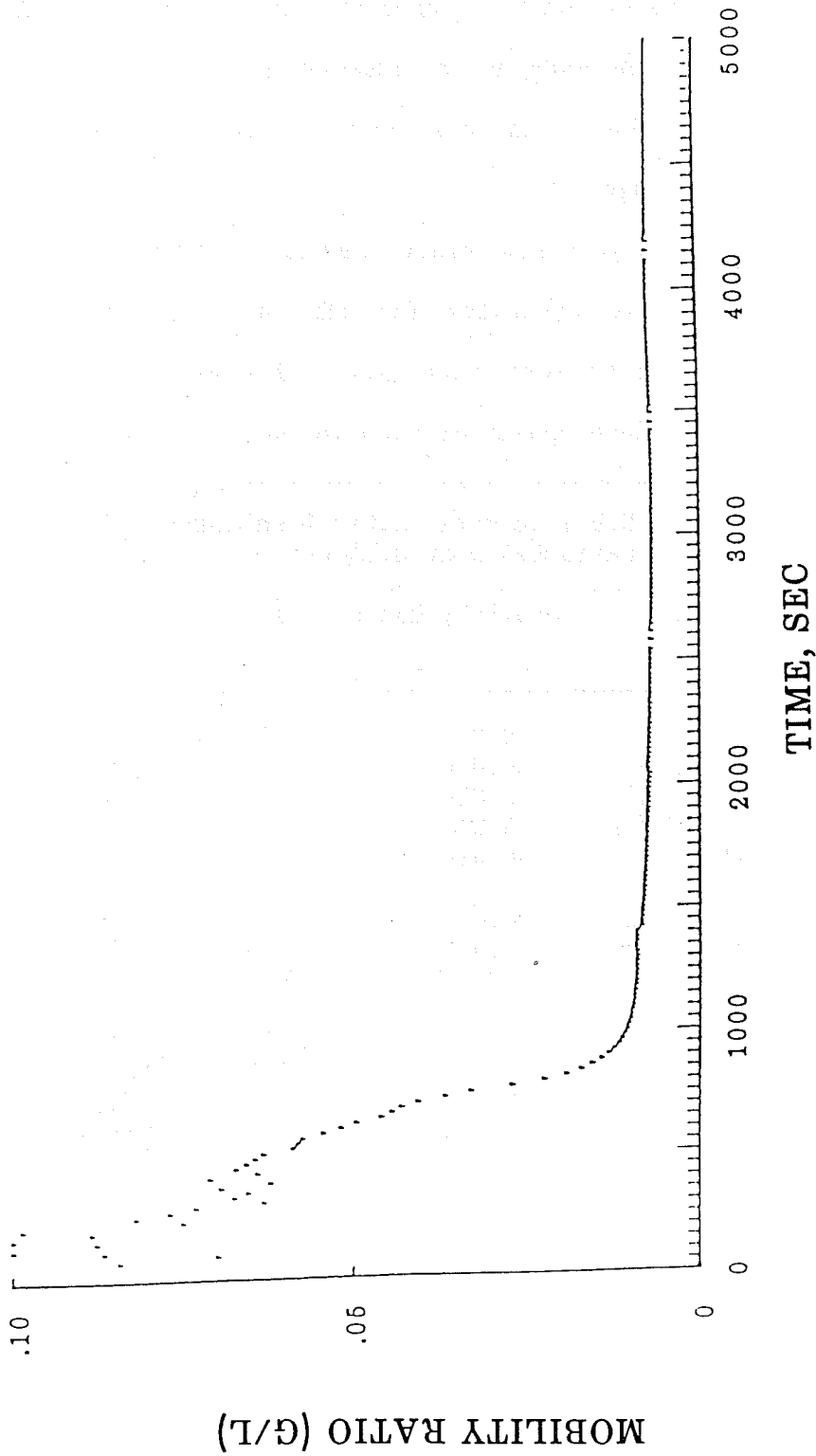


Figure 2.6

MOBILITY RATIO VS TIME FOR PLURONIC F68, pH = 2.9

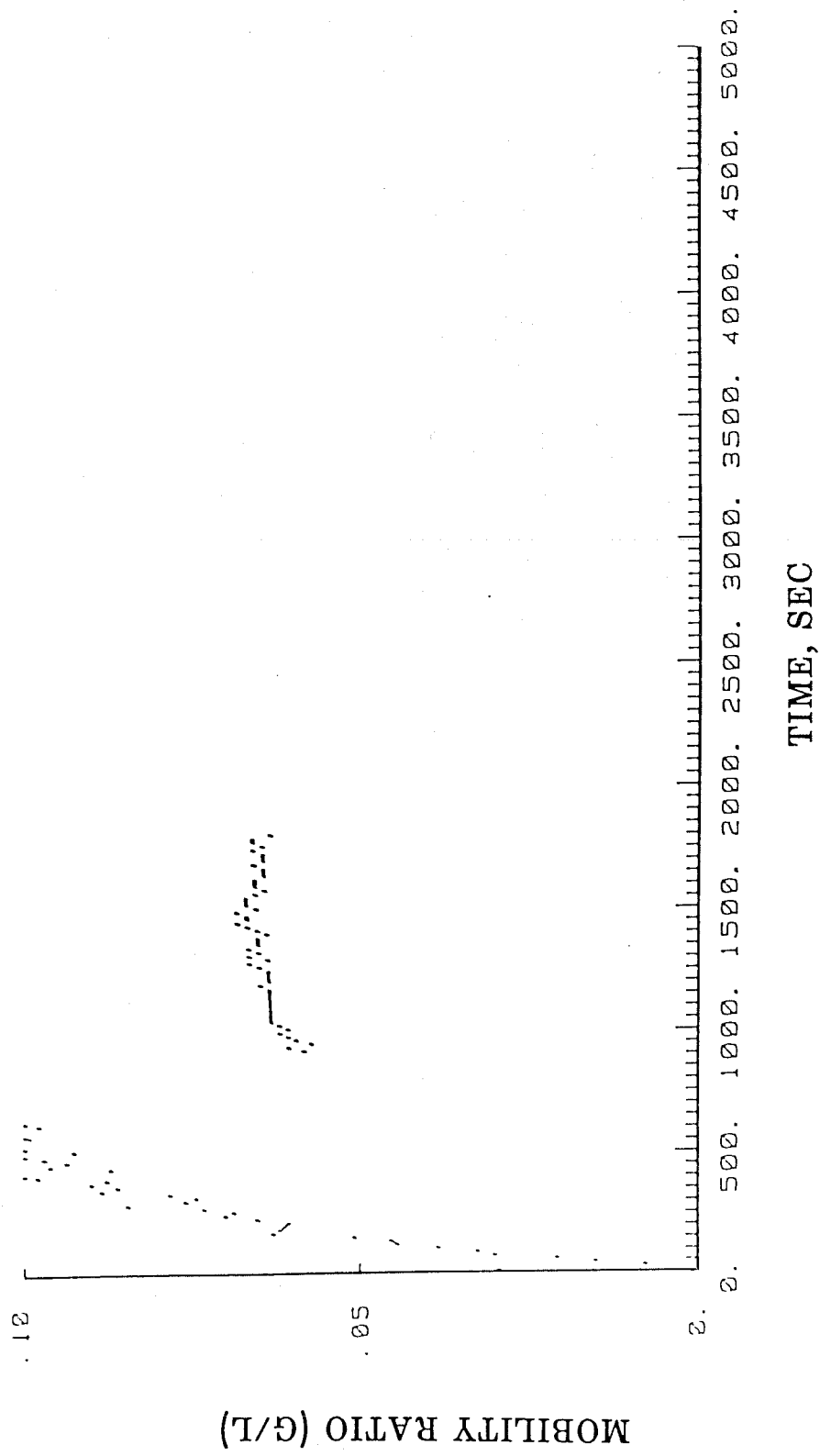


Figure 2.7

MOBILITY RATIO VS TIME FOR ALIPAL CD-128, pH =2.85

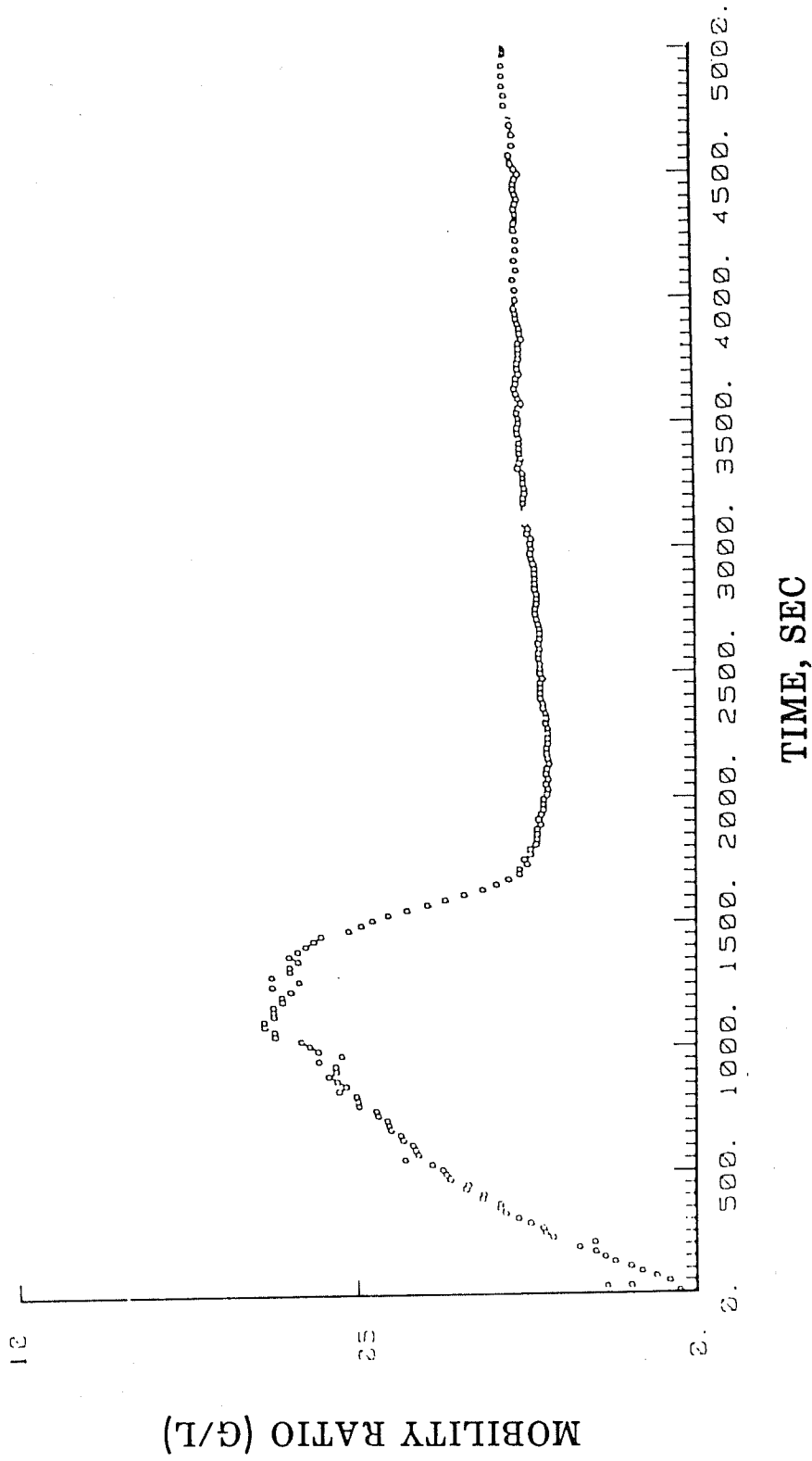


Figure 2.8

MOBILITY RATIO VS TIME FOR NEODOL 23-6.5, pH-2.9

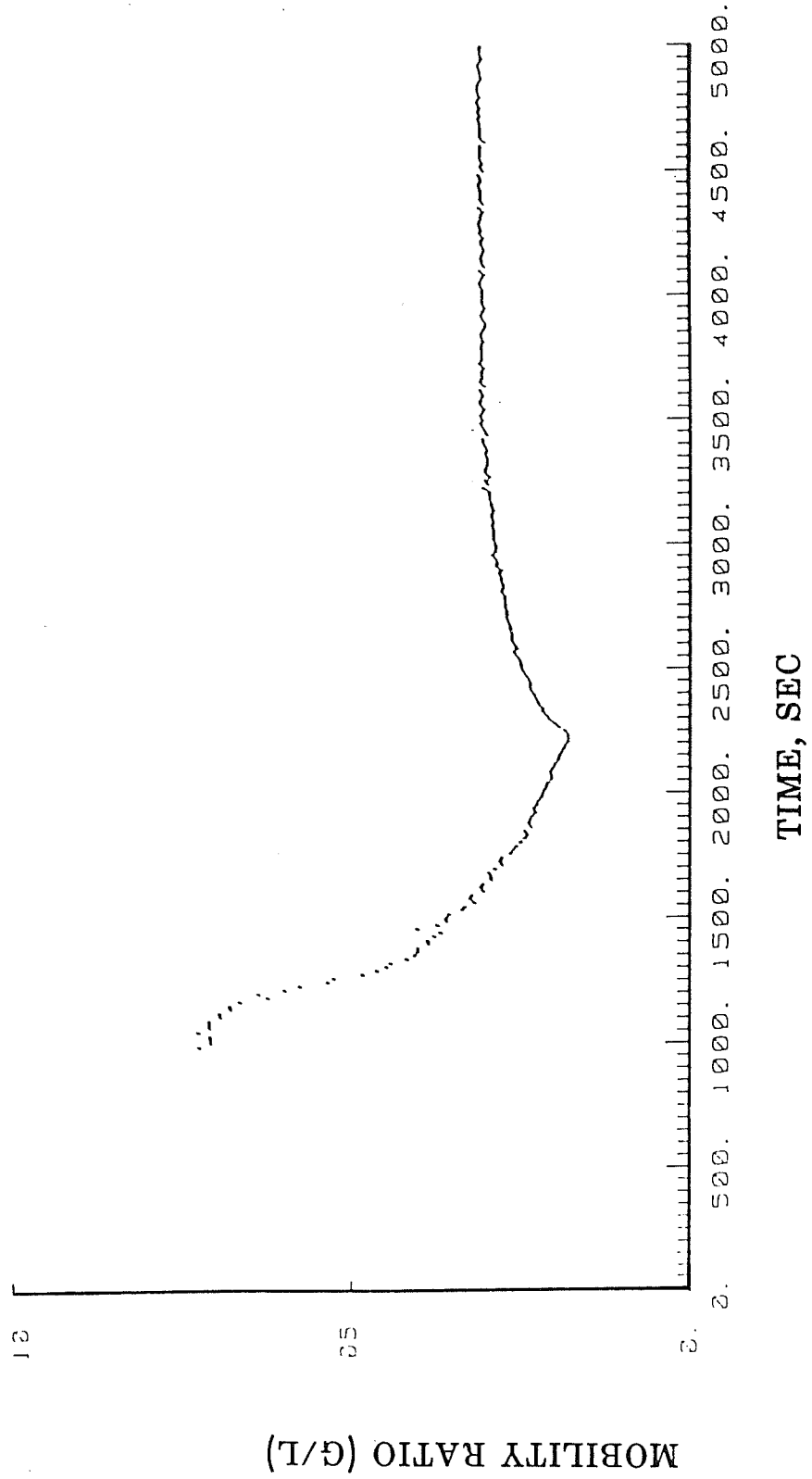


Figure 2.9

SECTION THREE

CO₂ RELATIVE PERMEABILITIES IN THE PRESENCE OF RESIDUAL OIL

3.1 Introduction

3.1.1 Need for Present Study

Conformance problems arise during CO₂ floods mainly because carbon dioxide has a higher mobility than that of the oil it is displacing. Consequently, the gas penetrates the oil and water, creating channels and by-passing the liquids. By definition, the mobility, M , of a fluid is the permeability of the porous medium to this fluid divided by the fluid's viscosity, as expressed in Eq. 3.1.1.

$$M = k/\mu \quad (3.1.1)$$

where

k is the permeability to the fluid, darcys, and

μ is the viscosity of the fluid, centipoise.

The mobility of CO₂ can be lowered by introducing surfactants that reduce the gas permeability, presumably by forming a foam in-situ. This improves the recovery of oil, because the gas mobility is now closer to that of the water and oil, and, thus, channeling and "fingering" by the gas are reduced. The mobility reduction manifests itself in the region behind the displacing front where gas is in contact with oil and water. Ahead of the displacing front, where no gas has yet penetrated, such improvement is not required.

The present experiments were needed in order to quantify the mobility reduction potential of commercially-available surfactants under typical reservoir conditions.

The surfactants studied had shown mobility control potential in preliminary laboratory screening tests discussed in Chapter 2.

The experiments also provided an opportunity to observe possible adverse interactions between the crude oil and the surfactants. Because the surfactants are present at low concentration and they exert their influence by affecting the gas-liquid interfaces, it is conceivable that the oil might hamper their effectiveness.

3.1.2 Experimental Approach

Because surfactants reduce the gas permeability but not its viscosity, changes in gas mobility can be inferred from changes in permeability. Permeability measurement can be made by performing either unsteady-state experiments or steady-state experiments.

In the case of unsteady-state experiments, a porous medium saturated with water and containing residual oil is flooded with carbon dioxide. The differential pressure across the porous medium can be kept constant (as was done in the present study) while measuring the injection rate of CO_2 and the flow rates of effluent water and gas as function of time. Alternatively, the injection rate of CO_2 can be held constant while the differential pressure across the medium is allowed to vary. Again, the flow rates of the effluents must be continually measured. In either case, the relative permeabilities must be calculated using a complex mathematical model that requires one know both the flow rates as a function of throughput and the first derivative. (The model is discussed in Section 3.2).

Considering only the time factor either type of unsteady-state experiment is preferable to a steady-state experiment, because a single

unsteady-state experiment provides relative permeabilities for a range of saturations. In contrast, a steady-state experiment yields the permeabilities at only one saturation. Accordingly, a large number of steady-state experiments must be performed to define accurately a relative permeability curve.

Keeping the pressure differential constant across the model was preferred to keeping the injection rate constant, because variations in the injection rate were not erratic and could be measured more accurately than changes in the pressure differential.

Steady-state experiments are more laborious than unsteady-state ones, because they require simultaneous injection of gas and water which entails certain experimental difficulties, and because it takes hours to establish steady-state conditions. Then the water and gas saturations must be determined. The results provide just a single point on each of the relative permeability curves (i.e., one for gas and one for water). Nevertheless, steady-state experiments have the advantage that the measured permeabilities are determined directly without recourse to an involved mathematical model, and the first derivative of the injection rate is not needed.

Because of the greater certainty inherent in the steady-state measurements, two types were made in the present study. The first was made at the end of an unsteady-state CO_2 flood, when the mobile water had been almost entirely removed and CO_2 was the only phase that was flowing. The flow rate and saturations were constant (i.e., the system was at steady-state), so the permeability to gas could be measured directly. This permitted the entire relative permeability curve for

gas (the one calculated using the mathematical model) to be correctly scaled if necessary.

The second type was made when the porous medium was being readied for another CO₂ flood. Brine alone was pumped into the medium until all the CO₂ had been displaced, and brine was the only phase that was flowing. Again, the flow rate and saturations were constant, so the water permeability could be measured. This permitted the relative permeability curve for water to be correctly scaled if necessary.

3.2 Calculation of Relative Permeabilities

3.2.1 Model Equations

The relative permeabilities to CO₂ and water were calculated using a procedure based on the original work of Buckley and Leverett [86] as extended by Welge [93] and Johnson, et al. [87]. According to this procedure, the fractional flow of water, f_w , is first calculated by means of Eq. 3.2.1

$$f_w = \frac{dL/dt}{dG_i/dt} \quad (3.2.1)$$

where

L is the cumulative volume of water produced

G_i is the cumulative volume of gas injected.*

The water relative permeability is then calculated using Eq. 3.2.2.

$$\frac{1}{K_{rw}} = \frac{g_o}{f_w} \frac{d(1/qG_i)}{d(1/G_i)} \quad (3.2.2)$$

* When CO₂ or another soluble is employed, this quantity must be reduced by the volume of gas that dissolves in the liquid within the model, as discussed below.

where

q is the gas injection rate, dG_1/dt

q_0 is the initial gas injection rate.

Finally, the gas relative permeability, k_{rg} , is calculated using Eq. 3.2.3.

$$k_{rg} = k_{rw} \frac{\mu_g^{1-f_w}}{\mu_w^{f_w}} \quad (3.2.3)$$

where

μ_g is viscosity of gas

μ_w is viscosity of water.

The viscosity of CO_2 at the reservoir conditions (124°F, 112 psia) is not readily available in the literature, and estimation methods based on empirical relationships are unreliable, because the reservoir conditions are so near the critical conditions (88°F, 1070 psia). For the above calculations, gas viscosity was obtained by interpolation from measurements made by Kestin, et al. [90] and Michels, et al. [91] on CO_2 at 122°F over a range of pressures.

Corresponding to each pair of relative permeabilities is the water saturation, S_w . Because the permeabilities calculated by Eqs. 3.2.2 and 3.2.3 pertain to the outlet face of the model, so, too, must the water saturation. It is not, in general, equal to the average saturation, but is significantly greater, as indicated by Eq. 3.2.4

$$S_w = 1 - S_o - S_{g,o} - L/P + G_i f_w / P \quad (3.2.4)$$

where S_o is the oil saturation,

$S_{g,o}$ is the initial gas saturation

P is the pore volume of the model.

3.2.2 Limitations

In practice there are four significant limitations in using Eqs. 3.2.1-3.2.4. The first arises from the fact that the equations were originally developed to describe the displacement of oil by water, i.e., one liquid by another. In that case the liquids are immiscible and incompressible, so the injection rate equals the total production rate (i.e., the rate at which water is injected equals the sum of the rates at which oil and water are being displaced). When a soluble gas such as CO₂ is the displacing fluid, however, the injection rate is significantly greater than the total production rate. In order to use the model equations in this case, the cumulative volume of injected gas must be reduced by the volume of gas that dissolves in the oil and water. (This adjustment is discussed more fully in section 3.5).

The second limitation is also due to the solubility of CO₂, namely, that the initial injection rate, q₀, to be used in Eq. 3.2.3 is much less than the observed rate. One way to estimate q₀, however, is to use the initial rate of water production. This is appropriate because, before CO₂ breaks through, the water production rate is the rate at which the volume of gas grows inside the model and is the appropriate dG/dt to use in Eq. 3.2.1.

The third limitation arises from the need to use both first and second derivatives of the cumulative volume of injected gas, G_i, when employing Eq. 3.2.2. This is because:

$$\frac{d/(1/qG_i)}{d(1/G_i)} = \frac{d(qG_i)^{-1}/dt}{d(G_i)^{-1}/dt} \quad (3.2.5)$$

Recalling that q, by definition is dG_i/dt, the numerator of Eq. 3.2.5 is

$$\frac{d}{dt} (qG_i)^{-1} = - \frac{(dG_i/dt)^2 + G_i d^2G_i/dt^2}{(qG_i)^2} \quad (3.2.6)$$

If raw data for G_i are used without first smoothing them, and the derivatives are approximated numerically by first and second differences, the resulting scatter in k_{rw} is prohibitive.* A more satisfactory approach is to fit the experimental data with suitable equations to smooth them and provide analytic expressions whose first and second derivatives are readily defined by accepted calculus procedures. (See Sections 3.3 and 3.4)

The fourth limitation arises from the fact that the model equations were developed for only the two-phase system. Because the oil phase was immobile in the present experiments, only two phases were flowing, and Eqs. 3.2.1-3.2.4 were still applicable.** However, in the sense in which the equations are used, the oil phase is considered inert and part of the porous medium. As a result, the equations assume $k_{rw} = 1.0$ when only water was being produced, because the water saturation and the fractional flow of water (as far as Eq. 3.2.1 was concerned) was 1.0.

In order to obtain relative permeability curves which are quantitatively correct once a basic relationship had been obtained from the model equations, independent values of k_g and k_w must be experimentally determined. These can then be used as scaling factors to adjust the basic relative permeability functions.

*The scatter in raw data from G_i arises from the difficulty involved in maintaining a constant pressure differential of 10 psi while the absolute pressure in the model is 1100 psig and the gas permeability of the model is continually increasing.

**The oil was present to test for any adverse effects it might have on CO_2 mobility. The model had been flooded with water until the oil was immobile; $S_o = 0.31$.

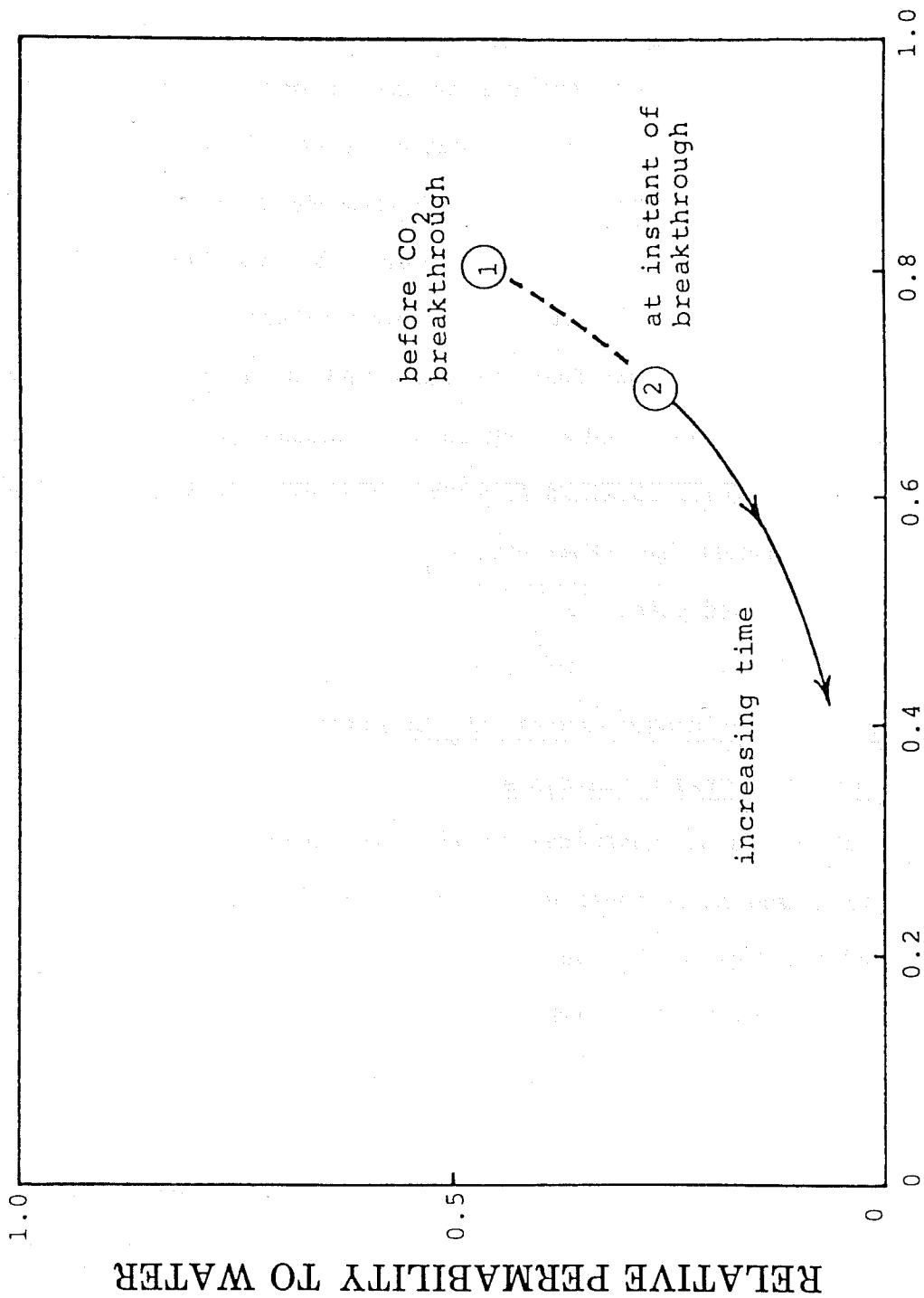
3.2.3 Methods to Scale Relative Permeability Curves

The water permeability of the laboratory model is easily measured before a CO_2 flood is started, because the saturations are known and constant, (e.g., $S_g = 0$). Dividing this result by the water permeability before oil has been introduced into the sand pack, provides a value for the relative permeability that is independent of the model equations.

To use this value of k_{rw} to scale those obtained during a CO_2 flood, we note that this independent value of k_{rw} must be larger than any other k_{rw} . This is because the water saturation during the CO_2 is always lower than it was at the start of the flood. (Alternately, one may say that S_g increases steadily from its initial value of zero). Similarly, at the outlet face of the model (where the model equations pertain), the water saturation remains at the original high value and S_g is zero until CO_2 breaks through. At the instant of breakthrough, the flow of CO_2 becomes finite, and S_w at the outlet face drops abruptly while S_g abruptly goes from zero to some finite value.

This discontinuous behavior is illustrated by Fig. 3.1 where Point 1 represents the water saturation and permeability at the model's outlet prior to CO_2 breakthrough, the Point 2 represents the situation the instant after breakthrough. The curve trailing from Point 2 illustrates the decline in water saturation and permeability as the CO_2 flood progresses.

To scale the set of k_{rw} values that are obtained from the model equations, one needs only divide each value by a suitable constant (determined by trial-and-error) such that when the values are plotted,



WATER SATURATION AT OUTLET FACE

Figure 3.1 Water Saturation and Permeability Drop Abruptly when CO₂ Breaks Through the Sand Pack.
 In This Example, Oil Saturation $S_o = 0.20$

the resulting curve (when extrapolated toward higher water saturation) passes through the independently-determined point, as in Fig. 3.1.

An analogous situation exists with the gas relative permeability curves, but in their case the scaling factor is most easily found by measuring the gas permeability at the end of a CO₂ flood (Point 2 in Fig. 3.2). The gas flow rate is determined from the slope of the curve that depicts the injected gas volume (cf. Fig. 3.5), and Darcy's law is used to calculate k_g . The corresponding water saturation is measured by sweeping the residual brine from the sand pack with deionized water and measuring the chloride content by Fajan's method (see Section 3). As before, the k_{rg} values obtained from the model equations are divided by a suitable constant so that the k_{rg} curve passes through the independently-determined point.

3.3 Equation for Water Production Vs. CO₂ Injection

3.3.1 Shape of Water Production Curve

When a CO₂ flood is conducted so that the pressure differential across the porous medium is constant, the curve depicting the cumulative volume of produced liquid, L_p , is S-shaped (see Fig. 3.3). The inflection point corresponds to the breakthrough of CO₂.

Before breakthrough, every volume of gas that is injected (and that does not dissolve in the liquids within the pores) produces an equal volume of water. As the gas saturation and mobility increase, the gas injection rate increases. As a result, the water production rate increases and the curve for L_p is concave upward.

In contrast, after CO₂ breaks through, the water permeability decreases rapidly as the water saturation drops, so the rate of water production declines, and the curve for L_p is concave downward.

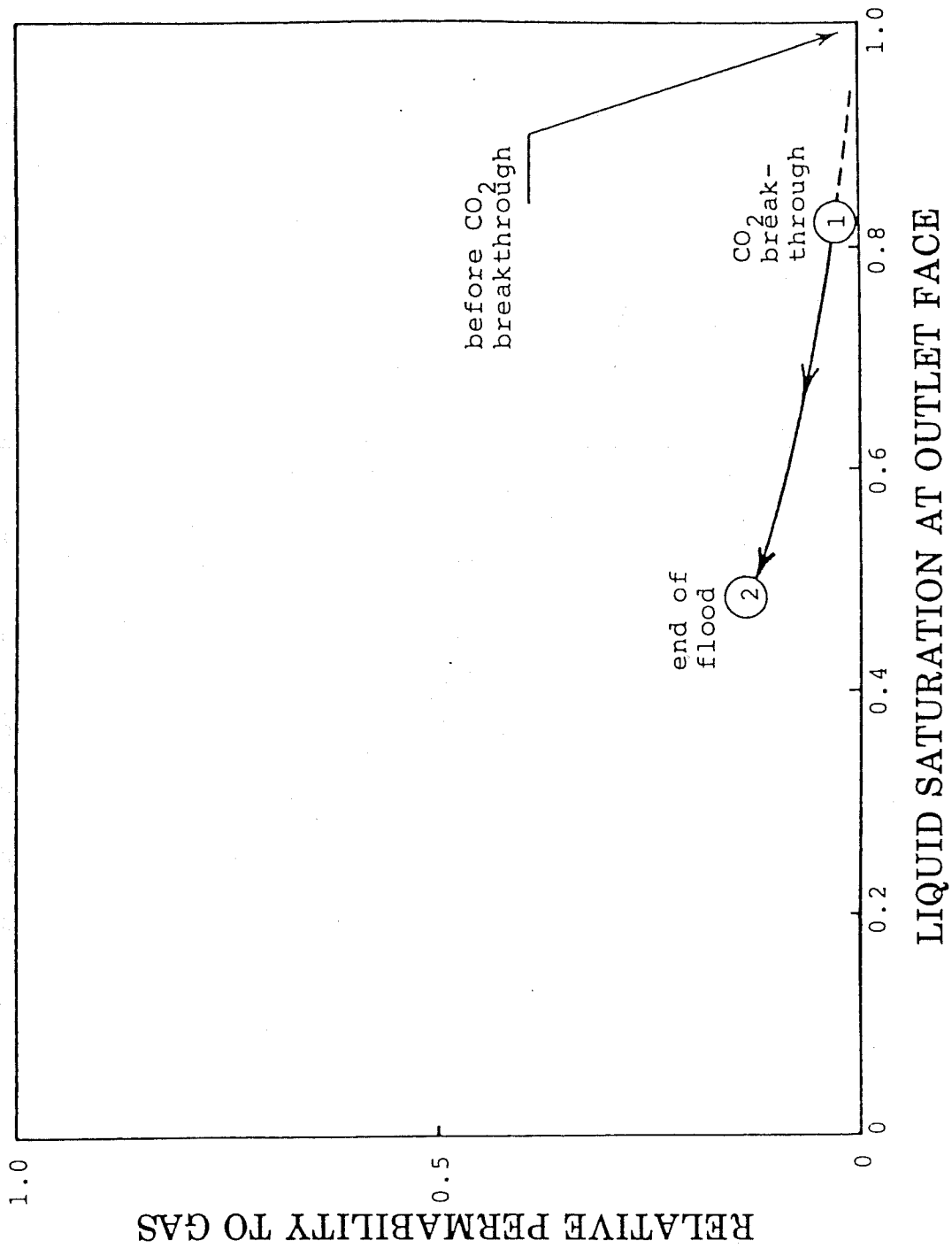


Figure 3.2 Gas Permeability at End of Flood Permits Scaling of k_{rg} Curve

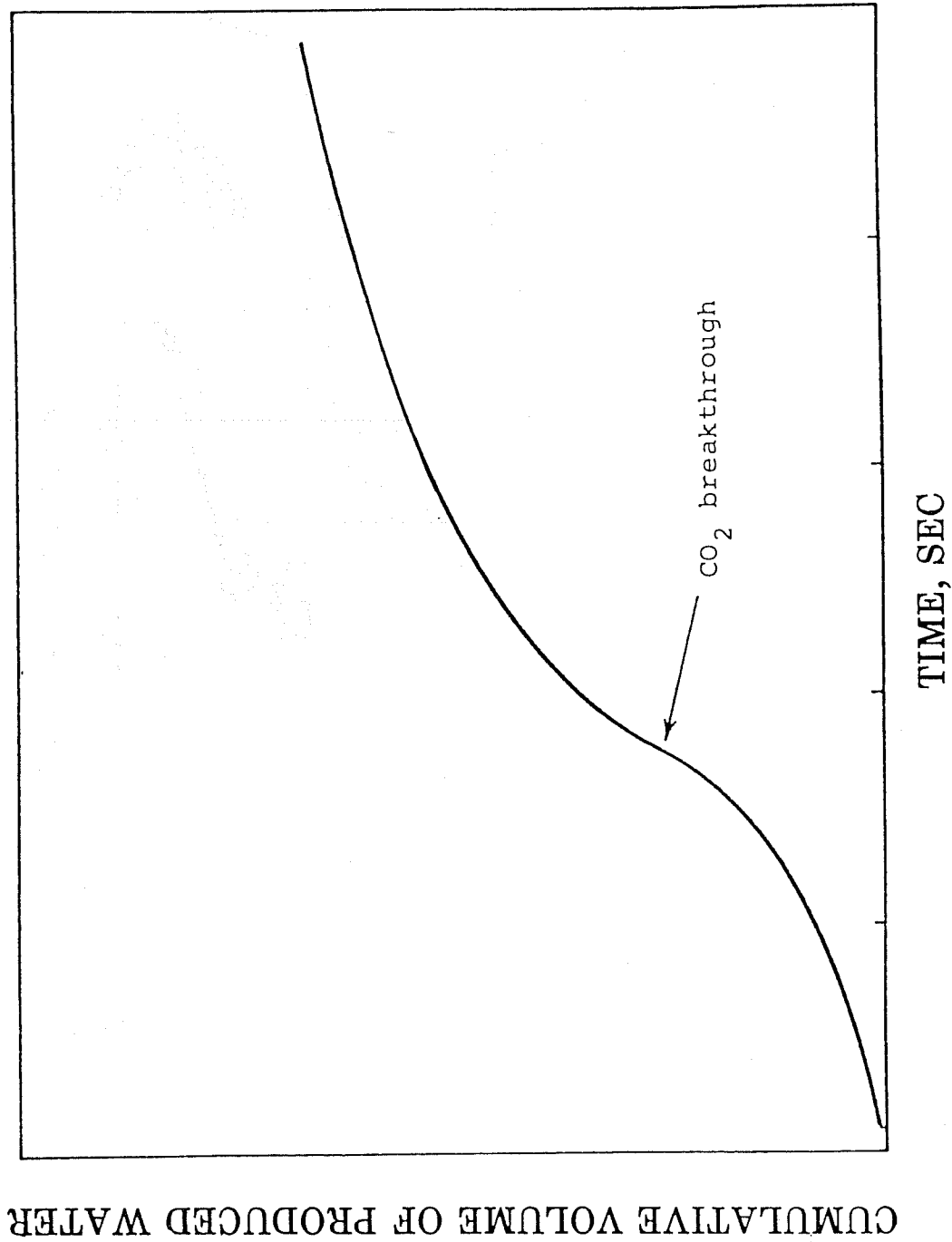


Figure 3.3 Water Production Rate Decreases After CO₂ Breaks Through the Sand Pack

3.3.2 Curve Modeled After CO₂ Breakthrough

Prior to CO₂ breakthrough, the fractional flow of water at the outlet face is constant at 1.0, and $k_g = 0$. Not until breakthrough do S_w , k_w and k_g change at the outlet, so there is no useful information in the L_p curve before that point.* Consequently, the only portion of the curve to which an equation must be fit is that following the inflection point.

3.3.3 Equation to Fit L_p Data

To obtain a suitable expression for L_p , a four-parameter equation having the form of Eq. 3.3.1 was fit to the experimental data. The

$$L_p = (d + at^2)/(1 + ce^{bt}) \quad (3.3.1)$$

parameters (a,b,c and d) were adjusted statistically so as to minimize the sum of squared deviations between the equation and the data. A VAX 780-11 computer performed the calculations using a software subroutine FITFUNCTION in the operating language RS/1 [94].

Equation 3.3.1 was superior to other forms that were tried (see Eqs. 3.3.2 - 3.3.6), because it provided the best least-squares fit, and its first and second derivatives retained the four parameters. Typical agreement between the equation and the raw data is shown in Figure 3.4.

3.3.4 Other Forms Considered

Five other equations were tested for their usefulness in fitting the experimental data. Not only was closeness of fit important, but the

*This is not strictly true because the initial liquid production rate may be used to estimate the initial gas injection rate, g_o . Moreover, the inflection point is often used to determine the time at which breakthrough occurred.

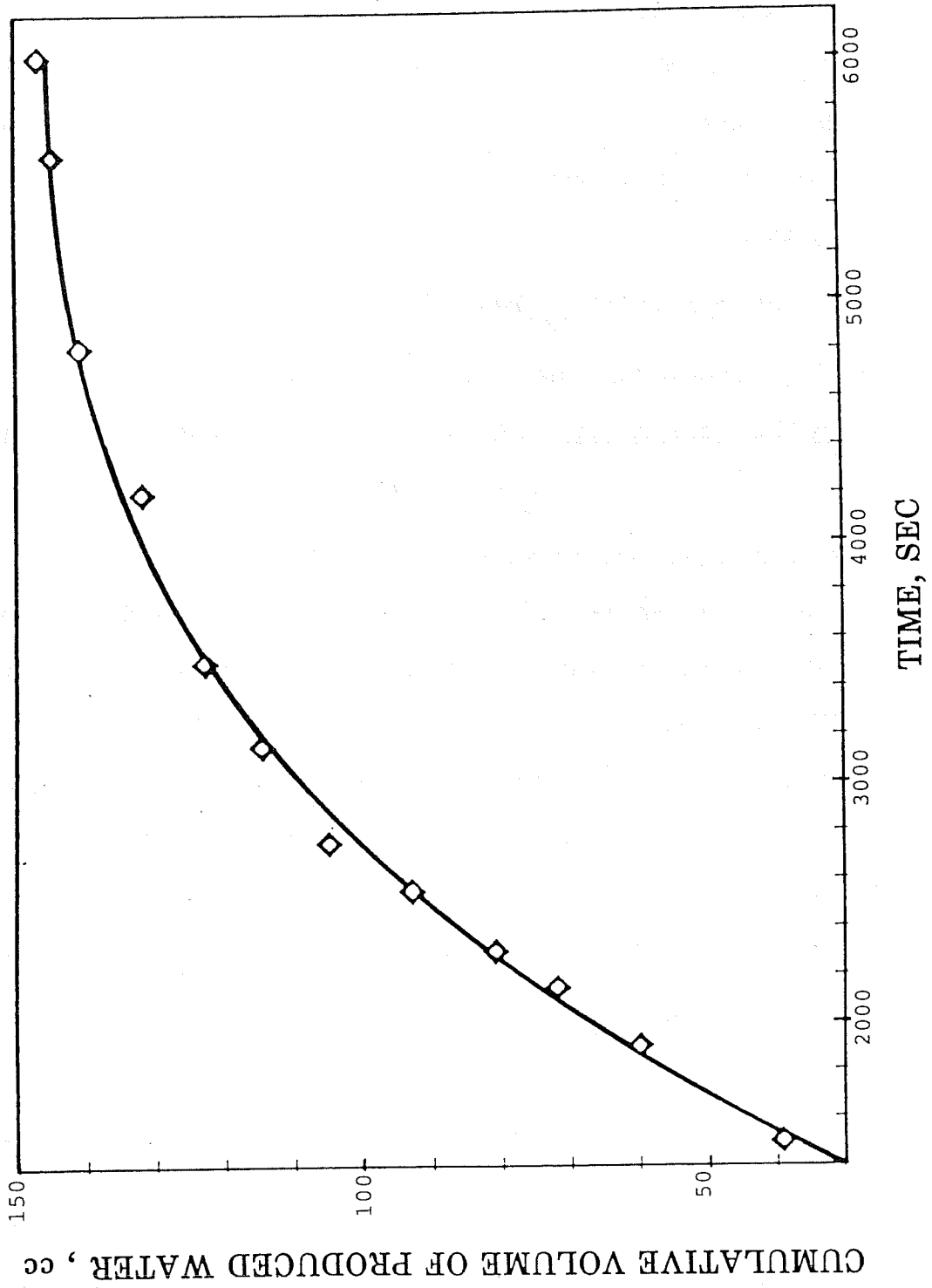


Figure 3.4 Eq. 3.3.1 Used to Smooth Water Production Data Following CO₂ Breakthrough

nature of the equations' first and second derivatives had to be considered. As in the case of Eq. 3.3.1, only data obtained after CO₂ breakthrough were employed.

- (a) Quadratic equations, such as Eq. 2.4.2, were inferior to Equation 3.3.1,

$$L_p = at^2 + bt + c \quad (3.3.2)$$

because the second derivative is a constant.

- (b) Cubics, such as Eq. 3.3.3, and higher polynomials generally have

$$L_p = at^3 + bt^2 + ct + d \quad (3.3.3)$$

inflection points. This implies the second derivative must be positive over some time interval(s). This behavior is physically unrealistic, because, in the present experiments, the water production rate decreased continuously as the gas saturation increased. This, in turn, meant the second derivative had to be less than zero for all times following CO₂ breakthrough, i.e., positive second derivatives could not occur.

- (c) An exponential equation with linear terms, Eq. 3.3.4, provided a

$$L_p = at + ce^{bt} + d \quad (3.3.4)$$

satisfactory fit because it has four parameters. However, its second derivatives has only two parameters (compared with four for Eq. 3.3.1), so it did not describe this higher-order behavior as accurately.

- (d) Exponential with quadratic terms, Eq. 3.3.5, has five adjustable

$$L_p = at^2 + bt + ce^{dt} + f \quad (3.3.5)$$

parameters and retains three parameters when differentiated twice. However, the statistical significance of the linear term (bt) was shown to be zero (i.e., it contributed so little to the goodness-of-fit as to be negligible). Moreover, the FITFUNCTION program frequently could not converge, presumably because of difficulty with the exponential term.

- (e) Mixed exponential, Eq. 3.3.6, had none of the above problems, and

$$L_p = at^2 + cte^{bt} + d \quad (3.3.6)$$

it fit the data nearly as well as Eq. 3.3.1, judging from the sum-of-squared-deviations. However, its fit was notably inferior to that of Eq. 3.3.1 in the vicinity of CO_2 breakthrough. This is the most important portion of the experimental data, because water saturation and flow rate are greater at breakthrough than at any subsequent time, and these properties are changing more rapidly at this instant than at any other. Thus, small errors in fitting the data in this region result in the largest errors in the rates of water production and gas injection. Finally, the relative rates of water production and gas injection determine the fractional flow of water (f_w in Eq. 3.2.1) and, hence, determine k_{rw} .

3.4 Equation for Cumulative Volume of Injected CO₂

3.4.1 Four-Parameter Equation

The equation used for smoothing the water production data also proved to be the best for the injected gas volumes, G_i , i.e.,

$$G_i = (d + at^2)/(1 + ce^{bt}) \quad (3.4.1)$$

As before, the values of the parameters were determined by the nonlinear regression program FITFUNCTION of the RS/1 operating language. Typical agreement between the equation and the raw data is depicted in Fig. 3.5. As it was for the equation used to describe liquid production, the pertinent domain is from the time of CO₂ breakthrough to the end of the experiment.

3.4.2 Need to Correct the Injected Gas Volumes

Before Eq. 3.4.1 can be fit to the experimental data the cumulative injected volume must be reduced by the volume of CO₂ that dissolved in the liquids inside the model. As mentioned earlier, the two-phase flow equations (Eqs. 3.2.1-3.2.6) assume the total volume of produced fluid equals the volume of fluid injected. This works well for an insoluble gas, but not for CO₂. Failure to make this correction causes the fractional flow of water, f_w , to be underestimated, because dG_i/dt in Eq. 3.2.1 is too large. This, in turn would cause k_{rw} to be underestimated by Eq. 3.2.2.

Another reason the cumulative gas volume must be corrected is this: The equation used to calculate the water saturation at the outlet face of the model includes a term containing the cumulative volume of injected gas. Thus, if dissolved gas is ignored, the gas saturation is grossly overestimated.

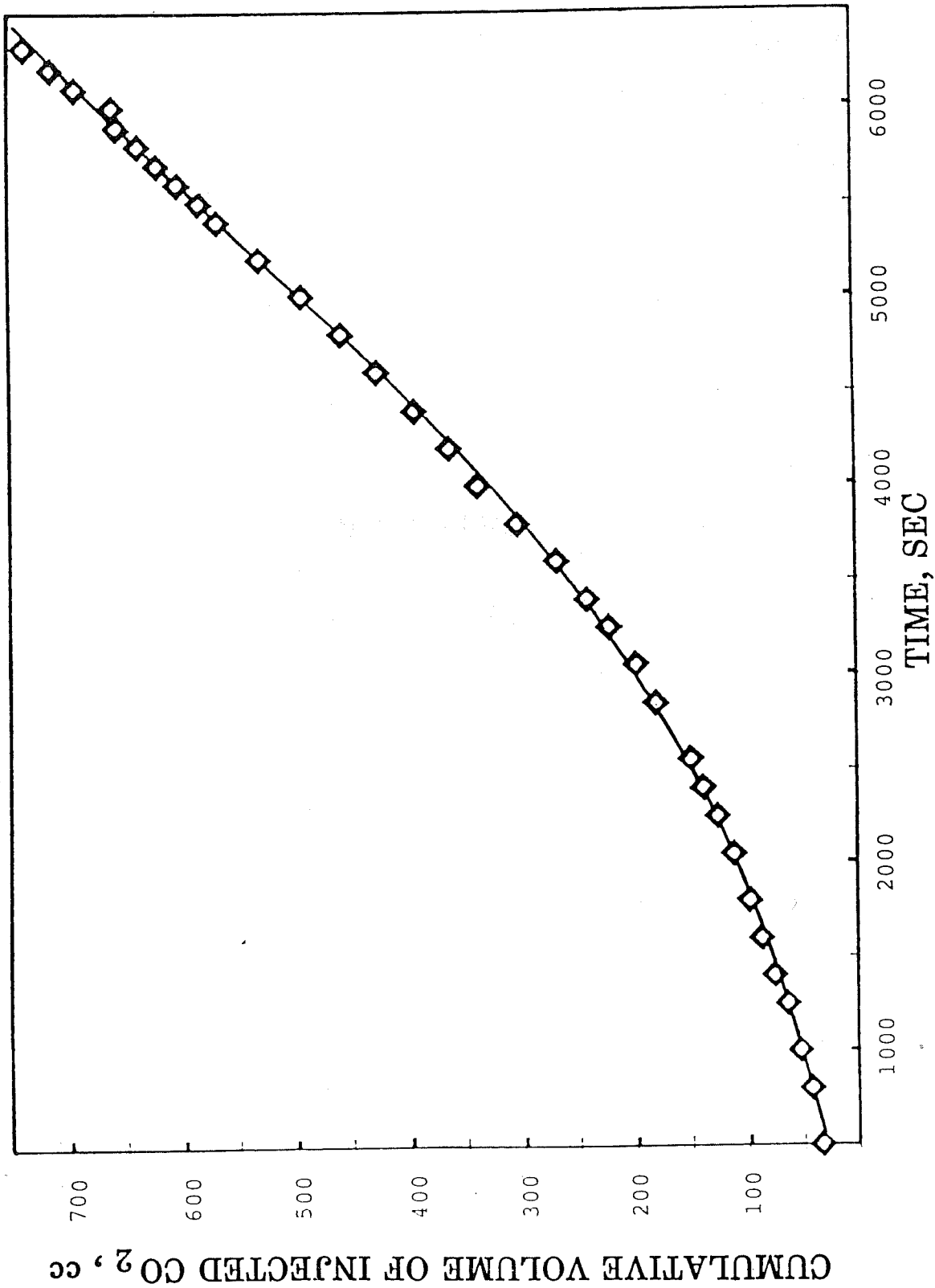


Figure 3.5 Eq. 3.4.1 Used to Smooth Gas Injection Data

3.4.3 Initial Attempts to Correct for or Avoid CO₂ Dissolution Problem

In principle, the volume of produced gas could be measured directly, and, in fact, that was done during the present experiments. However, some produced gas was invariably lost to the atmosphere when produced liquid was drained from the accumulator (see Fig. 3.8) making the cumulative volume uncertain.

One way to minimize the volume of CO₂ that dissolved during the experiments was to saturate the fluids in the model at the planned operating pressure (1100 psig) before starting the experiment. However, the rate of CO₂ dissolution was slow enough under these conditions that even after one hour, the model was not completely saturated with CO₂. The slow rate was largely due to the model being completely saturated with oil and water requiring the CO₂ to diffuse through liquids in order to completely saturate the fluids.

3.5 CO₂ Solubility Corrections

3.5.1 Comparison Between Injected Gas and Produced Water

As depicted in Fig. 3.6, the volume of CO₂ that is injected prior to CO₂ breakthrough is considerably greater than the volume of produced water. If all the injected CO₂ were to dissolve in the oil and water within the model, no water would be produced. The volume of produced water, then, is a measure of the CO₂ that failed to dissolve, and the difference between the volume injected and the volume produced is the volume of CO₂ that dissolves.

In the present experiments, the volume of CO₂ that dissolved before it broke through was typically 50 to 70 cc. For each experiment,

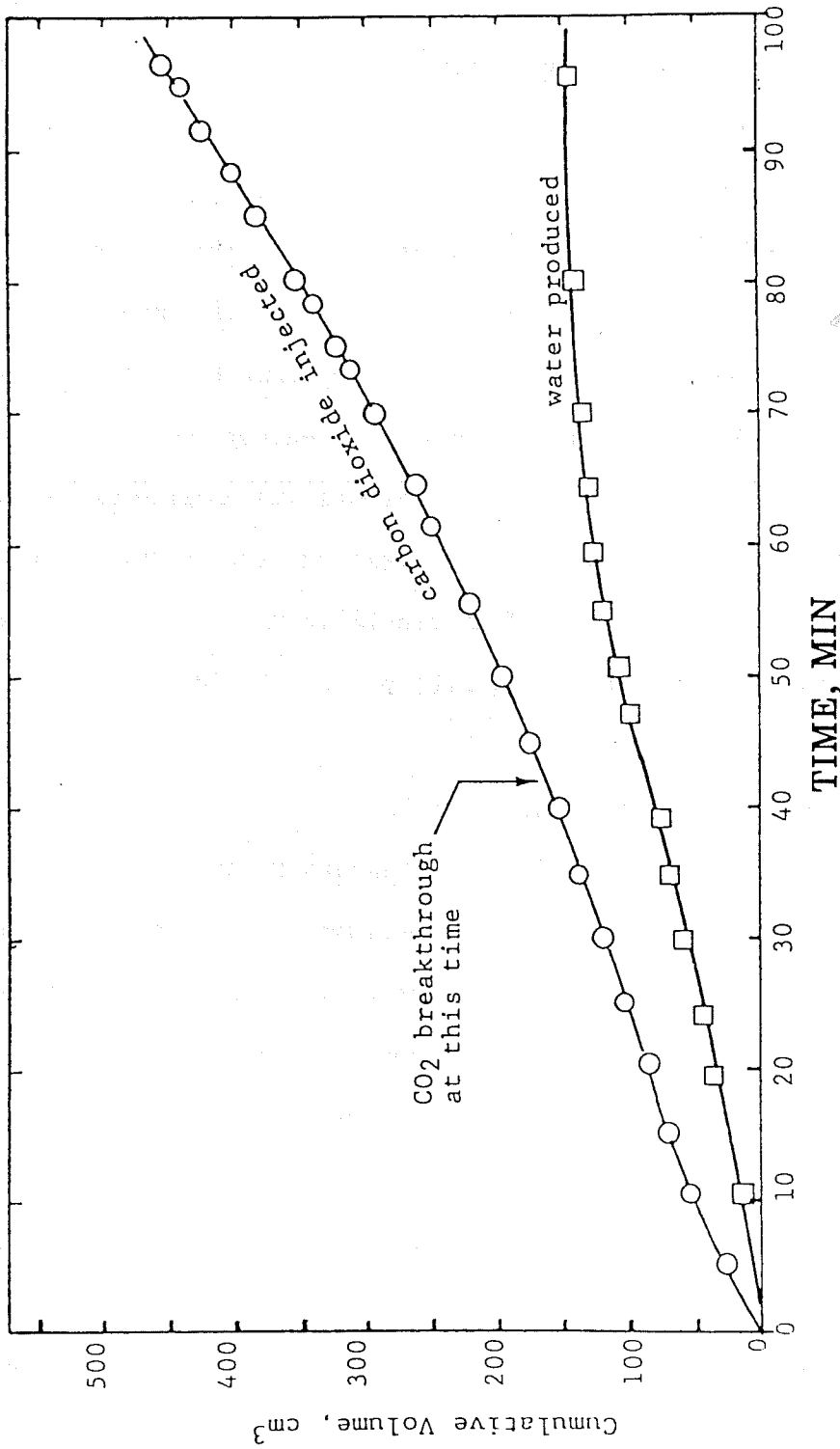


Figure 3.6 Volume of CO₂ Injected Exceeds Water Production Before Gas Breakthrough

the dissolved volume was subtracted from the measured injected volume to provide corrected values for G_i to be used in Eqs. 3.2.1-3.2.4.

3.5.2 Further Corrections to G_i

After CO_2 breaks through, some of the injected gas continues to dissolve in the liquids, of course. Although the rate of dissolution is not accurately known, experiments showed that, at breakthrough, the rate was less than 5% as great as the rate of CO_2 injection, and this percentage rapidly grew less as the experiment proceeded.

The discrepancy due to continued dissolution of CO_2 in the oil and water present in the model was accounted for by observing that, at the instant at CO_2 breakthrough, the rate of liquid production equals the rate of injection of the insoluble portion of CO_2 . (In the graphical terms of Fig. 3.7, the curve for the volume of insoluble CO_2 , G_i , must be tangent to the curve for liquid production, L_p , at the inflection point of the latter). To ensure this agreement, the measured volumes of injected gas in the period immediately following breakthrough were reduced further to make the rates equal at breakthrough. (Usually this amounted to 10 cc or less and could be estimated visually from the graph). The data for G_i in this region were smoothed to remove any discontinuity in the curve or its slope.

3.6 Apparatus

3.6.1 Reservoir Condition Model

An unconsolidated sand pack simulating an oil reservoir was used for the CO_2 permeability study at reservoir conditions. As depicted in Figure 3.8, the pack was contained within a 1.5-in. diameter seamless Sch. 40 stainless steel (316L) pipe, 24-in. long (62 cm). Welded to the ends of the pipe were two 316L stainless steel 900-lb, slip-on

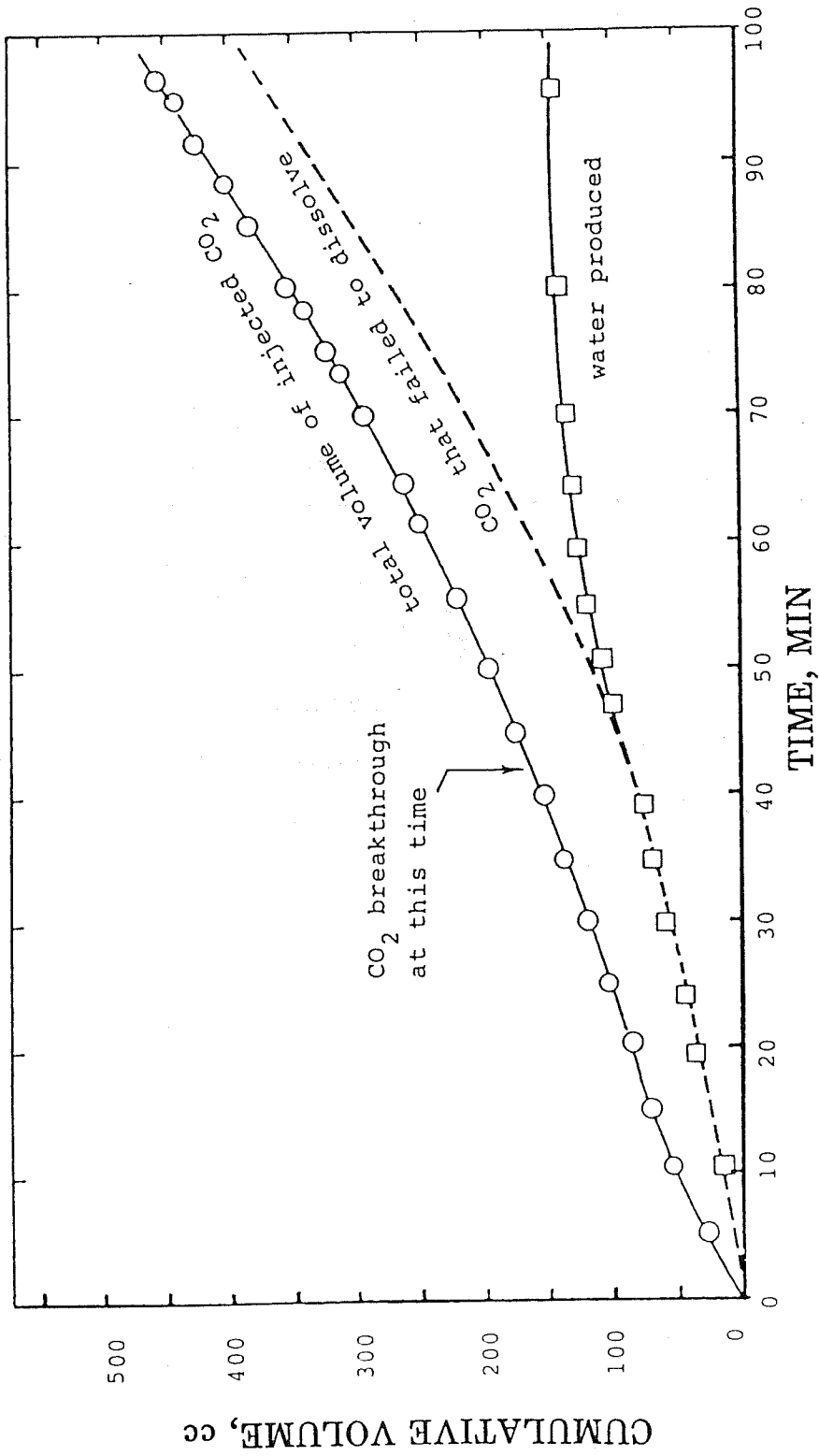


Figure 3.7 Undissolved Fraction of Injected CO₂ (dashed line)
 Provides Values for G_i to be Used in Eqs. 3.2.1-4

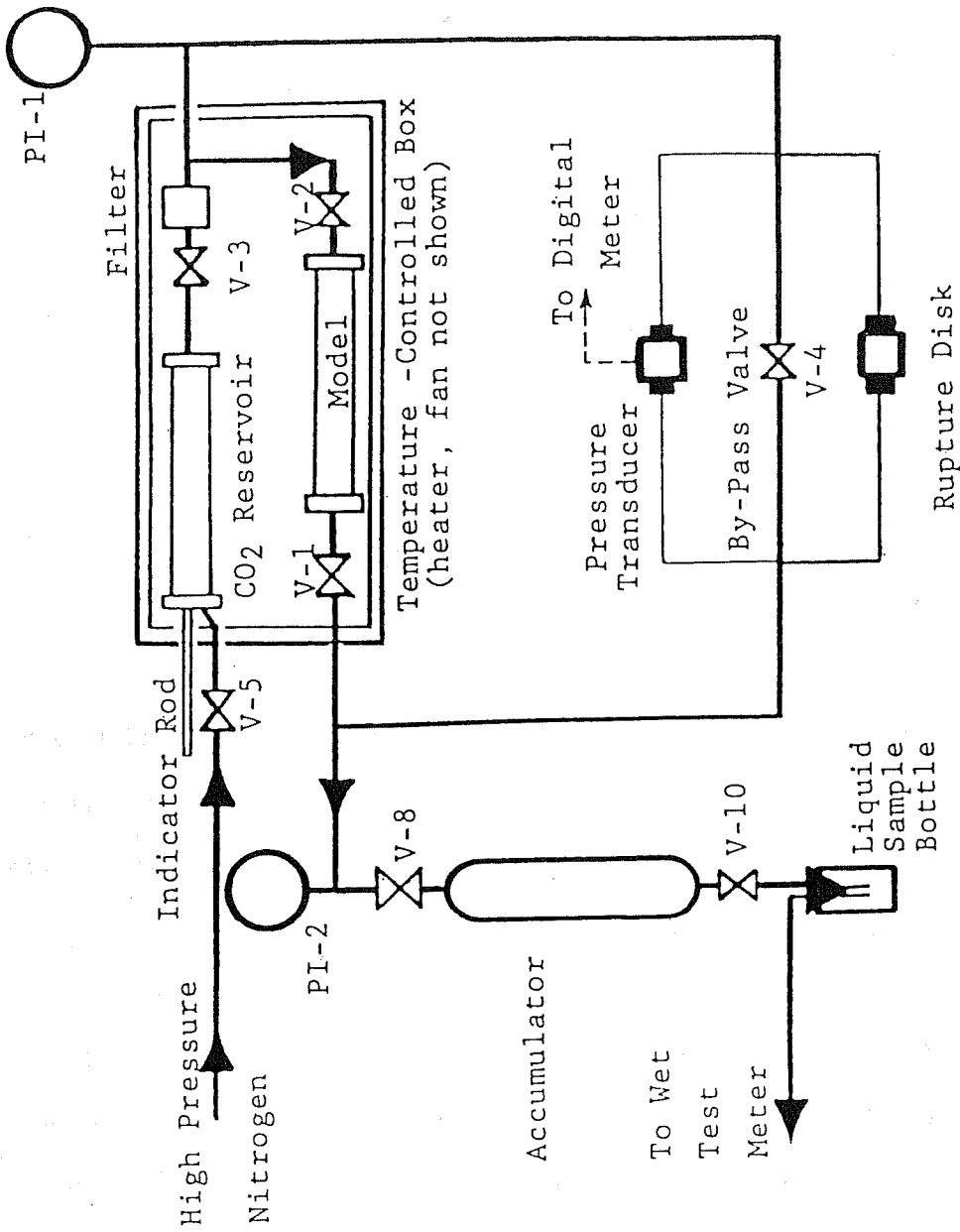


Figure 3.8 Schematic Diagram of Apparatus Used for CO₂ Mobility Study

flanges. The ends of the pipe were closed with blind flanges to secure spiral-wound asbestos-filled gaskets (Flexitallic, CG 9-1500 APT 601). Inlet and outlet ports were drilled and tapped in the center of the blind flanges for connection to 1/4-in. stainless steel valves, tubing, and other required fittings. Attached to the inside surface of each end flange was a 1.5-in. sintered stainless steel disk, 0.125-in. thick, with a maximum pore size of 100 microns. The physical parameters of the linear flow model are listed in Table 3.1.

TABLE 3.1

PARAMETERS OF RESERVOIR MODEL

| | |
|-------------------------|-----------------------|
| Length of Porous Medium | 59.6 cm |
| Porosity | 40.3% |
| Cross-sectional area | 12.73 cm ² |
| Pore Volume | 318 cc |
| Permeability to brine | 600 md |

The model was mounted horizontally in an insulated box where the temperature could be maintained at any desired reservoir temperature by heating elements (light bulbs) controlled by a thermostat (Johnson Controls, model A19AAF-12). Internal air circulation was maintained by a small blower (Dayton, model 1C939).

Pressure at the inlet of the model was measured by a Bourdon gage (Heise, model CM-29064) accurate to ± 2 psig. Pressure drop across the model was measured by a transducer (Validyne, model CD-223) that was protected from overpressure by a rupture disc in a parallel line.

3.6.2 Carbon Dioxide

An 800 cc stainless steel (304) rodded-piston transfer cylinder (Welker Engineering, sample cylinder style CP-2) served as the reservoir for carbon dioxide. Initially filled with liquid CO₂ from an inverted commercial cylinder, the reservoir was placed beside the model in the temperature-controlled box and brought to the same temperature.

To force carbon dioxide from the transfer cylinder, high-pressure nitrogen was admitted to one side of the piston (see Fig. 3.8). As CO₂ flowed from the other end of the cylinder, the position of the moving piston was indicated by the length of the attached calibration rod that protruded from the end of the cylinder.

3.6.3 Effluent Collection

As brine and carbon dioxide flowed from the model, they were separated in the accumulator. That vessel was wrapped with heating tape which kept it at 127°F to prevent condensation of liquid carbon dioxide.

Gas was taken through valve, V-7, to a "Wet-Test" meter (GCA Precision Scientific). The valve (Whitey, SS-14DKM4-S4) had been modified to serve as a back-pressure regulator. (The modification is described below).

Liquid was withdrawn from the bottom of the accumulator through valve V-10 which, like V-7, was also a pressure regulator.

Besides permitting gas and liquid to be separated, the accumulator served to dampen fluctuations in the downstream pressure. Small volumes of fluid could be withdrawn without appreciably changing the pressure-drop across the model. If gas was inadvertently withdrawn too rapidly, the system pressure would drop only slightly.

3.6.4 Modification of Valves

The valves, V-7 and V-10, had unthreaded sliding stems that facilitated their adaptation to act as pressure regulators. Also, the stems were smaller in diameter than the seats, a condition necessary for proper control. To modify the valves, the internal stem linkages were removed and replaced with coil springs which held the valves closed. After modification, each valve was installed in the system so that the upstream pressure was beneath the seat. When the pressure rose, it provided a force to oppose the spring force, and the valve opened to allow flow and cause a subsequent decrease in pressure. The handles of the valves were connected by threads to the bonnets and could be adjusted. Because the springs pressed against the inside of the handles, this adjustment changed the pressure at which the valve would open.

3.7 Procedure

3.7.1 Preparation of Model

One flange was bolted in place and the pipe was mounted vertically with the open end up. A 1-cm layer of glass beads (Potter Industries, type P, -70 +150 Tyler mesh) was carefully poured in using a funnel equipped with a long stem. On top of this was poured a 0.5-cm layer of -150 +200 mesh glass beads, then the pipe was filled with the silica flour. The silica flour (Midland Sand Co.) was nominally 20-micron in diameter and had been elutriated with water to remove most particles smaller than 10 microns.

To the upper flange was bolted a 12-in. length of pipe, and additional silica flour was poured into it while the model was struck firmly and repeatedly with a wooden mallet.

Air trapped in the model was purged with CO₂ at low pressure, then the CO₂ was removed by flowing pH 10.6 brine (3% NaCl by wt., 100 ppm Ca⁺⁺) through the sand while the outlet was connected to an aspirator. When the model was saturated with water, the upper section of pipe was removed, layers of glass beads were placed on top of the wet silica flour, another perforated stainless plate was placed on top of the beads, and the second flange was bolted in place.

The model was then mounted horizontally and flooded with deionized water to completely remove the brine; then it was flooded with a crude oil at 124°F to irreducible water saturation. The brine that had been produced during the waterflood was analyzed for chloride ion, by titration with silver nitrate solution (Fajan's method) to determine the porosity and pore volume of the sand pack.

3.7.2 Permeability to Brine

The model was flooded with brine (3% wt. NaCl) again until no more oil was produced. The brine's flow rate under constant pressure gradient (10 psid across the model) was measured and the brine permeability calculated using Darcy's law. If surfactant was also used, it was dissolved in the brine before the brine was injected. The usual concentration of surfactant was 0.5% wt.

3.7.3 Oil Saturation

Flooding the model again with deionized water to remove the brine and analysis of the effluent for chloride (Fajan's method) permitted the water saturation to be calculated. The difference between the value and 1.0 was the oil saturation.

3.7.4 Start-up Procedure for CO₂ Injection

First, the deionized water in the model was completely displaced with 3% NaCl (2.5 pore vol.). Then, to minimize gravity segregation within the sand pack, the model was revolved 180° about its longitudinal axis every 30 minutes for several hours before the experiment was begun. During this time, the temperature of the box containing the model and the CO₂ reservoir was set and allowed to become constant ($\pm 2^{\circ}\text{F}$) for 30 minutes. Finally, the following steps were followed to establish the desired system pressure (see Fig. 3.8):

1. Carbon dioxide was allowed to pass slowly through valve V-3, until the pressure of the system was 1100 psig. Valve V-2 was opened to raise the pressure in the model at the same time. The bypass valve, V-4, remained open to prevent damage to the transducer.
2. If the pressure exceeded 1100 psig, carbon dioxide was bled from the system through valve V-10, with valve, V-8 open.
3. Valve V-5 was opened next and the nitrogen pressure was increased until the piston in the CO₂ reservoir advanced enough to raise the system pressure to 1115 psig. Valve V-5 was left open so the CO₂ pressure would remain constant during the experiment.
4. The bypass valve, V-4, was closed and gas was bled from the accumulator through valve V-10 until the transducer showed that a differential pressure of 10 psid existed across the model.
5. The final step was to open valve V-1 and start the flow of CO₂ through the model.

3.7.5 Operation

Within seconds of opening valve V-1, the inlet pressure (indicated by PI-1) had dropped to 1110 psig, but then it remained constant throughout the flood. The pressure-drop across the model was maintained at 10 psi by manually adjusting valve V-10 and bleeding gas and water from the accumulator. Water was collected in a sample bottle while gas was vented through a Wet-Test meter. Continual adjustment of V-10 was required, because as the water saturation decreased, the flow of gas through the model increased.

3.7.6 Data Collection

The length of the position-indicator rod on the cylinder holding the CO₂ was measured frequently to determine the rate of gas injection.

The volume of gas leaving the model was measured by reading the Wet-Test meter.

The water produced during each time interval was determined by removing the sample bottle and weighing it. Each was replaced promptly with a new, tared bottle.

To determine the water saturation at the end of a CO₂ flood, the model was flooded with 800 cc (2.5 pv) deionized water at 500 psig to remove the remaining brine and CO₂*. The effluent liquid samples were combined with rinsing in a 1-liter volumetric flask. After filling the flask to the mark with deionized water and thoroughly mixing the contents, aliquot were titrated with 0.1 N AgNO₃ to determine chloride

*The procedure was analogous to that used for the CO₂ flood, but the CO₂ reservoir was filled with water. The differential pressure across the model was maintained at 10 psid as before.

by Fajan's method. The total effluent chloride was calculated, and then, knowing the concentration of brine originally in the model, the corresponding volume of brine and its saturation, % pv, were calculated.

3.8 Results

3.8.1 Surfactants Selection

Earlier studies in this laboratory had shown that several surfactants were capable of dramatically reducing gas mobility. When foams made with these compounds were passed through capillary tubes, gas mobility was reduced by a factor of 1000 or more [96]. Similarly, in tests using beds of glass beads, surfactants typically reduced the gas mobility by a factor of 10; the same surfactants reduced the gas mobility by a factor of 100 when nitrogen and brine were passed simultaneously through unconsolidated packs of silica flour [97]. Because the surfactants, Pluradyne SF-27* and Stepanflo-50**, has also been proven effective in tests using the bed of glass beads and has subsequently caused dramatic reductions of CO₂ mobility during miscible displacements of octane from unconsolidated sand packs [98], they were chosen for further testing in immiscible CO₂ floods.

3.8.2 Performance of Surfactants During Immiscible CO₂ Floods

Both Pluradyne SF-27 and Stepanflo-50 reduced the gas permeability measureably but not dramatically. As illustrated by the results depicted by Fig. 3.9, Pluradyne SF-27 reduced the permeability by 10-15%

*A registered trademark of BASF Wyandotte for a blend of ethoxylated alcohols having chain lengths between C₁₁ and C₁₅.

**A registered trademark of Stepan Chemical Company for a sulfated ethoxylated adduct of a linear alcohol.

compared to surfactant-free brine, while Stepanflo-50 reduced the permeability about 50%. In both cases, the surfactant concentration was 0.5% wt. in the brine phase.

Note that in Fig. 3.9, the scales have been expanded in order to emphasize the differences, and the liquid saturation (x-axis) is the sum of the water and oil saturations. The six points shown in Fig. 3.9 were determined experimentally and represent individual, independent measurements of the gas permeability (see Section 3.7.7 for procedure). The curves are provided only to help the reader compare those results. More accurate curves are presented in Section 3.8.5 and the associated experimental values for k_{rg} are tabulated in the Appendix.

It is not apparent why Stepanflo-50 did not have a greater effect upon the gas permeability. In miscible gas displacement experiments (using CO_2 to displace octane from sand packs), it has lowered the gas permeability by about 90 percent. The limited effectiveness of the Pluradyne SF-27 is even more perplexing. CO_2 displacing oil in a five foot long linear columns showed an 88 percent reduction in mobility due to the presence of Pluradyne SF-27. One plausible explanation was that, in the present experiments, the Pluradyne SF-27 had dissolved in the oil phase to such an extent that it was nearly absent from the brine. However, a third experiment with this surfactant disproved this hypothesis (see Section 3.8.4).

A possible conclusion is that the Pluradyne SF-27 requires more flow-length or reservoir volume to reach full effectiveness. The short column length utilized in the permeability tests may not have been sufficient to achieve a critical pressure differential at any specific point in the model.

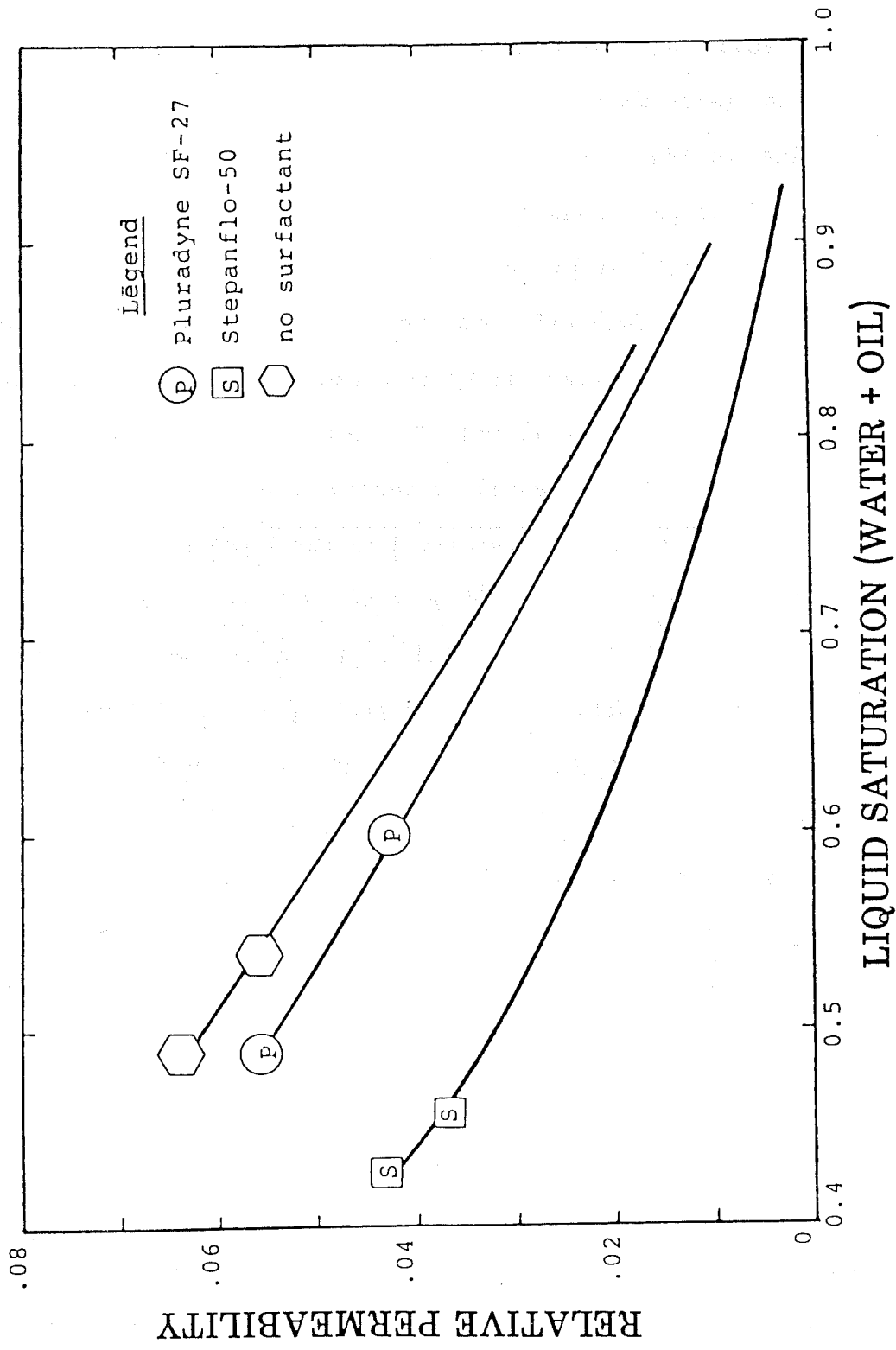


Figure 3.9. Effect of Surfactants on Gas Permeability

3.8.3 Additional Favorable Performance Factors

The superior performance exhibited by the Stepanflo-50 is borne out by the more efficient displacement of water effected by this additive. A higher displacement efficiency is manifested in a higher average gas saturations at gas breakthrough. These data are shown in Table 3.2.

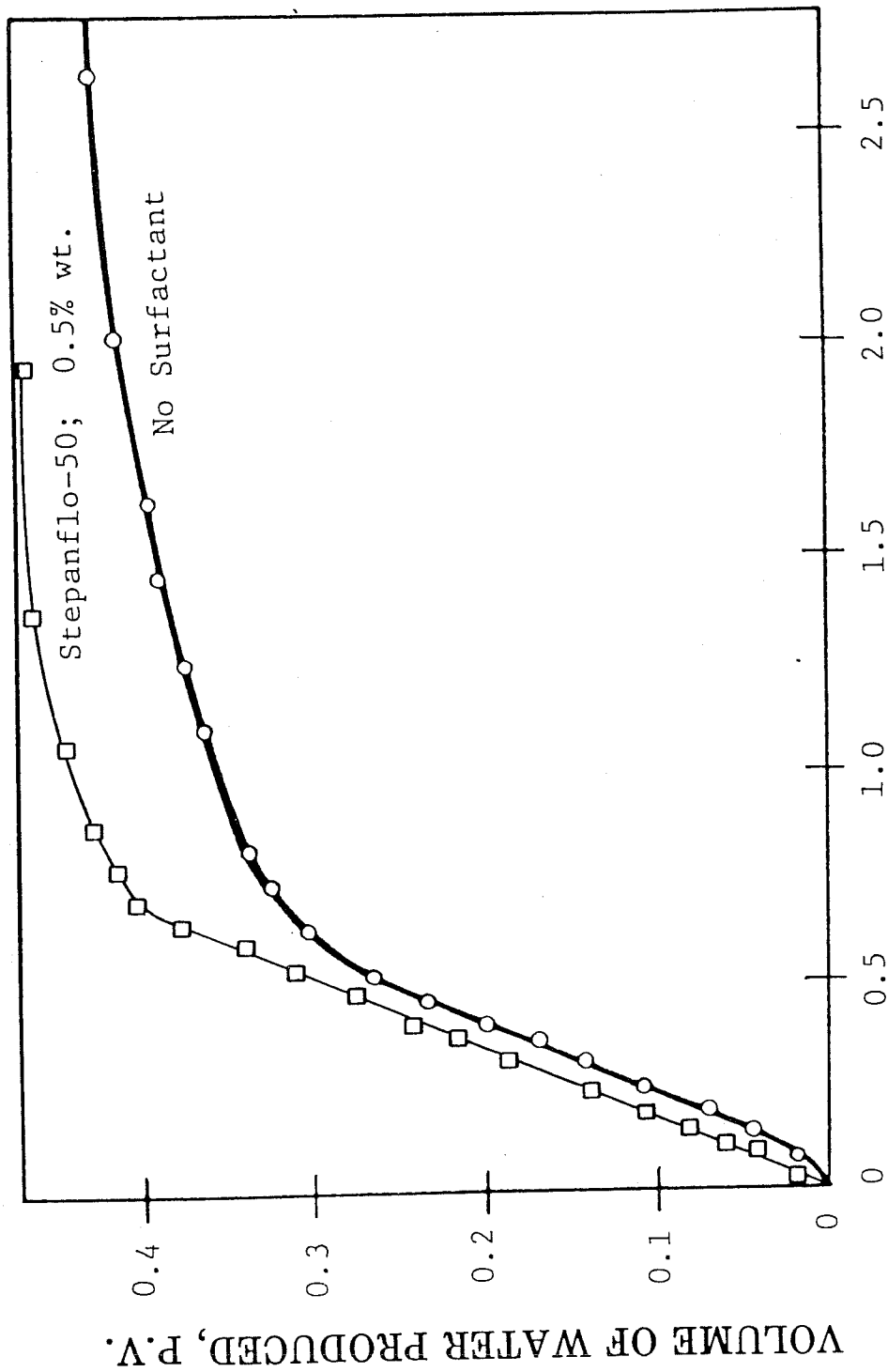
TABLE 3.2

GAS SATURATION AT BREAKTHROUGH
INCREASED BY SURFACTANTS

| Surfactant | Average Gas Saturation at Breakthrough |
|-----------------|---|
| None | 0.267 |
| Pluradyne SF-27 | 0.336 |
| Stepanflo-50 | 0.403 |

A plot of water produced versus pore volumes of CO₂ injected reveals another interesting facet relative to the effect of surfactants on the behavior of carbon dioxide in water as shown in Figures 3.10, and 3.11. Not only is the breakthrough of gas delayed significantly, but also the solubility of gas in the water seems to be measurably reduced. This is evident in Figures 3.10 and 3.11 where a distinct increase in water displaced for any given CO₂ injection is readily apparent in all tests with water containing a surfactant.

It is possible that the decreased water solubility is a transient, non-equilibrium phenomena, discernible only at the short contact times characteristic of laboratory work. On the other hand, if the phenomena



VOLUME OF CO₂ INJECTED, P.V.

Fig. 3.10 Mobility Control with Stepanflo-50
Increases Displacement Efficiency

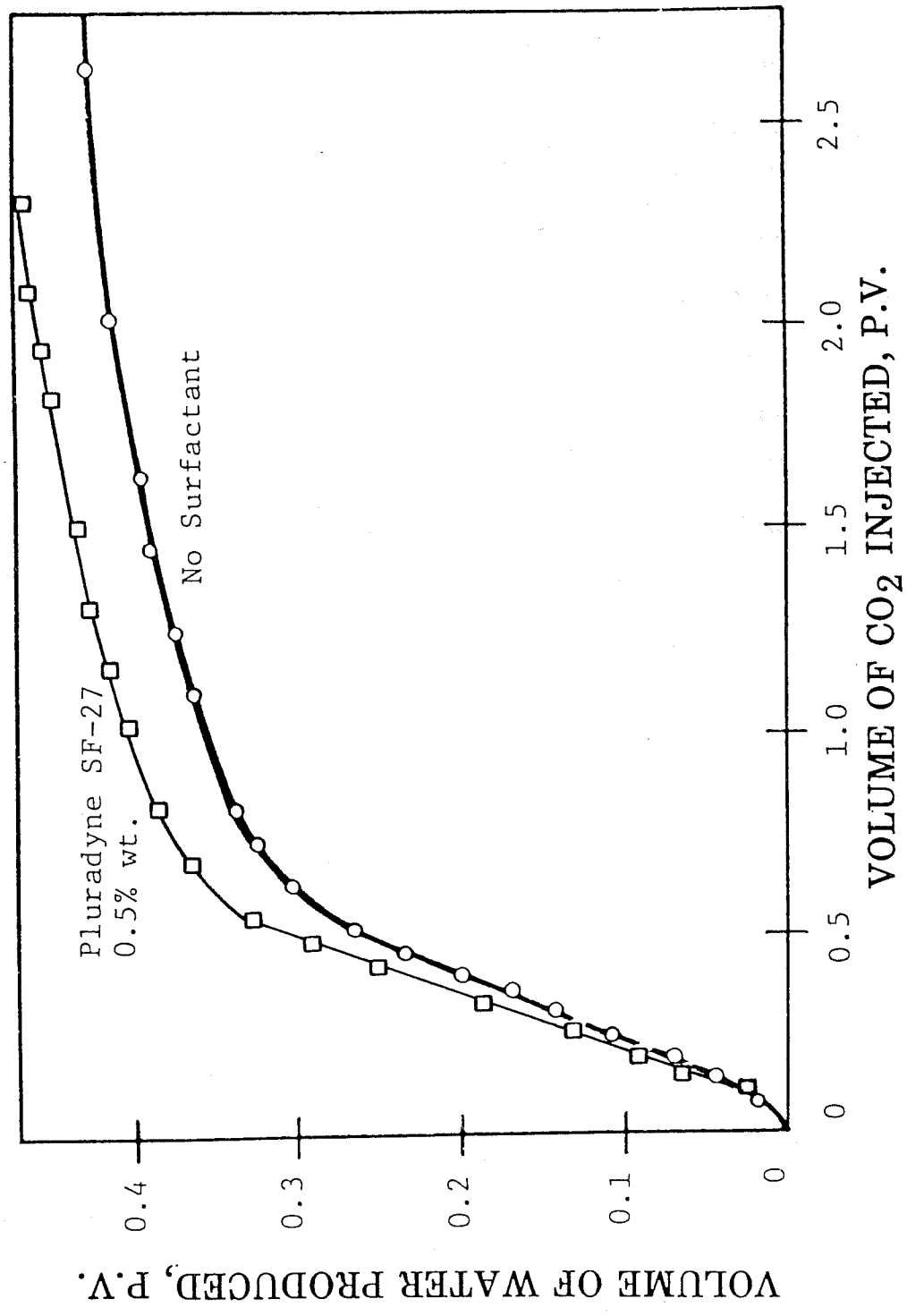


Fig. 3.11 Breakthrough of CO₂ Delayed by Pluradyne SF-27

is truly the result of a decreased carbon dioxide solubility in water, this mechanism would reduce the carbon dioxide lost by CO₂ dissolving in reservoir brine during field flooding operations. The savings on carbon dioxide would partially defray the cost of the mobility control additive, approximately 20 percent.

The apparent decrease in CO₂ solubility in water was consistently observed in all three-phase displacements in which a mobility control additive was present in the water phase. The additives have not been observed to have any effect on the solubility of CO₂ in crude oils or the minimum miscibility pressure.

3.8.4 Interaction of Surfactants With Oil

Only Pluradyne SF-27 appeared to interact with the oil in the model. It emulsified some of the oil as indicated by the muddy appearance of produced brine. Furthermore, in the course of four displacements with CO₂, the oil saturation decreased from 0.31 to 0.16.

In contrast, Stepanflo-50 did not emulsify the oil; the produced brine was clear and colorless, just as it was when no surfactant was present.

Because Pluradyne SF-27 had emulsified the oil it was thought that the surfactant might have also dissolved in the oil phase. Perhaps it had been almost completely extracted from the water by the oil; and thus it had been rendered ineffective in reducing gas permeability. To test this hypothesis, another immiscible displacement was conducted with this surfactant, but its concentration in the brine was doubled (to one percent wt.) compared to the previous experimental runs.

In this test, the surfactant was undoubtedly in sufficient excess, because its presence was evident in the produced brine. When portions of the brine were shaken, a stable foam formed above them. Nevertheless, the reduction in gas permeability was no greater than it had been before, as illustrated by the shaded center point shown on Fig. 3.12 (Fig. 3.12 is Fig. 3.9 with this new datum point added).

3.8.5 Relative Permeability Curves

The permeability of the model to gas and water when no surfactant is present is shown in Figs. 3.13 and 3.14. The solid lines in those figures show the experimentally determined values of k_{rg} and k_{rw} , while the dashed lines show extrapolated values. Circled points indicate independent measurements as described in Section 3.2.3. The experimental values are also presented in Tables A.1 in the Appendix.

Gas and water permeabilities when Pluradyne SF-27 was in the brine are shown in Figs. 3.15 and 3.16. Again, the solid lines show experimental results, dashed lines are extrapolated, and the circles are independent measurements. Numerical values are tabulated in the Appendix, Table A.2.

It is interesting to note that, when comparing Fig. 3.16 with Fig. 3.14, the surfactant appears to have increased the brine permeability by about 50% .

The permeabilities observed when Stepanflo-50 was in the brine are shown in Figs. 3.17 and 3.18, with the dashed and solid portions of the curves having the same significance as before. Numerical values are in Table A.3 in the Appendix. When comparing Fig. 3.18 with Fig.

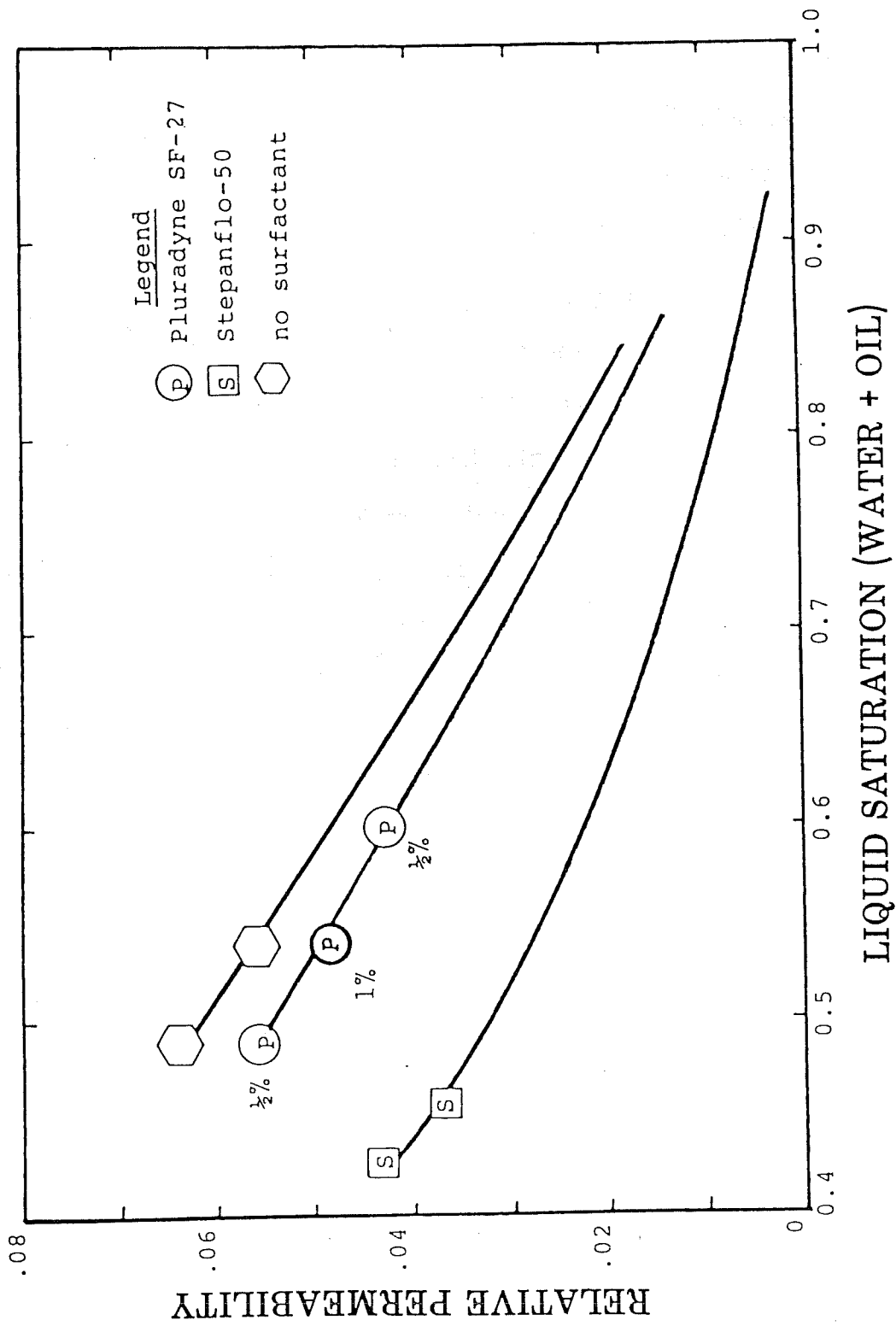


Figure 3.12 Performance of Pluradyne SF-27 Unchanged when Concentration Was Doubled

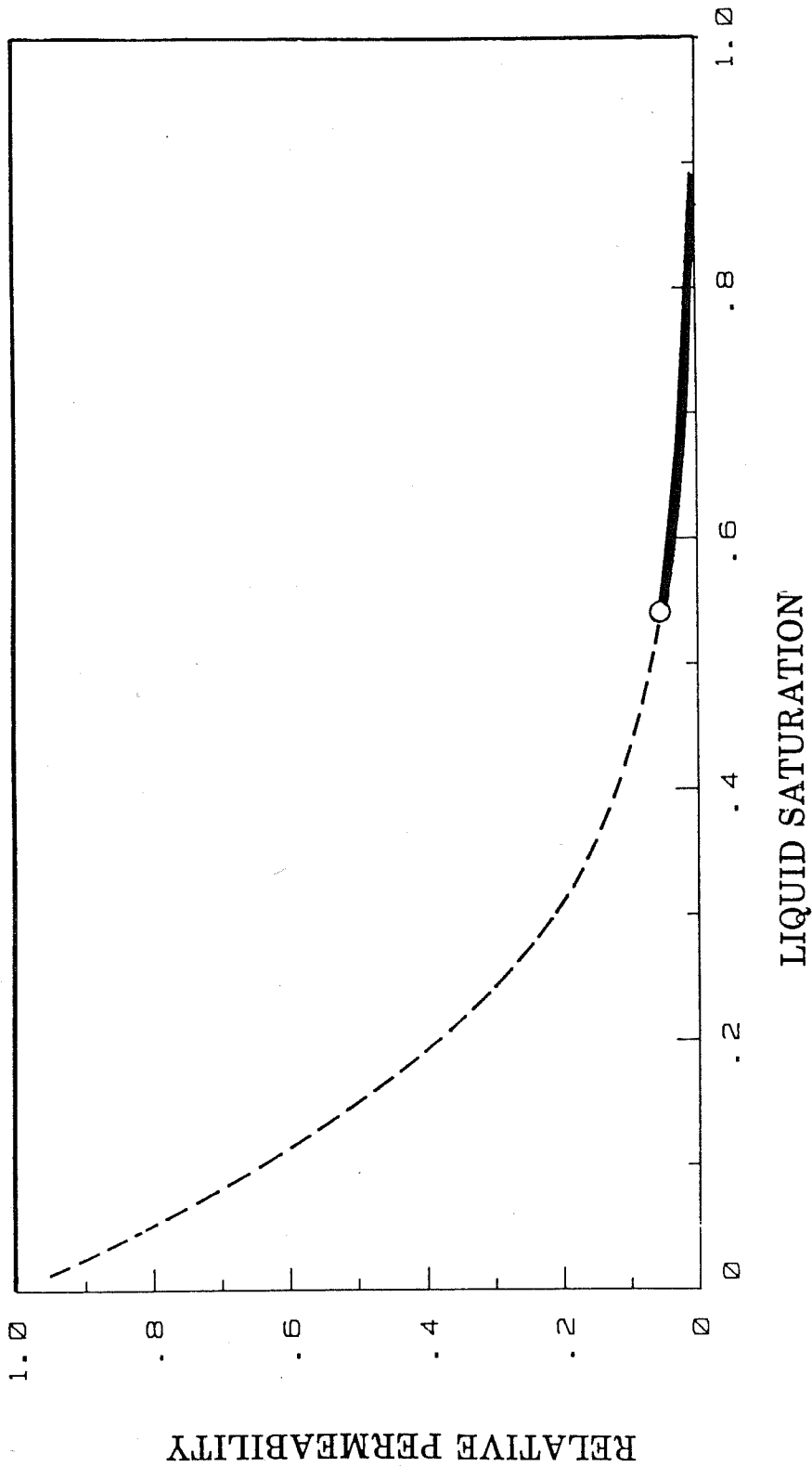


Fig. 3.13 Permeability to Gas in the Absence of Surfactant

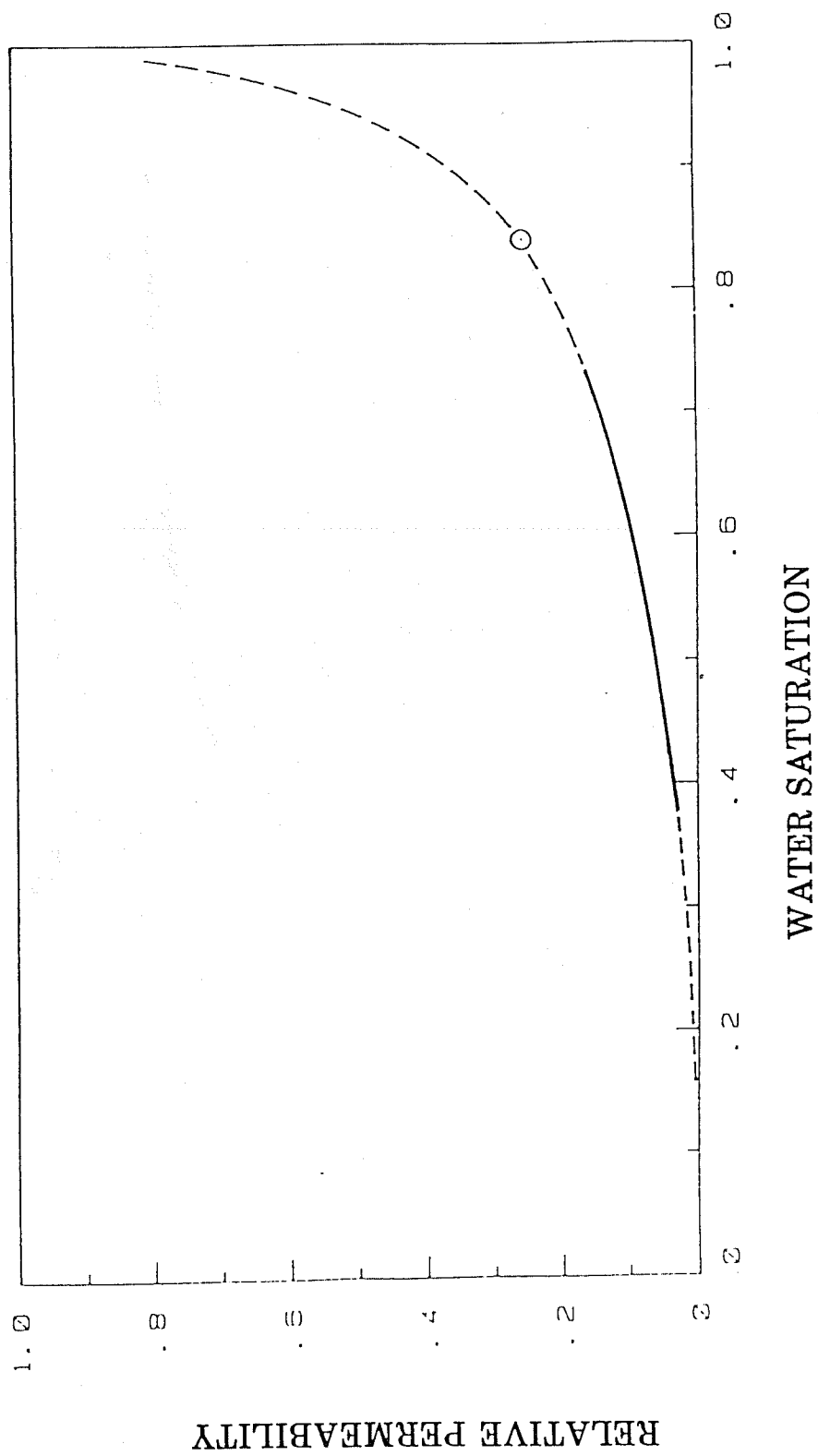
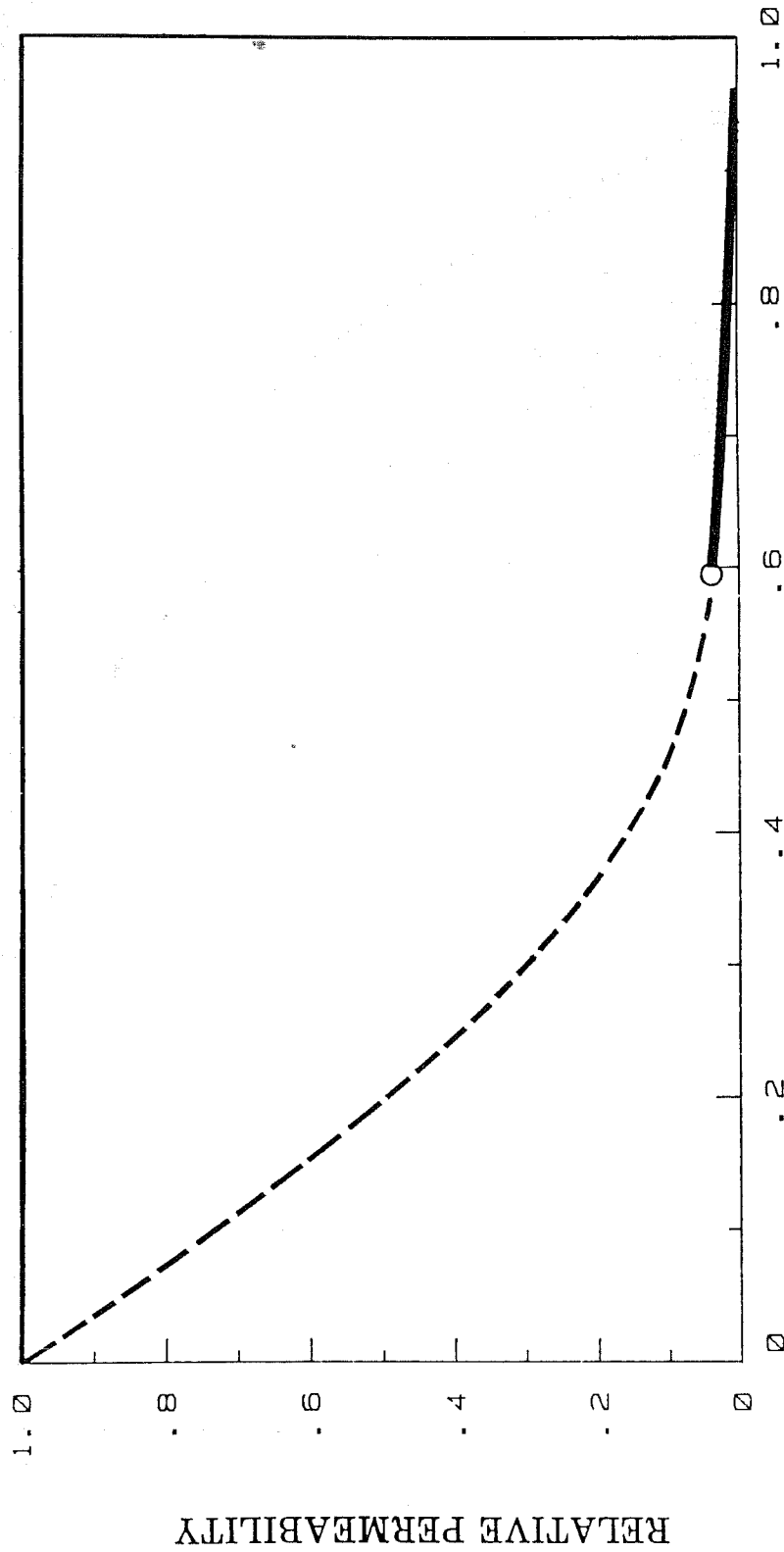
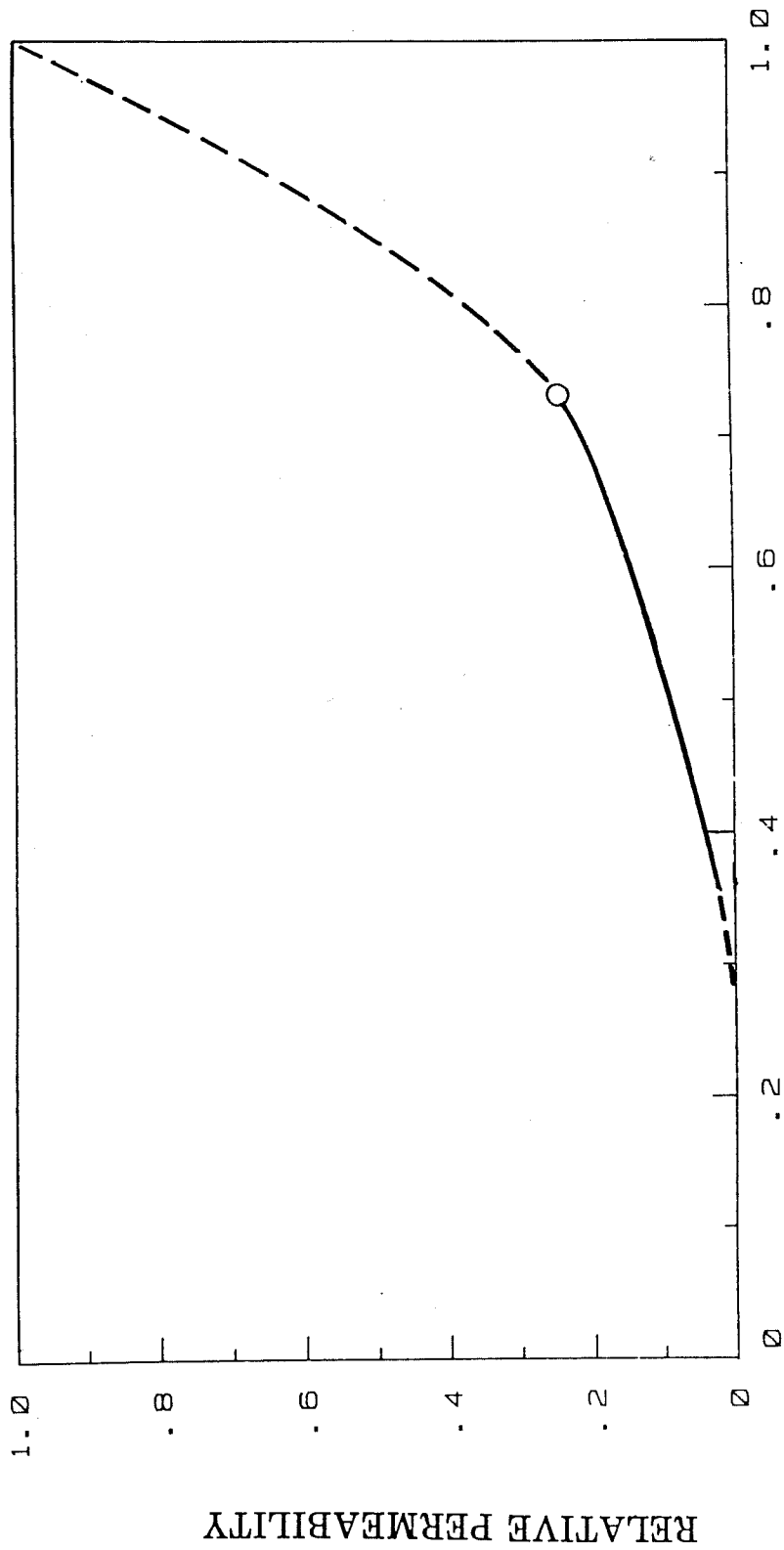


Fig. 3.14 Permeability to Water in Absence of Surfactant



LIQUID SATURATION

Fig. 3.15 Permeability to Gas when Pluradyne SF-27 Present



WATER SATURATION

Fig. 3.16 Permeability to Water when Pluradyne SF-27 Present

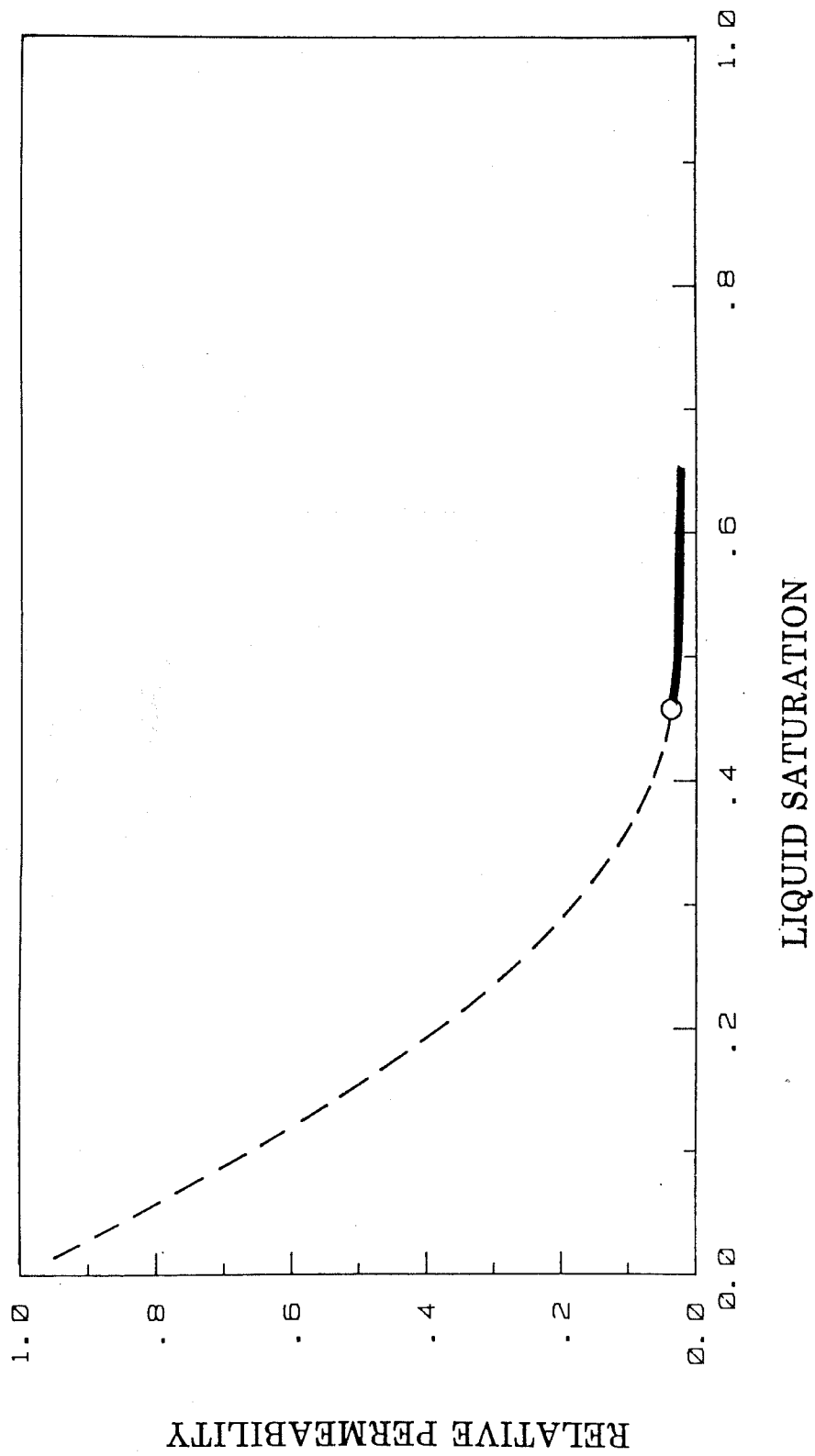


Fig. 3.17 Permeability to Gas when Stepanflo-50 Present

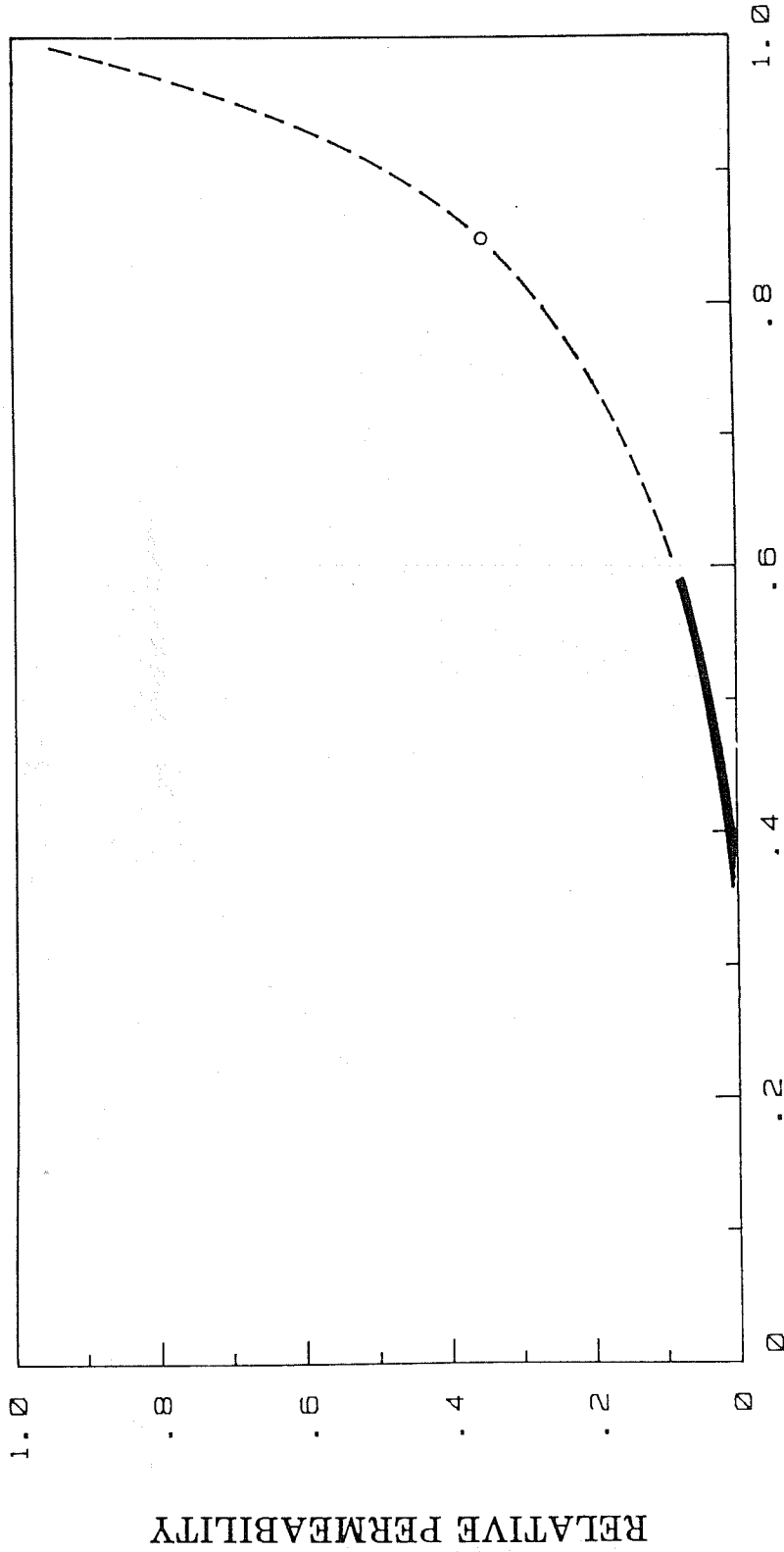


Fig. 3.18 Permeability to Water when Stepanflo-50 Present

3.14 it appears the surfactant lowered the brine permeability about 15 percent compared with the surfactant-free case.

SECTION FOUR

MISCIBLE DISPLACEMENT

4.1 Apparatus

4.1.1 Reservoir Condition Flow Model

Miscible oil displacement experiments were conducted in apparatus consisting of a tubular flow model, filter system, constant temperature box, three pressure gauges, a differential pressure transducer and a transfer cylinder. A schematic diagram of the apparatus is shown in Figure 4.1. The flow model is 54.3 in. (138 cm) long made from 1½ in. NPS, schedule 40, seamless, type 316L stainless-steel pipe. The ends are closed with 900-pound flanges welded to the pipe. The inside diameter of the column is 1.59 in. (4.03 cm) and, the cross-sectional area of the model is 1.976 in.² (12.75 cm²). The flange gaskets are teflon-stainless spiral type gaskets. The detail of the inlet section of the model is shown in Figure 4.2. A sintered stainless-steel disk confines the fine, unconsolidated sand packing. The column is filled with silica sand, elutriated to obtain a size range of 20 µm to 80 µm. Pore volume of the model was determined to be 42.0 in.³ (688 cm³) by fluid displacement tests, and the porosity was calculated to be 39.2 percent. The model is mounted in a constant temperature chamber, in which air is circulated to maintain the temperature of the model.

The fluid entering the column is filtered through two different types of filters in series. The first was a sand filter and second, a millipore-filter.

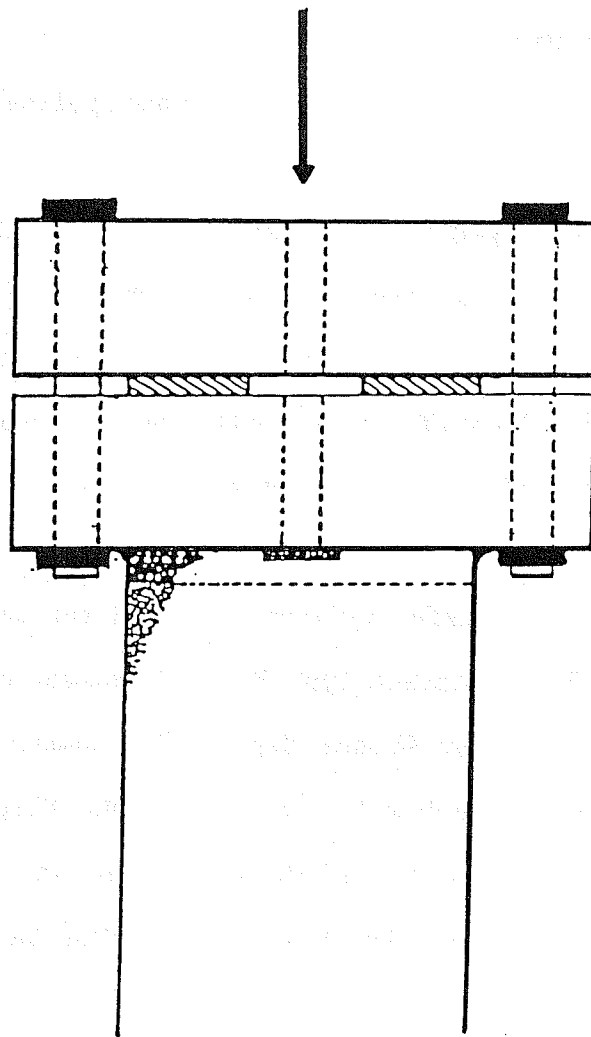


Figure 4.2 Model Entrance Construction

The upstream sand filter is designed to remove any particles or precipitates which possibly exist in the injection fluid. A diagram of the sand filter is shown in Figure 4.3. This filter is filled with + 20 μm silica-flour supported by a sintered-metal disk. To prevent channeling or shifting of the particles, glass wool is placed on top of the silica flour packing.

A 10 μm millipore-filter is for final polishing of the injected fluids.

Three pressure gauges were used to measure the inlet and outlet pressures. One 0-60 psi gauge and one pressure 0-1500 psi gauges were used for inlet pressure, and one 0-1500 psi was for outlet pressure. All were Ashcroft, Maxisafe gauges with type 316 tubes. The lower range pressure gauge was used when saturating the model. The higher ones were used for CO_2 injection tests.

A piston-type transfer cylinder is used for the injection of fluid in the model. Two different type 304 SS transfer cylinders, 500 cc and 2000 cc manufactured by Welker Engineering Company, were used. They were located inside the box to equilibrate the fluid temperature to the model temperature prior to injection. Fluid was injected by pumping hydraulic oil into one side of the piston in the transfer cylinder.

4.1.2 Injection Pump

For the injection of hydraulic fluid into the transfer cylinder, a modified Ruska pump was used. The body of the pump was manufactured by the Ruska Instrument Company in Houston, Texas. It was equipped with a totally electronically controlled drive train developed at New Mexico State University. It can be controlled to run in either a constant rate, constant pressure or constant differential-pressure mode.

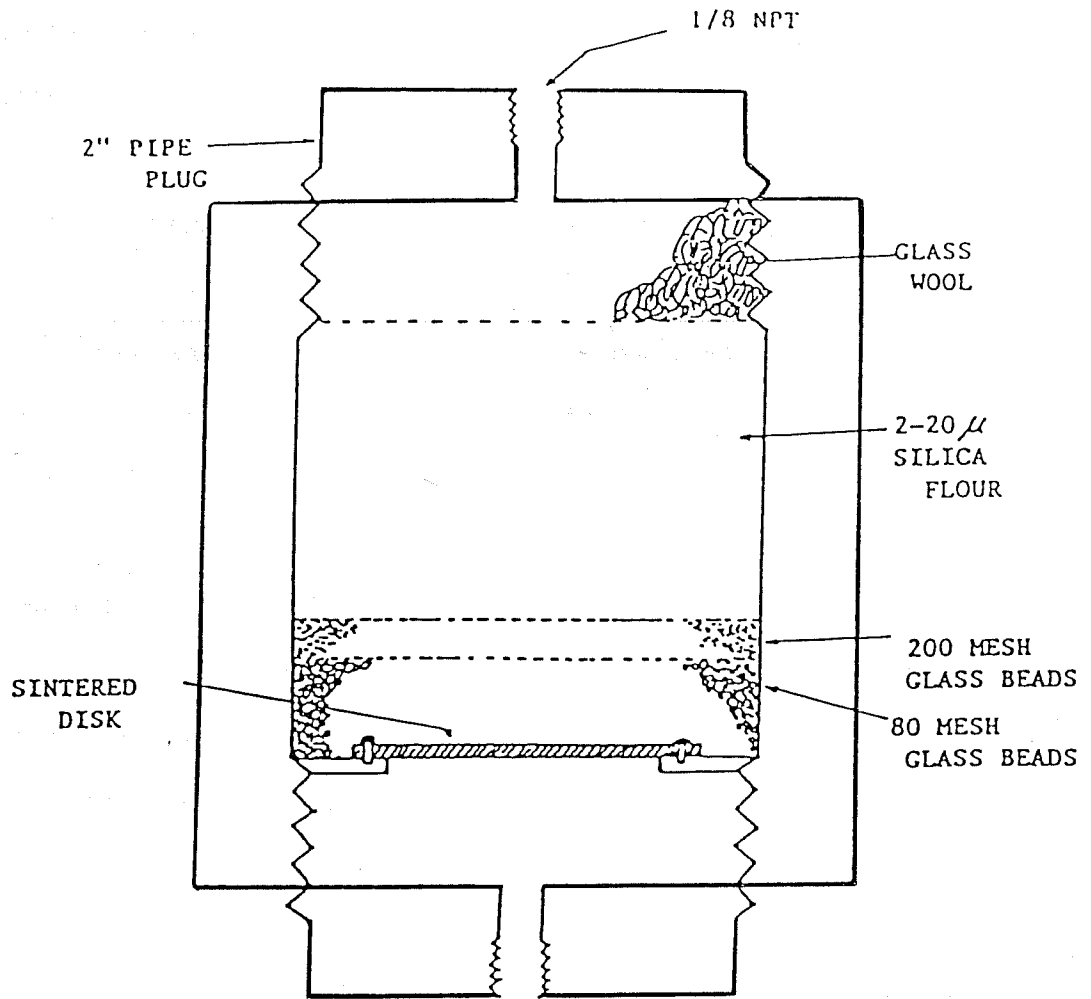


Figure 4.3 Injected Fluid Filter

4.2 Materials

Pure n-octane, 71°API, was used for all experiments to ensure miscibility with injected CO₂. Physical properties of the n-octane are given in Table 4.1. The octane was colored with Red LS 672 dye (Tricon Colors Inc.) to allow the volume of oil produced to be determined with a spectrophotometer. This is both more accurate and easier than the conventional volumetric measurement. The dye is essentially insoluble to the water phase.

Brine and deionized water were alternated in the experiments. The deionized water was prepared by reverse osmosis. Pore volume of the column after each process was checked by displacing one solution with the other and titrating the effluent for chloride ion. Preparation procedure of the brine solution which contained about 3.2% TDS, is given in Appendix A.

Three different types of surfactants, Pluradyne SF-27, Stepanflo-50 and Exxon LD 776-52 were evaluated. All are commercially available at present. Specific information on surfactant properties is given in Table 4.2. Surfactant solutions were mixed using a magnetic stirrer for several hours.

4.3 Procedure

4.3.1 Saturation of the Model

In preparation for an experiment, the model is saturated with n-octane and brine containing 100 ppm calcium ion 30,000 ppm sodium chloride to produce an environment similar to that encountered in a virgin oil reservoir. Brine is injected first and then displaced to its residual saturation with n-octane. The oil and water saturations were cal-

TABLE 4.1

PHYSICAL PROPERTIES OF N-OCTANE

| <u>Properties</u> | <u>n-Octane</u> |
|---------------------------|---|
| B. P. (°F) | 257.6 |
| Density | 0.7025 |
| M. W. | 114.23 |
| Formula | $\text{CH}_3(\text{CH}_2)_6\text{CH}_3$ |
| API Gravity @ 100°F | 71. |
| Critical Temperature (°F) | 565 |
| Critical Pressure psia | 364 |

TABLE 4.2

MOBILITY CONTROL SURFACTANTS

| | <u>Pluradyne SF-27</u> | <u>Stepanflo-50</u> | <u>Exxon LD 776-52</u> |
|------------------|------------------------|--------------------------|------------------------|
| Company Name | BASF Wyandotte | Stepan Chem. Co. | Exxon Co. |
| Chemical Name | Ethoxylated Alcohol | Sulfate Ester of Alcohol | Sulfonate |
| Concentration, % | 0.5 | 0.5 | 0.5 |
| Solution | Std. Brine | Std. Brine | Std. Brine |

culated by material balance. At the end of the experiment, the model was flooded with one or more pore volumes of deionized water, and the residual saturations were rechecked by titration of the effluent water.

4.3.2 Water and Surfactant Flood

After saturating the model with brine, a waterflood was initiated. This simulates the primary and secondary oil recovery processes. A differential pressure of 5 psi/ft was maintained through the waterflood. Initially, the waterflood produced water-free oil as is customary. After water breakthrough, oil production decreased abruptly until only the water phase was produced. After the waterflood, the oil saturation was checked by the injection of deionized water to obtain a baseline for the conventional miscible process. CO_2 was then injected and additional oil recovery recorded. For the CO_2 mobility control experiments, the model was flooded with one pore volume of the prescribed surfactant solution at a differential pressure of 2.0 psi/ft. No oil was produced during the surfactant injection phase.

4.3.3 Carbon Dioxide Tertiary Flood

The model was maintained at reservoir conditions of 1300 psig and 100°F for the CO_2 floods. During CO_2 injection, the pressure differential gradually increased from 2 to 10 psi/ft. Carbon dioxide was supplied from a transfer cylinder that was located inside the constant temperature box. To fill the transfer cylinder, it was packed in ice and then charged from a CO_2 tank configured to supply a flow of liquid CO_2 . The model was pressurized with CO_2 to 1300 psi before opening the outlet valve. Samples were then collected using the high pressure sample collecting system.

Three sample accumulators were alternated to achieve continuous operation. The maximum capacity of each sample accumulator is 40 cc. When an estimated 20 cc of fluid had been produced, a new accumulator was inserted. After installing a new accumulator, it was pressurized with nitrogen to 1300 psi before opening the valve connecting it to the model. This procedure was done as quickly as possible, so as not to disturb the steady-state operation of the process. Each sample accumulator removed from the system was weighed and then connected to a wet test meter (GCA/Precision Scientific Co.). Pressure was reduced very slowly using a needle valve, and the produced CO₂ was recorded. During the pressure reduction process, the sample accumulator was kept inside the ice-bath to prevent the loss of liquids by evaporation.

4.3.4 Sample Analysis

The samples collected usually contained two layers, oil and water. To analyze the amount of oil in the sample, a spectrophotometer response to the red dye in the oil phase was used. The optimum wavelength, determined for three different concentrations of oil diluted with octane, was 515 nm. Using this wavelength, a calibration curve of the wt% oil versus absorbance was generated. Actual oil produced was determined by diluting the produced sample of red n-octane with pure n-octane. The measured absorbance of the diluted sample coupled with the known dilution ratio allowed the actual oil produced to be easily and accurately calculated.

For surfactant free samples, pure n-octane was used for dilution and no problems were encountered. In the case where surfactants were present, a third layer of emulsion formed between the oil and water

phases. By substituting n-octanol followed by acetone as the diluent for n-octane, the two phases separated cleanly. The oil phase was then analyzed spectrophotometrically as before, using a different calibration curve.

4.4 Results

A total of four miscible displacement runs were conducted in the linear model. The results of these four runs are shown in Figures 4.4-4.7. Analyses of these data indicate no adverse effect on miscibility due to the presence of the surfactants, one run also reveals a dramatic improvement due to the decrease in CO₂ mobility. Together they offer strong support for the feasibility of utilizing mobility control additives in conjunction with carbon dioxide. Each of the tests included a base waterflood prior to the initiation of the tertiary carbon dioxide recovery process. The comparable performance observed in all four waterflood attests to the reliability of the data and justifies a quantitative comparison of the experiments. Model characteristics as well as fluid saturations, indicative of the performance of the different mobility control additives, are summarized in Table 4.3.

Referring first to Figure 4.4, the data represent a conventional CO₂ tertiary flood of a waterflooded light oil reservoir. It can be seen that the waterflood, represented by the data prior to CO₂ injection, recovered 0.5 PV of oil. This amount represented 76 percent of the oil initially in place and produced a residual oil saturation at the end of water flood of 0.16 PV. Both the recovery and residual saturation are consistent with values expected in a waterflood of a light oil.

TABLE 4.3

MOBILITY CONTROL FLOODS

| | Conventional CO ₂ Flood | II | Exxon LD 776-52 | Pluradyne SF-27 | Stepanflo- 50 |
|------------------------|---------------------------------------|------|--------------------|--------------------|------------------|
| S _{oi} , cc | I 444 | 464 | 465 | 477 | 445 |
| S _{oi} , PV | .65 | .67 | .68 | .69 | .65 |
| Waterflood | | | | | |
| Octane Produced: | | | | | |
| cc | 350 | 352 | 364 | 342 | 350 |
| PV | .51 | .51 | .53 | .50 | .51 |
| S _{rowf} , PV | .15 | .16 | .15 | .19 | .16 |
| CO ₂ Flood | | | | | |
| Octane Produced: | | | | | |
| cc | 29 | 46 | 98 | 48 | 34 |
| PV | .042 | .067 | .142 | .070 | .049 |

Injection of one pore volume of carbon dioxide (T = 100°F; 1370 psi) followed by additional water produced only 7 percent PV additional oil. Laboratory miscible floods normally produce over 10 percent additional oil. The low oil recovery shown in Figure 4.4 is due largely to inefficient macroscopic oil displacement induced by an unfavorable mobility ratio that exists between carbon dioxide and oil. The larger than usual model diameter allowed the phenomenon to be observed. This phenomenon has not been reported for experiments conducted in long, slim tube models where CO₂ injection was not preceded by waterflood.

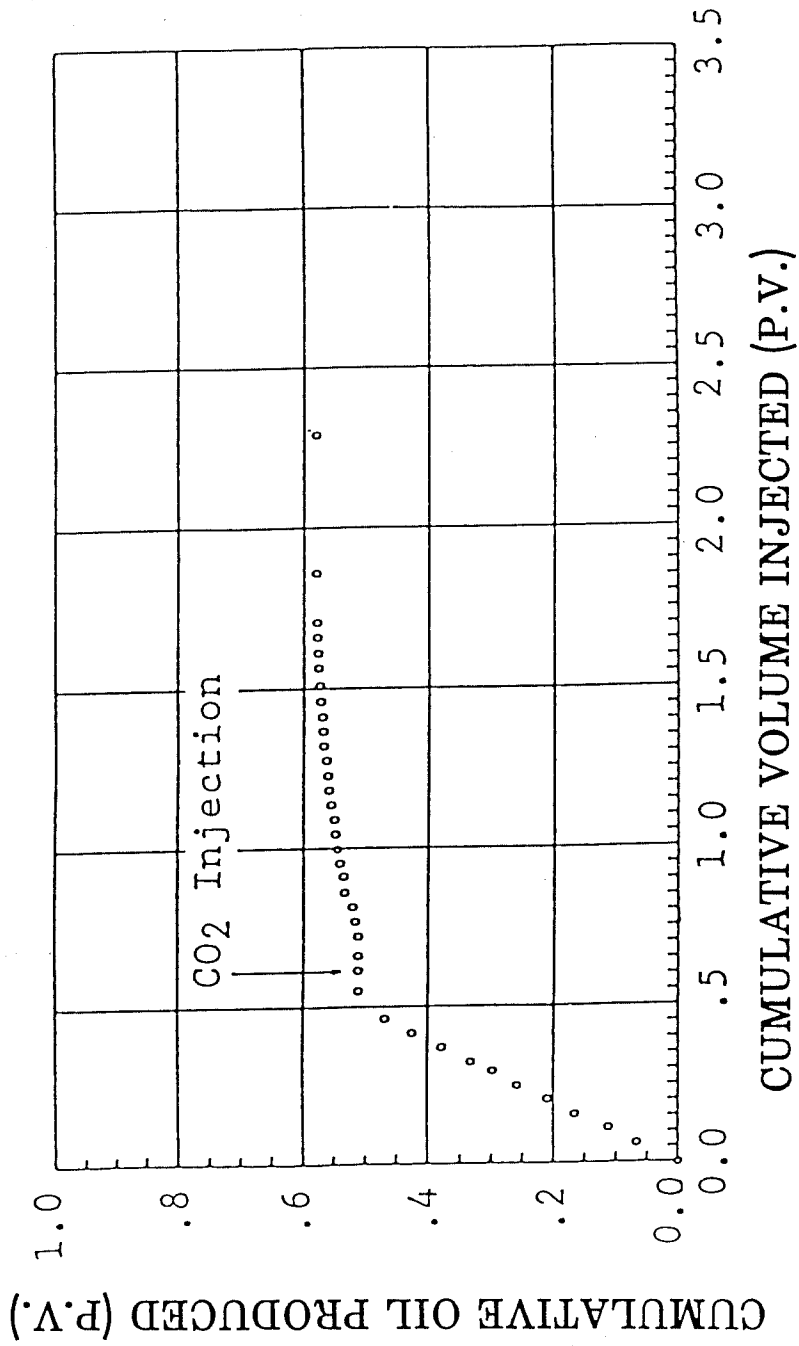


Figure 4.4 Conventional CO₂ Flood

The results of the conventional CO₂ flood I are presented in Table I for comparison. This was the first experiment performed which could account for the lower oil recovery. Conversely conventional flood II was the last experiment and benefited from the improved ability of the operator. For comparison with the mobility controlled floods the average of floods I and II will be used.

The results presented in Figure 4.5 were obtained using Stepanflo-50 as a mobility control additive. Stepanflo-50 is a sulfated ethoxylated adduct of a linear alcohol. It is the most effective additive, having this chemical structure, identified in this program. As was the case in the conventional CO₂ flood, the preliminary waterflood produced 0.5 pore volumes of oil. Prior to injecting carbon dioxide the model was carefully flooded at a low pressure drop 2 psi/ft, with a brine solution containing 0.5 percent Stepanflo-50. This surfactant does not reduce interfacial tension between n-octane and brine enough to encourage displacement of residual oil. This is indicated by the long period of surfactant injection without any oil production.

Supercritical CO₂ injection (T = 100°F; P = 1300 psi) was initiated after the Stepanflo-50 solution was in place. After injecting 0.6 PV of carbon dioxide, tertiary oil production commenced. Oil was produced at an approximately constant water oil ratio until 0.049 PV of tertiary oil had been produced. This is a slight decrease compared to the tertiary oil produced by carbon dioxide in the absence of a mobility control additive. The lower oil volume is not considered statistically significant.

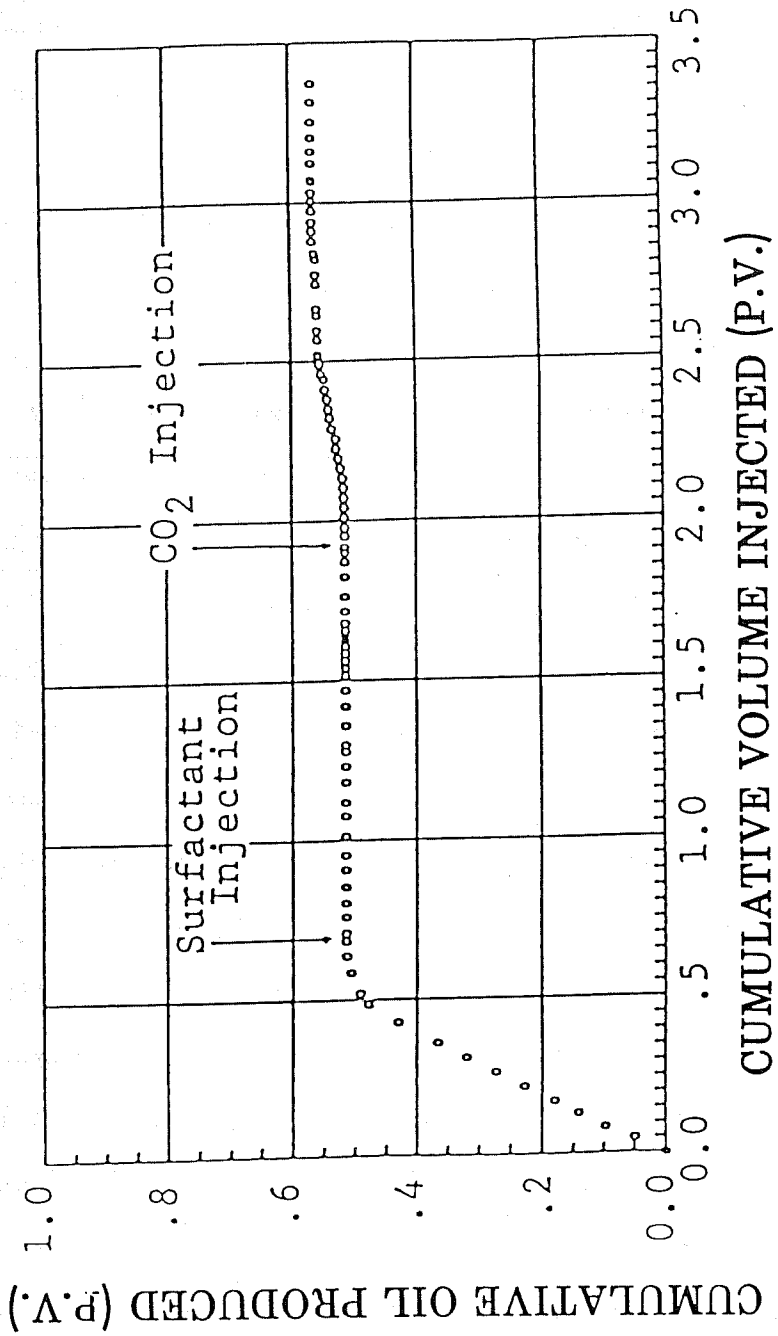


Figure 4.5 Stepanflo 50 Mobility Controlled CO₂ Flood

The results obtained for mobility control additive, Pluradyne SF-27, are shown in Figure 4.6. Pluradyne SF-27 is a blend of ethoxylated alcohols having chain lengths varying between C_{11} and C_{15} . It is superior to all other ethoxylated alcohol additives tested to date. However, additives having this general chemical structure show superior performance and several additives almost as effective are also commercially available. The waterflood performed in preparation for the Pluradyne SF-27 experiment again produced the expected 0.5 PV of oil. 1.3 PV of brine containing Pluradyne SF-27 was injected at 2.0 psi/ft pressure to prepare the model for the subsequent tertiary CO_2 flood. Tertiary oil production was delayed until 0.5 PV of carbon dioxide ($T = 100^\circ F$; $P = 1300$ psi) had been injected. This indicated a more efficient displacement of residual oil than was observed for either the conventional CO_2 flood or the experiment performed using Stepanflo-50. Oil recovery was slightly more erratic than previously observed but culminated in an ultimate recovery of 0.07 PV incremental oil, 30 percent greater than that obtained in a conventional CO_2 flood. The lower water-oil ratio indicated a more effective banking of oil. Also the higher cumulative recovery indicated the superiority of Pluradyne SF-27 for mobility control of carbon dioxide.

The most dramatic improvement in tertiary oil recovery was obtained using Exxon's LD 776-52. This is a synthetic sulfonate structure whose performance in brine is only average. Screening tests conducted in tap water containing very little calcium ion indicated that its potential for mobility reduction of gas flow in oil reservoirs flooded with freshwater was significantly higher than any additive previously investigated. To corroborate the superiority suggested by

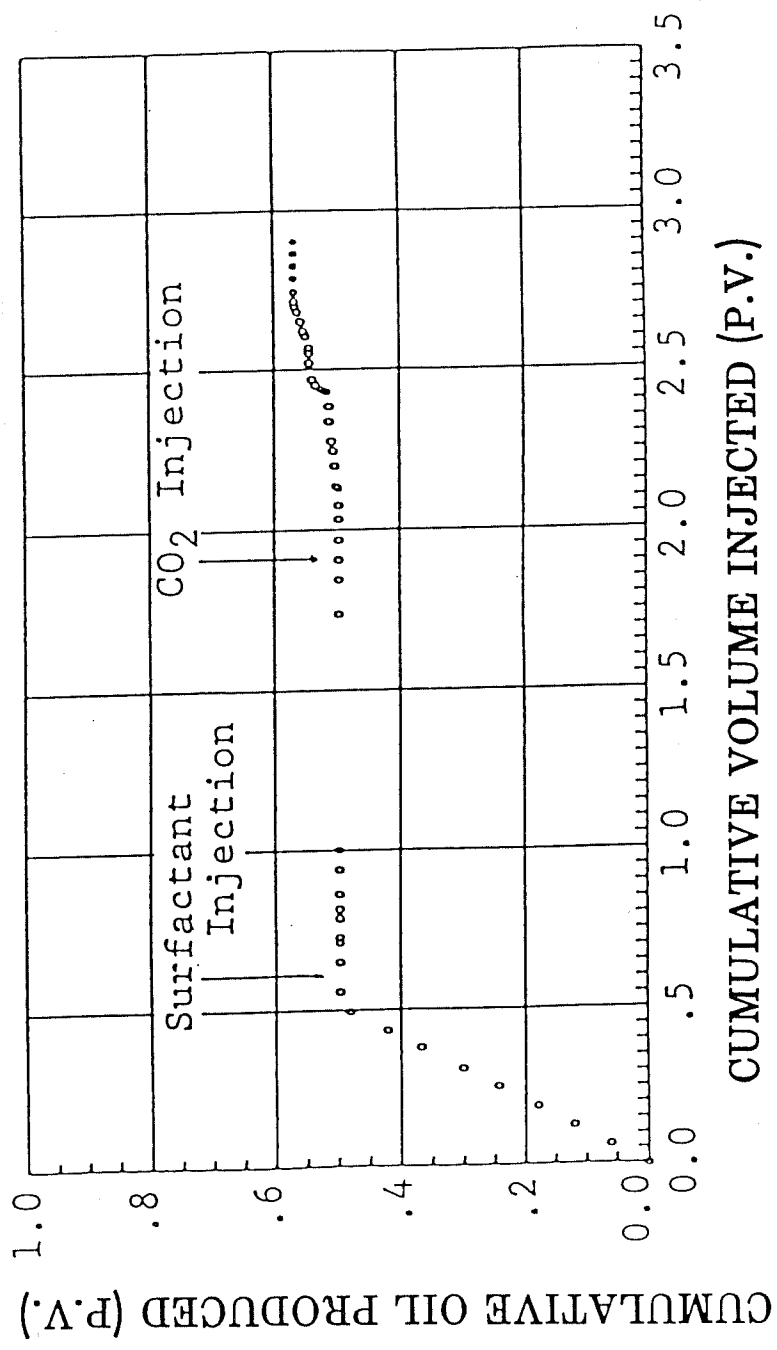


Figure 4.6 Pluradyne SF-27 Mobility Controlled CO₂ Flood

the dynamic screening tests, an experiment using LD 776-52 dissolved in tap water was conducted using the same model and technique previously used for miscible displacement studies in the presence of brine.

As shown in Figure 4.7, the waterflood produced about the same amount of primary plus secondary oil as observed in the other three experiments, 0.54 PV. The water phase was then carefully replaced with surfactant solution at a pressure drop of 2 psi/ft. Carbon dioxide injection was initiated and tertiary oil production did not occur until after 0.8 PV of supercritical carbon dioxide had been injected ($T = 100^{\circ}\text{F}$; $P = 1400$ psi). Enhanced oil production continued at a low water-oil ratio until 14 % PV additional oil had been produced and residual oil saturation had been reduced to zero. This amount of tertiary oil represents almost a three-fold increase over the average obtained in the conventional CO_2 floods. It is the strongest experimental corroboration of the feasibility of CO_2 mobility control. It also indicates that it may be possible to tailor molecular structures to obtain even more potent additives for use in brine.

These results essentially complete the work task relative to mobility control of carbon dioxide for miscible displacement of oil. The above experiments were conducted using octane as the oil phase to ensure that miscibility was obtained. The use of octane was adopted after queries of petroleum operators failed to identify an oil miscible with carbon dioxide at or below the 1500 psig pressure limitation of the experimental apparatus. The effort to find an oil miscible to carbon dioxide within the operating limits of the equipment will be continued and additional experiments performed if an oil from a candidate CO_2 flood reservoir is identified.

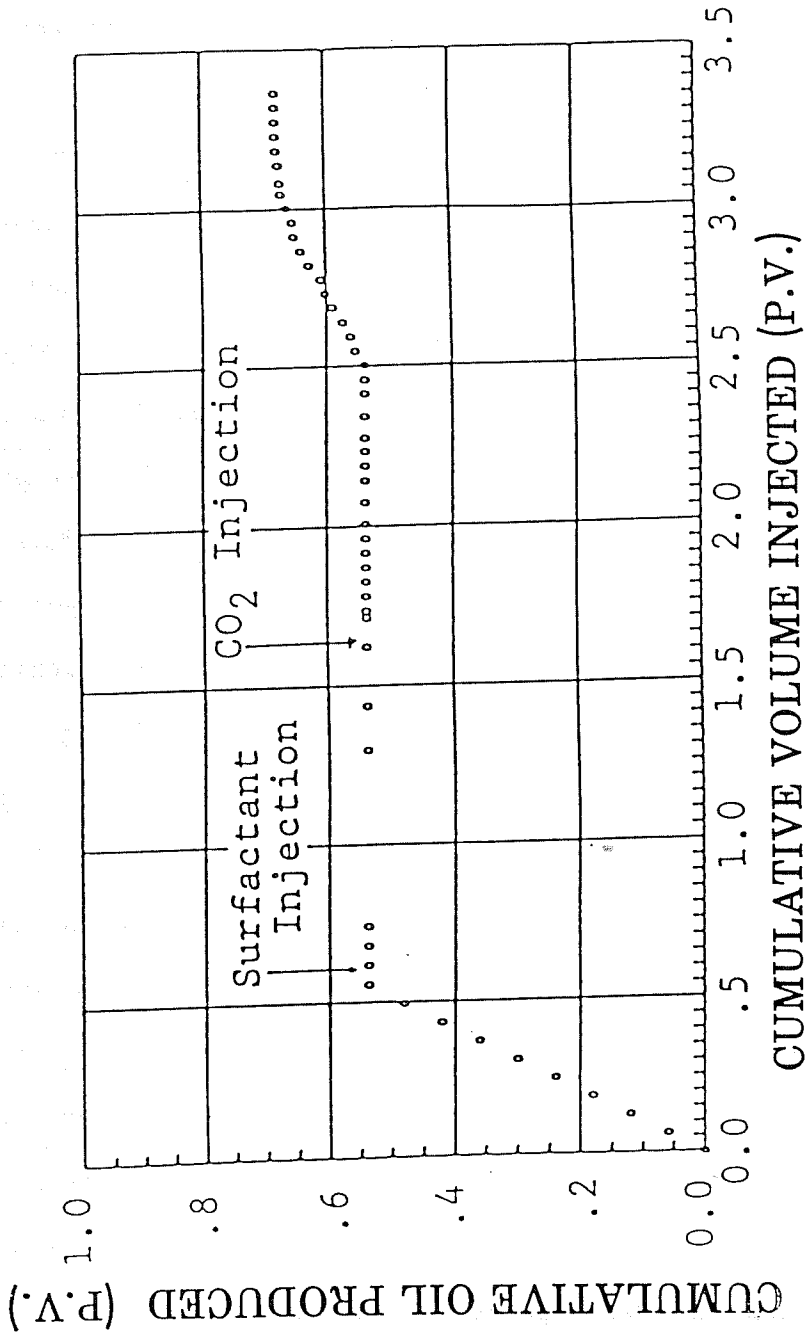


Figure 4.7. Exxon LD776-52 Mobility Controlled CO₂ Flood

4.5 Conclusions

Each of the additives tested significantly improve the tertiary oil recoverable by carbon dioxide miscible displacement process. The feasibility of utilizing mobility control additives in the miscible process appears good with one possible exception. One cannot lower the mobility of carbon dioxide without incurring additional pressure drop in the reservoir. There are many candidate fields where the properties of the oil, coupled with the depth and temperature of the reservoir, make miscibility difficult to obtain. For these fields, any additional pressure drop, induced by a mobility control additive, could reduce the carbon dioxide pressure below the level required to achieve miscible displacement. In so doing, the additive could conceivably act to decrease oil recovery rather than increase it.

While it is easy to speculate on such an occurrence, the actual benefit or loss is most difficult to calculate. The quantitative evaluation of the effect of mobility control in a particular reservoir is best handled by computer simulation. With appropriate software, oil displacement efficiency as function of reservoir pressure, influenced by mobility control, can be mapped to predict oil displacement at each point in the reservoir. The three dimensional nature of such simulators also can account for the improved conformance that will inevitably occur and contribute to the overall effect of mobility control on tertiary oil production. For floods below the miscibility pressure and those floods conducted well above the miscibility pressure, the use of mobility control additives should generate no adverse pressure effect and have an high potential for commercial success.

SECTION FIVE

IMMISCIBLE OIL DISPLACEMENT TESTS

5.1 Introduction

It has been shown in two-phase, gas-water, flow tests that the presence of a surfactant in the water phase lowers the flow mobility of a gas significantly. In capillary flow studies, the effect is manifested by an increased apparent viscosity, orders of magnitude greater than the viscosity of the surfactant solution. [95] In flow through a porous-medium model, the effect of lowered mobility seems more related to a decrease in the gas-phase relative permeability. Again, the effect is quite pronounced. [97,98]

Based on these earlier studies, linear oil displacement tests were designed to study the effect of surfactant-type, mobility-control agents on oil recovery in a linear sand-pack model. It was found that the mobility-control agents were effective in reducing the bypassing of oil by the CO₂. Further, it was shown that higher yields of tertiary oil were achieved when these agents were used as opposed to conventional CO₂ floods incorporating no mobility control.

5.2 Equipment

The equipment used in the oil-recovery flow tests consisted of a high-pressure stainless-steel flow model, Ruska pump, transfer cylinder, sample system, meters, regulator, controls and valves. A flow diagram for the system is shown as Figure 5.1.

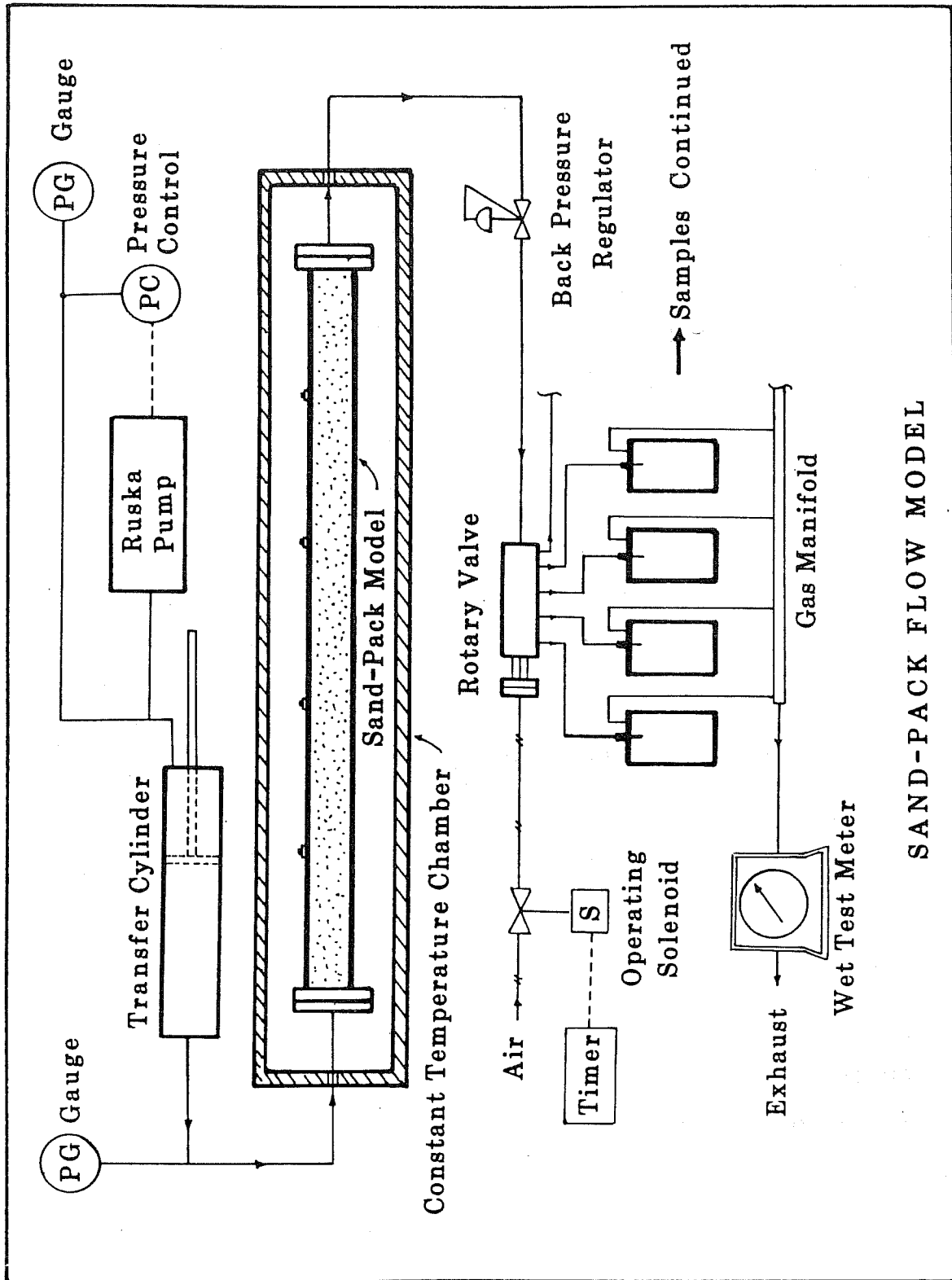


Figure 5.1 Reservoir Condition Flow Apparatus

The flow model is 200 cm long (6.6 ft) made from 1½ inch, schedule 40, seamless, type 316L stainless-steel pipe. The ends are closed with 900-pound flanges welded to the pipe. There are intermediate pressure taps along the pipe. They are made from a half of a 3000 psi coupling (¼ inch pipe size) welded to the pipe wall. A 1/8" hole is drilled through the wall to provide access to the model. The end flanges are blind flanges with 1/8" pipe-thread flow ports in the centers. The flange gaskets used are 0.254 mm (10 mil) thick teflon.

Attached to the inside surface of the end flanges is a 1½ inch sintered stainless disk 1/8 inch thick with a maximum pore size of 100 microns. This disk is used to retain the sand packing in the model. A thin layer of fine glass beads (-80 mesh size), approximately 0.1 inch deep, is used over the sintered disks to further prevent very small sand particles from being produced from the model.

The sand is a fine silica sand marketed as silica flour by the Midland Sand Company. It was necessary to remove the finest particles because the sandpacks originally tested had permeabilities less than 6 millidarcies. The major portion of the minus 20-micron particles was removed by water elutriation. Models packed with the fractionated silica were in the 150-200 millidarcy range, the permeability of many oil reservoirs.

A special technique was developed for packing the sand into the column. It consists of deaeration, packing and vibration steps. Packing by other methods resulted in non-uniform beds with dense sections and visible voids.

After packing by the above procedure the model was subjected to a pressure gradient of about 400 psi. It was vibrated simultaneously.

Water was used to provide the pressure differential. A small amount of compaction occurred. The resulting void was then filled with more wet deaerated sand. The column was then closed and installed in a constant-temperature chamber.

The constant-temperature chamber is an air bath unit. It is 8 ft long, 18 inches wide and 16 inches high. It is lined with 1" thick rigid polyurethane foam insulation with a heavy foil surface. It is heated with either heat lamps or light bulbs depending on the temperature range desired. The useful range is from about 5° above room temperature to about 140°C. The heat lamps are controlled by two methods. Some remain on continually but their intensity is set by adjusting a variable voltage transformer. The others are turned on and off with a thermostat. This combination is effective for good control over the working range. A small blower is installed inside the chamber to eliminate temperature gradients, by circulation of the air.

The injection system consists of a Ruska pump, a piston-type transfer cylinder, a pressure regulator, piping and gauges. The Ruska pump is a variable speed, 500 cc/stroke, 4000 psi unit. The transfer cylinder is made of 2.00 inch OD seamless tubing. It is type 304 stainless steel with a 0.120 inch wall thickness. It is fitted with O-ring sealed end caps and a floating piston. The piston is sealed by a viton seal with teflon on each side to protect the viton.

A pressure-control switch is installed on the line between the pump and the transfer cylinder. This switch is very helpful in controlling the injection pressure during the flood experiments.

A back-pressure regulator is placed in the discharge line to help control the operating pressure in the model. A problem with the back

pressure regulation was encountered. The viscosity of the crude oil is several orders of magnitude greater than that of the brine. Also the brine viscosity is much higher than that of the CO₂. Because the fluids come out of the column in slugs, the regulator action is erratic. When an oil slug comes out, the flow is very slow, and the pressure tends to rise. In contrast, when a CO₂ slug is encountered, the pressure drops rapidly, and the regulator must close rapidly to prevent a large pressure fluctuation in the model. As a consequence, a special back-pressure regulator was constructed having very small internal volume was constructed to resolve these problems.

The regulator consists of a ¼" tubing valve which has been modified to provide flow control according to the upstream pressure. The valve chosen is one with an unthreaded sliding stem, which was more easily adapted than threaded stem valves. Also the diameter of the stem is smaller than the diameter of the seat, a condition necessary for proper control. The internal stem linkage was removed and replaced with a coil spring which holds the valve closed. The valve is installed with the upstream pressure beneath the seat. As the pressure rises, it provides a force to oppose the spring force, and the valve then will open to allow flow, whereby the pressure will drop. The handle of the valve is connected by threads to the bonnet and may be adjusted. Since the spring presses against the inside of the handle, this adjustment changes the pressure at which the valve will open. This regulator as fabricated provided much better pressure control than had been previously accomplished. The valve in use is made from a Whitey, number SS-14DKM4-S4, valve.

A sample system is provided to enable the model to operate unattended. The system consists of a rotary valve with sample containers and a gas collection system connected to a wet test gas-flow meter.

The rotary valve is a six-position piston-operated valve which is available from Pierce Chemical Co. or Laboratory Data Control Division of Milton Roy Co. (catalogue number 4142530). The piston is operated with 85 psi nitrogen supplied from a cylinder and controlled by a multi-port solenoid valve. The solenoid valve is operated by an electrical timing clock. The clock can be set for intervals ranging from $\frac{1}{2}$ hour to several days. Typically samples are taken every 2 to 12 hours depending on the flow rates.

The gas flow is measured by collecting the gas from the sample containers where it enters a manifold and then passes through a laboratory-type precision wet-test meter.

The brine-oil samples are analyzed according to the analytical procedure reported below.

5.3 Analytical Procedure

An analytical procedure was developed for determining the oil content of samples from the flow tests. This procedure was found to give results with less than 1% error, even with 14°API crude. In the early tests the samples were analyzed by a procedure which consisted of the addition of a known volume of toluene. The sample was shaken well and allowed to settle. It was then poured into a separatory funnel and allowed to settle into two layers which were then separated and weighed. The weights of the two layers together with the volume of toluene added,

provided the basis for calculating the original composition of the sample.

A difficulty with reproducibility by this method was encountered. Accurate separation of the two layers was complicated by poor settling and by adhesion of the brine layer to the sides of the separatory funnel. Consequently, excessive settling time was required. Samples with high oil content required a considerable volume of toluene for dilution.

Because of these problems a better method was devised. This method is a spectrophotometric absorption method which overcomes the deficiencies noted above.

In this method a weighed sample is agitated well with a measured amount added of toluene. Enough toluene is added to allow light transmittance to be measured by the spectrophotometer. The agitation is accomplished with an adapted Cenco-Meinzer sieve shaker (Cat. #18480). This shaker provides an adjustable-speed motion which is ideal for mixing the toluene with the oil layer and yet does not cause excessive mixing of the two phases. The adaptation consists of a sample-bottle holder attached to the shaker plate.

Other methods of mixing were tried but either resulted in poor toluene blending or in excessive mixing of the brine phase with the oil phases. When these two phases are well mixed they tend to form a semi-stable emulsion which is slow in separating. When a surfactant is present in the brine phase, the problem is considerably aggravated. Some emulsions were very difficult to separate and required heating to about 85°C for 48 hours before the phase separation was accomplished.

After the sample is agitated for 4 minutes with the Cenco-Meinzer unit, it is allowed to settle until a clear layer forms in the upper portion of the oil phase. This step usually requires only a few moments. From this layer an aliquot of sufficient size for accuracy is then taken

and diluted with a measured amount of toluene. This test solution is then analyzed with a Bausch and Lomb spectrophotometer.

It was necessary to establish the proper absorption frequency and concentration range for the test samples. Consequently, tests were made at various frequencies with two different concentrations of crude oil in toluene. The results are shown in Figure 5.2. Note that no absorption peaks, typical of this method, are evident due to the fact that the crude oil consists of a diverse mixture of a large number of compounds. From these curves a frequency was chosen which is 635 nanometers (nm). This frequency was chosen because the absorption does not vary appreciably with frequency, particularly at the lower concentration of oil. Test reproducibility was studied at other frequencies, i.e. 580 and 660 nm because the absorption was greater at these points. It was found that the frequency setting and drift then became very critical and less accuracy was achieved.

The ideal concentration range was found to be between 0.04-0.08% for Wilmington crude. Dilution to this range is readily achieved by visual comparison of the diluted sample with a standard.

A number of calibration points were determined, and the resulting data were plotted on a log-log plot of wt% oil vs. absorbance. The plot resulted in a straight line, see Figure 5.3. A least square fit of the data provided an equation that was used for calculation of oil volumes.

The oil volume calculations are based on the measured absorbance and the appropriate weights taken during the analyses. An equation for the calculation is as follows:

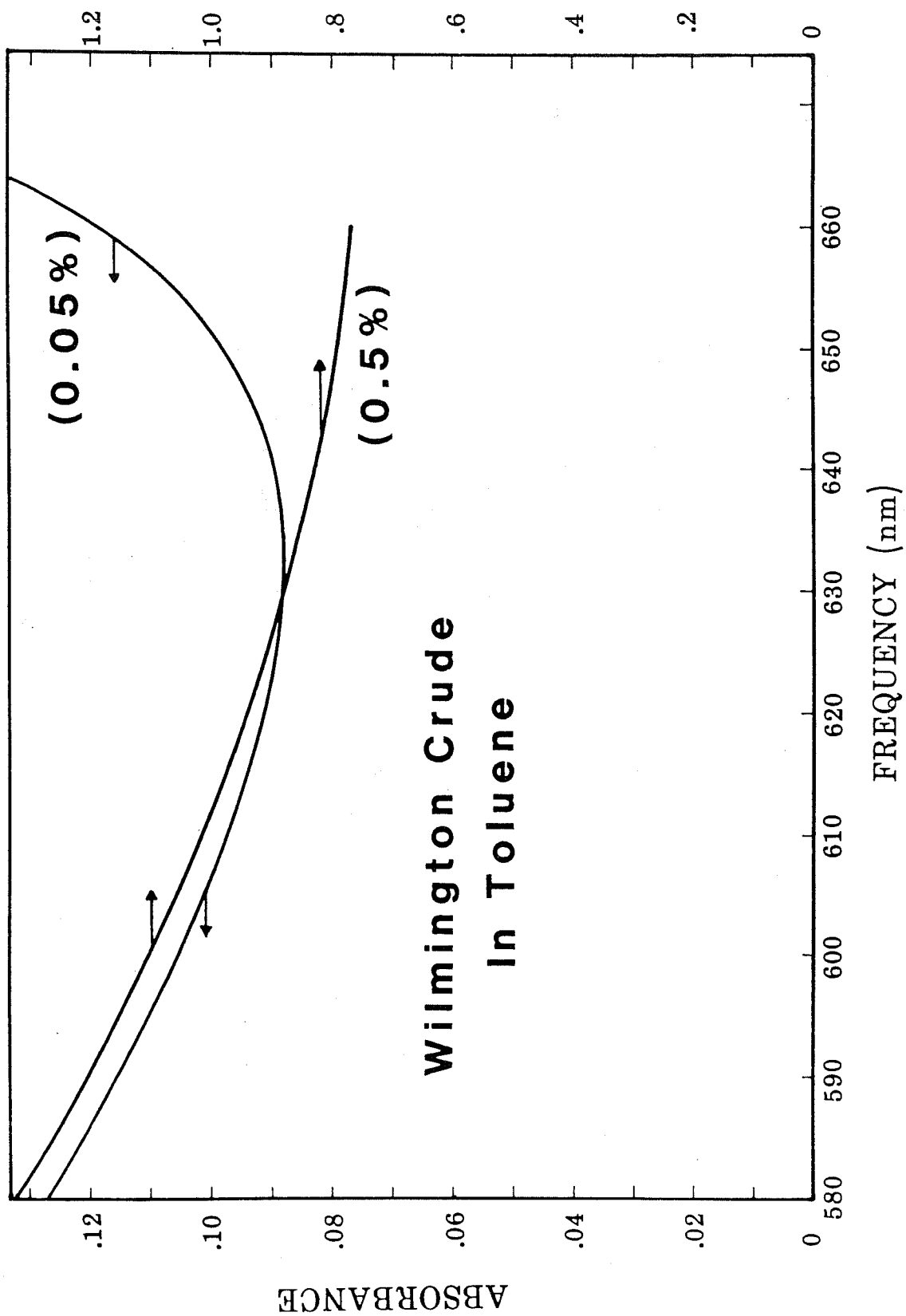


Figure 5.2 Absorption Spectra for Crude Oil-Toluene Solutions

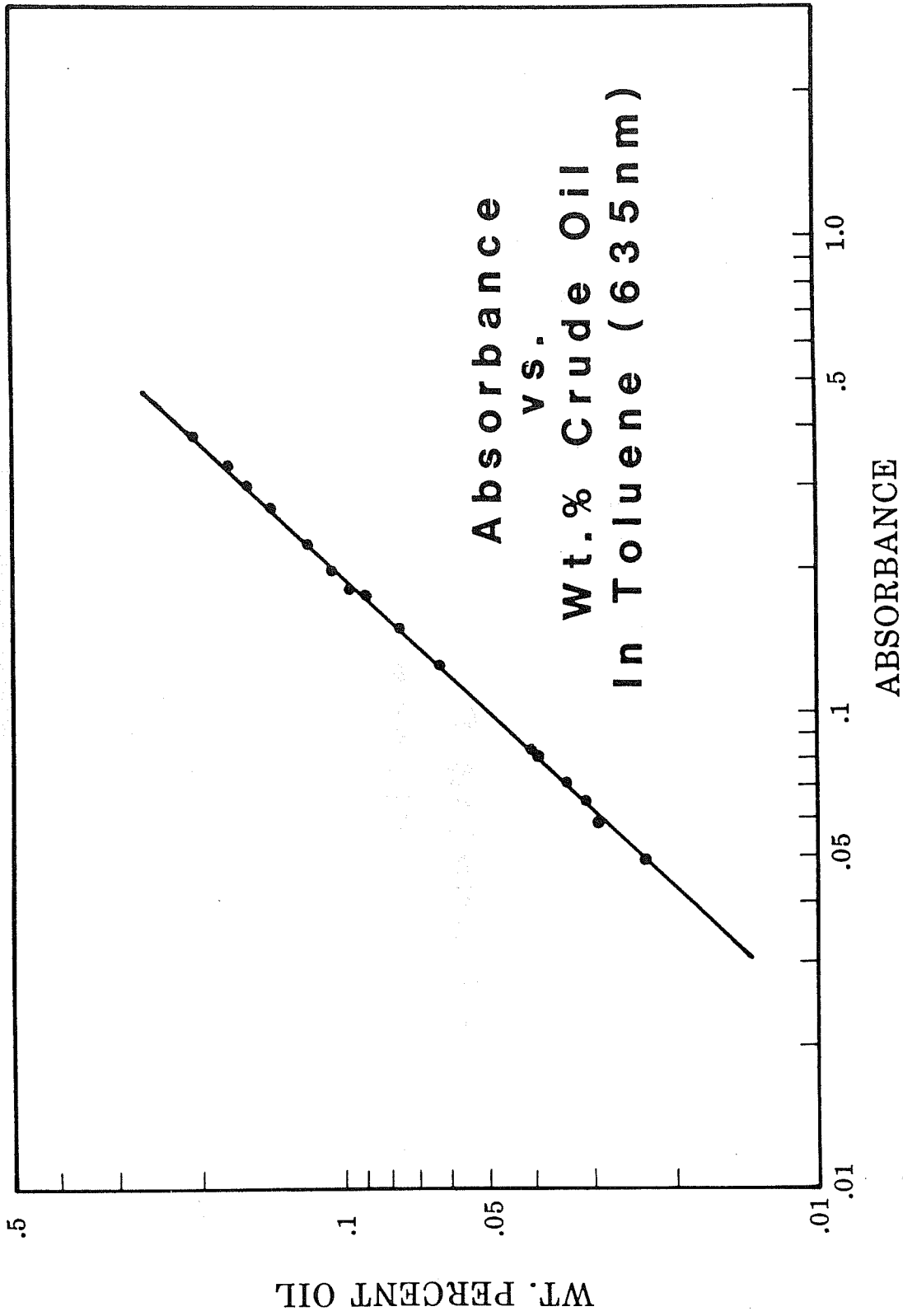


Figure 5.3 Calibration Curve for Spectra Photometric Analysis of Oil Concentration

$$\text{Oil Volume} = \frac{1}{\rho} A_c W_2 (TW - SW) / (W_1 A_c W_2)$$

where:

ρ is the oil density,

A_c is the corrected absorbance (Measured absorbance minus the constant for the sample vial used)

SW is the sample weight including tare

TW is the sample weight including toluene and the tare

W_1 is the aliquot weight

W_2 is the weight of the solution containing the diluted aliquot.

5.4 Experimental Procedure

The test procedure followed in this study consists of saturating the model with crude oil and brine to produce a condition similar to that encountered in a virgin oil reservoir. The model is then flooded with brine or water to recover primary production plus the oil produced by a waterflood. In mobility tests, brine containing a mobility-control additive is then injected; the delay is to insure no additional oil could be attributed to the presence of the additive in brine phase during a conventional waterflood. A carbon-dioxide flood is next initiated and continued to CO₂ breakthrough. Brine is then injected to recover the tertiary oil by a second waterflood.

Initially the column should contain only brine with no air or gas present. If gas is present, it can be removed by purging with CO₂ followed by water injection at 1500 psi. At 1500 psi, CO₂ dissolves in water readily and can be adequately removed with several pore volumes of water.

Three crude oils of different API gravities were used in this study. A summary of the crude oil's properties are shown in Table 5.1. Crude oil is loaded into a transfer cylinder very carefully so that no air is trapped. The crude is next displaced slowly into the model by hydraulic oil supplied by the Ruska pump. In this step it is most helpful to have the model and the transfer cylinder heated in the constant temperature chamber to lower the viscosity of the crude. In this study crude was injected at 95°C with a pressure differential of 200 psi.

Oil is injected until oil breakthrough and is then continued until no additional brine is produced. The model is now saturated with oil at residual brine content. This is the usual condition found in oil bearing formations.

The oil production step now begins with the injection of water or brine. This step was conducted at 51°C (124°F), which is the temperature of the tar-zone reservoir, source of Wilmington crude. The pressure gradient used was about 10 psi per ft. The resulting flow rate is slow enough to give similar results to those encountered in the field. The waterflood is continued until the oil cut becomes very small, about 3%. The point at which water breakthrough occurs is noted.

If a mobility control agent is to be used, it is now injected. It is necessary to reduce the pressure differential in this step because the surfactant reduces the interfacial tension in the model. If this is not done, oil will be produced in this step. In an actual reservoir the pressure gradient would be low enough that this would not happen. After sufficient volume of solution has been injected so that the additive begins to break through (about 0.6 pore volume), the injection is stopped.

The next step in the study is the carbon dioxide flood. The pressure of the liquids in the model is adjusted to the CO₂ flood pressure between 1000 psi and 1600 psi.

Carbon dioxide is next injected into the column. The pressure at the column outlet is maintained at the selected operating level. Samples are collected and analyzed. The point at which CO₂ breakthrough occurs is noted, and the cumulative CO₂ volume produced is recorded from that point on.

At the point of CO₂ breakthrough the injection is stopped and a second waterflood is started. The waterflood is continued until the oil cut again is reduced to 3%.

5.5 Results

The results of the tests are presented in Table 5.2. They show that immiscible CO₂ flooding followed by a waterflood can be effective in increasing, substantially, the oil recoverable after water flooding of a low-gravity viscous oil. However, higher gravity oils, i.e. is, Maljamar, waterflood to a low residual and leave little oil to be recovered by immiscible CO₂ displacement.

For Wilmington Tar Zone crude the oil recovered by primary plus waterflood was equal to about 30.4% of a pore volume. Immiscible CO₂ flooding increased the recovery 66% to a total recovery of 50.5% PV. The addition of a mobility control agent increased the recovery further to 58.3% PV. This amounts to 39% additional tertiary oil by CO₂ flooding attributable due to the effectiveness of the mobility-control process.

It was also noted that the CO₂ produced increased abruptly when no mobility control was used. In contrast, when the Pluronic F68 was used, the CO₂ production increased much more gradually.

Table 5.1. Immiscible Displacement

Crude Oils

| Crude Oil | Gravity °API | Reservoir Temp., °F | Viscosity CP |
|---------------------------|--------------|---------------------|--------------|
| Wilmington Tar Zone | 14 | 123 | 283 |
| Wilmington Upper Terminal | 22 | 148 | 23 |
| Maljamar | 37 | 90 | 1 |

Table 5.2. Immiscible CO₂ Flood Results

Crude Oils

| | Wilmington Tar Zone | Wilmington Tar Zone | Wilmington Upper Terminal | Wilmington Upper Terminal | Maljamar |
|-------------------------------|---------------------|---------------------|---------------------------|---------------------------|----------|
| Mobility Control Additive | - | Pluronic F-68 | - | Plurafoam SF-27 | PSF-27 |
| Conc., wt% | - | 0.5 | - | 0.5 | 0.5 |
| S _{oi} | .86 | .84 | .78 | .78 | .81 |
| <u>Water Flood</u> | | | | | |
| Oil prod. pv | .30 | .30 | .42 | .42 | .58 |
| S _{rowf} | .56 | .54 | .36 | .36 | .23 |
| <u>CO₂ Flood</u> | | | | | |
| | .20 | .28 | .09 | .14 | .01 |
| S _{roCO₂} | .36 | .26 | .27 | .22 | .22 |

A plot of the cumulative oil produced versus the cumulative volume injected is shown for core floods with and without mobility control. See Figures 5.4 and 5.5. Note, in the immiscible flood without mobility control, Figure 5.4, little additional oil was produced during the CO₂ injection. During the final waterflood almost all of the tertiary oil production occurred. In contrast the effect of mobility control is reflected in greater oil production during CO₂ injection as shown in Figure 5.5.

The average oil produced in the two base-case waterfloods is 305 cc. With an initial oil volume of 870 cc, the recovery in the primary plus secondary phases is 35% of the original oil in place. The total oil produced in the case of the conventional CO₂ flood is 510 cc which 58.6% of the initial oil. When mobility control was used the total oil recovered increased to 585 cc which represents 67.2% of the original oil.

A comparison of the data in Table 5.2 shows the enhanced recovery of Upper Terminal crude oil by carbon dioxide was significantly less than Tar Zone crude due to its higher gravity. The higher gravity, and hence, lower viscosity enabled the initial waterflood and primary production phases of the producing operation to recover 56% of the oil in place or 0.42 pv of oil. Immiscible CO₂ injection followed by tertiary waterflood recovered an additional 0.09 pv of oil; possibly commercial but less than 50% of the CO₂ recovery obtained with Tar Zone crude.

After the tertiary waterflood was complete, the water in the model was replaced with brine containing 0.5% Pluradyne SF-27. Carbon dioxide was again injected until breakthrough and only a minor amount of additional oil was produced. A second tertiary waterflood was then conducted and it produced an additional 0.05 pv of enhanced oil. The recovery

CONVENTIONAL CO₂ FLOOD

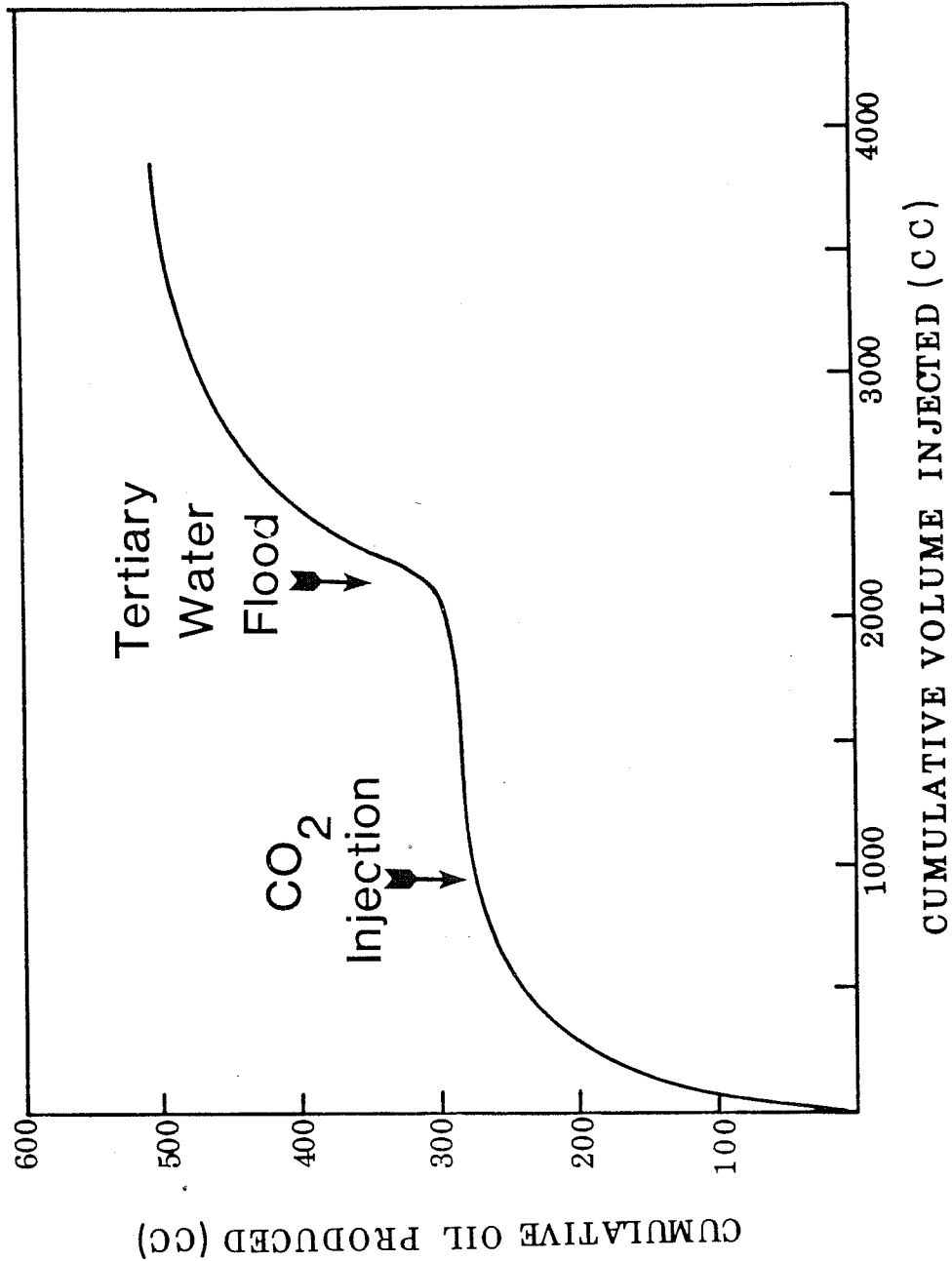


Figure 5.4 Immiscible CO₂ Displacement of Wilmington Tar Zone Crude Oil

CO₂ FLOOD WITH MOBILITY CONTROL

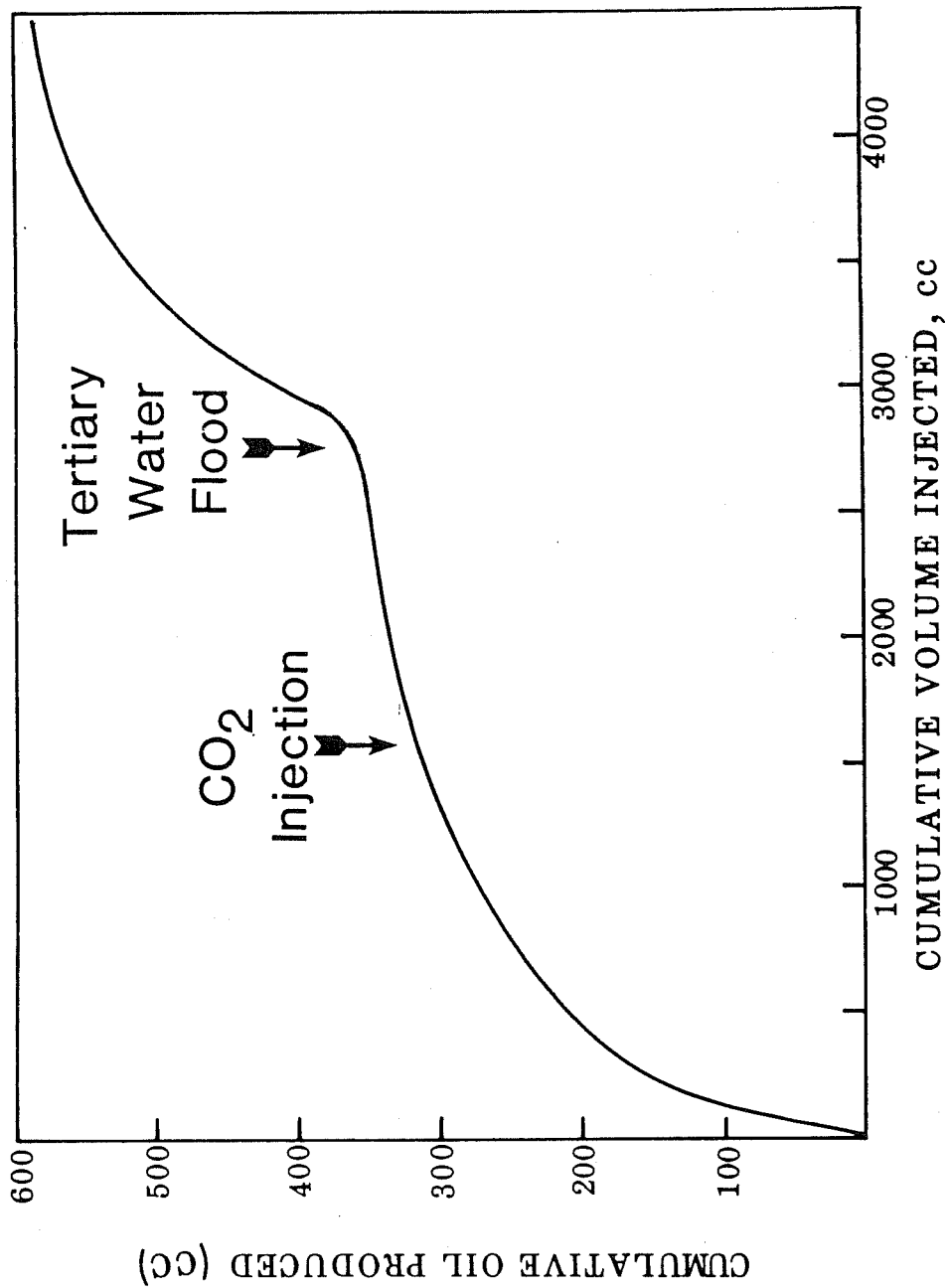


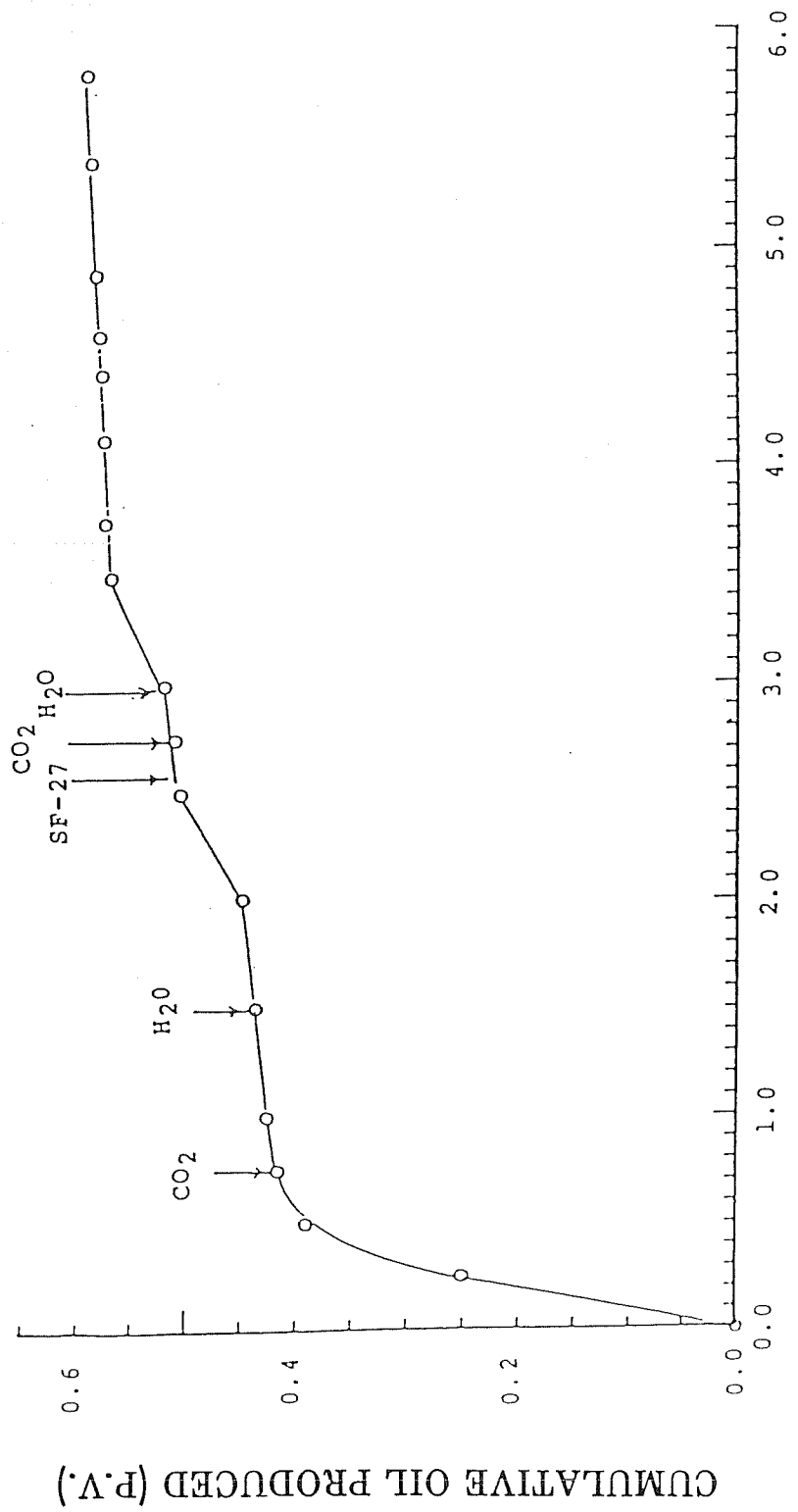
Figure 5.5 Pluronic F68 Mobility Controlled Immiscible CO₂ Displacement of Wilmington Tar Zone Crude Oil

curves for the complete sequence of fluids injected during the experiments is shown in Figure 5.6.

Based on the results of the sequential experiment it appears that mobility control additives can increase the oil recoverable by immiscible CO₂ flooding of Upper Terminal crude by approximately 50%. The added tertiary production due to the use of the mobility control additive would be profitable and its contribution to the overall process could be the difference between commercial recovery for Upper Terminal Zone type oils or having to abandon the lease with mobile oil still left in the reservoir.

One of the key objectives of the experiment was to assess the mobility control imparted by Pluradyne SF-27. To do this pressure differential was recorded at steady-state flow rates at the end of the first CO₂ injection phase with only brine present in the model and at the end of the second CO₂ injection phase when the brine contained the mobility control additive. In the first case with no additive present, the relative permeability to carbon dioxide was 23.5 md at the end of the carbon dioxide flood. When Pluradyne SF-27 was dissolved in the water phase the permeability was only 2.5 md; approximately an order of magnitude reduction in the mobility of carbon dioxide.

A third immiscible test was conducted with an even lighter crude, 26 °API, from the Maljamar reservoir in southeastern New Mexico. This crude is miscible with CO₂ above 3000 psi and a field test is now being conducted by Conoco, Inc. Due to the pressure limitation of the flow model, the test had to be conducted at 1600 psig, well below the miscible pressure. As a result, the CO₂ floods with and without mobility control recovered only a minor amount of oil, less than 0.02 pv.



CUMULATIVE VOLUME INJECTED (P.V.)

Figure 5.6 Carbon Dioxide Displacement of Upper Terminal Zone Crude

However, the mobility of the gas was reduced eight-fold by Pluradyne SF-27. This is similar to the reduction noted in the case of the experiment with Upper Terminal Zone crude.

SECTION SIX

RESERVOIR SIMULATION OF MOBILITY CONTROLLED CO₂ FLOODS

6.1 Introduction

The problem of accurately simulating the enhancement of oil displacement by injection of carbon dioxide in the presence of a mobility control additive is much more complex than generally recognized. This may explain the dearth of published papers dealing with this emerging enhanced oil recovery process. Complicating the problem is the fact that the enhancement of oil production by CO₂ injection occurs by two different modes of operation; namely miscible and immiscible displacement. In the miscible process, the carbon dioxide is either first-contact miscible with the crude or extracts enough light hydrocarbons from the crude initially contacted that a CO₂ enriched bank forms that is miscible with the crude oil in all proportions. The bank of miscible gas has been shown to effectively displace most of the crude oil from the reservoir.

Under immiscible conditions, carbon dioxide dissolves in the crude oil it contacts in the reservoir; reducing the crude oil's viscosity and swelling its volume. The resulting low-viscosity, swollen oil can then be displaced by water to obtain enhanced oil production.

Modeling either process is extremely difficult and complex because of the interaction between the carbon dioxide and the crude which results in changes in viscosity, residual oil saturation and the mobility of the oil, water and even the CO₂. Although the basic miscible process is much simpler to model, the addition of mobility control adds

one or more orders of magnitude of difficulty to the problem. At present it appears that current simulators are not capable of accurately simulating the mobility controlled miscible process. On the other hand, although the immiscible displacement is also more complex when mobility control is considered, new techniques were developed in the course of this research that allowed Scientific Software-Intercomp's simulation program to accurately model the immiscible CO₂ process under mobility controlled conditions process.

6.2 Immiscible Displacement

In modeling the immiscible displacement of crude oil by carbon dioxide, it is necessary to accurately describe the solubility relationship of carbon dioxide in crude oil as a function of reservoir pressure. This is extremely important as the pressure will vary both during the life of the flood and also with position in the reservoir. The necessary algorithm was developed by utilizing the conventional equilibrium K value approach to describe the concentration of carbon dioxide in the crude oil solution that is in equilibrium with carbon dioxide in the vapor phase. In modelling the immiscible displacement process, the oil can be assumed to be dead; i.e., no volatile components, and, hence, the gas phase in the reservoir always consists of pure carbon dioxide. Although this assumption is not perfectly rigorous for most oil reservoirs, it is close enough to yield acceptable simulation results. It is possible to modify the algorithm to accommodate any light hydrocarbon gases present in the gas phase should the simulation accuracy warrant.

Calculating the viscosity of the carbon dioxide crude oil mixtures also presents a challenge. Normally, the viscosity of binary fluid

mixtures, gases or liquids, can be calculated by the relationship:

$$\mu = \mu_1^{x_1} \mu_2^{x_2} \quad (1)$$

where μ_1, μ_2 = Component viscosities

x_1, x_2 = Component mol fractions

In the case of liquid solutions containing carbon dioxide, this equation is not accurate unless one uses a pseudo-viscosity for liquid phase carbon dioxide; not the handbook value. Laboratory data are available that describe the viscosity of crude oil-carbon dioxide mixtures at different concentrations of carbon dioxide. These data can then be used to back calculate, by equation 1, the liquid phase viscosity of carbon dioxide for use in the simulation process. The viscosity so calculated for this simulation was 1.003 cp.

The mobility reduction of carbon dioxide was modelled by increasing the viscosity of the gaseous carbon dioxide to reflect the hypothetical presence of the additive vaporized from the water phase in the reservoir. It is assumed that the mobility additive will be injected as an aqueous solution in slugs; ahead of and alternating with CO₂ injection. Equation 1 was utilized to predict the gas phase viscosity using a pseudo-viscosity for the mobility control additive, the second component in the gas phase selected to provide the desired amount of mobility control. By this technique, it is possible to simulate the mobility reduction experimentally determined for any given additive. In this study CO₂ mobility lowering by factors of 1.5, 2 and 10 were examined to cover the range of additive performances measured in the laboratory. Mobility lowering is defined as the ratio of CO₂ mobilities with additive to that without additive, MR.

Since in actual operations the additive will be supplied dissolved in the water phase, some mechanism had to be devised to transfer it to the gas phase where its mobility lowering could be calculated. This was accomplished by a simple volatility function using the conventional K value approach. The value of K was selected so that only a small mass of additive would be transferred to the gas phase. Although small in mass, the additive was assigned a high psuedo-viscosity in order to provide the desired mobility lowering with a minimum amount of mass transfer from the water to the gas phase.

The reservoir chosen for the simulation is the Wilmington Tar Zone that has been under commercial CO₂ enhancement since 1980. The CO₂ flood, operated by the Champlin Petroleum Company, is described in detail by Saner and Patton [105]. Reservoir conditions at the start of the simulation are presented in Table 6.1. The pattern chosen was a five acre 5-spot with the smallest geometrical unit, 1/8 of the 5-spot serving as the basis for the calculation. The reservoir was divided into three communicating vertical layers. The reservoir was further divided into rectangular matrix oriented parallel to the direction of flow between the injector and producer. The x-axis (line connecting the wells) was divided into eight segments. The y-dimension was divided into four segments to conform with the standard simulator matrix. Other pertinent parameters relative to the simulation, including relative permeability data are included in Appendix D.

The results obtained for the 3-D simulations corresponding to varying improvements in carbon dioxide mobility ratio are shown in Figure 6.1. These results quantify the degree to which mobility control does indeed enhance the quantity of crude oil recovered by the CO₂ process.

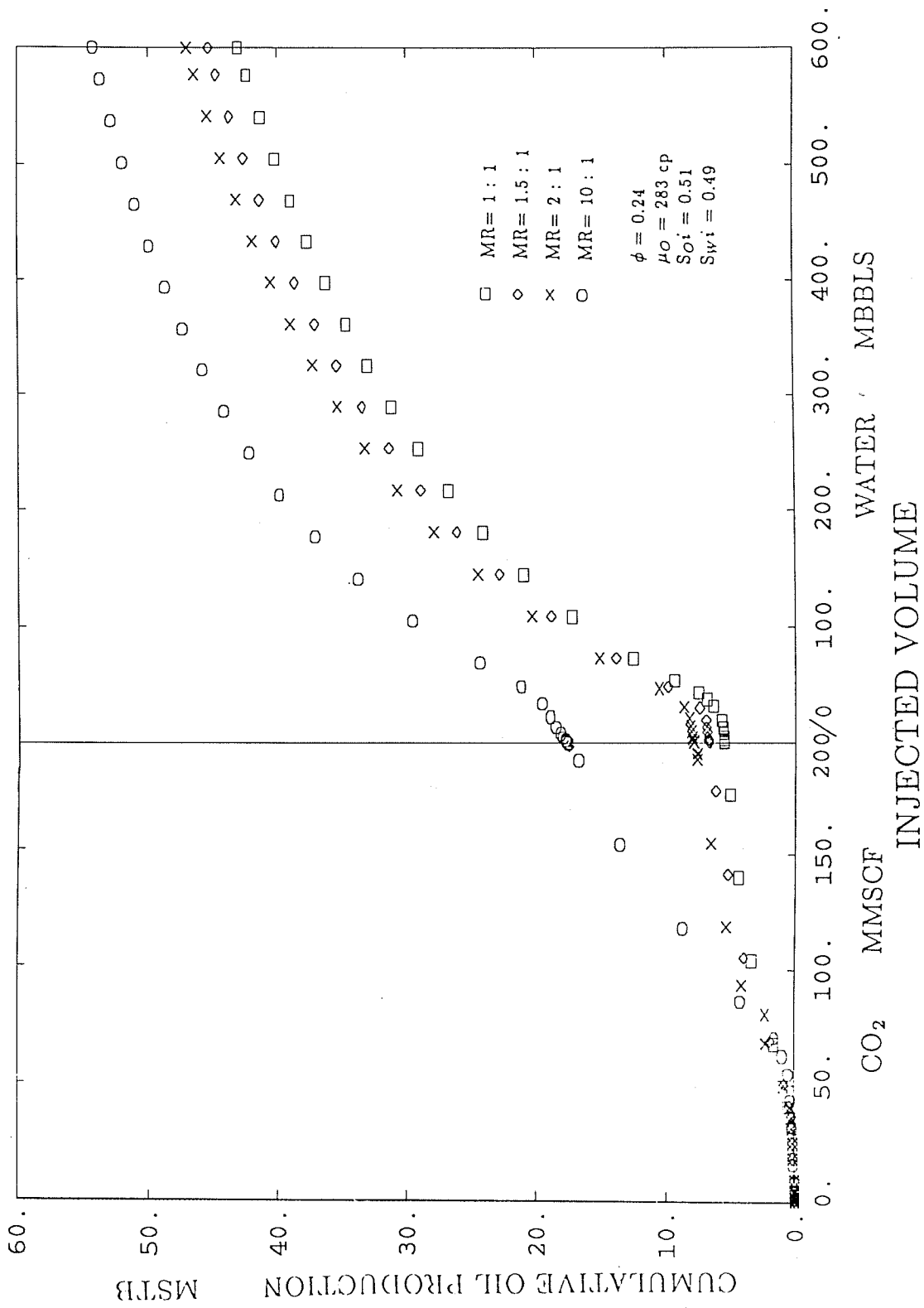


Figure 6.1 Enhanced Oil Production - Immiscible CO₂

TABLE 6.1
RESERVOIR AND FLUID PARAMETERS-
IMMISCIBLE CO₂ SIMULATION

Reservoir

Area = 20 acres

Net Sand = 66 ft.

Depth = 2500 ft.

Temperature, $T_i = 123^\circ\text{F}$

Pressure, $p_i = 1000$ psia

Porosity, $\phi = 0.24$

Saturations

Oil $S_{oi} = 0.51$

Water $S_{wi} = 0.49$

Viscosities

Oil, $\mu_o = 283$ cp

Water, $\mu_{uo} = 0.41$ cp

CO₂, $\mu_{CO_2} = 0.02$ cp

Complete reservoir response as a function of cumulative injection is also tabulated in Appendix D.

One surprising result was observed; namely, the additional oil production enhanced by mobility lowering of CO₂, was obtained during carbon dioxide injection. The tertiary waterflood maintained oil production at a comparable rate for all cases studied. For example, the lowering of the CO₂ mobility by a factor of 10 resulted in the production of 12,200 stock tank barrels of oil during the carbon dioxide

phase of the simulation, a 125 percent increase over that obtained during the injection of conventional carbon dioxide. Much of this incremental production was maintained throughout the subsequent waterflood phase. At the end of the simulation approximately 8900 total additional stock tank barrels had been produced due to the mobility control additive. This equates to a 20 percent final incremental improvement due to the mobility control additives.

From the commercial point of view, this is a very favorable situation. The fact that the enhanced oil production comes during the initial CO₂ injection process generates additional cash flow early in the process. The result is a very positive impact on the economics of the field operation.

The importance of simulating the displacement process in three dimensions is illustrated in Table 6.2. In this table the results obtained for 2-D simulation are compared with those of 3-D simulation. It can be seen that by considering permeability variations in the vertical direction, i.e., reservoir layering, one obtains a significant influence on the predicted oil recovery. Oil recovery is expectedly reduced by the addition of the vertical layering. However, the effect of the additive on enhancing oil recovery is increased as the additive partially overcomes the heterogeneous nature of the reservoir which is responsible for fostering lower production.

Figures 6.2-6.5 show the CO₂ saturation profiles at a time well into the CO₂ injection phase of the simulation. It is apparent by comparison of these contours that the addition of the mobility control additive increased the carbon dioxide saturation propagated throughout the reservoir at a comparable time in the project life; i.e., equal

TABLE 6.2
COMPARISON OF 3-D VS. 2-D SIMULATION
OF IMMISCIBLE CO₂ FLOODING

| | <u>3-D</u> | <u>2-D</u> |
|---|------------|------------|
| Oil Recovery After CO ₂ Injection, M bbL | | |
| MR = 1 (No Additive) | 5.5 | 12.0 |
| MR = 1.5 | 6.7 | 13.1 |
| MR = 2.0 | 7.9 | 14.0 |
| MR = 10.0 | 17.7 | 20.8 |
| Oil Recovery After Water Injection to Economic Limit, M bbL | | |
| MR = 1 (No Additive) | 43.1 | 51.1 |
| MR = 1.5 | 45.4 | 51.6 |
| MR = 2.0 | 47.1 | 52.5 |
| MR = 10.0 | 54.2 | 56.1 |

amount of carbon dioxide injection. Stated another way, the low viscosity, highly mobile carbon dioxide tends to finger through the reservoir displacing neither water nor oil efficiently. As a result, high saturations of carbon dioxide do not develop in the reservoir unless a mobility control additive is employed. This phenomenon is not necessarily bad because only a small gas phase saturation is required to guarantee that the oil in a given pore space is fully CO₂ saturated and, hence, any additional carbon dioxide saturation does little to promote enhanced flow of oil. However, as the oil is produced from the reservoir the void volume so generated must be compensated for with replacement by an injected fluid. In the case of carbon dioxide having a lower mobility, the CO₂ phase serves the purpose of filling the void created by the production

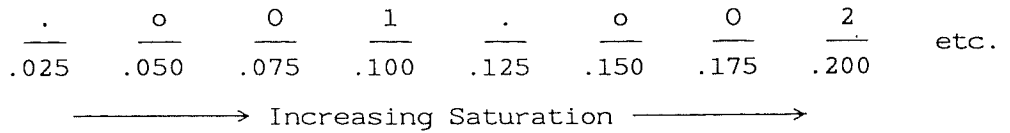
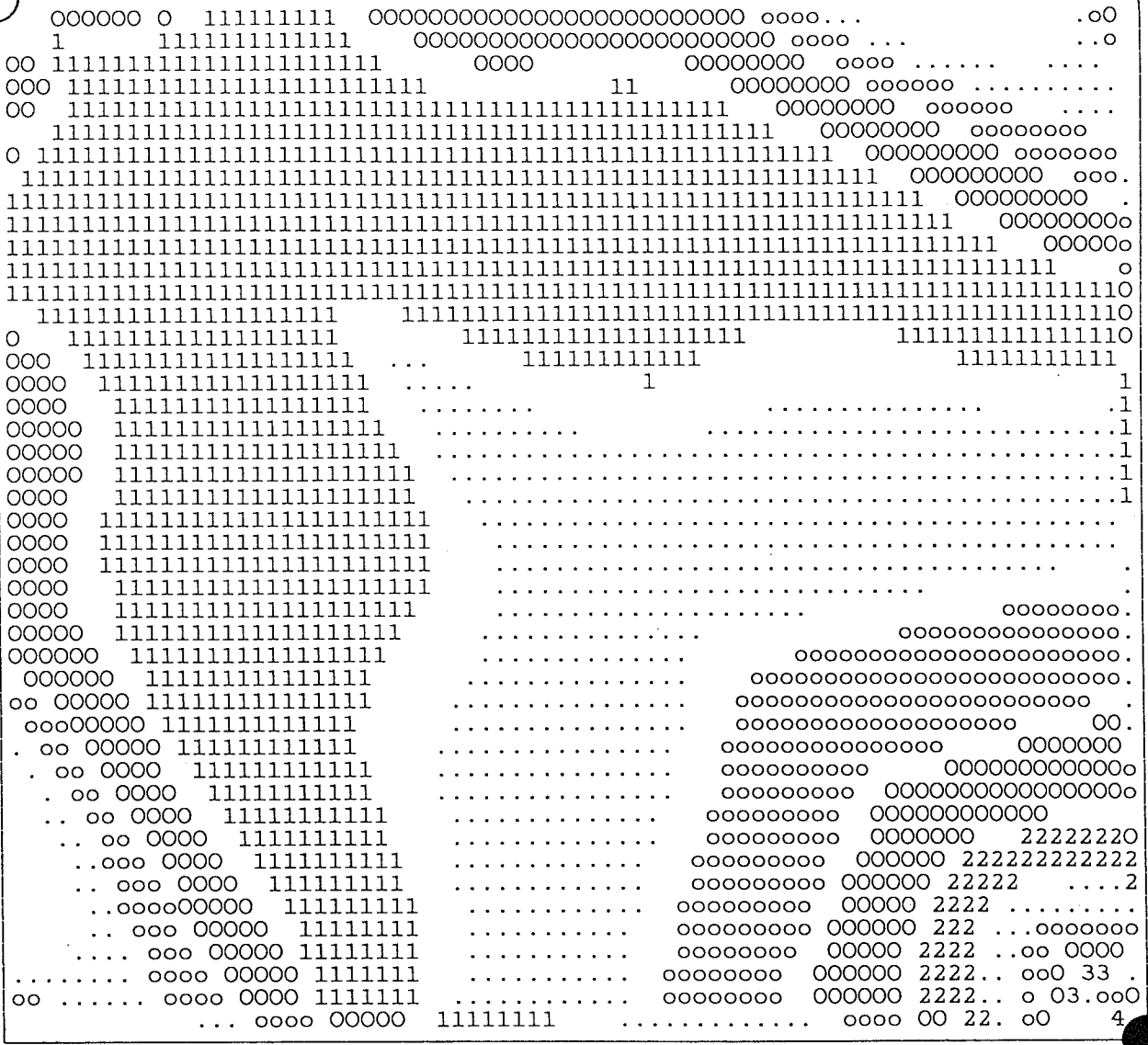


Figure 6.2 Base Case – No Mobility Control
 CO₂ Saturation Profile @ 0.24 P.V.
 Injected; 1/4 five spot pattern.

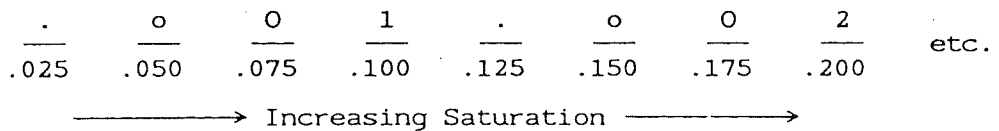
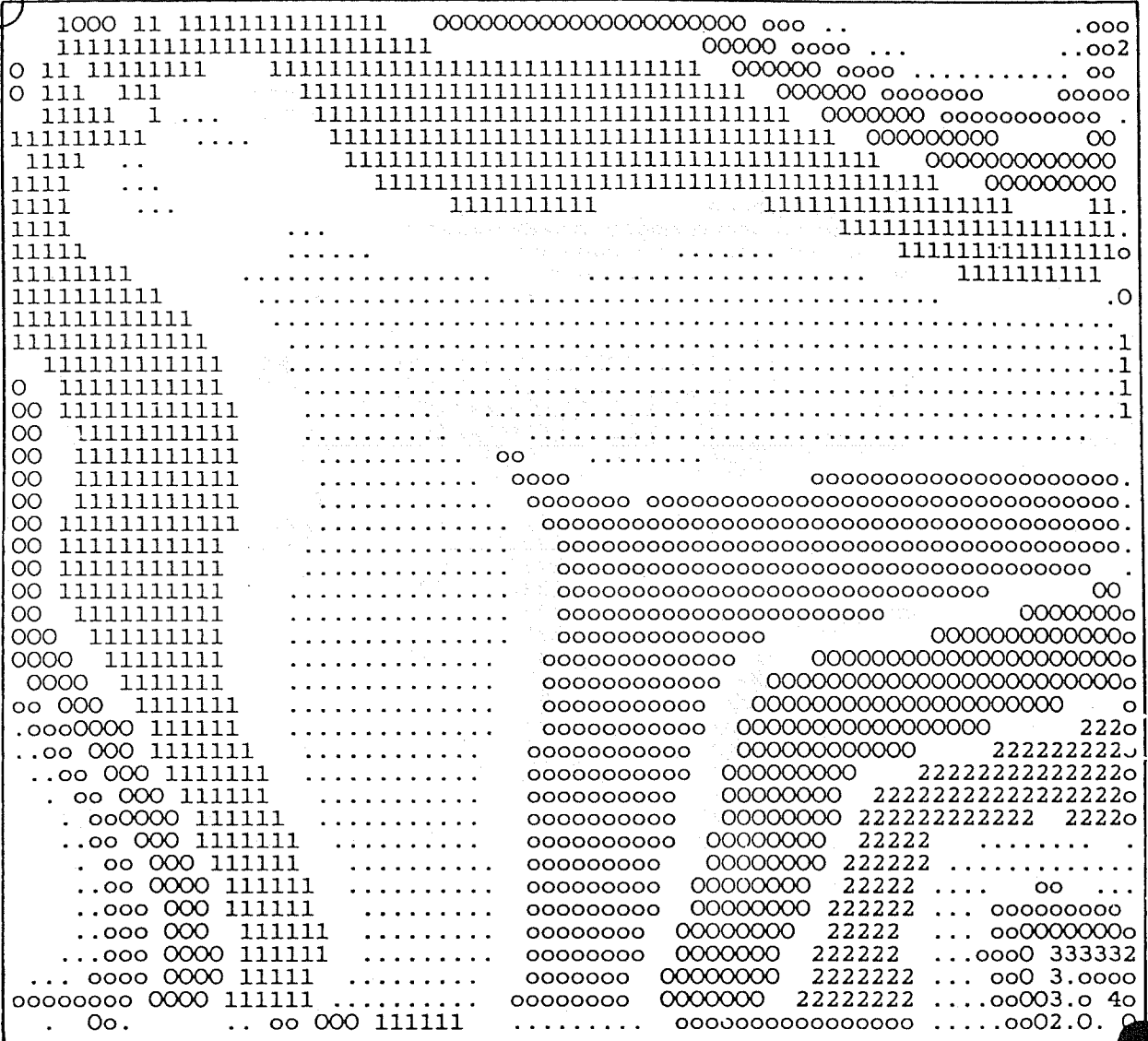


Figure 6.4 MR = 2.0 – CO₂ Saturation Profile @ 0.24 P.V. Injected; 1/4 five spot pattern.

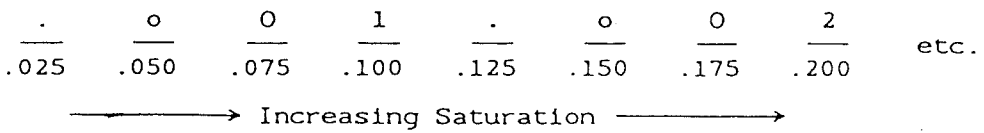
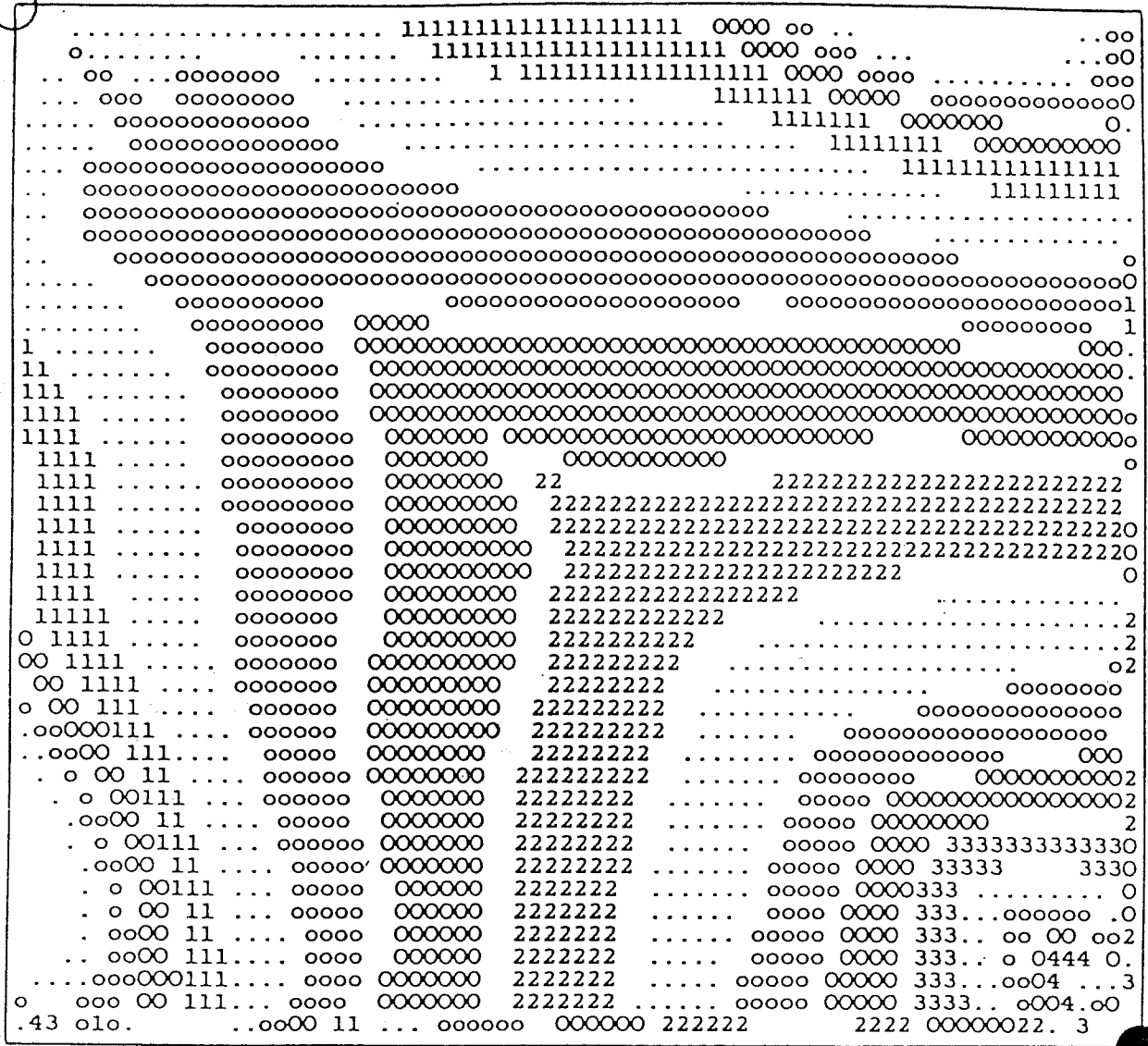


Figure 6.5 MR = 10. - CO₂ Saturation Profile
 @ 0.24 P.V. Injected; 1/4 five spot
 pattern.

of oil. In the base case, i.e., no mobility control, the voidage must be satisfied by the injection of additional quantities of water.

6.3 Miscible Displacement

The problem of simulating miscible displacement is relatively straightforward. The injected CO₂ phase can be assigned the properties of oil and, as such, will be miscible with the reservoir hydrocarbons in all proportions. This technique works in an acceptable manner for conventional CO₂ miscible displacement simulations and computer results usually match those obtained in laboratory floods.

The novel condition of carbon dioxide having a lowered mobility offers additional complexities far in excess of what one might expect. Mobility is defined as the relative permeability of a fluid divided by its viscosity, k_{rf}/μ_f . From this relationship, it is apparent that mobility can be lowered by either reducing relative permeability, k_{rf} , or increasing viscosity, μ_f . Unfortunately, this simplistic approach causes insurmountable problems in the simulation of a miscible carbon dioxide flood. For example, if one arbitrarily reduces k_{rCO_2} , it is found that the computer model also reduced k_{ro} since it is using the same relative permeability curve for both the hydrocarbon oil and the CO₂ "oil". It is, therefore, apparent that if the mobility of CO₂ is reduced by changing the relative permeability curve the mobility of the oil is erroneously also reduced. The net result is a low efficiency flood and little or no enhancement due to the carbon dioxide injection.

A similar problem arises if one chooses to lower mobility by increasing the viscosity of CO₂. This can be accomplished independently of the oil viscosity and is the approach that was adopted for

simulating miscible displacement during this research project. Unfortunately, it was discovered that when an increased viscosity assigned to the CO₂ was subsequently used to calculate the viscosity of the oil-CO₂ mixture flowing in the reservoir, an error was introduced that completely masked any enhancement due to lowering the mobility of CO₂. Due to the artificially high CO₂ liquid viscosity assumed, the calculated CO₂-oil solution also had a high viscosity and, as such, would not flow with the same facility as the low viscosity oil-CO₂ solution in the absence of mobility control.

The reservoir chosen for the simulation was the Maljamar reservoir. Located in Southwest New Mexico, this field has been under experimental CO₂ enhancement since 1980. The CO₂ test is operated by the Conoco, Inc. with offices in Hobbs, New Mexico. Reservoir conditions at the start of the simulation are presented in Table 6.2. The pattern chosen was a five acre 5-spot with the smallest geometrical unit, 1/8 of the 5-spot serving as the basis for the calculation.

The results of the 2-D simulations are the prediction shown in Figure 6.6. This Figure is obviously in error and is presented only to demonstrate the spurious results that result when mobility control is simulated by increasing the viscosity of injected carbon dioxide in the miscible displacement process. Lowering of the relative permeability function, since it affects both oil and carbon dioxide "oil", is anticipated to give similar spurious results.

Additional work on simulation development or more ingenious use of available software will be required in order to adequately simulate miscible CO₂ displacement with mobility control. The magnitude of this work is beyond the scope of this project. However, it is felt that this work is valuable and should be undertaken in the future.

TABLE 6.3
RESERVOIR AND FLUID PARAMETERS -
MISCIBLE CO₂ SIMULATION

Reservoir

Area = 20 acres

Net Sand = 66 ft.

Depth = 4033 ft.

Temperature, $T_i = 90^\circ\text{F}$

Pressure, $p_i = 1720$ psia

Porosity, $\phi = 0.10$

Saturations

Oil $S_{oi} = 0.30$

Water $S_{wi} = 0.70$

Viscosities

Oil, $\mu_o = 1.0$ cp

Water, $\mu_{uo} = 0.79$ cp

CO₂, $\mu_{CO_2} = 0.073$ cp

OIL PRODUCTION DUE TO MISCIBLE CO₂ INJECTION

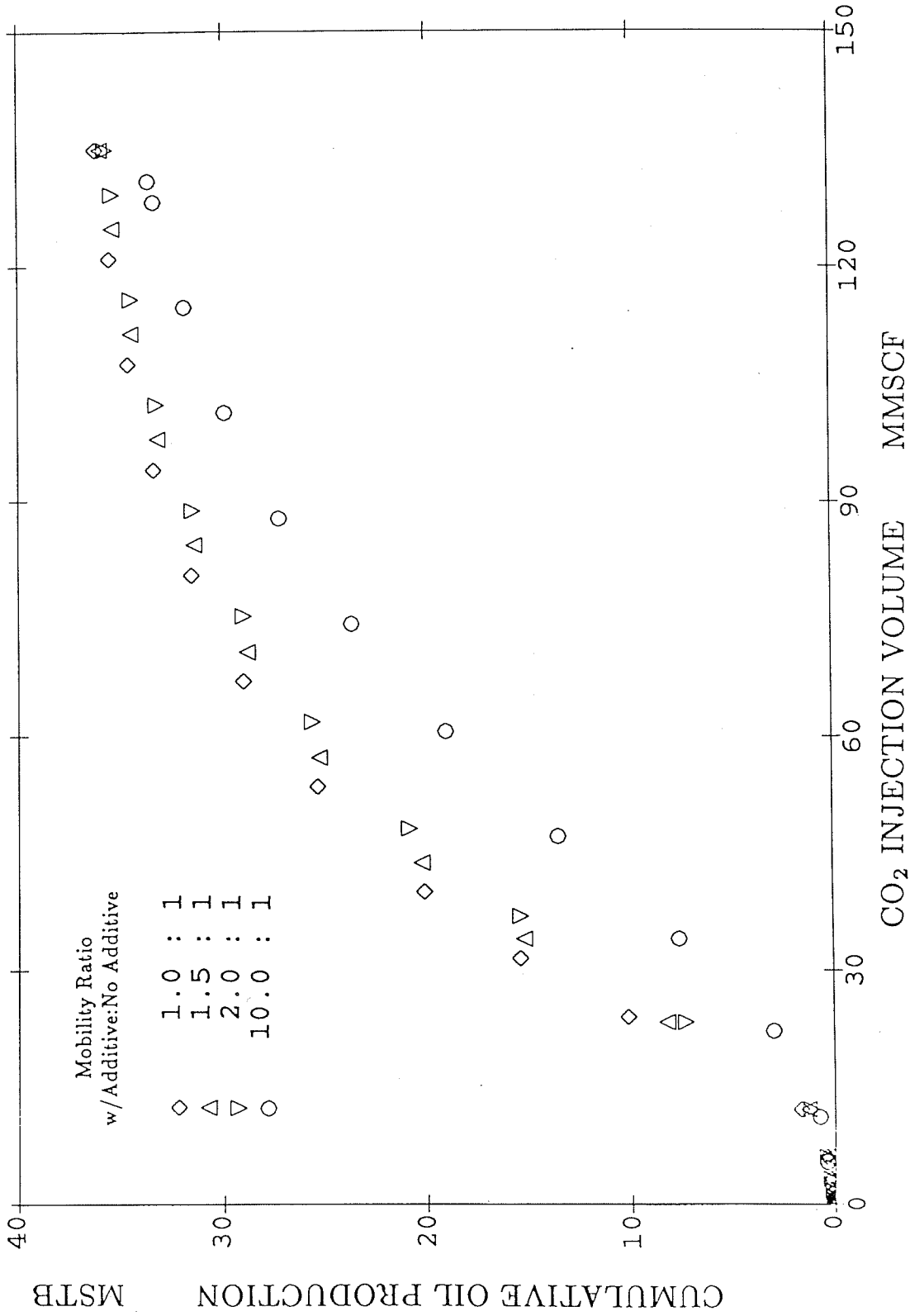


Figure 6.6 EOR - Miscible CO₂

SELECTED BIBLIOGRAPHY

1. Albrecht, R. A. and Marsden, S. S. "Foams as Blocking Agents in Porous Media." Soc. Pet. Eng. J. 10, (1970), 51-55.
2. Batra, V. K. and Holm, L. W. "Model Study as a Sealant for Leaks in Gas Storage Reservoirs." Soc. Pet. Eng. J. 10, (1970), 9.
3. Beeson, D. M. and Ortloff, G. D. "Laboratory Investigation of the H₂O-Driven CO₂ Process for Oil Recovery." J. Pet. Tech. (April 1959), 63-66.
4. Bernard, G. G. "Effect of Foam on Recovery of Oil by Gas-Drive." Prod. Monthly (January 1963), Vol. 27. No. 1, 18-21.
5. Bernard, G. G. and Holm, L. W. "Effect of Foam on Permeability of Porous Media to Gas." Soc. Pet. Eng. J. (September 1964), 267-274.
6. Bernard, G. G. and Holm, L. W. "Model Study of Foam as a Sealant for Leaks in Gas Storage Reservoirs." Soc. Pet. Eng. J. 10, (1970), 9-16.
7. Bernard, G. G., Holm, L. W. and Jacobs, W. L. "Effect of Foam on Trapped Gas Saturation and on Permeability of Porous Media to H₂O." Soc. Pet. Eng. J. (December 1965), 295-300.
8. Bird, R. B., et al., Transport Phenomena, Wiley, 1960.
9. Blauer, R. E., et al., Determination of Laminar, Turbulent, and Transitional Foam Flow Losses in Pipes, SPE 4885, presented at SPE 44th Annual California Regional Meeting, San Francisco, April 4-5, 1974.
10. Bond, D. C. and Bernard, G. G. "Rheology of Foams in Porous Media." Paper presented at SPE-AIChE Joint Symposium, AIChE 58th Annual Meeting, Dallas, TX (February 1966), 7-10.
11. Brown, A. G., Thuman, W. C. and McBain, J. W. "The Surface Viscosity of Detergent Solutions as a Factor in Foam Stability." J. Colloid. Sci. 8, (1953), 491-507.
12. Chatenever, Alfred and Inora, Whit, K. and Kyte, John R. "Microscopic Observation of Solution Gas-Drive Behavior." Journal of Pet. Tech. (August 1961), 806-816.
13. "CO₂ Grows as Recovery Tool." Oil & Gas J. (August 7, 1972), 22.
14. Craig, F. F. and Lumms, J. L. "Oil Recovery by Foam Drive." U.S. Patent (1965) 3,185,634.

15. Crawford, H. R., Neill, G. H., Buck, B. J., and Crawford, P. B. "CO₂-A Multipurpose Additive for Effective Well Stimulation." J. Pet. Tech. (March 1963), 237-242.
16. Crockety, D. H. "CO₂ Profile Control at Sacroc." Pet. Eng. (November 1975), 44-52.
17. David, A. and Marsden, S. S. "The Rheology of Foam." Soc. Pet. Eng. AIME, SPE No. 2544.
18. De Nevers, N. "A Calculation Method for Carbonated Water Flooding." Soc. Pet. Eng. Journal (March 1964), 9-20.
19. De Vries, A. J. "Foam Stability." Rubber Chemistry and Technology, 1957.
20. Dicharry, R. M. "Landmark CO₂ Injection Project Pacing Off At Sacroc." Pet. Engr. (December 1974), 22-25.
21. Dicharry, R. M., Perryman, T. L., and Ronquille, J. D. "Evaluation and Design of a CO₂ Miscible Flood Project-Sacroc Unit, Kelly-Snyder Field." J. Pet. Tech. (November 1973), 1309-1318.
22. Dodds, W. S., Stutzman, L. F., Sollami, B. J. "CO₂ Solubility in H₂O." Ind. & Eng. Chem. (1956), 92.
23. ERDA "Enhancement of Recovery of Oil & Gas." Progress Review #9 (January 1977).
24. Eugenev, A. E. and Turnier, V. N. "Rheological Properties of Foam in Porous Medium." Neft-I-Gaz Vol. 10 No. 12 (1967), 78-80.
25. Eydt, A. J. "Study of the Foamability of Solutions Using the Tensiolaminometric Technique." Jour. Am. Oil Chem. Soc., Vol. 45 (September 1968), 607-610.
26. Francis, A. W. "Ternary Systems of Liquid CO₂." J. Phys. Chem. Vol. 58 (December 1954), 1099-1114.
27. Fried, A. N. "The Foam-Drive Process For Increasing the Recovery of Oil." R. I. 5866, USBM (1961).
28. Gooktekin, A. "Experimental Studies on the Production of Foams in Porous Media with a View to Increasing the Recovery of Oil from a Reservoir." Erdoel-Erdgas-Z. Vol. 84, No. 6 (1968), 208-226.
29. Henderson, L. E. "The Use of Numerical Simulation to Design a CO₂ Miscible Displacement Project." J. Pet. Tech. (December 1974), 1327-1334.
30. Herschel, W. H., and R. Bulkley, Proceedings, ASTM, 26, Part II, 621-633, (1926).

31. Hoffer, M. S. and Rubin, E. "Flow Regimes of Stable Foams." Ind. Eng. Chem. Fundam. Vol. 8, No. 3 (August 1969), 438-489.
32. Holbrook, S. T., et al. "Rheology of Mobility Control Foams." Paper SPE/DOE 9809 presented at the 1981 SPE/DOE Second Joint Symposium on EOR, Tulsa, April 5-8, 1981.
33. Holm, L. W. "A Comparison of Propane and CO₂ Solvent Flooding Processes." AIChE Journal Vol. 7, No. 2 (June, 1961), 179-184.
34. Holm, L. W. "CO₂ Requirements in CO₂ Slug and Carbonated H₂O Oil Recovery Processes." Prod. Monthly (September 1963), 6-8, 26-28.
35. Holm, L. W. "CO₂ Solvent Flooding for Increased Oil Recovery." Pet. Trans. AIME Vol. 216 (1959), 225-231.
36. Holm, L. W. "Foam Injection Test in the Siggins Field, Illinois." J. Pet. Tech. Vol. 22 (1970), 1449-1506.
37. Holm, L. W. "Model Study of Foam as a Sealant for Leaks in Gas Storage Reservoirs." Soc. Pet. Engrs. Jour. Vol. 10 (1970), 9.
38. Holm, L. W. "Status of CO₂ and Hydrocarbon Miscible Oil Recovery Methods." J. Pet. Tech. (January 1976), 76-84.
39. Holm, L. W. "The Mechanism of Gas and Liquid Flow Through Porous Media in the Presence of Foam." Soc. Pet. Eng. J. (December 1968), 359-369.
40. Holm, L. W. and Josendal, V. A. "Mechanisms of Oil Displacement by CO₂." J. Pet. Tech. (December 1974), 1427-1438.
41. Holm, L. W. and O'Brian, L. J. "CO₂ Test at the Mead-Strawn Field." J. Pet. Tech. (1971), 431-442.
42. Huang, E. T. S., and Tracht, J. H. "The Displacement of Residual Oil by CO₂." Paper SPE 4735 Presented at the SPE-AIME 3rd Symposium on Improved Oil Recovery, Tulsa (April 22-24, 1974).
43. Jacob, W. M., Woodcock, K. E. and Grove, C. S. "Theoretical Investigation of Foam Drainage." Ind. & Chem. Vol. 48, No. 11 (November 1956), 2046-2051.
44. Kanda, M., Schechter, R. S. "On the Mechanism of Foam Formation in Porous Media." Paper SPE 6200, Society of Petroleum Engineers of AIME, 5200 North Central Expressway, Dallas, TX. 75206 1976.
45. Kohler, N. and G. Chauveteau. "Polysaccharide Plugging Behavior in Porous Media: Preferential Use of Fermentation Broth." Paper SPE 7425 presented at SPE 53rd Annual Fall Meeting, Houston, October 1-4, 1978.

46. Lacy, J. W., Faris, J. E. and Brinkman, F. H. "Effect of Bank Size on Oil Recovery in High Pressure Gas-Driven LPG-Bank Process." Journal of Pet. Tech. (August 1961), 806-816.
47. Marsden, S. S. and Khan, S. A. "The Flow of Foam through Short Porous Media and Apparent Viscosity Measurements." Soc. Pet. Eng. J. (March 1966), 17-25.
48. Marsden, S. S., Jr., Earligh, J. J. P., and Albrecht, R. A. "Use of Foam in Petroleum Operations." Paper presented at Seventh World Pet. Cong., Mexico City (April 2-7, 1967).
49. Mast, R. F. "Microscopic Behavior of Foam in Porous Media." Paper SPE 3997, Society of Petroleum Engineers of AIME, 6200 North Central Expressway, Dallas, TX 75206 1972.
50. Menzie, D. E., and Nielson, R. F. "A Study of the Vaporization of Crude Oil by CO₂ Repressurization." J. Pet. Tech. (November 1963), 1247-1252.
51. Metzner, A. B. "Flow of Non-Newtonian Fluids." Handbook of Fluid Dynamics, McGraw Hill, 1st Edition, 1961.
52. Michels, A., Botzen, A., and Schuurman, W. "The Viscosity of CO₂ Between 0°C and 75°C and at Pressures up to 2000 Atm." Physica XXIII (1957), 95-102.
53. Mies, G. D., Shedlousky, L., and Ross, J. "Foam Drainage." Jour. Phys. Chem. Vol. 49 (1949), 93-107.
54. Minnsieux, L. "Oil Displacement by Foams in Relation to Their Physical Properties in Porous Media." J. Pet. Tech. (January 1974), 100-107.
55. Oh, S. G. and Slattery, J. C. "Interfacial Tension Required for Significant Displacement of Residual Oil." Soc. Pet. Eng. J. Vol. 19 (1979).
56. Patton, J. T. "Enhanced Oil Recovery by Carbon Dioxide Flooding," Energy Communications (January 1978), 1-24.
57. Patton, J. T. and W. E. Holman. "Removal of Water from Boreholes," U.S. Patent 3,251,417, i. May 17, 1966.
58. Rathmell, J. J., Stalkup, F. I., and Hassinger, R. C. "A Laboratory Investigation of Miscible Displacement by CO₂." Paper SPE 3483 presented at the SPE-AIME 46th Annual Fall Meeting, New Orleans, October 3-6, 1971.
59. Raza, S. H. "Foam in Porous Media: Characteristics and Potential Applications." Soc. Pet. Engr. J. (December 1970), 328-336.

60. Raza, S. H. "Plugging Formations with Foam." U.S. Patent (January 27, 1970) 3,491,832.
61. Raza, S. H. and Marsden, S. S. "The Streaming Potential and the Rheology of Foam." Soc. Pet. Eng. J. (December 1967), 359-368.
62. Rogers, W. F. "Lab Apparatus for Studying Oil Well Subsurface Corrosion." Corrosion, Vol. 9 No. 25 (January 1953).
63. Rosen, M. J. and Solash, J. "Factors Affecting Initial Foam Height in the Ross-Miles Foam Test." Jour. Am. Oil Chem. Soc. (August 1969), 399-402.
64. Ross, S. "Bubbles and Foam: New General Law." Ind. & Eng. Chem., Vol. 61 No. 10 (October 1969), 49-57.
65. Scheideger, A. E. The Physics of Flow Through Porous Media, McMillan Company, 2 ed. New York, 1960.
66. Scott, J. O. and Forrester, C. E. "Performance of Domes Unit Carbonated Waterflood-First Stage." J. Pet. Tech. (September 1965), 1379-1384.
67. Shah, D. O. and Syslesui, C. A. "Molecular Interactions in Monolayers: Molecular Association and Foam Stability of Fatty Acids and Alcohols." Jour. A. Oil. Chem. Soc. (December 1969), 645-648.
68. "Shell Starts Miscible CO₂ Pilot in Mississippi's Little Creek Field." Oil & Gas J. (September 2, 1974), 52-53.
69. Shelton, J. L. and Schnieder, F. N. "The Effect of H₂O Injection on Miscible Flooding Methods Using Hydrocarbons and CO₂" Soc. Pet. Eng. J. (June 1975), 217-226.
70. Shelton, J. L. and Yarborough, L. "Multiple Phase Behavior in Porous Media During CO₂ or Rich-Gas Flooding." J. Pet. Tech. (September 1977), 1171-1178.
71. Shih, F. S. and Lemlich, R. "Continuous Foam Drainage and Overflow." Ind. Eng. Chem. Fundam. Vol. 10 No. 2 (1971), 2547-259.
72. Sibree, T. O. "The Viscosity of Froth." Trans. Farad. Soc. Volume 30 (1934), 325-331.
73. Simon, R. and Graue, D. J. "Generalized Correlations for Predicting Solubility, Swelling, and Viscosity Behavior of CO₂ - Crude Oil Systems." J. Pet. Tech. (January 1965), 102-106.
74. Slattery, J. C. "Interfacial Effects in the Displacement of Residual Oil by Foam." AICHE Journal. Vol. 25 No. 2 (March 1979), 283-289.

75. Smith, R. L. "Sacroc Initiates Landmark CO₂ Injection Project." Pet. Eng. (December 1971), 43-47.
76. Snyder, R. E. "Shell Starts CO₂ Injection Project in West Texas." World Oil (September 1972), 75-76.
77. Spangler, W. G. "Dynamic Foam Test." Jour. Am. Oil. Chem. Soc. Vol. 41 (April 1964), 300-306.
78. Stright, D. H., Aziz, K., Settari, A., and Starratt, F. E. "CO₂ Injection into Bottom-Water Undersaturated Viscous Oil Reservoirs." J. Pet. Tech. (October 1977), 1248-1258.
79. Van Meures, P. "The Use of Transparent Three-Dimensional Models for Study of the Mechanisms of Flow Processors in Oil Recoveries." Trans. AIME 210 (1957), 205-301.
80. Van Waxer, J. R., et al., Viscosity and Flow Measurement - A Laboratory Handbook of Rheology, Interscience Publishers, 1963.
81. Warner, H. R., Jr. "An Evaluation of Miscible CO₂ Flooding in Waterflooded Sandstone Reservoirs." J. Pet. Tech. (October 1977), 1339-1347.
82. White, R. W. "Oil Recovery by CO₂: Past and Future." Pet. Engr. (December 1971), 58-59.
83. Whorton, L. P. Brownscombe, E. R. and Dyes, A. B. "Method for Producing Oil by Means of CO₂." U.S. Patent (December 30, 1952) 2,623,596
84. Wilson, Keith. "Enhanced Recovery Inert Gas Processes Compared." Oil & Gas J. (July 31, 1978) 76.
85. Bernard, G. G., Holm, L. W. and Harvey, C. P. "Use of Surfactant to Reduce CO₂ Mobility in Oil Displacement." Soc. Pet. Eng. J. (August 1980), 281-292.
86. Buckley, S. E. and Leverett, M. C. "Mechanisms of Fluid Displacement in Soils." Trans. AIME 142, (1942) 152.
87. Johnson, E. F., Bossler, D. P. and Naumann, V. O., "Calculation of Relative Permeability from Displacement Experiments," Trans. AIME 216, 370 (1959).
88. Patton, J. T. "Enhanced Oil Recovery by CO₂ Foam Flooding." Final Report, U.S. Doe DE8200905 (April 1982).
89. Collines, R. E. Flow of Fluids Through Porous Media, The Petroleum Publishing Co., Tulsa (1976).
90. Kestin, J., Whitelaw, J. H. and Zien, T. F., Physica 30, 161 (1964).
91. Michels, A., Bolzen, A., and Schuurman, Physica 20, 1141 (1941).

92. Perry, R. H. and Chilton, C. H. "Chemical Engineers' Handbook," 3rd ed., McGraw-Hill, New York (1973).
93. Welge, H. J. "A Simplified Method for Computing Oil Recovery by Gas or Water Drive," Trans. AIME 195, 91 (1952).
94. Bolt, Beranek and Newman, Inc., RS/1 Users Guide (version 12.00), Cambridge, Mass. (1983).
95. Patton, J. T. Holbrook, S. T. and Hsu, W., "Rheology of Mobility-Control Foams," Soc. Pet. Eng. J., 456 (1983).
96. Dellinger, S. E., Patton, J. T., and Holbrook, S. T., "CO₂ Mobility Control," Soc. Pet. Eng. J., 191 (1984).
97. Holbrook, S. T., "Mobility Control of Gases in Enhanced Oil Recovery Processes," in preparation.
98. Patton, John T., "Enhanced Oil Recovery by CO₂ Foam Flooding. Annual Report for October 1, 1982 - September 30, 1983. U.S. Publ. DOE/MC/16551-10 (1984).

PATENTS & THESES

101. Bernard, G. G.: "Foam Drive Oil Recovery Process," U.S. Patent No. 3,529,668 (1970).
102. Bernard, G. G. and Bond, D. C.: "Forming Foam Under Reservoir Conditions in Petroleum Recovery Process", U.S. Patent No. 3,318,379 (1967).
103. Bernard, G. G. and Bond, D. C.: "Secondary Recovery Method," U.S. Patent No. 3,369,601 (1968).
104. Bernard, G. G. and Holm, L. W.: "Method for Recovering Oil from Subterranean Formations," U.S. Patent No. 3,342,256 (1967).
105. Bernard, G. G. and Rai, C.: "Method of Secondary Recovery Employing Successive Foam Drives of Different Ionic Characteristics," U.S. Patent No. 3,323,588 (1967).
106. Bond, D. C. and Holbrook, O. C.: "Gas Drive Oil Recovery Process," U.S. Patent No. 2,866,507 (1958).
107. Craig, F. F. and Lummus, J. L.: "Oil Recovery by Foam Drive," U.S. Patent (1965), 3,185,634.
108. Deming, J. R.: "Fundamental Properties of Foams and Their Effects on the Efficiency of the Foam Drive Process," M.S. Thesis, The Pennsylvania State U. (1964).
109. Holm, L. R. W.: "Secondary Recovery Process Using Gas-Liquid Drive Fluids," U.S. Patent No. 3,177,939 (1965).
110. Holman, W. E. and Patton, J. T.: "Removal of Water Boreholes," U.S. Patent No. 3,251,417 (1966).
111. Patton, J. T., "Modified Heteropolysaccharides," U.S. Patent 3,729,460, i. May 24, 1973.
112. Raza, S. H.: "Plugging Formations with Foam." U.S. Patent No. 3,491,832 (January 27, 1970).
113. Whorton, R. W.: "Oil Recovery by CO₂: Past and Future." Pet. Engr. (December 1971), 58-59).

APPENDIX A

APPENDIX A

COMPUTER SIMULATION OF MOBILITY CONTROL CO₂ FLOOD

A.1 Linear Displacement with Two Phases Flowing

A.1.1 Objective

The procedure detailed below predicts the volume of water that will be produced as CO₂ is injected into a porous medium during an immiscible CO₂ flood where the pressure difference across the porous medium is held constant. The procedure is appropriate even when oil is present, if the oil is immobile. A means of extending the procedure to the case where three phases are flowing simultaneously is described in Section 2.2.

A.1.2 Required Data

To use the present method; one must know:

- (a) the pressure difference (ΔP) across the porous medium;
- (b) the permeability (k) of the porous medium;
- (c) the initial saturations with respect to oil (S_{oi}), water (S_{wi}) and gas (S_{gi});
- (d) the relationship between the relative water permeability (k_{rw}) and water saturation (S_w);
- (e) the relationship between the relative gas permeability (k_{rg}) and total liquid saturation (S_L). The latter is the sum of the water and oil saturations;
- (f) the viscosities of the gas (μ_g) and water (μ_w).

In general, the relationships between the relative permeabilities and liquid saturations must be determined experimentally. A procedure for such determination is described in Section Three, and the underlying mathematical basis is provided in Sections 2.3 and following.

A.1.3 Simulation Strategy

The porous medium is envisioned as being divided into a number of segments by imaginary partitions perpendicular to the direction of flow. The time required for the flood is divided into numerous small intervals. During any given interval, the properties of each segment (i.e., saturations, permeabilities and pressure gradient) are taken as constant.* Flows of gas and water into and out of each segment are calculated for the first time increment, then the saturations and relative permeabilities in every segment are revised, and the pressure gradients are calculated anew. The next time interval is considered, and the flows and properties are calculated for each segment as before. The procedure is repeated for successive time intervals. An example follows.

A.1.4 Example

Let the segments shown (cell blocks perpendicular to flow) be of equal length (L) and designate them (from inlet to outlet) as 1,2,3, ...i...n. Designate time increments as 1,2,3...j... For example, initially (at time 0), the third segment has water saturation $S_{w,3,0}$ and its relative permeability to water is $k_{rw}(S_{w,3,0})$ where the latter denotes that k_{rw} is a function of S_w . Assume time intervals (Δt) are equal.

*This is a satisfactory assumption if the segments and time intervals are short enough.

Step 1: Calculate the pressure gradient across each segment. Initially, if liquid saturations are equal in all segments, the gradients are equal and are given by Eq. A.1.1:

$$\left(\frac{\Delta P}{\Delta L}\right)_{i,o} = \frac{\Delta P}{\Delta n} \quad (\text{A.1.1})$$

where

ΔP is the pressure drop across the segment;

ΔL is the length of the segment; and

n is the total number of segments.

Step 2: Starting at the outlet of the porous medium (segment n), calculate the incremental flow rates of gas and liquid for the first time interval using Darcy's Law in finite difference form as given by Eqs. A.1.2 and A.1.3.

$$\left(\frac{\Delta G}{\Delta t}\right)_{n,1} = \frac{-kk}{\mu_g A} r_{g,n,o} \left(\frac{\Delta P}{\Delta L}\right)_{n,o} \quad (\text{A.1.2})$$

$$\left(\frac{\Delta L}{\Delta t}\right)_{n,1} = \frac{-kk}{\mu_w A} r_{w,n,o} \left(\frac{\Delta P}{\Delta L}\right)_{n,o} \quad (\text{A.1.3})$$

where

A is the cross-sectional area of the segment perpendicular to the director of flow, and

ΔG and ΔL denote the incremental volumes of gas and liquid leaving the segment. They may be calculated using Eqs. A.1.4.

$$\Delta G_{n,1} = \left(\frac{\Delta G}{\Delta t}\right)_{n,1} \Delta t \quad (\text{A.1.4a})$$

$$\Delta L_{n,1} = \left(\frac{\Delta L}{\Delta t}\right)_{n,1} \Delta t \quad (\text{A.1.4b})$$

Step 3: Move left to the adjacent segment, (i.e., decrement the index i). Calculate $\Delta G_{n-1,1}/\Delta t$ using Darcy's Law again, and thence $\Delta G_{n-1,1}$.

Step 4: Noting that the total volume leaving a segment must equal the total volume that enters its neighbor to the right, calculate the incremental volume of liquid leaving segment n-1 using Eq. A.1.5.

$$(\Delta L + \Delta G)_{n-1,1} = (\Delta L + \Delta G)_{n,1} \quad (\text{A.1.5})$$

Step 5: Move left again and calculate ΔG and ΔL for segment n-2 as was done for segment n-1. Repeat the process for successive segments until the inlet of the porous medium is reached (i.e., until $\Delta L_{1,1}$ and $\Delta G_{1,1}$ have been calculated).

Step 6: Calculate the volume of gas injected during the increment 1 using Eq. A.1.6:

$$\Delta G_{o,1} = (\Delta G + \Delta L)_{1,1} \quad (\text{A.1.6})$$

Note that $\Delta G_{o,1}$ is the volume of injected gas which produced a volume of liquid $\Delta L_{n,1}$ at the opposite end of the porous medium. This is just the relationship that is desired.

Step 7: Calculate new values for the volumes of water and gas residing in each segment and the saturations in each segment:

$$G_{i,1} = G_{i,0} - \Delta G_{i,1} + \Delta G_{i-1,1} \quad (\text{A.1.7})$$

$$L_{i,1} = L_{i,0} - \Delta L_{i,1} + \Delta L_{i-1,1} \quad (\text{A.1.8})$$

$$S_{w,i,1} = L_{i,1} / (\phi A L) \quad (\text{A.1.9})$$

$$S_{L,i,1} = S_{w,i,1} + S_o \quad (\text{A.1.10})$$

where

$G_{i,1}$ is the volume of gas in the ith segment after one time increment;

$L_{i,1}$ is the volume of water in the ith segment;

ϕ is the porosity of the medium; and

S_o is the oil saturation, a constant.

Step 8. Update the values of k_{rg} and k_{rw} for each segment using tables of experimental results that relate k_{rg} to S_L and k_{rw} to S_w .

Step 9: Revise the pressure gradients using Darcy's Law and the values for $\Delta L_{i,j=1}$ which were previously calculated by difference (see Eq. A.1.5).

$$\left(\frac{\Delta P}{\Delta L}\right)_i = - \frac{\Delta_w A}{kk_{rw,i,1}} \left(\frac{\Delta L}{\Delta t}\right)_{i,1} \quad (A.1.11)$$

To prevent round-off errors from accumulating, it is advisable to normalize the resulting values for p so that

$$\sum_i (\Delta_{pi}) = \Delta P \quad (A.1.12)$$

This may be done by multiplying each Δ_{pi} by the ratio $\Delta P / \sum (\Delta_{pi})$.

Step 10: Proceed to the next time interval (i.e., increment j by one).

Step 11: Calculate the volumes of gas and liquid produced during the second time interval using Eqs. A.1.2 and A.1.3 and the revised values for pressure gradients and relative permeabilities. Add the value obtained for $\Delta L_{n,2}$ to that obtained during the first time interval to get the cumulative water production at the end of two time intervals.

Step 12: Proceed as described in Steps 3-5 to calculate the volumes of gas and liquid produced from each segment; and, as in Step 6, to calculate the volume of gas injected during the second time interval. Add the value of $G_{o,2}$ to that obtained during the first time interval to get the cumulative volumes of gas injected at the end of two time intervals.

Step 13: Revise the saturations, relative permeabilities, and pressure gradients for all segments as described in Steps 7-9.

Step 14: Repeatedly increment the time and perform the calculation sequence of Steps 2-9 to find how cumulative water production is related to cumulative gas injection.

A.1.5 Allowance for CO₂ Solubility

To provide a more realistic model, the dissolution of CO₂ in the water and oil must be included in the above procedure. This may be done by amending Step 3 in the preceding example thusly: When gas enters a segment for the first time, the volume of gas leaving the preceding segment ($\Delta G_{i-1,j}$) is increased by the amount that is predicted (from experimental results) to dissolve in the liquids that are present in the invaded segment.

Table A.1. Relative Permeabilities to Gas and Water
When No Surfactant is Present

| Liquid Saturation | Gas Relative Permeability | Water Saturation | Water Relative Permeability |
|-------------------|---------------------------|------------------|-----------------------------|
| | | .836* | .255* |
| .881 | .005 | .734 | .162 |
| .871 | .006 | .724 | .157 |
| .858 | .008 | .710 | .149 |
| .832 | .011 | .684 | .136 |
| .801 | .014 | .654 | .120 |
| .767 | .018 | .620 | .104 |
| .722 | .023 | .574 | .084 |
| .680 | .028 | .532 | .067 |
| .643 | .032 | .495 | .054 |
| .606 | .038 | .458 | .042 |
| .578 | .043 | .430 | .033 |
| .554 | .050 | .407 | .028 |
| .541* | .056* | .393 | .025 |

*Independently-measured values used to scale others in the column.

Table A.2. Relative Permeabilities to Gas and Water
When Pluradyne SF-27 Present

| Liquid Saturation | Gas Relative Permeability | Water Saturation | Water Relative Permeability |
|-------------------|---------------------------|------------------|-----------------------------|
| .981 | .003 | .740* | .255* |
| .967 | .004 | .726 | .239 |
| .953 | .006 | .712 | .225 |
| .938 | .007 | .697 | .211 |
| .915 | .009 | .674 | .193 |
| .892 | .011 | .651 | .176 |
| .870 | .013 | .629 | .160 |
| .840 | .015 | .599 | .141 |
| .812 | .018 | .571 | .124 |
| .785 | .021 | .544 | .108 |
| .754 | .024 | .513 | .091 |
| .725 | .027 | .484 | .074 |
| .699 | .031 | .458 | .059 |
| .671 | .034 | .430 | .043 |
| .645 | .038 | .404 | .029 |
| .622 | .041 | .381 | .016 |
| .600* | .044* | .359 | .003 |

*Independently-measured values used to scale others in the column.

Table A.3. Relative Permeabilities to Gas and Water
When Stepanflo-50 Present

| Liquid Saturation | Gas Relative Permeability | | Water Saturation | Water Relative Permeability |
|-------------------|---------------------------|------|------------------|-----------------------------|
| | | | .85* | .35* |
| .651 | .024 | .024 | .586 | .079 |
| .639 | .024 | .024 | .574 | .072 |
| .628 | .025 | .025 | .563 | .064 |
| .611 | .026 | .026 | .546 | .055 |
| .595 | .027 | .027 | .530 | .047 |
| .580 | .027 | .027 | .515 | .040 |
| .561 | .028 | .028 | .496 | .033 |
| .544 | .029 | .029 | .479 | .026 |
| .527 | .029 | .029 | .462 | .021 |
| .508 | .030 | .030 | .433 | .016 |
| .491 | .031 | .031 | .426 | .012 |
| .476 | .033 | .033 | .411 | .009 |
| .460* | .037* | | .395 | .007 |

*Independently-measured values used to scale others in the column.

The following table shows the results of the survey conducted in the year 1998. The data is presented in a tabular format, with columns representing different categories and rows representing individual data points. The table is organized into two main sections, each containing a list of items and their corresponding values.

| Category | Item 1 | Item 2 | Item 3 | Item 4 | Item 5 |
|-----------|--------|--------|--------|--------|--------|
| Section 1 | 101 | 102 | 103 | 104 | 105 |
| | 106 | 107 | 108 | 109 | 110 |
| | 111 | 112 | 113 | 114 | 115 |
| | 116 | 117 | 118 | 119 | 120 |
| | 121 | 122 | 123 | 124 | 125 |
| | 126 | 127 | 128 | 129 | 130 |
| | 131 | 132 | 133 | 134 | 135 |
| | 136 | 137 | 138 | 139 | 140 |
| | 141 | 142 | 143 | 144 | 145 |
| | 146 | 147 | 148 | 149 | 150 |
| Section 2 | 151 | 152 | 153 | 154 | 155 |
| | 156 | 157 | 158 | 159 | 160 |
| | 161 | 162 | 163 | 164 | 165 |
| | 166 | 167 | 168 | 169 | 170 |
| | 171 | 172 | 173 | 174 | 175 |
| | 176 | 177 | 178 | 179 | 180 |
| | 181 | 182 | 183 | 184 | 185 |
| | 186 | 187 | 188 | 189 | 190 |
| | 191 | 192 | 193 | 194 | 195 |
| | 196 | 197 | 198 | 199 | 200 |

A P P E N D I X B

FIGURE B.1

STATIC FOAM TEST #1: ALIPAL CD-128

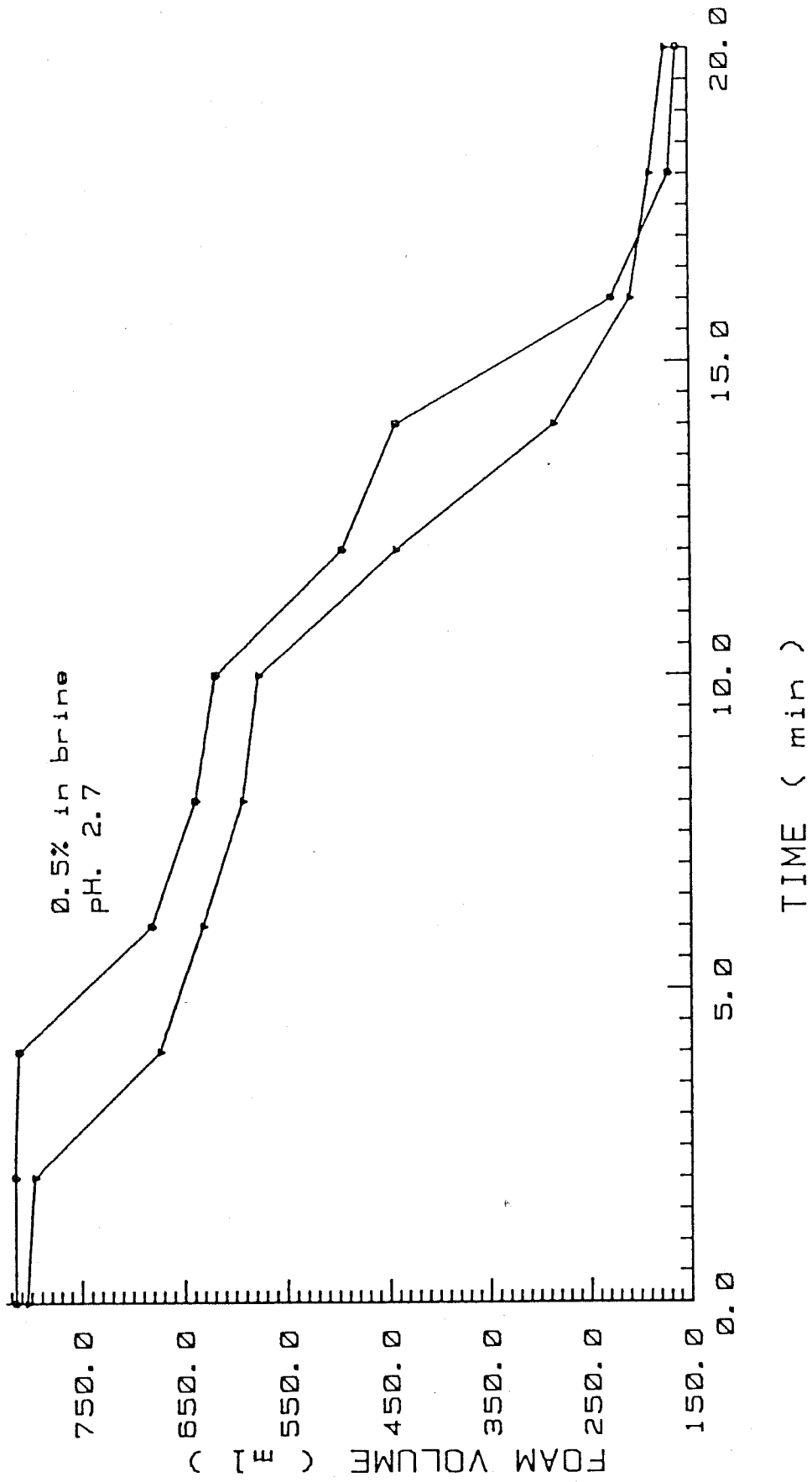


FIGURE B.2

STATIC FOAM TEST #'s 1&2: ALIPAL CD-128 w/10cc OF CRUDE

0.5% in brine
pH=2.5
▽ Run #1
○ Run #2

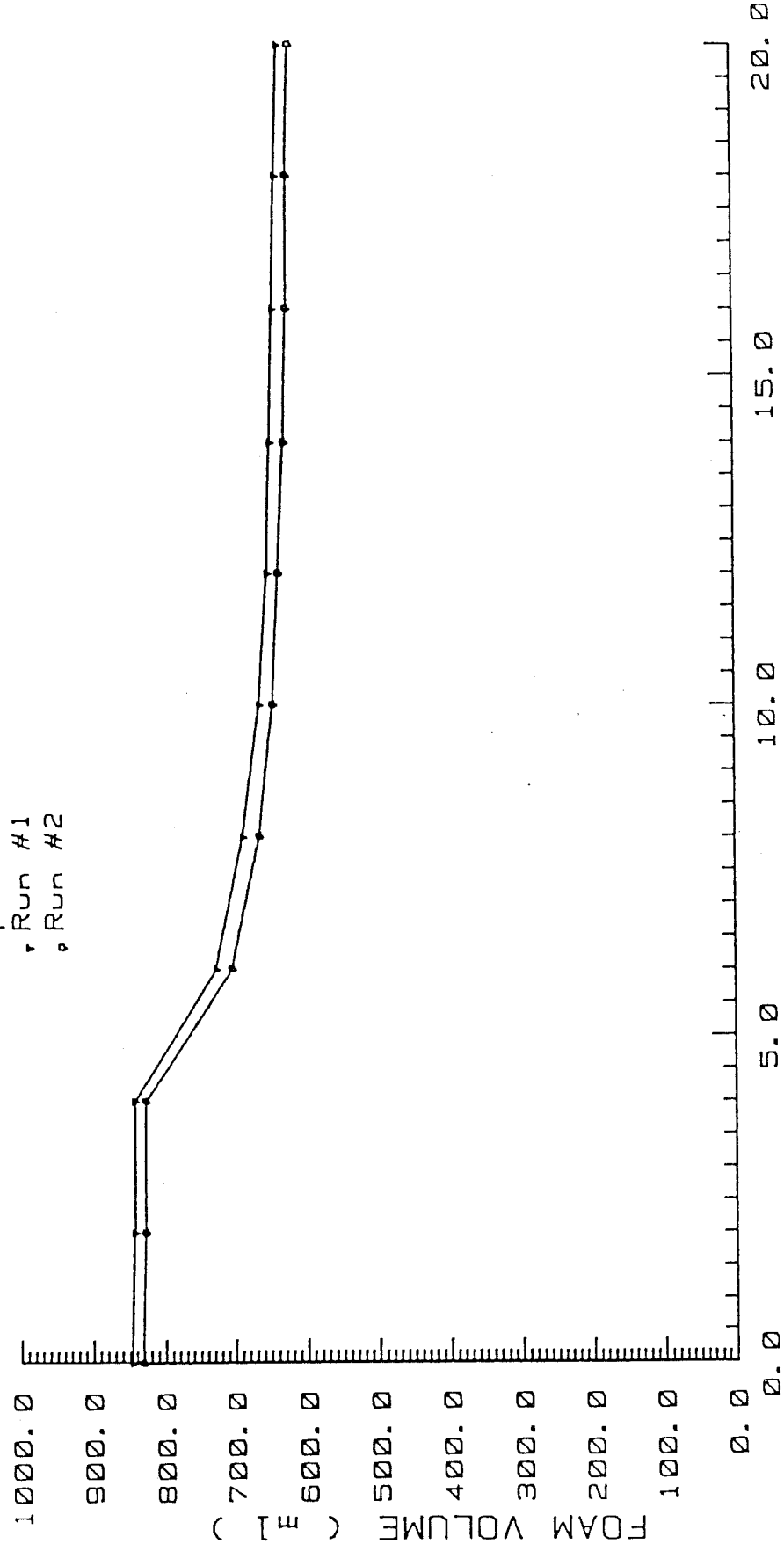


FIGURE B.3

STATIC FOAM TEST #4: WITCOLATE 1276

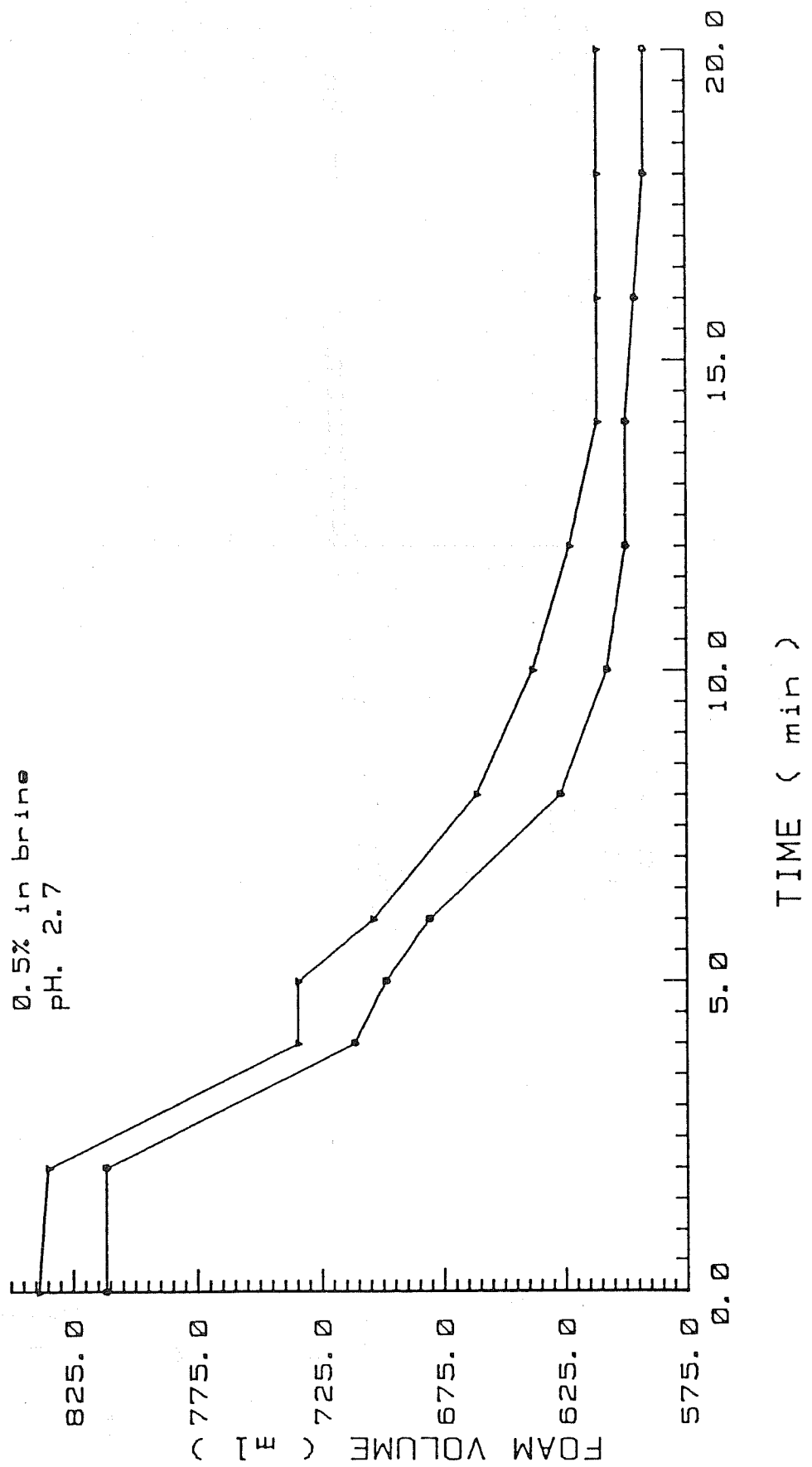


FIGURE B.4

STATIC FOAM TEST #'s 788: WITCOLATE 1276 w/10cc OF CRUDE

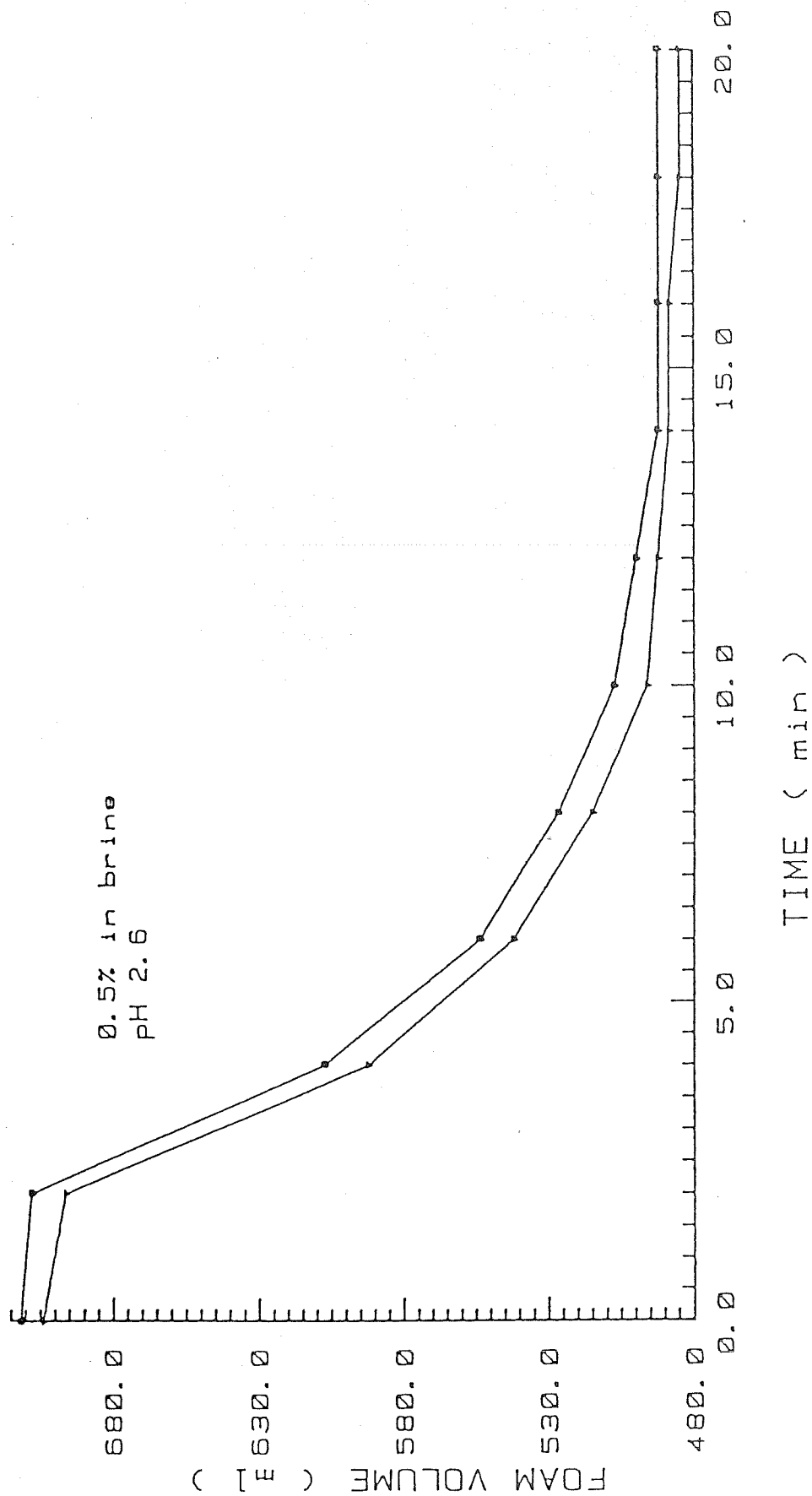


FIGURE B.5

STATIC FOAM TEST #2: NEODOL 23-6.5

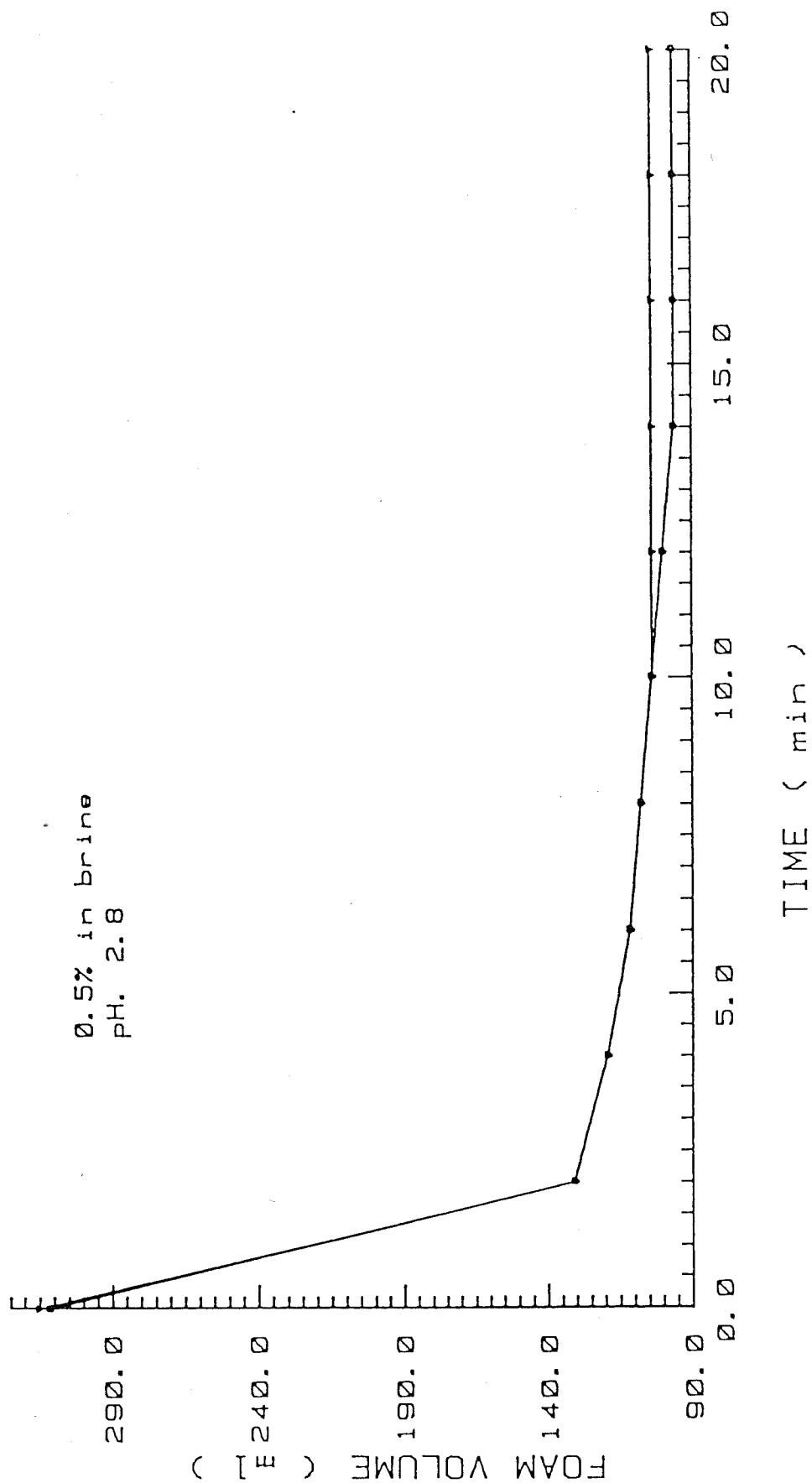


FIGURE B.6

STATIC FOAM TEST #'s 384: NEODOL 23-6.5, w/10cc OF CRUDE

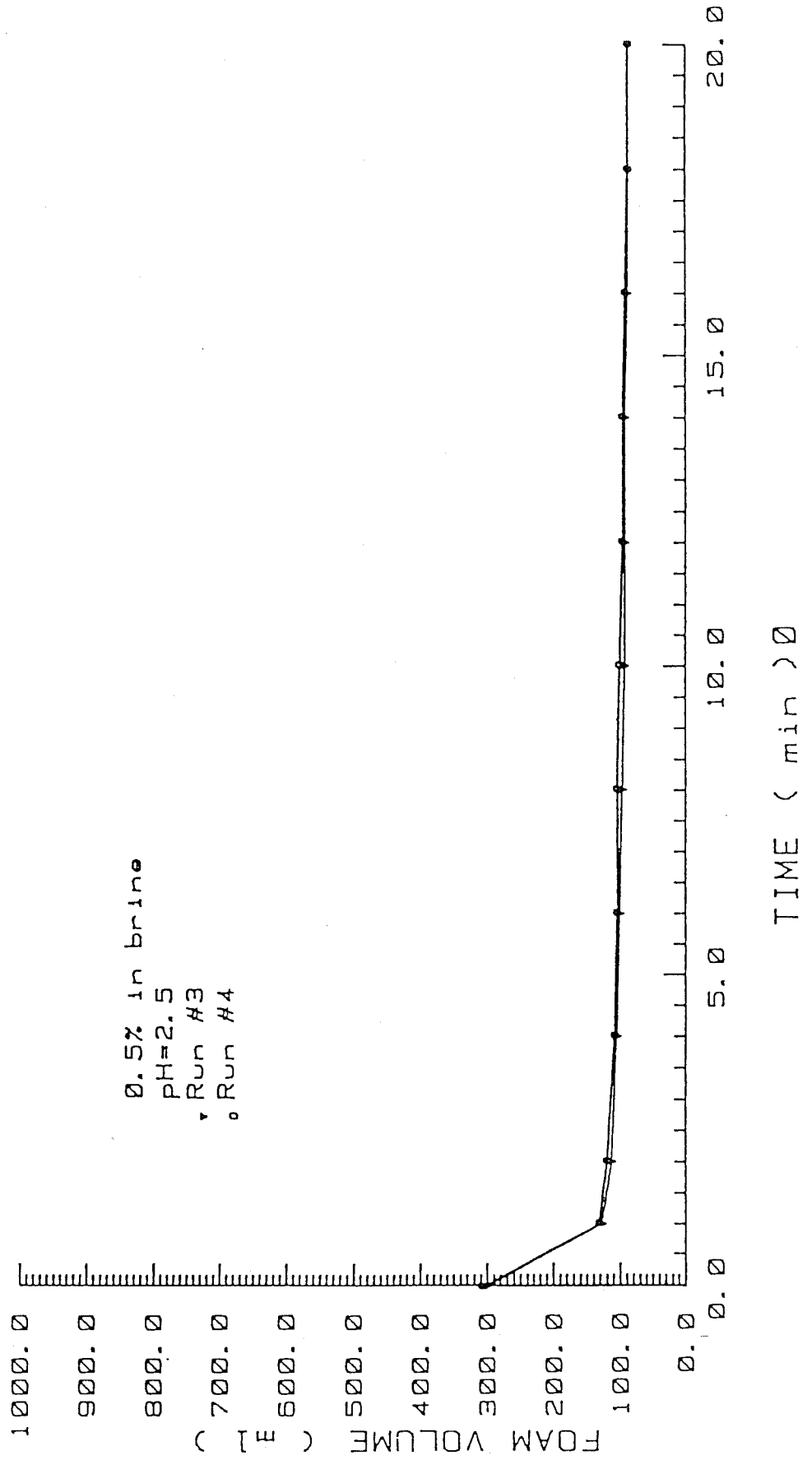


FIGURE B.7

STATIC FOAM TEST #3: PLURONIC F-68

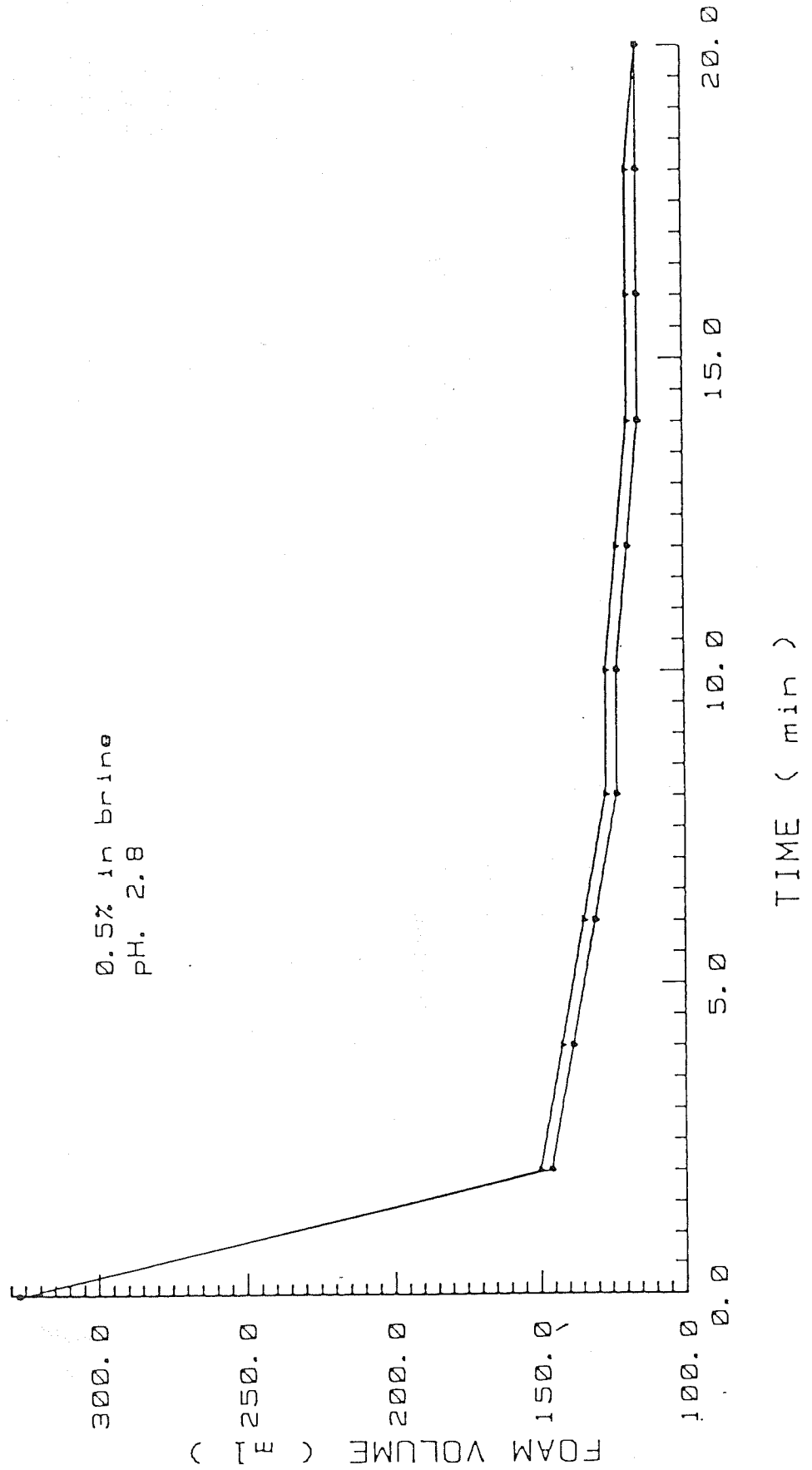


FIGURE B.8

STATIC FOAM TEST #'s 586: PLURONIC F-68, w/10cc OF CRUDE

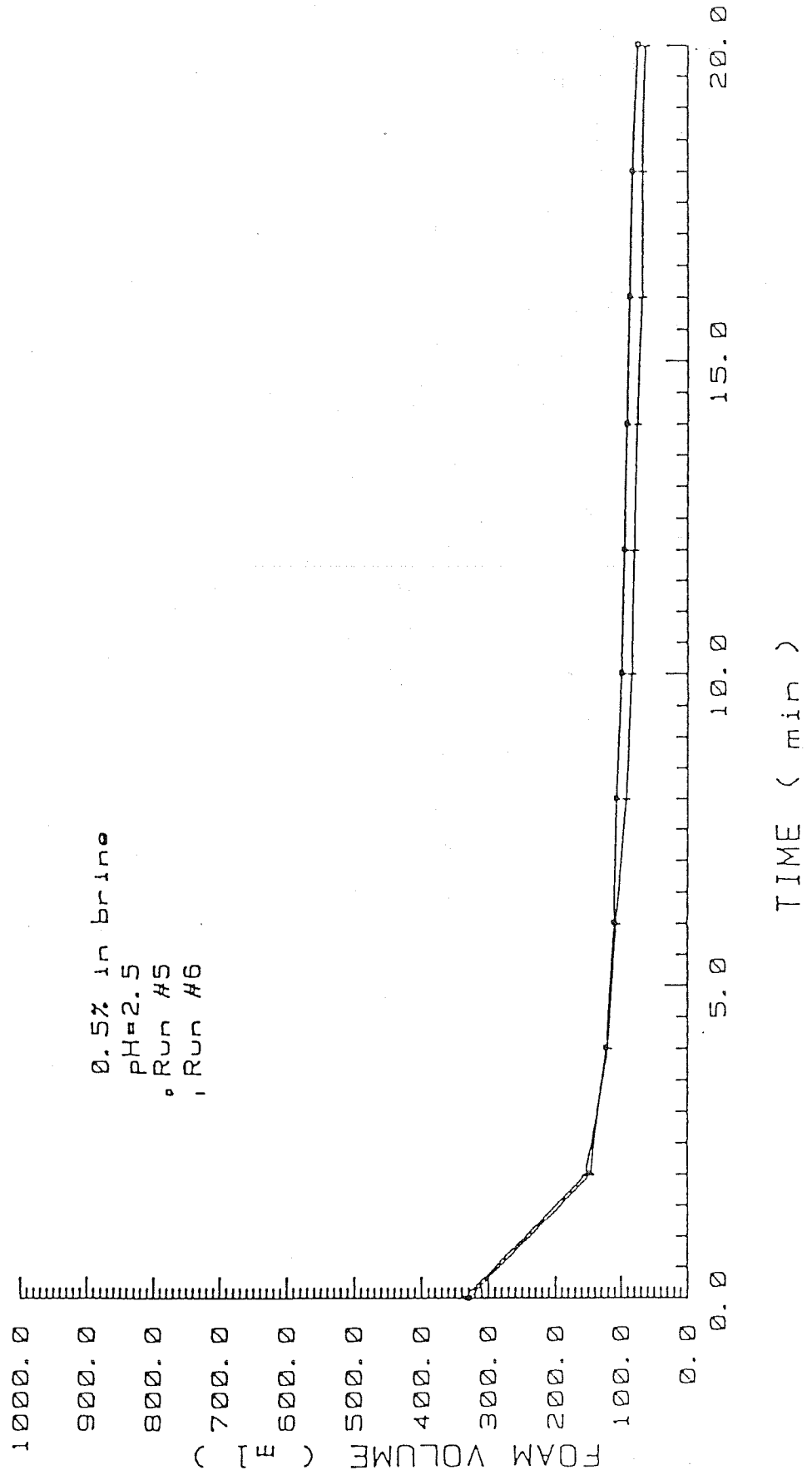


FIGURE B.9

STATIC FOAM TEST #5: STEPANFLO #50

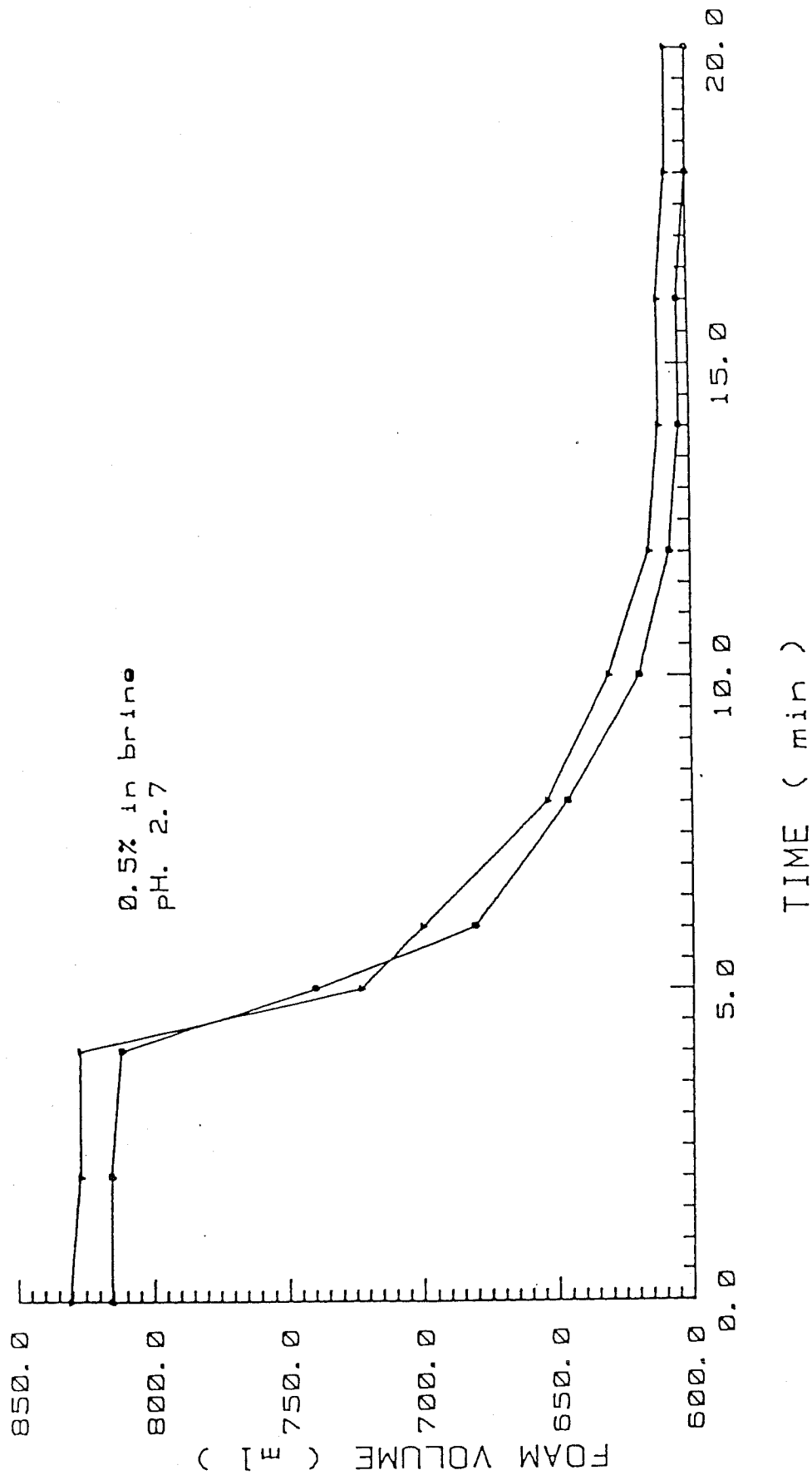


FIGURE B.10

STATIC FOAM TEST #'s 9810: STEPANFLO 50 w/10cc OF CRUDE

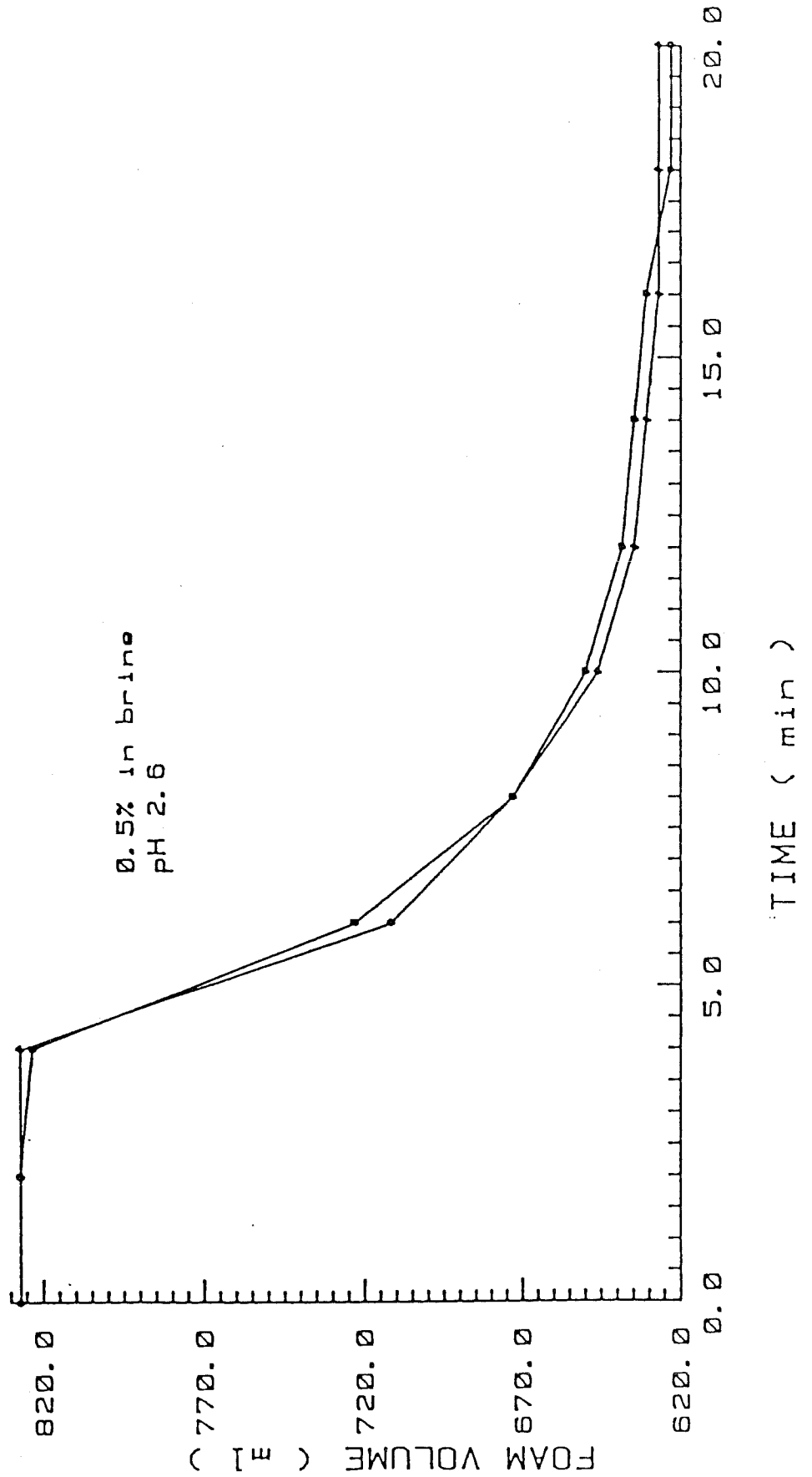


FIGURE B.11

STATIC FOAM TEST #6: TETRONIC 1508

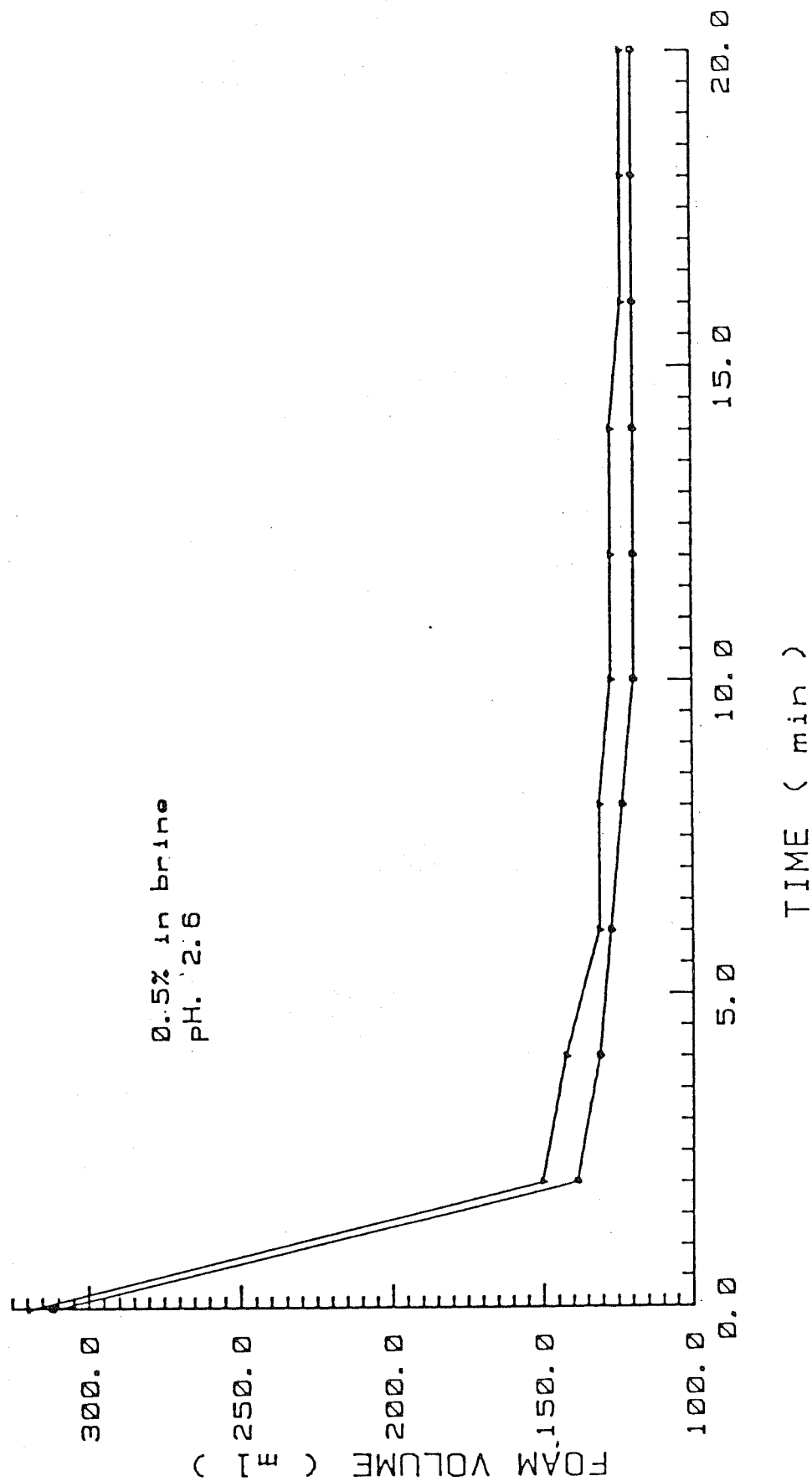


FIGURE B.12

STATIC FOAM TEST #'s 11&12: TETRONIC 1508 w/10cc OF CRUDE

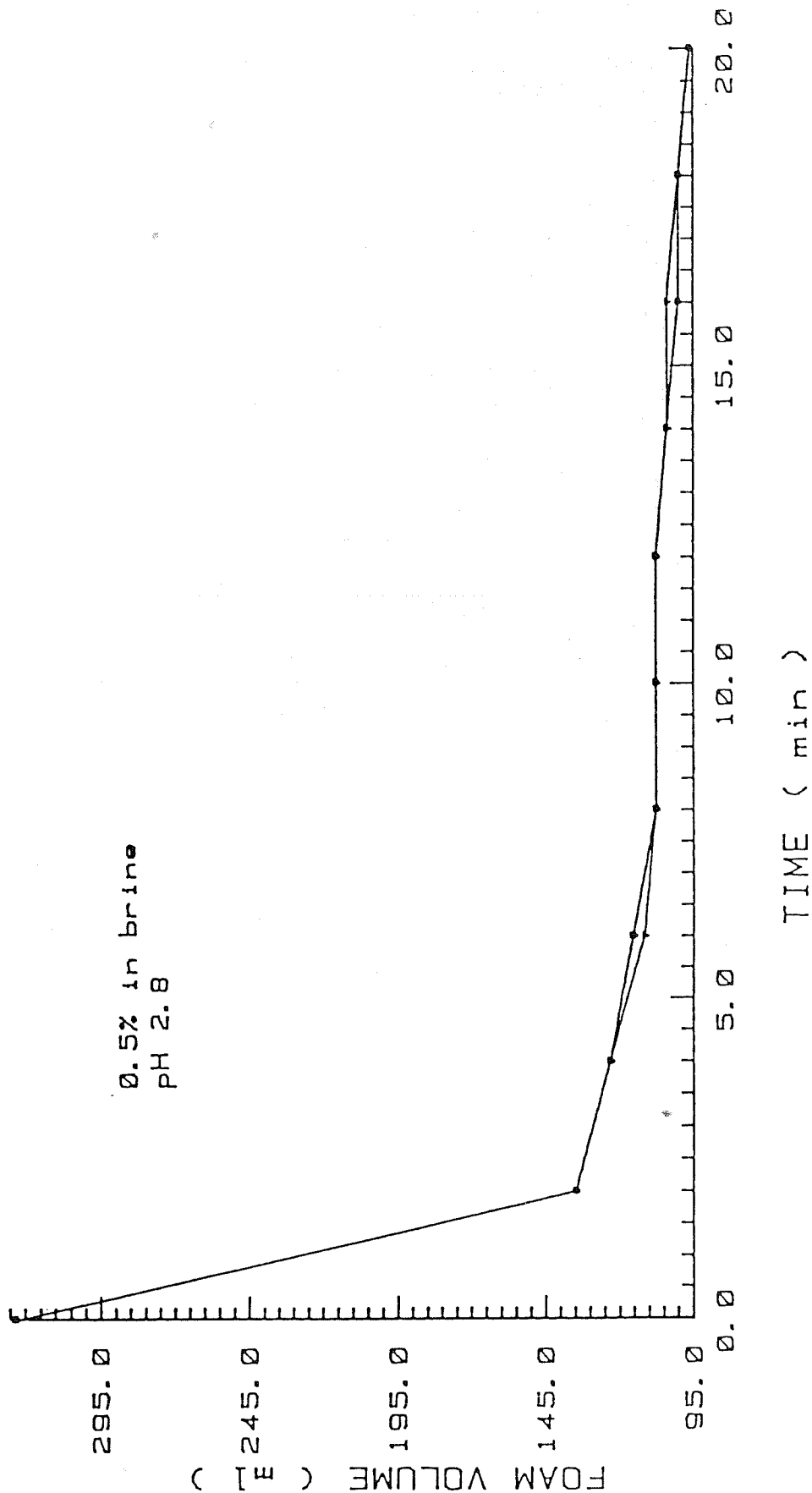


FIGURE B.13

STATIC FOAM TEST #7: ICONOL

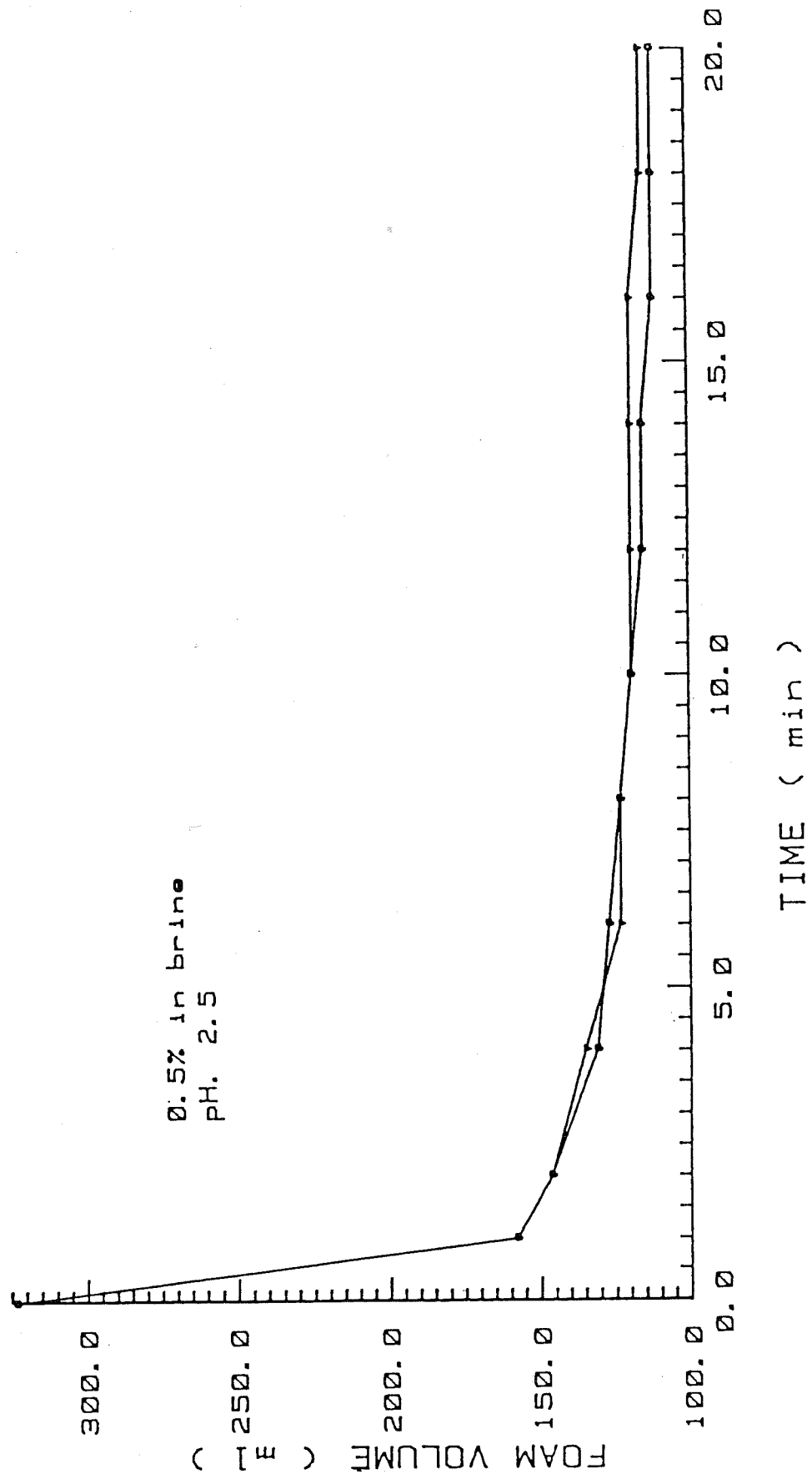


FIGURE B.14

STATIC FOAM TEST #'s 13&14: ICONOL w/10cc OF CRUDE

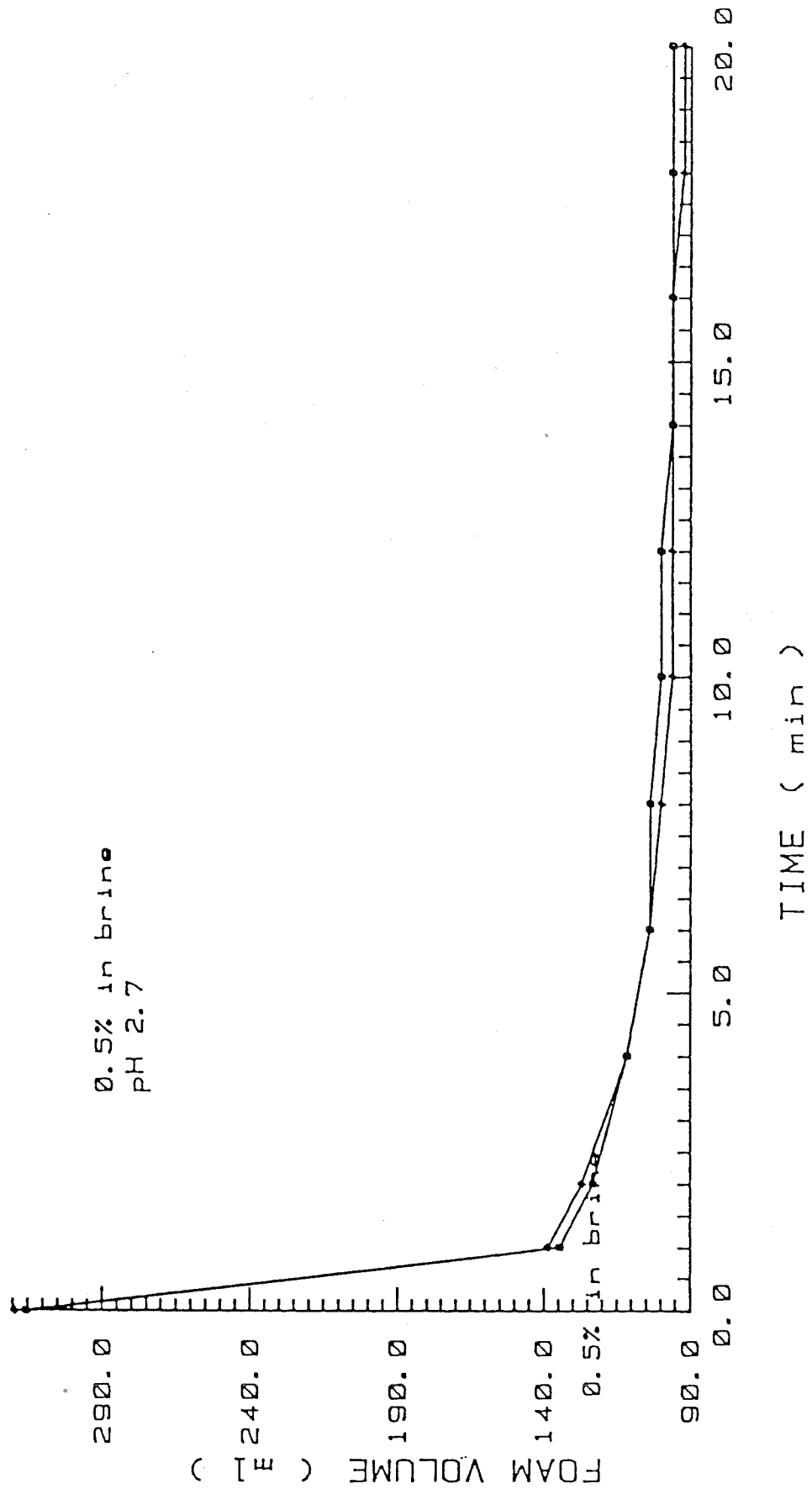


FIGURE B.15

STATIC FOAM TEST #'s 15&16: PLURADYNE OF-90

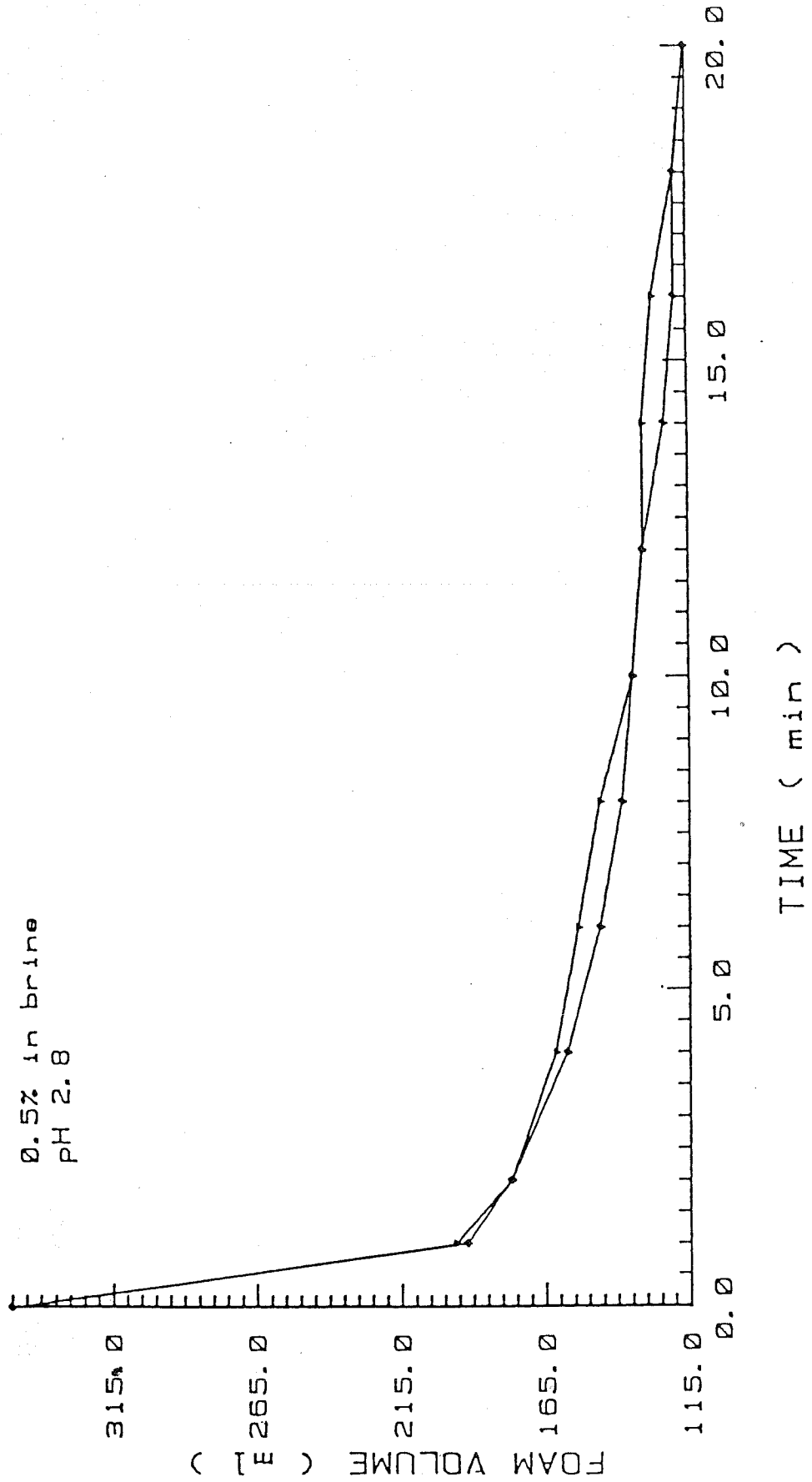
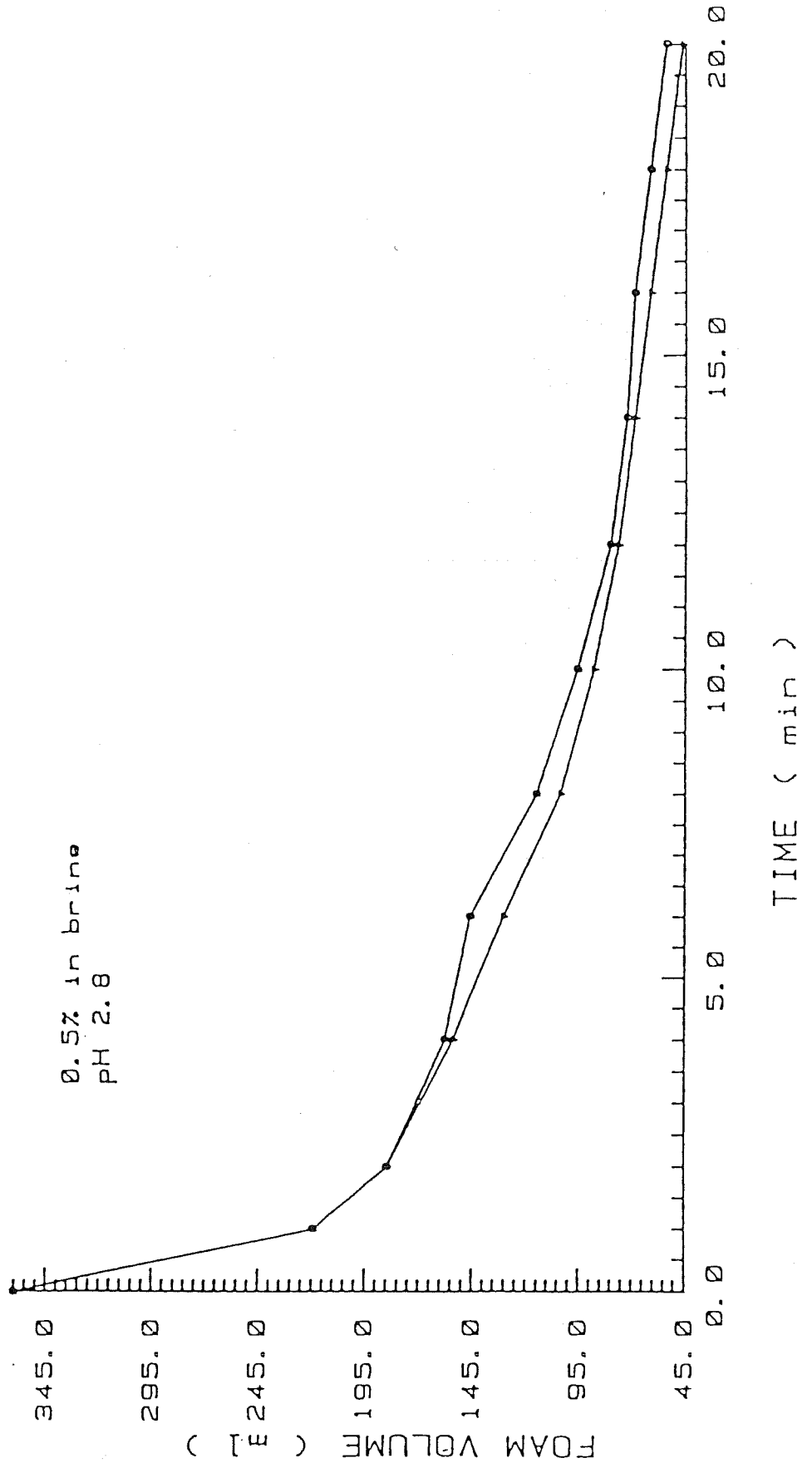


FIGURE B.16

STATIC FOAM TEST #'s 17&18: PLURADYNE OF-90 w/10cc OF CRUDE



A P P E N D I X C

FIGURE C.1

MOBILITY RATIO VS TIME FOR BRINE pH=2.8

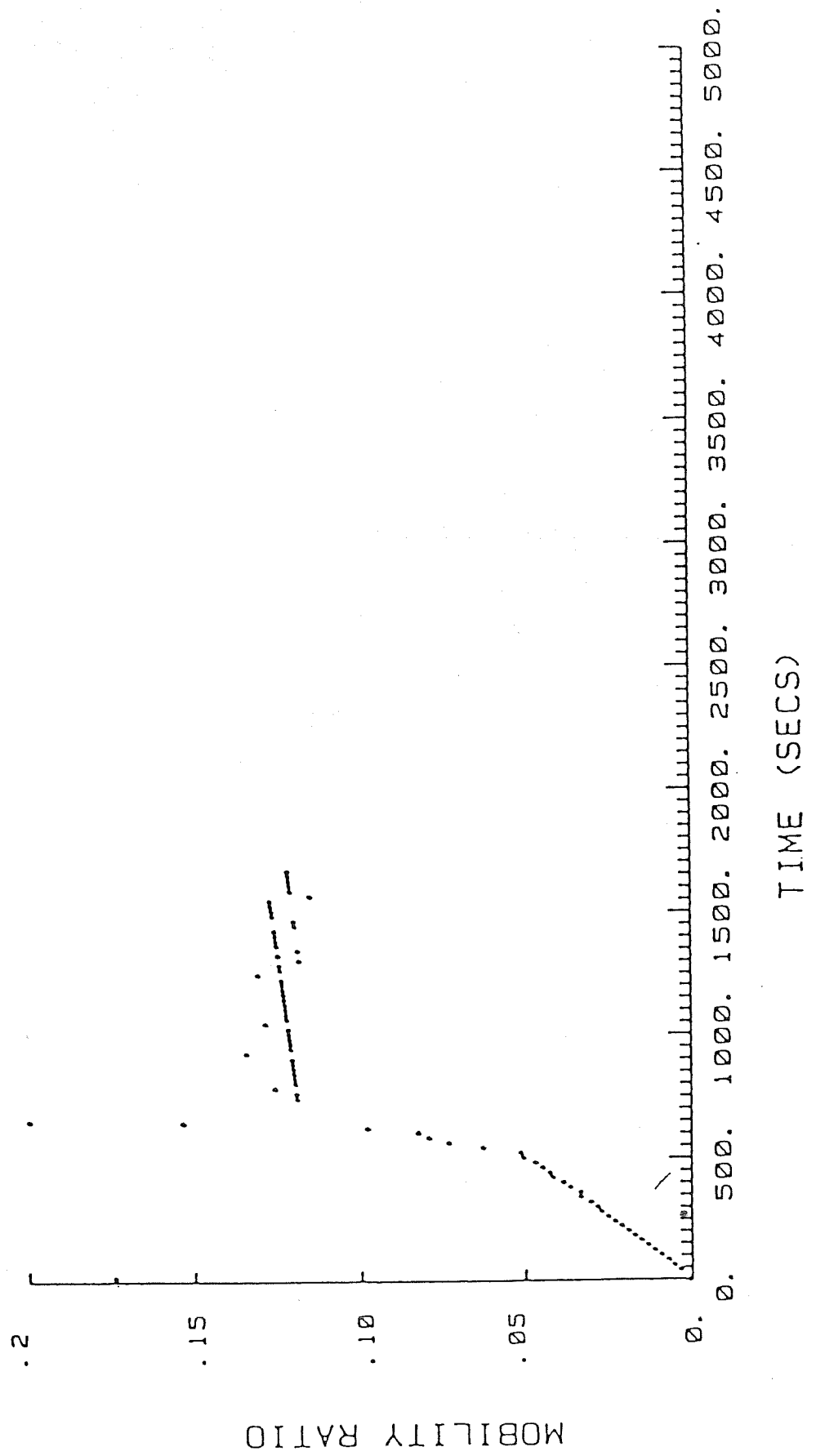


FIGURE C.2

MOBILITY RATIO VS TIME FOR ALIPAL CD-128, pH=2.85, 20/11/82

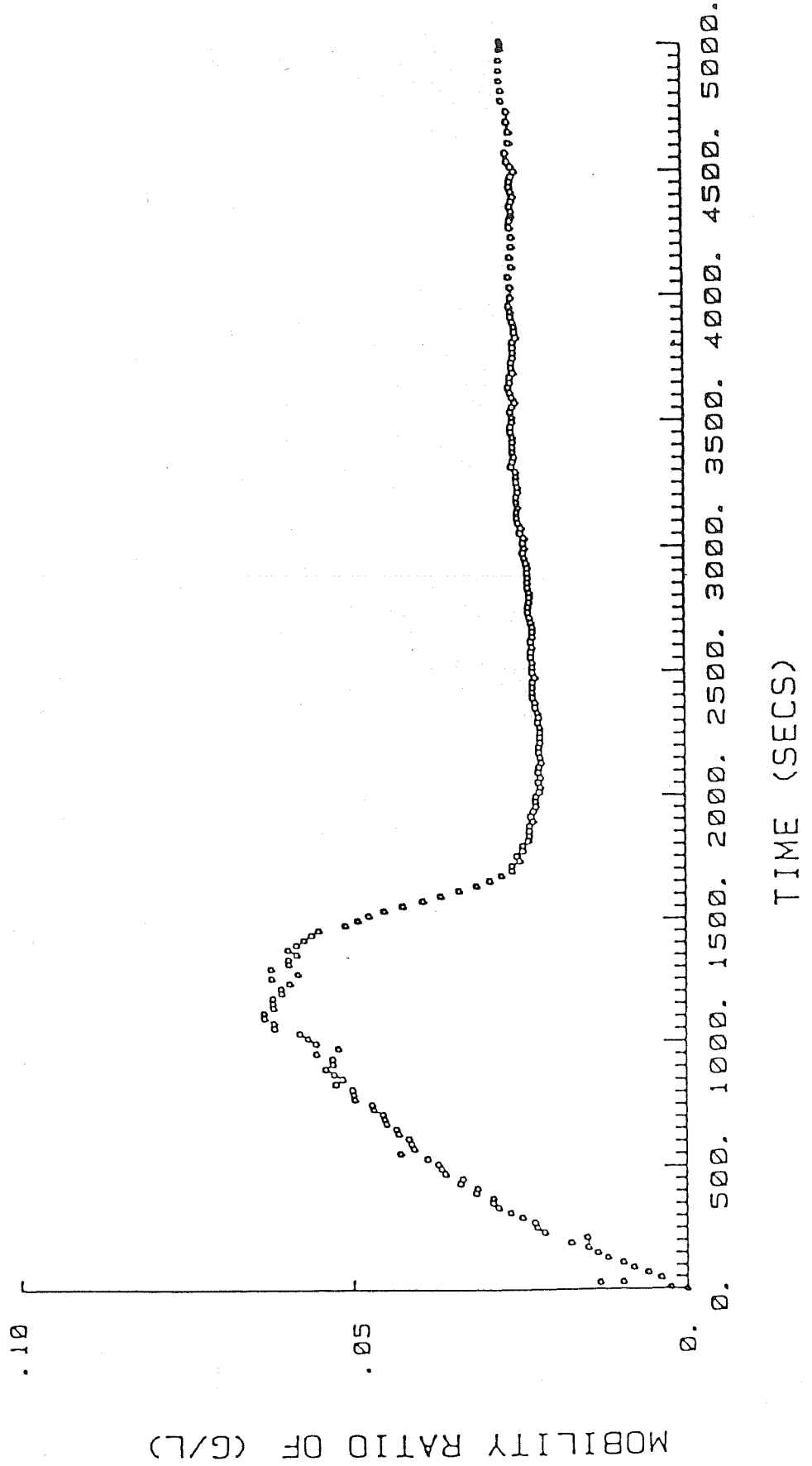


FIGURE C.3

MOBILITY RATIO VS TIME FOR WITCOLATE 1276, pH=2.5, 29/11/82

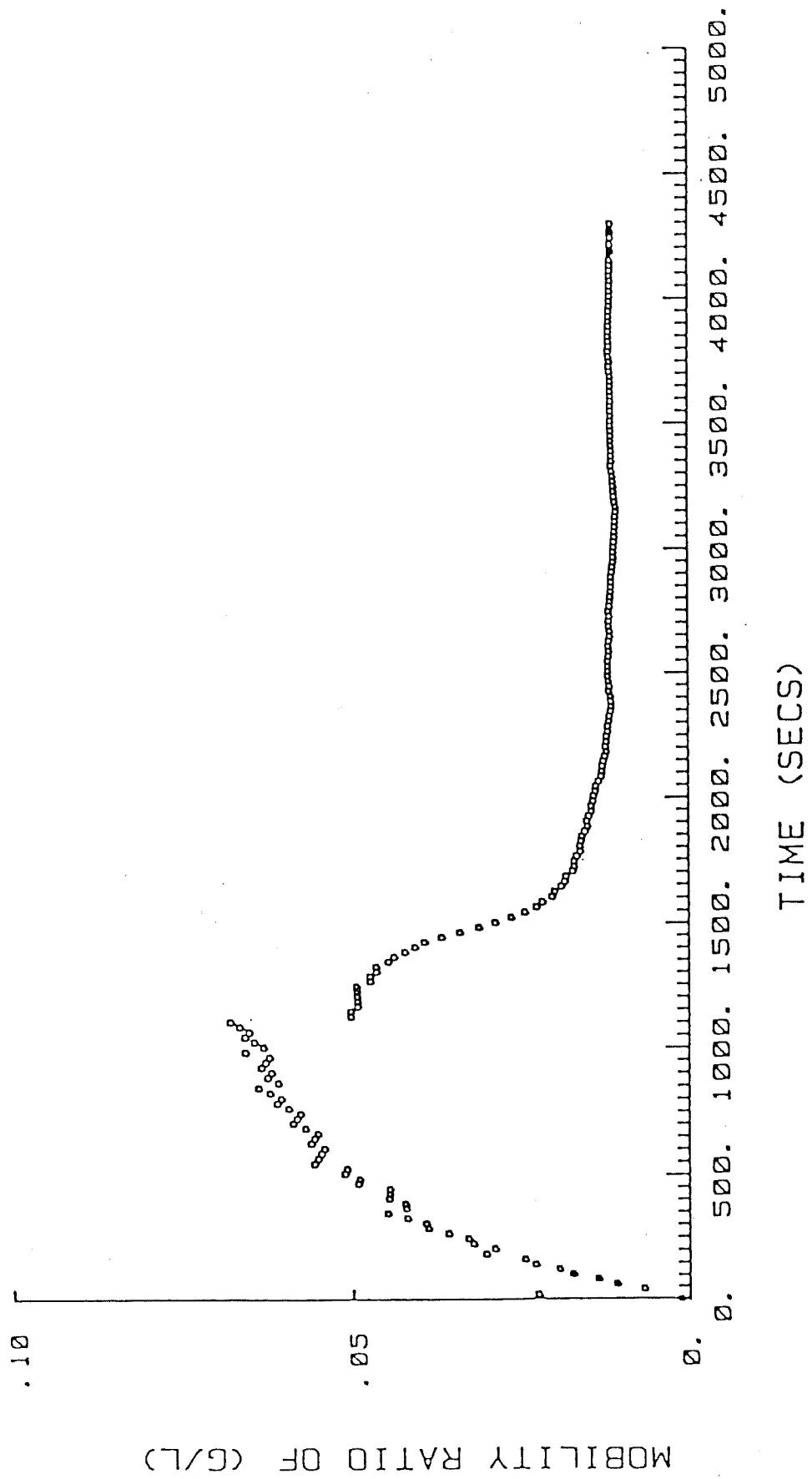


FIGURE C.4

MOBILITY RATIO VS TIME FOR NEODOL 23-3.

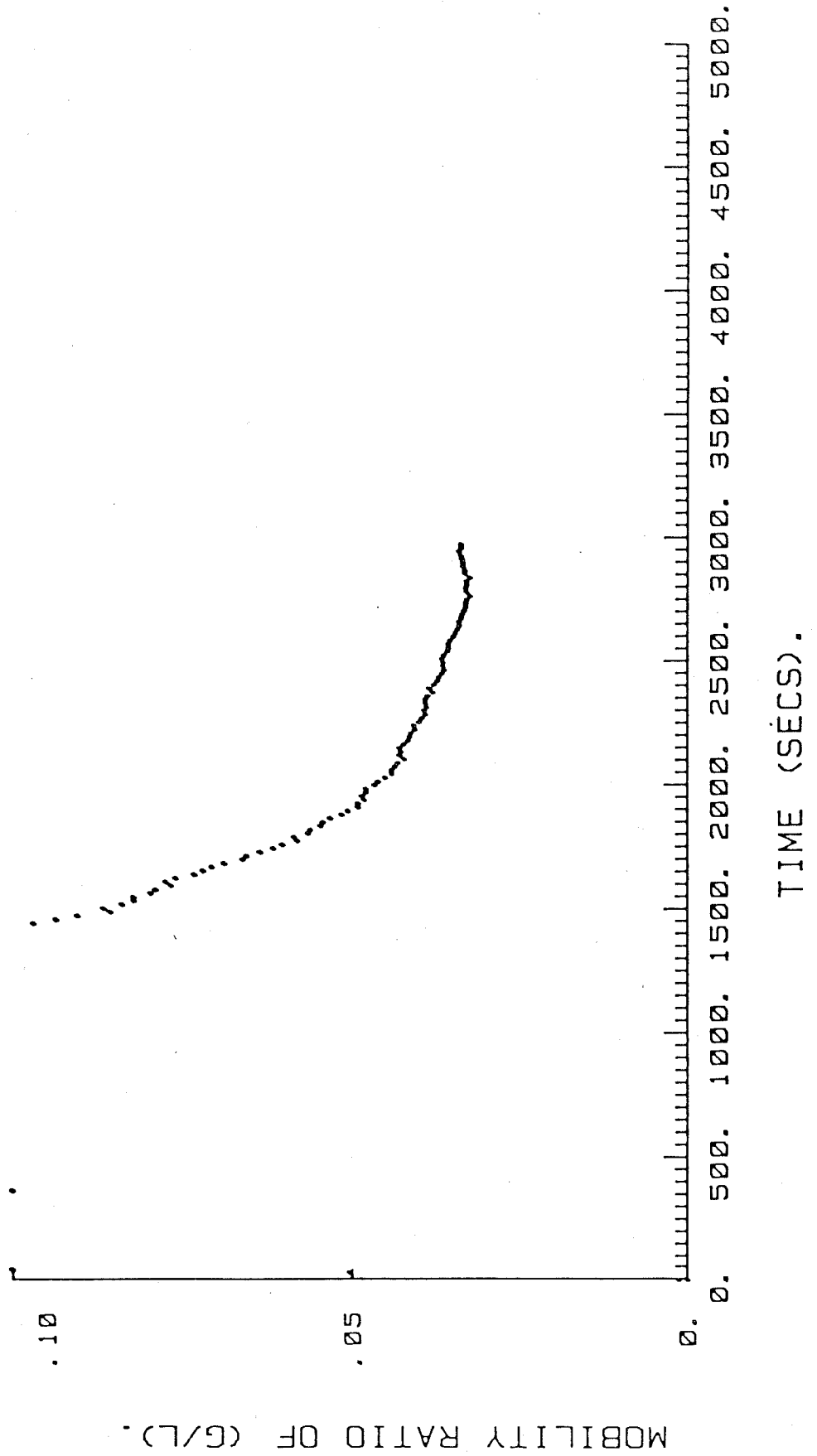


FIGURE C.5

MOBILITY RATIO VS TIME FOR PLURONIC F68, pH=2.9, 1/27/83.

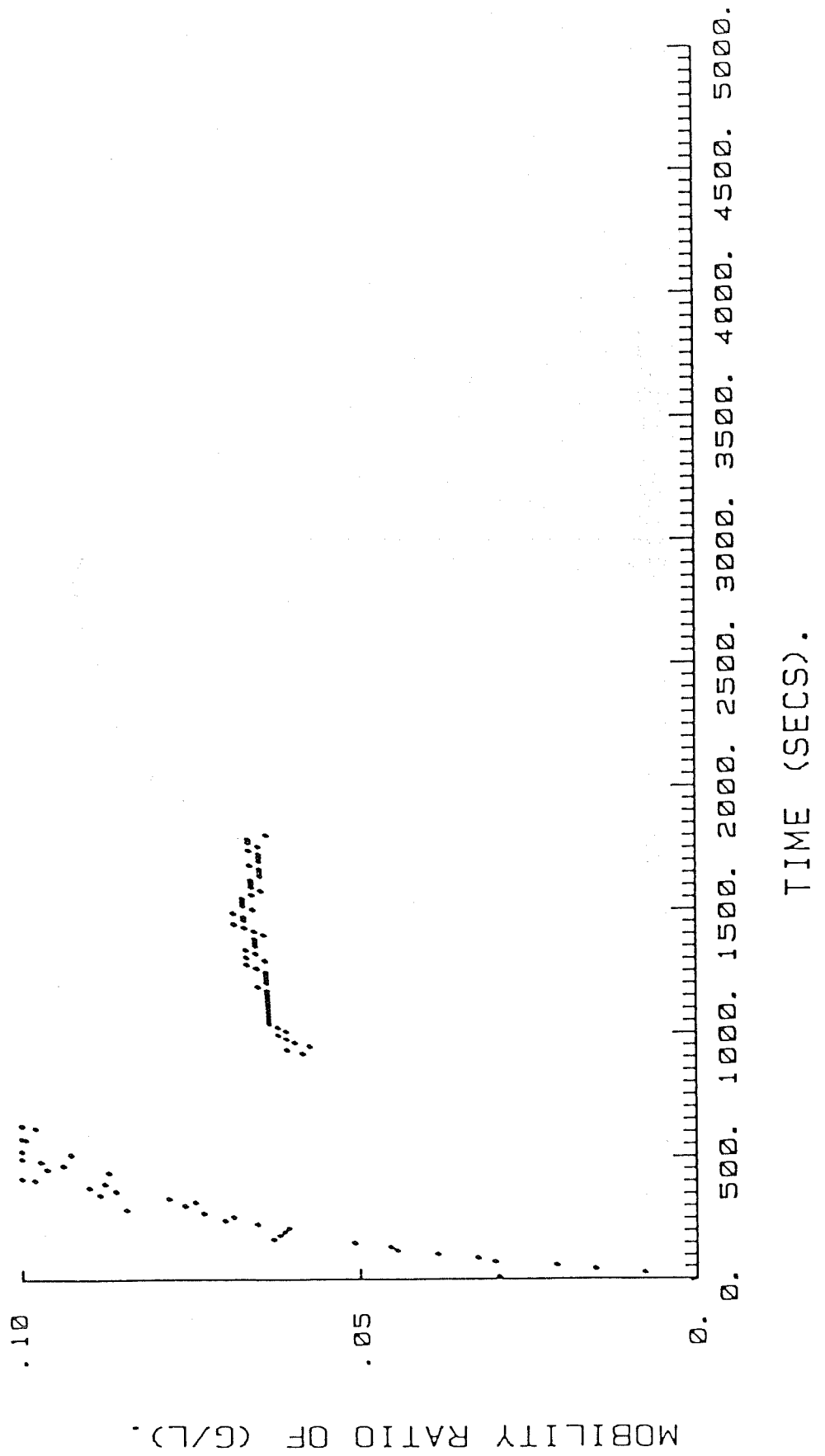


FIGURE C.6

MOBILITY RATIO VS TIME FOR STEPANFLO 50 , PH=2.8

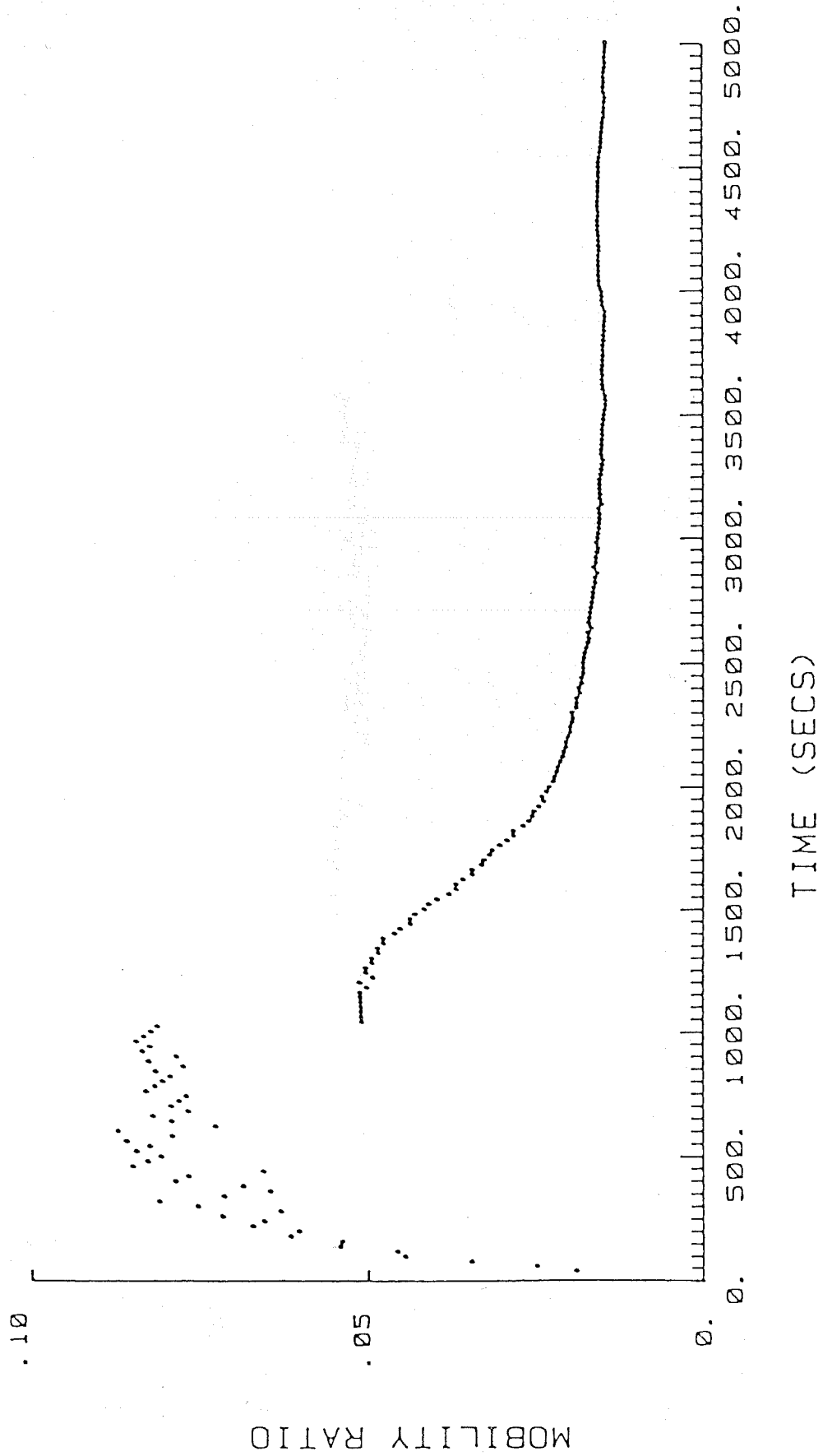


FIGURE C.7

MOBILITY RATIO VS TIME FOR TETRONIC 1508, pH=2.6, 11/26/82.

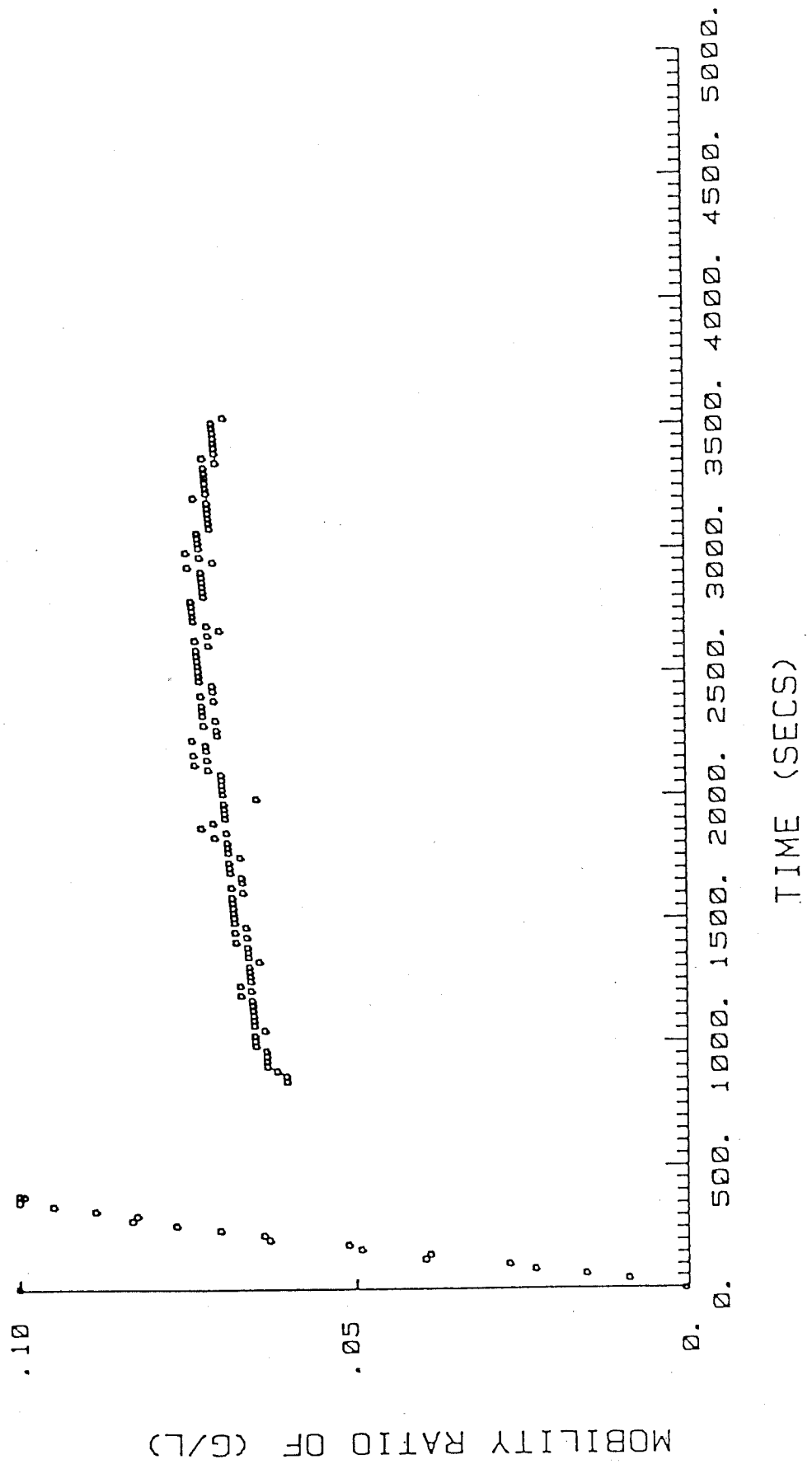


FIGURE C.8

MOBILITY RATIO VS TIME FOR ICONOL, pH=2.5, 24/1/83.

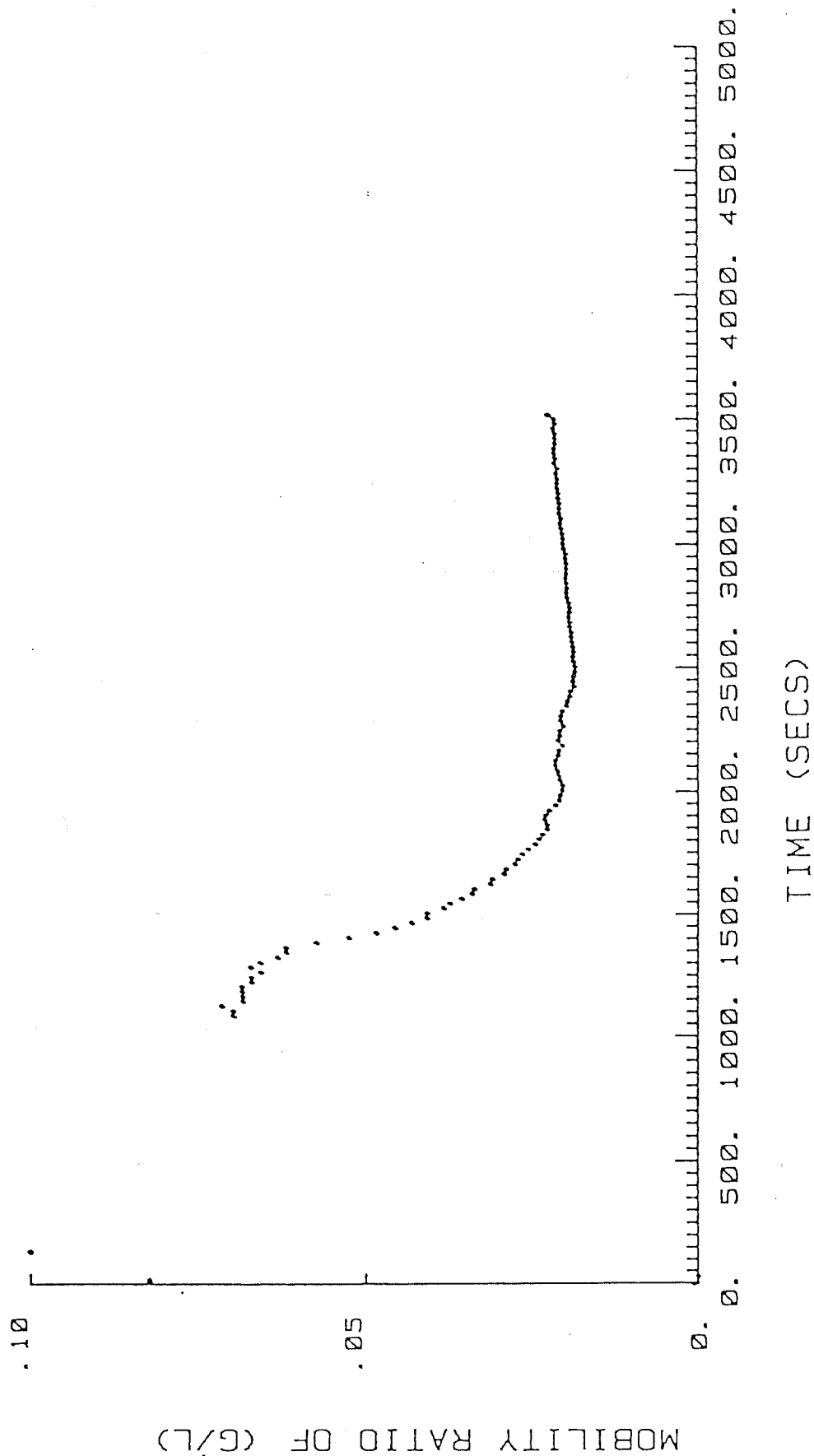


FIGURE C.9

MOBILITY RATIO VS TIME FOR PLURADYNE OF -90, pH=2.75, 22/1/83.

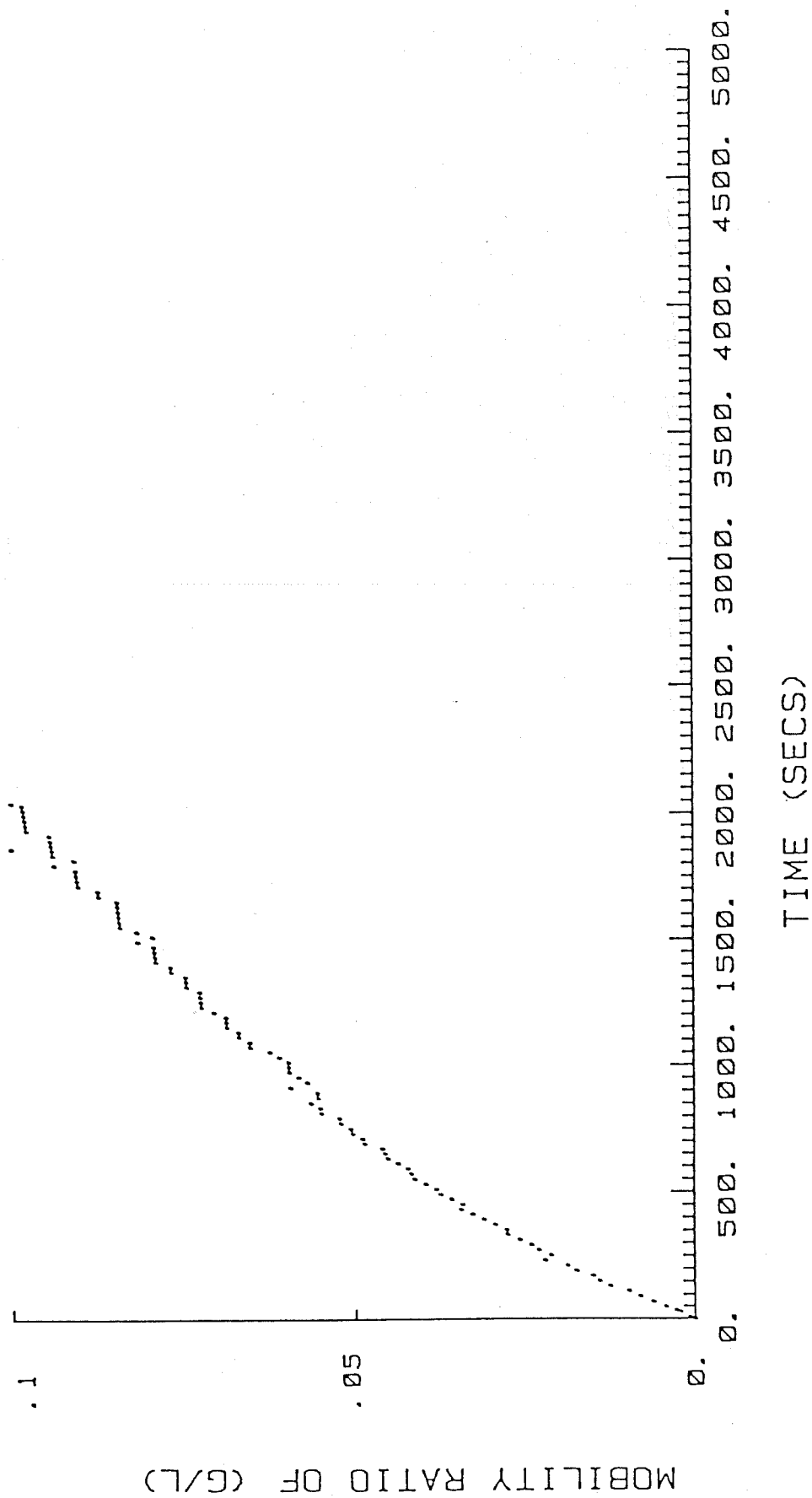
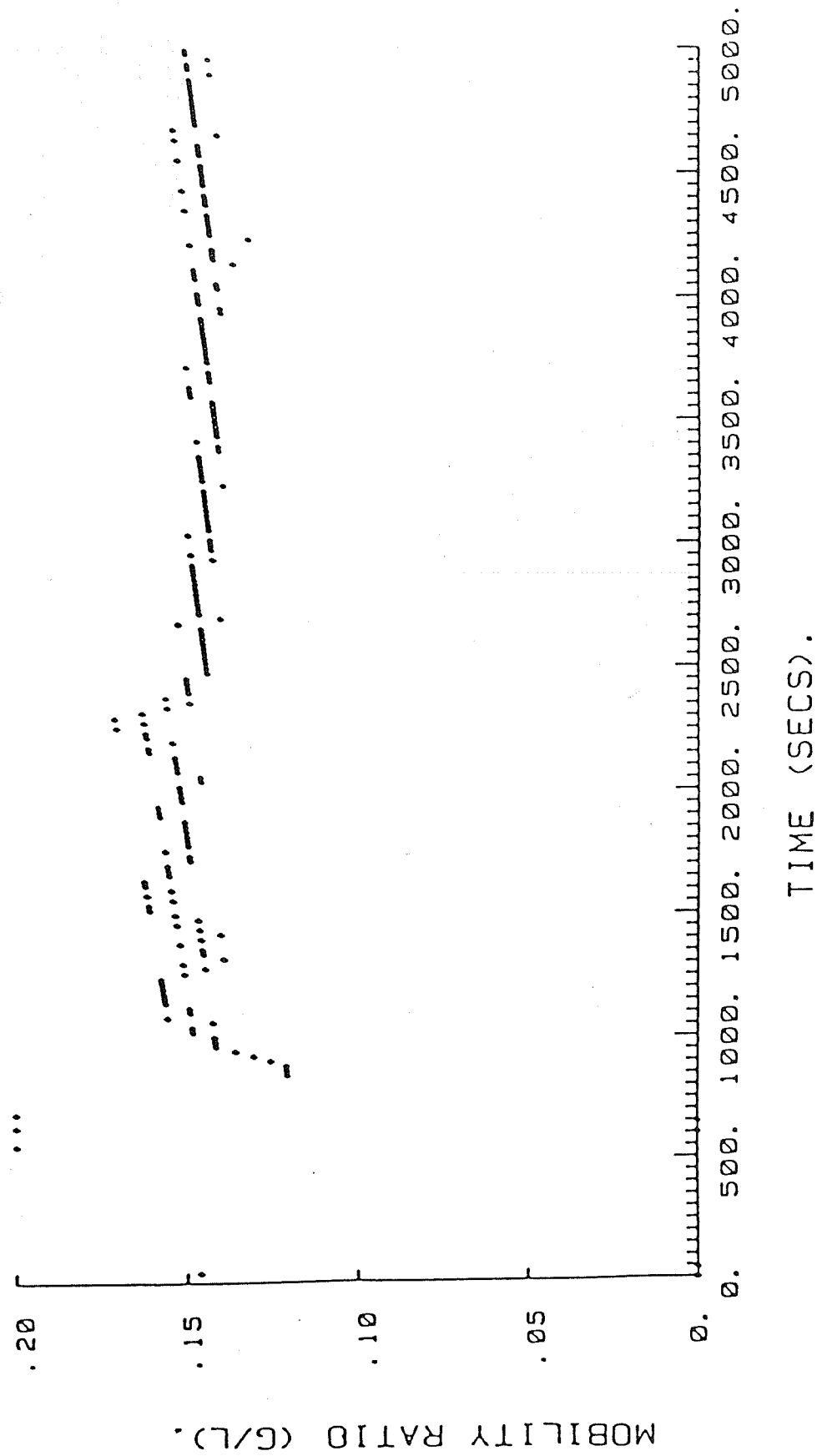


FIGURE C.10

MOBILITY RATIO VS TIME FOR SUN TECH 4



APPENDIX D

Appendix D-1

| INITIALIZATION DATA - REGION 1 | | |
|---|-----------------------------------|--------------------|
| EQUILIBRIUM CALCULATION METHOD | = | CON.PRES. |
| INITIAL TEMPERATURE | = | 123.0 (DEG.F) |
| INITIAL PRESSURE | = | 1000.0 (PSIA) |
| DEPTH AT INITIAL PRESSURE | = | 2500.0 (FT.) |
| DEPTH AT WATER-OIL CONTACT | = | 0.0 (FT.) |
| DEPTH AT GAS-OIL CONTACT | = | 0.0 (FT.) |
| CAPILLARY PRESSURE AT WATER-OIL CONTACT | = | 0.0 (PSI) |
| CAPILLARY PRESSURE AT GAS-OIL CONTACT | = | 0.0 (PSI) |
| SWING COMPONENT | = | 3 |
| REGION BOUNDARIES | | |
| I = 1- 8 | J = 1- 4 | K = 1- 3 |
| WATER SATURATION | OIL SATURATION | GAS SATURATION |
| 0.4900 | 0.5100 | 0.0000 |
| COMPONENT | MOLE FRACTION IN PRIMARY PHASE | |
| H2O | 1.0000 | |
| OIL | 1.0000 | |
| CO2 | 0.0000 | |
| ACD | 0.0000 | |
| NUMBER OF ACTIVE GRID BLOCKS | = | 60 |
| INITIAL AVERAGE PRESSURE | = | 1000.0 PSIA |
| MASS IN PLACE | | |
| COMPONENT | FIELD UNITS | MOLES(BTU) |
| 1 H2O | 0.1486E+06 | 0.3893E+07 |
| 2 OIL | 0.1538E+06 | 0.1131E+06 |
| 3 CO2 | 0.0000 | 0.0000 |
| 4 ACD | 0.0000 | 0.0000 |
| 5 HEAT | 0.4570E+10 | 0.4570E+10 |
| INITIAL WATER-IN-PLACE | = | 0.1486E+06 STB |
| INITIAL OIL-IN-PLACE | = | 0.1538E+06 STB |
| INITIAL GAS-IN-PLACE | = | 0.0000 MSCF |
| TOTAL PORE VOLUME WITH SOIL ABOVE | = | 0.1725E+07 CU. FT. |

.....
 * SATURATION FUNCTIONS *
 * FOR ROCK TYPE I *
 *

| WATER-OIL SATURATION FUNCTIONS | | | | | | | | | | GAS-OIL SATURATION FUNCTIONS | | | | | | | | | |
|--------------------------------|-------------|------------|----------------|------------|--------------------------------|----------|-------------|------------|-----------|------------------------------|--------|----------|-------------|------------|--------------------------------|------------|--------|--|--|
| RELATIVE PERMS | | | | | CAP PRESS (PCMO) / (D(SW) PSI) | | | | | RELATIVE PERMS | | | | | CAP PRESS (PCGO) / (D(SG) PSI) | | | | |
| SAT (SW) | WATER (KRW) | OIL (KROV) | RELATIVE PERMS | PCMO (PSI) | D(SW) | SAT (SG) | LIQUID (SL) | OIL (KROG) | GAS (KRG) | PCGO (PSI) | D(SG) | SAT (SG) | LIQUID (SL) | OIL (KROG) | GAS (KRG) | PCGO (PSI) | D(SG) | | |
| 0.0000 | 0.0000 | 0.0000 | 0.0000 | 0.0000 | 0.0000 | 0.0000 | 0.0000 | 0.0000 | 0.0000 | 0.0000 | 0.0000 | 0.0000 | 0.0000 | 0.0000 | 0.0000 | 0.0000 | 0.0000 | | |
| 0.2500 | 0.6010 | 0.5000 | 0.0505 | 0.0000 | 0.0000 | 0.3000 | 0.0001 | 0.5000 | 0.0000 | 0.0000 | 0.0000 | 0.3000 | 0.0001 | 0.5000 | 0.0000 | 0.0000 | 0.0000 | | |
| 0.3300 | 0.5030 | 0.3427 | 0.0000 | 0.0000 | 0.0000 | 0.3800 | 0.0004 | 0.4000 | 0.0000 | 0.0000 | 0.0000 | 0.3800 | 0.0004 | 0.4000 | 0.0000 | 0.0000 | 0.0000 | | |
| 0.4200 | 0.4070 | 0.2100 | 0.0000 | 0.0000 | 0.0000 | 0.4600 | 0.0000 | 0.3500 | 0.0000 | 0.0000 | 0.0000 | 0.4600 | 0.0000 | 0.3500 | 0.0000 | 0.0000 | 0.0000 | | |
| 0.5000 | 0.0268 | 0.1240 | 0.0000 | 0.0000 | 0.0000 | 0.5300 | 0.0149 | 0.2380 | 0.0000 | 0.0000 | 0.0000 | 0.5300 | 0.0149 | 0.2380 | 0.0000 | 0.0000 | 0.0000 | | |
| 0.5800 | 0.0223 | 0.0597 | 0.0000 | 0.0000 | 0.0000 | 0.6100 | 0.0373 | 0.1690 | 0.0000 | 0.0000 | 0.0000 | 0.6100 | 0.0373 | 0.1690 | 0.0000 | 0.0000 | 0.0000 | | |
| 0.6700 | 0.0217 | 0.0192 | 0.0000 | 0.0000 | 0.0000 | 0.6900 | 0.0762 | 0.1100 | 0.0000 | 0.0000 | 0.0000 | 0.6900 | 0.0762 | 0.1100 | 0.0000 | 0.0000 | 0.0000 | | |
| 0.7500 | 0.2104 | 0.0020 | 0.0000 | 0.0000 | 0.0000 | 0.7700 | 0.1366 | 0.0620 | 0.0000 | 0.0000 | 0.0000 | 0.7700 | 0.1366 | 0.0620 | 0.0000 | 0.0000 | 0.0000 | | |
| 0.8300 | 0.3341 | 0.0000 | 0.0000 | 0.0000 | 0.0000 | 0.8400 | 0.2237 | 0.0260 | 0.0000 | 0.0000 | 0.0000 | 0.8400 | 0.2237 | 0.0260 | 0.0000 | 0.0000 | 0.0000 | | |
| 0.9200 | 0.0000 | 0.0000 | 0.0000 | 0.0000 | 0.0000 | 0.9200 | 0.0000 | 0.0000 | 0.0000 | 0.0000 | 0.0000 | 0.9200 | 0.0000 | 0.0000 | 0.0000 | 0.0000 | 0.0000 | | |
| 1.0000 | 0.7110 | 0.0000 | 0.0000 | 0.0000 | 0.0000 | 1.0000 | 0.6500 | 0.0000 | 0.0000 | 0.0000 | 0.0000 | 1.0000 | 0.6500 | 0.0000 | 0.0000 | 0.0000 | 0.0000 | | |
| END POINTS | | | | | | | | | | END POINTS | | | | | | | | | |
| SWC | SWIR | SORW | KRW0 | KROCV | | SORG | SGC | SGR | KRG0 | SOINIT | | SORG | SGC | SGR | KRG0 | SOINIT | | | |
| 0.000 | 0.0000 | 0.1710 | 0.3341 | 0.6500 | | 0.000 | 0.1800 | 0.0000 | 0.6300 | 0.0000 | | 0.000 | 0.1800 | 0.0000 | 0.6300 | 0.0000 | | | |

IMMISCIBLE CO₂ FLOOD - MOBILITY RATIO = 1.5

DATE FILED: MAR 28 1983
 ABSTRACT VISC GAS PRESSURE: 11.1
 IMBIBITION CASE: 1/0 2/1 ACHE 5-1501
 40% PRODUCTION POSITIVE 0.2

EGIP UNIT # 14 RUN SUMMARY

WATER - CUM WATER PRODUCED..... WS18
 OIL - CUM OIL PRODUCED..... OS18
 GAS - CUM GAS PRODUCED..... GSP18
 WOR - CUM WOR PRODUCED..... WOR18
 WATER PRODUCTION RATE..... WS18/D
 OIL PRODUCTION RATE..... OS18/D
 GAS PRODUCTION RATE..... GSP18/D
 WOR PRODUCTION RATE..... WOR18/D
 WATER INJ. WATER..... WS18/STB
 GAS OIL RATIO..... WS18/OS18
 CUM WATER INJECTED..... WS18
 CUM OIL INJECTED..... OS18
 CUM GAS INJECTED..... GSP18
 WATER INJECTION RATE..... WS18/D
 OIL INJECTION RATE..... OS18/D
 GAS INJECTION RATE..... GSP18/D
 WOR INJECTION RATE..... WOR18/D
 VOLUMETRICALLY WEIGHTED FIELD AVERAGE PRESSURE..... PSIA
 PERCENTAGE OF EGIP PRODUCED.....
 RESERVOIR PRESSURE IN LAYER WHERE WELL BOTTOM HOLE PRESSURE IS SPECIFIED..... PSIA
 WELLBORE PRESSURE IN LAYER WHERE WELL BOTTOM HOLE PRESSURE IS SPECIFIED..... PSIA

WELL NUMBER: 14-1-1-1

| TIME | WATER | OIL | GAS | GVAT | GOIL | GGAS | WOR | GOR | WATERI | OILI | GASI | GVATI | GOILI | GGASI | PAVE | REC | |
|----------|--------|-------|--------|-------|------|-------|-------|-------|--------|------|-------|-------|-------|-------|------|------|-------|
| 1.000 | 0.11 | 3.66 | 0.10 | 109.8 | 1.4 | 0.0 | 76.03 | 3.80 | 0.0 | 0.0 | 0.4 | 0.0 | 0.0 | 403.0 | 998 | 0.00 | |
| 3.000 | 0.29 | 0.00 | 0.00 | 89.6 | 1.2 | 0.0 | 75.91 | 0.00 | 0.0 | 0.0 | 1.2 | 0.0 | 0.0 | 403.0 | 1813 | 0.00 | |
| 5.347 | 0.56 | 0.00 | 0.00 | 11.7 | 0.0 | 0.0 | 75.98 | 0.00 | 0.0 | 0.0 | 2.4 | 0.0 | 0.0 | 403.0 | 1818 | 0.00 | |
| 11.048 | 1.20 | 0.02 | 0.00 | 108.9 | 1.4 | 0.0 | 76.26 | 0.00 | 0.0 | 0.0 | 4.7 | 0.0 | 0.0 | 403.0 | 1852 | 0.00 | |
| 23.626 | 0.04 | 0.10 | 0.10 | 141.6 | 1.8 | 0.0 | 76.94 | 0.00 | 0.0 | 0.0 | 9.5 | 0.0 | 0.0 | 403.0 | 1185 | 0.00 | |
| 47.207 | 7.52 | 0.09 | 0.10 | 175.9 | 2.2 | 0.0 | 78.26 | 3.00 | 0.0 | 0.0 | 16.9 | 0.0 | 0.0 | 403.0 | 1158 | 0.00 | |
| 63.701 | 10.13 | 0.13 | 0.10 | 188.8 | 2.4 | 0.0 | 79.03 | 3.20 | 0.0 | 0.0 | 23.5 | 0.0 | 0.0 | 403.0 | 1176 | 0.00 | |
| 84.202 | 13.42 | 0.17 | 0.10 | 197.5 | 2.6 | 0.0 | 76.81 | 3.20 | 0.0 | 0.0 | 32.1 | 0.0 | 0.0 | 403.0 | 1203 | 0.11 | |
| 91.753 | 15.67 | 0.22 | 0.10 | 194.3 | 3.8 | 0.0 | 51.23 | 8.01 | 0.0 | 0.0 | 36.7 | 0.0 | 0.0 | 403.0 | 1209 | 0.18 | |
| 103.304 | 17.78 | 0.42 | 0.14 | 182.7 | 17.4 | 3.6 | 11.47 | 0.21 | 0.0 | 0.0 | 44.3 | 0.0 | 0.0 | 403.0 | 1223 | 0.27 | |
| 126.405 | 21.12 | 0.80 | 0.11 | 144.4 | 16.5 | 17.6 | 0.75 | 10.67 | 0.0 | 0.0 | 50.6 | 0.0 | 0.0 | 403.0 | 1215 | 0.32 | |
| 172.609 | 25.44 | 1.87 | 18.46 | 34.4 | 23.1 | 319.3 | 4.08 | 13.82 | 0.0 | 0.0 | 63.0 | 0.0 | 0.0 | 47.0 | 1173 | 1.21 | |
| 262.689 | 30.14 | 4.00 | 52.79 | 51.4 | 23.7 | 377.0 | 2.19 | 15.90 | 0.0 | 0.0 | 195.0 | 0.0 | 0.0 | 403.0 | 1182 | 2.00 | |
| 332.699 | 32.92 | 5.26 | 26.44 | 31.0 | 14.0 | 416.3 | 2.21 | 29.84 | 0.0 | 0.0 | 141.0 | 0.0 | 0.0 | 403.0 | 1933 | 3.02 | |
| 492.609 | 34.93 | 6.20 | 126.89 | 22.3 | 10.4 | 405.0 | 2.45 | 38.85 | 0.0 | 0.0 | 177.0 | 0.0 | 0.0 | 403.0 | 333 | 4.03 | |
| 508.000 | 36.03 | 6.73 | 149.89 | 19.3 | 9.2 | 400.7 | 2.50 | 43.70 | 0.0 | 0.0 | 208.0 | 0.0 | 0.0 | 403.0 | 379 | 4.30 | |
| 508.000 | 36.03 | 6.73 | 150.46 | 18.9 | 8.9 | 394.0 | 2.51 | 43.28 | 0.0 | 0.0 | 200.0 | 0.0 | 0.0 | 403.0 | 373 | 4.35 | |
| 508.000 | 36.03 | 6.73 | 151.24 | 18.1 | 8.5 | 355.0 | 2.52 | 42.94 | 0.0 | 0.0 | 200.0 | 0.0 | 0.0 | 403.0 | 373 | 4.40 | |
| 506.788 | 36.19 | 6.75 | 152.31 | 16.6 | 7.8 | 334.0 | 2.54 | 42.89 | 2.7 | 0.0 | 200.0 | 400.0 | 0.0 | 0.0 | 6.0 | 923 | 4.41 |
| 513.173 | 36.24 | 6.83 | 153.08 | 14.1 | 6.5 | 328.1 | 2.57 | 42.76 | 5.3 | 0.0 | 200.0 | 400.0 | 0.0 | 0.0 | 0.0 | 953 | 4.44 |
| 532.293 | 36.35 | 6.87 | 155.99 | 11.3 | 5.0 | 309.2 | 2.63 | 41.43 | 6.9 | 0.0 | 200.0 | 400.0 | 0.0 | 0.0 | 0.0 | 951 | 4.47 |
| 533.536 | 36.46 | 6.92 | 157.37 | 7.6 | 4.1 | 140.8 | 2.33 | 34.16 | 13.4 | 0.0 | 200.0 | 400.0 | 0.0 | 0.0 | 0.0 | 959 | 4.50 |
| 548.873 | 36.46 | 6.93 | 158.73 | 15.7 | 4.4 | 76.8 | 2.40 | 17.29 | 19.5 | 0.0 | 200.0 | 400.0 | 0.0 | 0.0 | 0.0 | 994 | 4.54 |
| 575.416 | 37.51 | 7.44 | 158.98 | 33.8 | 17.8 | 4.8 | 1.99 | 0.52 | 30.2 | 0.0 | 200.0 | 400.0 | 0.0 | 0.0 | 0.0 | 1199 | 4.84 |
| 621.416 | 43.81 | 9.45 | 159.64 | 136.9 | 52.5 | 14.3 | 0.61 | 0.27 | 46.6 | 0.0 | 200.0 | 400.0 | 0.0 | 0.0 | 0.0 | 1308 | 6.41 |
| 681.429 | 60.58 | 13.51 | 160.81 | 279.5 | 67.6 | 19.5 | 4.13 | 0.29 | 72.6 | 0.0 | 200.0 | 400.0 | 0.0 | 0.0 | 0.0 | 1487 | 9.82 |
| 771.429 | 91.62 | 18.52 | 162.23 | 344.9 | 55.6 | 15.4 | 4.20 | 0.28 | 108.6 | 0.0 | 200.0 | 400.0 | 0.0 | 0.0 | 0.0 | 1661 | 13.32 |
| 861.429 | 124.32 | 22.92 | 163.34 | 363.3 | 44.4 | 12.3 | 4.16 | 0.28 | 144.6 | 0.0 | 200.0 | 400.0 | 0.0 | 0.0 | 0.0 | 1397 | 16.90 |
| 951.429 | 157.38 | 26.21 | 164.23 | 370.3 | 36.5 | 9.9 | 15.13 | 0.27 | 180.6 | 0.0 | 200.0 | 400.0 | 0.0 | 0.0 | 0.0 | 1386 | 17.04 |
| 1031.429 | 191.00 | 29.00 | 164.97 | 374.8 | 31.0 | 8.2 | 12.09 | 0.27 | 216.6 | 0.0 | 200.0 | 400.0 | 0.0 | 0.0 | 0.0 | 1308 | 18.82 |
| 1131.429 | 225.45 | 31.42 | 165.61 | 378.5 | 26.9 | 7.8 | 14.07 | 0.26 | 252.6 | 0.0 | 200.0 | 400.0 | 0.0 | 0.0 | 0.0 | 1283 | 20.43 |
| 1221.429 | 259.81 | 33.55 | 166.16 | 381.8 | 23.7 | 6.1 | 16.09 | 0.26 | 288.6 | 0.0 | 200.0 | 400.0 | 0.0 | 0.0 | 0.0 | 1256 | 21.82 |
| 1311.429 | 294.39 | 35.46 | 166.64 | 384.3 | 21.2 | 5.9 | 14.15 | 0.26 | 324.6 | 0.0 | 200.0 | 400.0 | 0.0 | 0.0 | 0.0 | 1237 | 23.00 |
| 1401.429 | 329.13 | 37.17 | 167.08 | 385.9 | 19.0 | 4.8 | 2.27 | 0.25 | 360.6 | 0.0 | 200.0 | 400.0 | 0.0 | 0.0 | 0.0 | 1221 | 24.17 |
| 1491.429 | 363.99 | 38.72 | 167.47 | 387.3 | 17.2 | 4.3 | 23.49 | 0.25 | 396.6 | 0.0 | 200.0 | 400.0 | 0.0 | 0.0 | 0.0 | 1206 | 25.14 |
| 1581.429 | 399.00 | 40.13 | 167.82 | 389.0 | 15.7 | 3.9 | 24.85 | 0.25 | 432.6 | 0.0 | 200.0 | 400.0 | 0.0 | 0.0 | 0.0 | 1192 | 26.10 |
| 1671.429 | 434.13 | 41.43 | 168.15 | 390.4 | 14.4 | 3.7 | 27.17 | 0.26 | 468.6 | 0.0 | 200.0 | 400.0 | 0.0 | 0.0 | 0.0 | 1179 | 26.94 |
| 1761.429 | 469.34 | 42.62 | 168.46 | 391.2 | 13.3 | 3.4 | 29.52 | 0.25 | 504.6 | 0.0 | 200.0 | 400.0 | 0.0 | 0.0 | 0.0 | 1167 | 27.71 |
| 1851.429 | 504.60 | 43.72 | 168.73 | 391.8 | 12.3 | 3.1 | 31.90 | 0.25 | 540.6 | 0.0 | 200.0 | 400.0 | 0.0 | 0.0 | 0.0 | 1154 | 28.43 |
| 1941.429 | 539.92 | 44.75 | 168.99 | 392.4 | 11.4 | 2.8 | 34.38 | 0.25 | 576.6 | 0.0 | 200.0 | 400.0 | 0.0 | 0.0 | 0.0 | 1147 | 29.10 |
| 2030.000 | 562.92 | 45.34 | 169.15 | 392.7 | 10.9 | 2.7 | 36.04 | 0.25 | 600.6 | 0.0 | 200.0 | 400.0 | 0.0 | 0.0 | 0.0 | 1141 | 29.50 |

